"Solidified liquid lipids" for oral solid dosage forms: Characterisation and processing

Dissertation

zur Erlangung des

Doktorgrades der Naturwissenschaften (Dr. rer. nat.)

der

Naturwissenschaftlichen Fakultät I – Biowissenschaften –

der

Martin-Luther-Universität
Halle-Wittenberg

vorgelegt von

Frau Apothekerin Claudia Kutza

geboren am 13.07.1983 in Dresden

1. Gutachter: Prof. Dr. rer. nat. habil. Karsten Mäder
2. Gutachter: Prof. Dr. rer. nat. habil. Alfred Blume
3. Gutachter: Prof. Dr. Benjamin Boyd

Datum der Verteidigung: 19.02.2016

Table of Contents

1. Introduction

The application of high-throughput screening and combinatorial chemistry in drug discovery generates more compounds with poor aqueous solubility [1–3]. Even though high-throughput solubility assays and computational methods for solubility prediction were developed to select leads with better physicochemical profiles [1, 3–7], approximately 40 % of potent drug candidates are poorly water-soluble resulting in low and highly variable oral bioavailabilities [8, 9]. Often, those poorly water-soluble compounds are classified as class II (low aqueous solubility, high permeability) or class IV drug candidates (low aqueous solubility, low permeability) based on the Biopharmaceutical Classification System (BCS). The BCS classification is composed of four classes and divides active pharmaceutical ingredients according to their aqueous solubility and membrane permeability [10–13]. It is an important tool for predictions and estimations of drug absorption and therefore used in formulation development [7, 10, 11, 14, 15]. There are different options to formulate poorly water-soluble drugs and it is the task of the formulation scientist to choose the most appropriate one for a drug candidate. The most important formulation strategies to tackle this issue are nanosizing, amorphous systems (e.g. amorphous solid dispersions) and lipid formulations [16–20].

1.1. Classification of lipid formulations

Lipid formulations should present the drug in a dissolved or solubilized state *in vivo*. The bioavailability is improved by avoidance of the dissolution step [21–23]. Pouton introduced a lipid formulation classification system (LFCS) for oral administration of lipophilic drugs for the first time in 2000 [24]. With the final classification published in 2008 these formulations were basically divided in four formulation types with increasing polarity from type I to type IV systems. Table 1 on page 2 gives an overview over the lipid formulation systems modified from Pouton and Porter [25, 26]. The most simple lipid formulations are oily solutions (LFCS type I) containing mono-, di- and triglycerides. The group of self-emulsifying drug delivery systems (SEDDS) is much more diversified. Lipid formulations referred to as SEDDS are divided in type II and type III formulations. The most important criterion is the type of surfactant. Type II formulations normally use surfactants with an HLB around 11 which are less water soluble while type III formulations contain at least one hydrophilic surfactant with an HLB above 12. LFCS type II systems result in turbid and relatively coarse o/w (oil in water) emulsions under very gentle agitation. For instance, type II systems were produced with oleate esters as polysorbate 85 or polyoxyethylene (25) glyceryl trioleate [21, 26, 28, 32]. The inclusion of water-soluble surfactants generates LFCS type III systems. Depending on the composition and characteristic

Table 1: *Classification of lipid formulation systems modified from Pouton and Porter*

LFCS class	Excipients	Characteristics	Examples
Type I	Simple oily solution	Non-dispersing	Medium-chain triglycerides [27]
Type II (SEDDS)	Oils, surfactants with HLB 8–12	Self-emulsification to a turbid o/w dispersion	Medium-chain triglycerides, Tagat® TO[a] [28]
Type III (SEDDS, SMEDDS)	Oils, water soluble (and water insoluble) surfactants, cosolvents	Self-emulsification or self-microemulsifica-tion resulting in more or less clear dispersions	Castor oil, medium-chain mono-/diglycerides, Cremophor®EL[b], Cremophor®RH 40[c] [29] Propylene glycol monocaprylate, Cremophor® EL[b] [30]
Type IV	Water soluble surfactants and cosolvents	Formation of micellar solution	TPGS[d], PEG[e] 400, propylene glycol [31]

[a] Polyethylene glycol 25 glyceryl trioleate
[b] Macrogolglycerol ricinoleate (PEG-35 castor oil)
[c] Macrogolglycerol hydroxystearate (PEG-40 hydrogenated castor oil)
[d] Tocopheryl polyethylene glycol 1000 succinate
[e] Polyethylene glycol (=macrogol)

of the excipients those systems have self-emulsifying or self-microemulsifying properties. When dispersed in aqueous media emulsions or microemulsion-like clear dispersions are formed spontaneously. Typical surfactants used to formulate these systems are pegylated castor oil related substances (Cremophor®EL and RH40) or pegylated mixed glycerides (Labrasol®and Gelucire®) [25, 26, 33]. With the classification published in 2006 type III systems were further subdivided in two categories (IIIa and IIIb) depending on the amount of oil, surfactant and cosolvent predicting the performance of the lipid formulation [25]. But with an increasing complexity of such systems, e.g. the use of several oils/partial glycerides, surfactants and cosolvents in one formulation, a clear sub-classification of type III systems only based on excipient amounts is very difficult. Consequently, the final classification in 2008 differentiates between four basic lipid formulation types as demonstrated in table 1. The most hydrophilic type IV systems distinguish from the other formulation types as they contain no oil component [25, 26]. These formulations are composed of surfactants only or a mixture of surfactants and cosolvents. Typical cosolvents are propylene glycol, glycerol, ethanol and liquid PEGs [26]. Type IV formulations form micellar

solutions [26]. Further examples can be found at Kawakami et al. including excipients as Gelucire®44/14, Tween®80 as hydrophilic surfactant and ethanol, PEG 400 and glycerol as cosolvents [34, 35]. Nevertheless, the terminology used in the literature to differentiate the lipid formulations is ambiguous. Especially in the case of SMEDDS, the term "SNEDDS" (self-nanoemulsifiying drug delivery systems) is used, too. Müllertz et al. described the difference based on the thermodynamic stability [36]. SMEDDS result in microemulsions which are thermodynamically stable. Nanoemulsions formed from SNEDDS are kinetically stable. Yet, nanoemulsions can exhibit a very high kinetic stability and they have particles in the nanometre range. Thus, it is sometimes difficult to distinguish between both forms [36]. Exemplary formulations for SNEDDS with Cremophor® EL were developed by Villar et al. reaching an enhanced dissolution of gemfibrozil [37].

The different performance of lipid formulations is mostly caused by their fate in the gastrointestinal tract. It is the aim to maintain the drug in solution in the stomach and throughout the absorption period in the intestine [23]. Therefore, the lipid formulation should disperse easily in the gastrointestinal tract and should be resistant to drug precipitation on dispersion and during digestion of the formulation [23, 38]. The tendency for drug precipitation is dependent on the formulation. Oily solutions need digestion to disperse more easily in the gastrointestinal tract. Therefore, the presence of bile (bile acids and phospholipids) serving as emulsifier and pancreatic juice (digestion enzymes) is necessary [39]. The properties of the digestion products of the formulation components are crucial for the extent of drug precipitation and consequently for the bioavailability as well. Furthermore, the properties of the drug itself, e.g. its distribution in digestion products, have an important impact, too [39, 40]. Different studies can be found in the literature showing an enhanced solubilization during *in vitro* lipolysis or increased bioavailability for long-chain triglycerides (LCT) compared to medium-chain triglycerides (MCT) [40–42]. Investigations with the drug fenofibrate by Mohsin et al. suggest that MCT solutions are relatively fast digested and that their fatty acids often lead to a higher rate of drug precipitation compared to the LCT formulation [41]. In contrast, several studies can be found without any difference in bioavailability between medium- and long chain triglycerides [40, 43–45]. Another cause for the diverse results in this field was given by Porter et al. suggesting an influence of the lipid amount used in lipolysis experiments [46]. Fatouros and Müllertz studied the digestion of self-emulsifying lipid formulations in a simulated gastrointestinal tract and found the presence of micelles, unilamellar vesicles, lipolytic product phases and liquid crystalline phases [47–51]. Self-emulsifying systems which are more hydrophilic will disperse/dilute more easily in the digestive system. But the supersaturation of the dissolved drug is a disadvantage because it is often followed by a drug precipitation which could lead to a reduced bioavailability [23, 52]. However, a supersaturation followed by a drug precipitation does not necessarily result in a lower

bioavailability. Thomas et al. produced super-SNEDDS with the poorly soluble drug halofantrine [53]. The drug precipitation occurred in the amorphous form which finally enhanced the absorption. Furthermore, self-emulsifying drug delivery systems showing drug precipitation *in vitro* do not always show the precipitation *in vivo* [54].

In the meantime, the principle of lipid formulations is applied for marketed drug products (table 2 on page 5). The most famous example among marketed lipid formulations is the ciclosporin formulation Sandimmun®. Ciclosporin is an immunosuppressant drug and according to the literature usually classified as BCS class IV drug [14, 55]. The original soft gelatine capsule formulation contained a pre-concentrate which formed a coarse o/w emulsion when getting in contact with the aqueous gastrointestinal fluids. Bile and pancreatin of the digestive system are needed to disperse the lipid droplets and to incorporate the active ingredient in mixed micelles. This process facilitates the drug absorption in the intestine. The drug absorption is dependent from the digestive performance, in this case. Consequently, the inter- and intra-individual variability of the ciclosporin absorption was relatively high. Finally, the variability of the ciclosporin absorption could be reduced by the development of a type III lipid formulation, the self-microemulsifying system (Sandimmune® Neoral) [14, 31, 56–58].

1.2. Solid lipid formulations

Solid dosage forms, e.g. tablets, are the most accepted way by patients to take a drug [61]. But the majority of marketed lipid formulations (compare table 2) appear as bulk oral solution or soft gelatin capsule where the liquid mixture is incorporated.

1.2.1. Capsule filling of lipid formulations

For the manufacturing of soft gelatin capsules, the liquid or semi-solid is for instance filled by application of the rotary die process [59, 62, 63]. Only a few specialised companies are able in manufacturing soft gelatin capsules [63]. Hence, the production usually needs to be outsourced [63]. Hard gelatin capsules increasingly come into focus for a filling of liquids and semi-solids (e.g. liquid or semi-solid lipid formulations, PEG solid dispersions) using special equipment and different sealing technologies, e.g. banding or LEMS™ which means liquid encapsulation by microspray [61–63]. However, in many cases, the filling process might be difficult due to viscosity problems which is challenging for the content uniformity of low dose and/or highly potent drugs [63]. Furthermore, unintended interactions between the filling and the capsule shell occur due to migration processes which may affect the performance of the lipid formulation (e.g. drug precipitation, loss of self-emulsifying capacity) or the capsule shell (leaky capsules, brittle or sticky soft capsules)

Table 2: *Examples of marketed products containing lipid formulations [14, 36, 59, 60]*

Product name	API[a]	Company	Excipients[b]	Formulation type[c]	Dosage form
Rocaltrol®	Calcitriol	Roche	Medium-chain triglycerides	I	Soft gelatine capsule, oral solution
Avodart®	Dutasteride	GlaxoSmithKline	Mono- and diglycerides of caprylic/capric acid	I	Soft gelatine capsule
Sandimmun® Neoral	Ciclosporine A	Novartis	Corn oil glycerides (mono-,di- and triglycerides), Cremophor® RH 40, propylene glycol, ethanol, α-tocopherol	III	Soft gelatine capsule, oral solution
Ciprobay®	Ciprofloxacin	Bayer	Medium-chain triglycerides, Lecithin, Tween® 20[d]	III	Methacrylic acid copolymer microcapsules for constitution to an oral suspension
Kaletra®	Lopinavir and ritonavir	Abbott	Cremophor® RH 40, ethanol, glycerin, propylene glycol	IV	Oral solution
Aptivus®	Tipranavir	Boehringer Ingelheim	TPGS, PEG 400, propylene glycol	IV	Oral solution

a Active pharmaceutical ingredient
b Excipients contributing to the lipid formulation
c Based on LFCS classification of Pouton and Porter
d Also known under the name of polysorbate 20 or polyethylene glycol sorbitan monolaurate or polyoxyethylene sorbitan monolaurate

[25, 63]. The interactions between the filling and the shell are not easy to predict and the optimization of the formulation and the capsule material might be a time consuming and expensive process. Therefore, alternative solid and capsule free formulation approaches with lipids are highly attractive [61, 64]. They combine the solubilization enhancement in lipid vehicles with the advantages of solid dosage forms [9].

1.2.2. Formulation techniques of solid lipids

Lipids which are solid at room temperature can be processed for instance by melt extrusion, melt granulation or spray cooling (spray congealing) [9, 61]. By means of high pressure homogenisation solid lipid nanoparticles can be obtained representing a highly various and broad research field which, for this reason, will not be covered in this introduction.

Melt extrusion with lipids is mostly used to produce sustained release formulations of hydrophilic compounds [9, 61]. Thereby, lipids serve as co-excipients or processing aids also known as functional excipients (e.g. Gelucire®, Vitamin E TPGS) to improve the extrusion of principal carriers like MCC (microcrystalline cellulose) or polymers (e.g. poly(vinyl pyrrolidone), Soluplus®) or to modify the properties of the formulation [20, 65–67]. Studies aimed at solubility enhancement of poorly soluble drugs are mainly based on melt extrusion with polymer matrices [20, 68]. Most of the examples given in reviews of solid lipid formulations and pertaining to melt extrusion of lipids are, going into detail, not based on a melt extrusion process but rather on adsorption with a subsequent conventional extrusion step. Just a few extrusion matrices based on lipids only are reported, for instance with Gelucire® 50/02 (blend of mono-, di- and triglycerides with mono- and di-esters of fatty acids and poly(ethylene glycol)). This is one example for a wet extrusion with lipids where the lipid is crushed in the frozen state prior to the extrusion at ambient temperatures [69]. Windbergs et al. studied the extrusion of powdered lipids (e.g. Dynasan® 118, a triglyceride of stearic acid) with theophylline as model drug [70, 71]. This extrusion form is named solid lipid extrusion and is known in food science under the name cold extrusion [72, 73]. In pharmaceutical technology, solid powdered lipids are usually extruded at temperatures below the lipid melting point/range so that the bulk part of the lipid is not in a molten state [68]. Solid lipid extrudates are mainly intended to modify dissolution profiles, e.g. sustained release formulations [68, 74, 75]. Indeed, with melt/lipid extrusion high drug loads can be achieved, but recrystallisation during storage or ageing is the major problem of these products besides incompatibilities between excipient and API [66, 67]. Furthermore, dependent on the type of excipient and the extrusion parameters, the thermal stress is disadvantageous. Finally, the process based on solid lipid matrices is quite challenging due to the special plasticity which is required for melt/lipid extrusion and due to the existence of polymorphic modifications [20, 68, 70].

Moreover, for melt extrusion, the formation of eutectic mixtures should be considered if several lipid excipients are combined [66].

Lipids used for melt granulation usually act as binders. Examples can be found using the excipient family Gelucire® as well as lecithin, partial glycerides and polysorbates [9]. A combination of a lipid granulation and adsorption with a subsequently performed extrusion/spheronization step was investigated by Abdalla et al. [76]. A semi-solid mass containing glycerol monostearate, Solutol® HS15 (macrogol-15-hydroxystearate) and diazepam was achieved after addition of water and was then processed with MCC in a kneader to form a mass suitable for extrusion. Dissolution experiments showed that the release rate of the self-emulsifying pellets was increased compared to pellets containing MCC and glycerol monostearate only [76]. Again, the process is challenging due to the plasticity which is needed for the extrusion or granulation process.

In the literature, microparticles of the lipid excipient Gelucire® 50/13 (stearoyl polyoxylglycerides) produced by spray cooling were reported [77–79]. A reliable drug incorporation of 10 % could be demonstrated by Passerini et al [77]. DSC measurements of the 30 % formulation exhibits the melting peak of the drug implying an incomplete incorporation or the expulsion of the drug out of the formulation. However, the majority of lipid formulations are still liquid or semi-solid [9]. Probably, the explained disadvantages of solid lipid matrices may be the reason for it. Moreover, many lipid excipients used in lipid formulations are in a liquid or semi-solid state at ambient temperature [9]. To be processable as a solid dosage form they have to be 'solidified'.

1.2.3. Solidification techniques of liquid lipids

'Solidification' of liquid lipids does not necessarily mean that the lipid mixture is actually in a solid state. It means that the powder or the granules behave like a solid in the formulation process, but they may contain liquid lipid microdomains. The solidification of liquid lipid systems can be achieved by different techniques such as spray drying and lyophilisation of emulsions, the incorporation of lipid mixtures into solid polyethylene glycols (PEGs) and the adsorption at solid carriers [9, 39, 61, 80].

1.2.3.1. Spray-drying/lyophilisation of emulsions

Spray drying and lyophilisation (also freeze-drying) of o/w emulsions are two of the oldest solidification techniques, well known and often applied in food and pharmaceutical science [39, 80–83]. A solid carrier is needed (e.g. carbohydrates, polymers) to encapsulate the liquid oil phase during removal of the aqueous phase [39, 81, 82]. Both techniques differ in the manner of removing the aqueous phase. Afterwards, the powder containing the encapsulated lipid (dry emulsion) should easily reconstitute to an emulsion *in vitro* and *in*

vivo, respectively. For spray-drying, the use of carbohydrates as carrier can be associated with a physical instability caused by a recrystallisation of the amorphous form. By the application of polymers like hydroxypropylmethyl cellulose (HPMC) the stability of dry emulsions could be improved [80, 84, 85]. Yi et al. produced dry SMEDDS by spray-drying with dextran as solid carrier [80]. Based on DSC and X-ray diffraction analysis an amorphous state of the incorporated drug nimodipine was assumed but stability studies with regard to recrystallisation are missing. An interesting study with fumed silica as solid carrier (referred to as pickering emulsion) was performed by Adelmann et al. in 2012 [83]. They applied spray- and freeze-drying to a pickering emulsion containing olive oil. The spray-dried product appeared as more or less sticky powder with an oil content up to 90 % but with a tendency to oil leakage at the surface. Depending on the silica content, the freeze-dried product appeared in form of a compressed dry powder to a porous solid and even a gel-like formulation with up to 98 % oil content [83]. Yet, further process steps, e.g. compression to a tablet, are questionable for these high oil contents due to oil leakage. Dry emulsions on silica basis were investigated by different scientists [86–88]. High MCT loading levels with more than 40 % are reported. The addition of mannitol (together with nanosized silica) after the high pressure homogenisation resulted in spray-dried microparticles which were suitable for direct compression [88]. Furthermore, it was found that the nanostructured silica network of these silica-lipid-microparticles enhanced the lipid digestion[88–90]. Similar studies were performed with self-emulsifying systems resulting in an increased bioavailability of lovastatin [91]. However, the elevated temperature during the spray drying process could be a problem for temperature sensitive drugs. In this case, lyophilisation is the more gentle process [82]. The formation of a tablet was obtained by a direct lyophylisation of an emulsion-filled tablet blister [92]. Nevertheless, both solidification techniques often result in cohesive powders with poor flowability or lead to tablets of poor quality [85, 88, 92]. This necessitates further processing steps like wet granulation or the addition of excipients improving the direct compression process [88]. Furthermore, the lyophilisation process is a relatively slow and expensive drying process and it is generally only applied for products with high added value [93–97].

1.2.3.2. Solidification of lipids in solid polymers - Solid dispersions

Solid dispersions are obtained by incorporation of drug compounds in polymers (e.g. polyethylene glycols, polyvinylpyrrolidone). They are usually prepared by co-melting or solvent evaporation [19]. Also liquid lipid mixtures, wherein the drug is dissolved, can be incorporated in solid polymers just as solid lipids by co-melting [19, 98]. Exemplary studies for incorporation of solid lipids were done by Unga et al. with PEG 4000 [99]. The incorporation of liquid lipid mixtures was predominantly performed in solid PEGs like PEG 4000 [30, 99–102]. Therefore, a homogeneous blend of the molten PEG and the

liquid lipid is prepared with a subsequent cooling until the mass solidifies which usually happens at room temperature [30, 99]. Characterization of such systems with different lipids were done by Mahlin et al. and Unga et al. focusing on the impact of the lipid type (molecular size and polarity) on the crystallisation behaviour of PEGs [99–101]. Li et al. solidified a SMEDDS pre-concentrate in solid PEG 3350 [30]. The poorly soluble API was dissolved in the molten mixture of propylene glycole monocaprylate (oil), polyoxyl 35 castor oil (surfactant) and PEG 3350 (solid matrix) and the mixture was filled in hard gelatine capsules afterwards. The analysis of the solidified mixture concluded a two-phase system with crystalline PEG as solid matrix. The liquid lipid pre-concentrate is separately dispersed between the PEG crystals and contains the drug in a dissolved state. In vitro dissolution studies demonstrated a fast self-microemulsification [30]. Disadvantages of this solidification method are the thermal stress applied by co-melting and the necessity of filling the viscous mixture in capsules. Consequently, the same challenges as explained for capsule filling (see chapter 1.2.1) are relevant, too.

1.2.3.3. Adsorption at solid carriers

Adsorbates are an attractive option to obtain solid lipid formulations systems because of the simple process by mixing liquid and solid components. Depending on the excipient further processing like compression and pelletizing is feasible [9, 103, 104]. Abdalla et al. demonstrated that it is possible to include up to 40 % (w/w) of a liquid self-emulsifying system into MCC pellets. Progesterone was used as lipophilic drug. The pellets were obtained by extrusion/spheronization. Despite the high lipid load, they were not leaky and had a solid character with spherical shape. Besides MCC, a variety of excipients with sufficient high specific surface area or porosity offer good liquid adsorption properties such as inorganic compounds like silicates, organic compounds like special cellulose derivatives as well as polymers [9]. An ideal adsorbent should have the following main characteristics:

1. High loading capacity

2. Facilitates easy processing with standard processes of solid dosage forms

3. High storage stability

4. No negative impact on drug stability

5. Complete drug release in the body

6. No toxicity

Polyvinylpyrrolidone (PVP) as an example for polymeric adsorbents was investigated by Boltri et al. An adsorbate formulation containing a surfactant/lipid mixture was com-

Table 3: *Properties of the adsorbent excipients according to the supplier*

Excipient	Particle size [μm]	Specific surface area [$\frac{m^2}{g}$]	Oil adsorption capacity [$\frac{ml}{g}$]	Mean pore size [nm]
Fujicalin®	115[a]	40	0.94	7.35
Neusilin® US2	<75: less than 40 %[b] 75–250: more than 60 %[b]	300	2.7–3.4	5–6
Neusilin® UFL2	0.02[c]	300	2.0–2.4	5–6

[a] Mean particle size
[b] Particle size distribution
[c] Single particle diameter

pared to a marketed liquid filled capsule formulation of etoposide (Vepesid® 50, Bristol-Myers Squibb) [105]. Aerosil®, an inorganic carrier, is a well-known excipient with good adsorption potential [86–88]. The silica-lipid-microparticles using Aerosil®380 presented in chapter 1.2.3.1 were obtained by spray-drying. The final powder can also be considered as adsorbate because it contains solid carriers and the remaining lipid component.

Recently, new materials have been developed with improved properties regarding liquid adsorption and suitability for pharmaceutical processes. Fujicalin® and Neusilin® are novel processed materials from the groups of calcium phosphates and silicates which offer a good adsorbing capacity. Fujicalin® is a dibasic calcium phosphate in a spray-dried form. Neusilin® is a magnesium aluminometasilicate which is provided in different types. A selection of excipient specific data according to product information and enquiry at the supplier are presented in table 3 for Fujicalin® and two Neusilin® types. Neusilin® UFL2 appears as fine powder and Neusilin® US2 is the spray-dried product in form of spherical granules [106, 107]. Several examples can be found in the literature studying these materials as adsorbents for liquid lipids. Ito et al. solidified solutions of lansoprazole in surfactants with different Neusilin® types and calcium silicates. They improved the bioavailability of this drug in rats after intestinal administration [108]. Another study with gentamicin sulfate (a BCS class III compound) compared the bioavailibility of formulations differing in the used adsorbent [109]. An anhydrous silicic acid, a magnesium aluminometasilicate (Neusilin® US2) and a porous calcium silicate was included in this study. The calcium silicate had the lowest surface area and it showed the highest bioavailability in rats among the investigated adsorbents [109]. During the preparation of this thesis new studies concerning lipid adsorption were published. Milović et al. produced SMEDDS adsorbates with aluminometasilicates and porous silica. The type of adsorbent and its surface area affected the release rate of carbamazepine [110]. Another approach in this area is the

liquisolid technique introduced by Spireas in 1992 as concept of powdered solutions maintaining a sufficient flowability [111]. This technique comprises a simple blending of liquid medications with solid excipients in powder form. The resulting product can be considered as adsorbate. The research of Spireas et al. comprised the investigation of liquisolid compacts with regard to the effect of powder composition [112–114]. These compacts were composed of an compression enhancing carrier (e.g. MCC) and a flow-enhancing adsorptive material (e.g. amorphous silicon dioxide). For example, methyclothiazide dissolved in PEG 400 and formulated as liquisolid system was directly compressed to tablets [114]. The research on adsorbate systems is ongoing and still in focus [115]. Recently, Hentzschel et al. investigated the release of griseofulvin in liquisolid compacts using Neusilin® US2 and water miscible liquids [116]. A higher release rate of the drug was observed from tablets produced with a prior adsorption of a drug solution in PEG 300 on this excipient.

Furthermore, different methods of adsorbate preparation or adsorbing techniques can be found in the literature. The previous examples adsorbed the liquid prior to a processing such as compaction or pelletizing. Sander and Holm applied an alternative method. They prepared tablets of Neusilin® US2 by direct compression and loaded them successfully with liquid SMEDDS afterwards [117]. Meanwhile, studies with different lipids and adsorbents in combination with dissolution experiments with poorly s soluble drugs or model drugs were published [118, 119]. But so far, there are no detailed investigations in the field of adsorbate formation with liquid lipids focusing on interactions between liquid and solid excipients. The process of liquid adsorption is characterised mainly macroscopically. However, the seemingly simple adsorption process is challenging: First of all, there is the choice of the appropriate excipient which differs in its adsorption capacity and suitability to the desired pharmaceutical process. Moreover, storage conditions as well as pharmaceutical processing could influence the adsorption strength of excipients or the immobilisation of the liquid, respectively. The interactions between liquid and solid components could be crucial for processability, storage stability, and finally for the *in vivo* performance.

1.3. Aim of this thesis

Liquid lipid adsorbates are simple and promising solid lipid formulation systems. Detailed investigations of the interactions between the liquid lipid and the adsorbent are missing. In this thesis, novel adsorbent excipients and different lipid systems (non-emulsifying and emulsifying) will be chosen to form solid adsorbate systems. It is the aim to look deeper inside the adsorbate formation and to provide a detailed characterisation of possible physicochemical interactions. Thereby, certain influencing parameters will be included as different homogenisation methods, different storage conditions and a further processing of the adsorbate. Additionally, the release properties of the adsorbate will be considered

with respect to the physicochemical interactions built between the liquid and the solid adsorbent.

The inorganic adsorbents Fujicalin® and Neusilin® are novel processed excipients and available in pharma grade. Besides, the excipients offer a sufficient adsorbing capacity (see table 3). Fujicalin® is available in form of spherical granules produced by spray drying. Neusilin® is available in different qualities, e.g. in powder and granulated form and further divided in alkaline and neutral grades with different water content, specific surface area, particle size and adsorbing capacity. Adsorbates from the substance classes calcium phosphates and silicates will be investigated in this thesis. Fujicalin® and the adsorbent Neusilin® US2, a spray dried silicate in form of spherical granules, were selected. Additionally, Neusilin® UFL2, the fine powder form of the silicate, will be included to compare adsorbents with different particle sizes of the same substance class. It is important to choose a rather simple lipid adsorbate system to be able to study interactions between the solid adsorbent and the liquid lipid in detail and to gain deeper insight on possible alterations of the lipid properties after the adsorption. Medium-chain triglycerides (MCT) are perfectly suited as model oil to form simple adsorbate systems. MCT is often used as solvent for poorly water-soluble drugs in marketed lipid formulations and it is often part of self-emulsifying systems.

The oil adsorbates should be obtained by simple standard technologies and by use of standard equipment. For this purpose, the common homogenisation method mortar and pestle will be used which was present in most of the recent publications concerning adsorbate production. In addition to the conventional blending by mortar/pestle, a novel mixing method, the dual asymmetric centrifugation will be applied. Previous publications investigated this method for the production of liposomal formulations [120–122] and phospholipid gels [122, 123]. It will be applied for adsorbate production for the first time. By means of the subsequently presented methods, it is intended to find out whether the type of homogenisation will influence the physicochemical interactions between the adsorbate components.

Methods for a comprehensive characterisation of the MCT adsorbate and especially the solidified MCT have to be developed. The morphology of the solid particles will be compared before and after oil adsorption by use of environmental scanning electron microscopy and confocal laser scanning microscopy. Furthermore, the absolute density will be measured by use of helium pycnometry to get a better knowledge about the oil distribution. The impact on the properties of the oil caused by the adsorption is a very central issue and will be investigated by different methods. Thereby, the impact of different storage conditions will be included. The microviscosity can be used as a measure for the adsorption state and strength. NMR relaxometry and imaging (Benchtop NMR and MRI) are excellent methods to study the microviscosity by measuring the mobility of the protons of a proton-bearing liquid. NMR relaxometry is frequently used in food techno-

logy [124, 125] and newly applied in the pharmaceutical field [126, 127]. This technique offers short measurement times which are important for the observation of time-dependent processes as for example release studies. Furthermore, it is also possible to measure at certain temperatures. The electron spin resonance (ESR) spectroscopy is a powerful analytical tool which offers clues to different physicochemical parameters of drug delivery systems and is successfully applied in the pharmaceutical research [128–131]. It will serve as second method to investigate the microviscosity of the adsorbed oil. Therefore, the spin probe Tempol, a paramagnetic molecule, will be incorporated because most of the pharmaceutical samples are ESR silent [76]. Furthermore, ESR shall clarify a possible impact on the micropolarity of the adsorbed oil. Changes in the environmental polarity could be a very crucial alteration for a dissolved drug. Therefore, the micropolarity will be additionally investigated by fluorescence analytics. The fluorescence emission of the dye Nile red is sensitive to the polarity of the environment [132–135] and will be measured by use of the multispectral fluorescence imaging technique. Finally, the release of the adsorbed oil from the solid excipient is an important issue. A strong and permanent binding may have a bad influence on drug absorption. Abdalla et al. discovered an incomplete Progesterone release from self-emulsifying microcrystalline cellulose (MCC) pellets [104]. Therefore, a desorption test in aqueous media will be included in the characterisation study of Benchtop-NMR/MRI and multispectral fluorescence imaging.

For a pharmaceutical application of lipid adsorbates it will be important to prove a simple handling in common pharmaceutical processes. The feasibility of the production of pellets by extrusion/spheronization will be investigated by means of the example of Fujicalin® and a self-emulsifying mixture as a more complex lipid system. MCC is the most common extrusion/spheronization aid with properties suitable for the production of strong and spherical pellets [136] and will be used in a first trial in combination with the Fujicalin® adsorbate. Due to known disadvantages of MCC concerning the release of poorly soluble drugs [136], it is planned to include native pea starch as second carrier. By means of reflected light microscopy and ESEM, the morphology of the products of the different process steps will be studied. The application of NMR relaxometry will be used to see a possible influence of the extrusion process on the microviscosity of the adsorbed self-emulsifying system. Further investigations of the pellets such as a complete size and shape analysis will not be performed as it is planned as a feasibility study and thus would go far beyond the scope of this thesis.

Finally, a detailed investigation of the release properties of the adsorbates shall be performed as a comparative study of the three adsorbents with a complex lipid system. The release of a lipophilic fluorescence dye will be measured as model for drugs of poorly aqueous solubility but of good oil solubility. A possible selective release of components of the lipid system will be clarified by dynamic light scattering and ^{1}H-NMR spectroscopy.

2. Materials and methods

2.1. Materials

2.1.1. Adsorbing materials and excipients used for extrusion/spheronization

Product name	Chemical name	Supplier
Fujicalin®	Dibasic calcium phosphate anhydrous	Fuji Chemical Industry (Japan)
Neusilin® UFL2	Magnesium aluminometasilicate	Fuji Chemical Industry (Japan)
Neusilin® US2	Magnesium aluminometasilicate (spray-dried)	Fuji Chemical Industry (Japan)
Vivapur®101	Microcrystalline cellulose	JRS Pharma GmbH + Co KG (Germany)
Pea starch	Starch	Roquette (France)

2.1.2. Lipids

Product name	Chemical name	Supplier
Miglyol® 812	Medium-chain triglycerides	Caelo (Germany)
Captex® 355 EP/NF	Medium-chain triglycerides	Abitec Corporation (USA)
Capmul® MCM C10	Glycerol monocaprate	Abitec Corporation (USA)
Capmul® MCM EP	Glycerol monocaprylocaprate	Abitec Corporation (USA)
Capmul® PG8	Propylene glycol monocaprylate	Abitec Corporation (USA)
Solutol® HS 15	Macrogol-15-hydroxystearate	BASF (Germany)
Cremophor® ELP	Polyoxyl-35 castor oil	BASF (Germany)

2.1.3. Dyes and spin probes

Substance name	Chemical name	Supplier	Absorption maximum [nm]	Emission maximum [nm]
DiI	1,1-Dioctadecyl-3,3,3',3'-tetramethyl-indocarbocyanine perchlorate	SIGMA Aldrich Chemie GmbH (Germany)	551	570
Rhodamine 110 chloride	Xanthylium-3,6-diamino-9-(2-carboxyphenyl)-chloride	SIGMA Aldrich Chemie GmbH (Germany)	498	520
Nile red	9-Diethylamino-5-benzo[α]phenoxazinone	SIGMA Aldrich Chemie GmbH (Germany)	polarity shift	
Sudan red 7B	N-Ethyl-1-[4-(phenylazo)phenylazo]-2-naphthylamine	SIGMA Aldrich Chemie GmbH (Germany)	-	
Tempol	2,2,6,6-Tetramethyl-4-hydroxy-piperidin-1-oxyl	SIGMA Aldrich Chemie GmbH (Germany)	-	

2.1.4. Solvents

2.1.4.1. Aqueous solvents

Purified water was obtained by a combination of ion exchangers and reverse osmosis and distilled water was produced by double distillation. Both conforms to the monograph of purified water of the European Pharmacopoeia. Deuterated water (deuterium oxide 99.9 atom% D) was obtained from SIGMA Aldrich Chemie GmbH (Munich, Germany). For NMR spectroscopy measurements deuterated water containing $0.75\,\%$(w/w) 3-(trimethylsilyl) propionic-2,2,3,3-d4 acid, sodium salt was used. Phosphate buffer pH 6.8 (Sørensen) was obtained by dissolving the buffer agents sodium hydrogen phosphate dihydrate and potassium dihydrogen phosphate (both purchased from Carl Roth, Germany) in distilled water or deuterated water.

Table 4: Overview over the prepared adsorbate samples dedicated to the applied analytical method.

Method	Fujicalin®	Neusilin® US2	Neusilin® UFL2
	percentage of MCT or SMEDDS [%]		
ESEM	30	50	50
CLSM	30	50	50
Helium pycnometry	10/30/50	10/30/50	10/30/50
NMR relaxometry	30/50	30/50/70	30/50/70
NMR imaging	30	50	50
NMR spectroscopy	30	50	50
ESR spectroscopy	30	30	30
Multispectral fluorescence imaging	30	50	50
Fluorescence microplate reader	30	50	50
PCS	30	50	50

2.1.4.2. Organic solvents

All used organic solvents were of analytical quality and were used without further purification.

2.2. Methods

2.2.1. Preparation of the adsorbates

The adsorbates consisted of two components: The solid adsorbing excipient (e.g. Fujicalin®, Neusilin® US2, Neusilin® UFL2) and medium-chain triglycerides (MCT) or a liquid pre-concentrate respectively. Different percentages were prepared depending on the solid excipient and the analytical method: 10 %, 30 %, 50 % and 70 % (w/w). Due to the higher oil adsorption capacity, the Neusilin® adsorbates were the only adsorbates prepared with a MCT loading of 70 %. For some investigations, it was necessary to have a similar powder appearance or similar bulk volumes. Because of the different adsorption capacity, this was only possible if Fujicalin® as 30 % adsorbate was compared to Neusilin® as 50 % adsorbate. Table 4 gives an overview over the prepared adsorbates for the different analytical methods.

Two preparation methods were applied. The mortar method comprehends the weighing of the components in a glass vial and a premixing with a spatula prior to a gentle blending by mortar and pestle. As second method, the components were blended by use of dual asymmetric centrifugation (SpeedMixer™ DAC 150 SP, Hauschild GmbH & Co KG, Germany). The mixing is based on a double rotation of a container. Figure 1 on page 18 shows the principle of this centrifugation method. The components were weighed in a closable polypropylene container (volume: 12 ml or 50 ml) and directly mixed. The mixing program followed the same procedure for all samples involving three steps, a 30 second period with a rotation speed of 3500 rpm at the beginning, and two further mixing periods for 30 seconds at 2000 rpm. In between each step, a rest period of 30 seconds at 300 rpm was inserted to avoid overheating of the material.

2.2.2. Storage conditions

The excipients as well as the produced adsorbates were generally stored in a climatic chamber at 20 °C and 40 % relative humidity. In addition, different levels of relative humidity (RH), 32–33 % (over a saturated $CaCl_2$ solution) and 75–76 % (over a saturated NaCl solution), were prepared in a desiccator at a constant temperature of 20 °C [137]. The humidity values were controlled with a hair hygrometer. Prior to thermogravimetric analysis (see section 2.2.7) and preparation of the adsorbates, the excipients were stored for 4 weeks at these conditions. The adsorbates were then stored for a further week prior to the NMR relaxometry study.

2.2.3. Preparation of pellets by extrusion/spheronization

For extrusion, a twin screw radial extruder (Fuji-Paudal, Japan) with dies of 1 mm hole diameters and a wall thickness of 1 mm was used. The resulting extrudates were spheronized for 5 min in a 250 mm radial plate spheronizer (Fuji-Paudal, Japan). The frictional plate was designed with a grid pattern of pyramidal segments of 3 mm × 3 mm base size and 1.5 mm height. The extrudates which were intended for further analysis and the pellets were dried in an oven at 40 °C for 2 h. Two pellet formulations were produced. Table 5 shows the composition of both pellet formulations. The batch size was 350 g. The first step was the adsorption of the liquid. For this purpose, Fujicalin® was blended according to the mortar/pestle method with the liquid concentrate using an enamel bowl and a pistil in appropiate size. The liquid concentrate was taken from Abdalla et al. [104] and is equivalent to pre-concentrate C whose composition is given in table 6. Afterwards, the extrusion aid (MCC or pea starch) was added and blended. Then, an appropriate amount of purified water was added to form a mass suitable for extrusion.
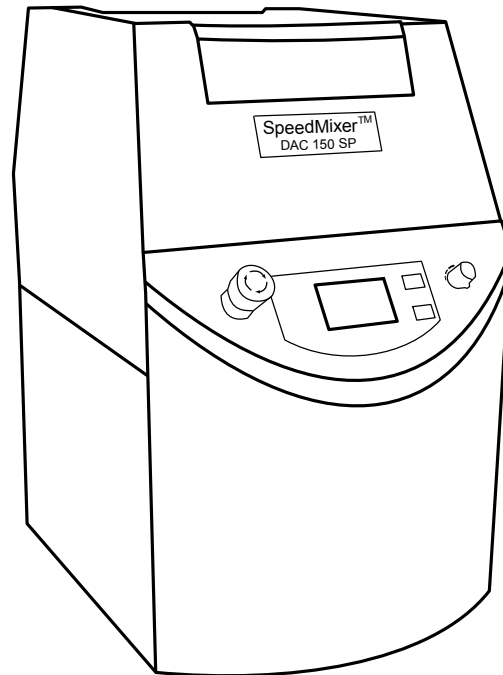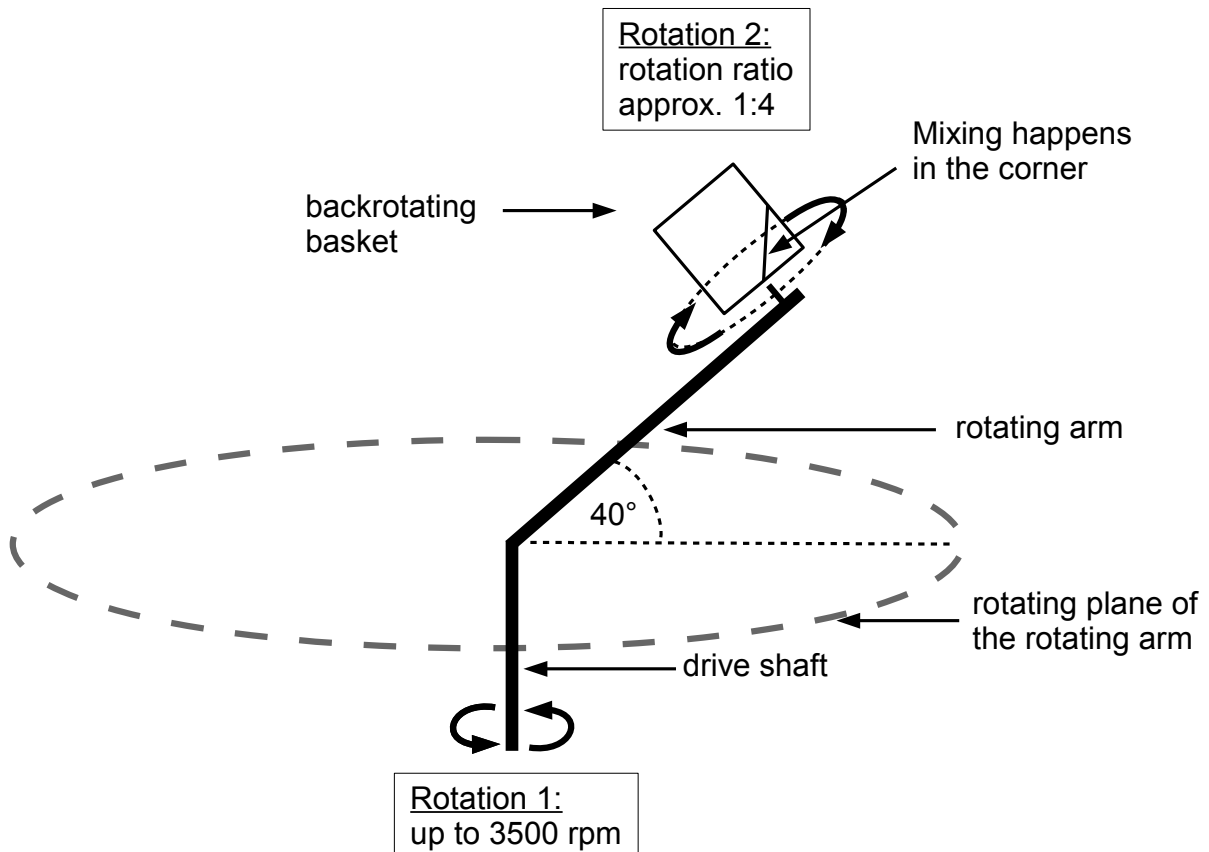
Figure 1: *Principle of the SpeedMixer™ method modified from Massing et. al. [122]. Top: Model of the device. Bottom: Principle of dual asymmetric centrifugation (DAC). Two rotation processes happens simultaneously. The main rotation 1 describes the conventional centrifugation with a rotating movement around a vertical axis at a defined angle to the rotating plane. Thereby and due to the angle of about 40° the material is pushed outwardly to the corner between bottom and container wall. A second rotation is performed by the basket/container component on its own in the opposite direction pushing the material inwardly.*

Table 5: *Composition of the pellet formulations in [%(w/w)]*

Excipient	Formulation I	Formulation II
Fujicalin®	40	20
Vivapur®101	40	-
Pea starch	-	70
Liquid concentrate	20	10

Table 6: *Composition of the liquid pre-concentrates in [%(w/w)]*

Excipient	Pre-concentrate A	Pre-concentrate B	Pre-concentrate C
Capmul® MCM C10	20	-	-
Captex 355® EP/NF	40	-	40
Solutol® HS 15	40	-	40
Capmul® PG8	-	50	-
Cremophor® ELP	-	50	-
Capmul ® MCM EP	-	-	20

2.2.4. Set up of the release study of adsorbed self-(micro)emulsifying systems

2.2.4.1. Selection of the pre-concentrates

Table 6 shows the composition of two self-microemulsifying pre-concentrates (A + B) and of one self-emulsifying pre-concentrate (C). Pre-concentrate (C) was not included in the release study. Pre-concentrate B was taken from Li et al. [30]. Pre-concetrate C was taken from Abdalla et al. [104] and was not included in the release study described in chapter 2.2.4.2 on page 20. Pre-concentrate A is a modified mixture based on pre-concentrate C. For the selection, 0.1 g of each pre-concentrate was covered with 2 ml phosphate buffer pH 6.8 (Sørensen). For pre-concentrate B, a second preparation with distilled water was done. The samples were shaken by use of an orbital shaker by 400 min^{-1} at 37 °C for 1 h. The pre-concentrates were partly coloured with Sudan red for a better visibility of the distribution of the pre-concentrate in the medium.

For further analysis, samples of the selected pre-concentrates A and B were re-prepared at room temperature by covering 0.1 g of a pre-concentrate with 2 ml phosphate buffer pH 6.8 or distilled water, respectively. The samples were shaken by use of an orbital shaker by 400 min^{-1} at 25 °C for 15 min .

2.2.4.2. Preparation of release samples of the adsorbates

Adsorbates of pre-concentrate A and B were prepared as listed in table 4 referring to the methods fluorescence micro plate reader, NMR spectroscopy and PCS. Dual asymmetric centrifugation was used as preparation method. Samples for the release study were obtained following the procedure in Figure 2 on page 21. For the pre-concentrate reference, the liquid mixture was first filled into the test tube. Subsequently, 10 ml of phosphate buffer pH 6.8 with a temperature of 37 °C was added. For the adsorbates samples, 10 ml of the buffer was first filled into a test tube and tempered to 37 °C. Then, an appropriate quantity of adsorbate containing 0.5 g of liquid pre-concentrate was added (equates 1.67 g Fujicalin® adsorbate and 1.00 g Neusilin® adsorbate). 1 h rotation in an end over end apparatus with 10 rpm at 37 °C followed with a subsequent rest period of 5 min to achieve a primary sedimentation of the adsorbate. 5 ml of the supernatant was transferred via a glass frit G3 (pores of 16–40 μm) into a test tube. 1.5 ml of the obtained release medium was transferred into an 1.7 ml Eppendorf reagent tube and centrifuged in an Eppendorf Minispin for 1 min at 5000 rpm to remove the remaining solid particles of the adsorbent. Subsequently, the supernatant was analysed via florescence, PCS and NMR spectroscopy.

For the preliminary visual study, 10 g of the pre-concentrate was coloured with 1 mg Sudan red prior to preparation of the adsorbate. Instead of the filtration step in Figure 2, a centrifuge Labofuge 300 (Heraeus, Germany) was used. The hereof resulting samples were compared as received and not further treated.

2.2.5. Microscopical methods

2.2.5.1. Environmental scanning microscopy

Surface properties of the raw material and the MCT adsorbates were observed with a Philips ESEM XL 30 FEG microscope at a pressure of 1.3 mbar in WET mode and with use of the GSE (gaseous secondary electron) detector which provided a sufficient resolution. First a test with pure MCT was performed which resisted the evacuation of the chamber. The pellet study (see chapter 3.2) was additionally performed by use of the backscatter electron detector (BSE).

2.2.5.2. Confocal laser scanning microscopy

The oil distribution on the excipient particles were investigated with a LSM 710 microscope (Carl Zeiss MicroImaging GmbH, Germany). 1 g solid excipient was moistened with an ethanolic solution of the fluorescent dye Rhodamine 110 chloride (Rh 110) (concentration: 0.5 $\frac{μg}{ml}$). Fujicalin® was moistened with 0.5 ml solution, for Neusilin® an amount of 2 ml was used because of the larger surface area. The moistened excipient was imme-
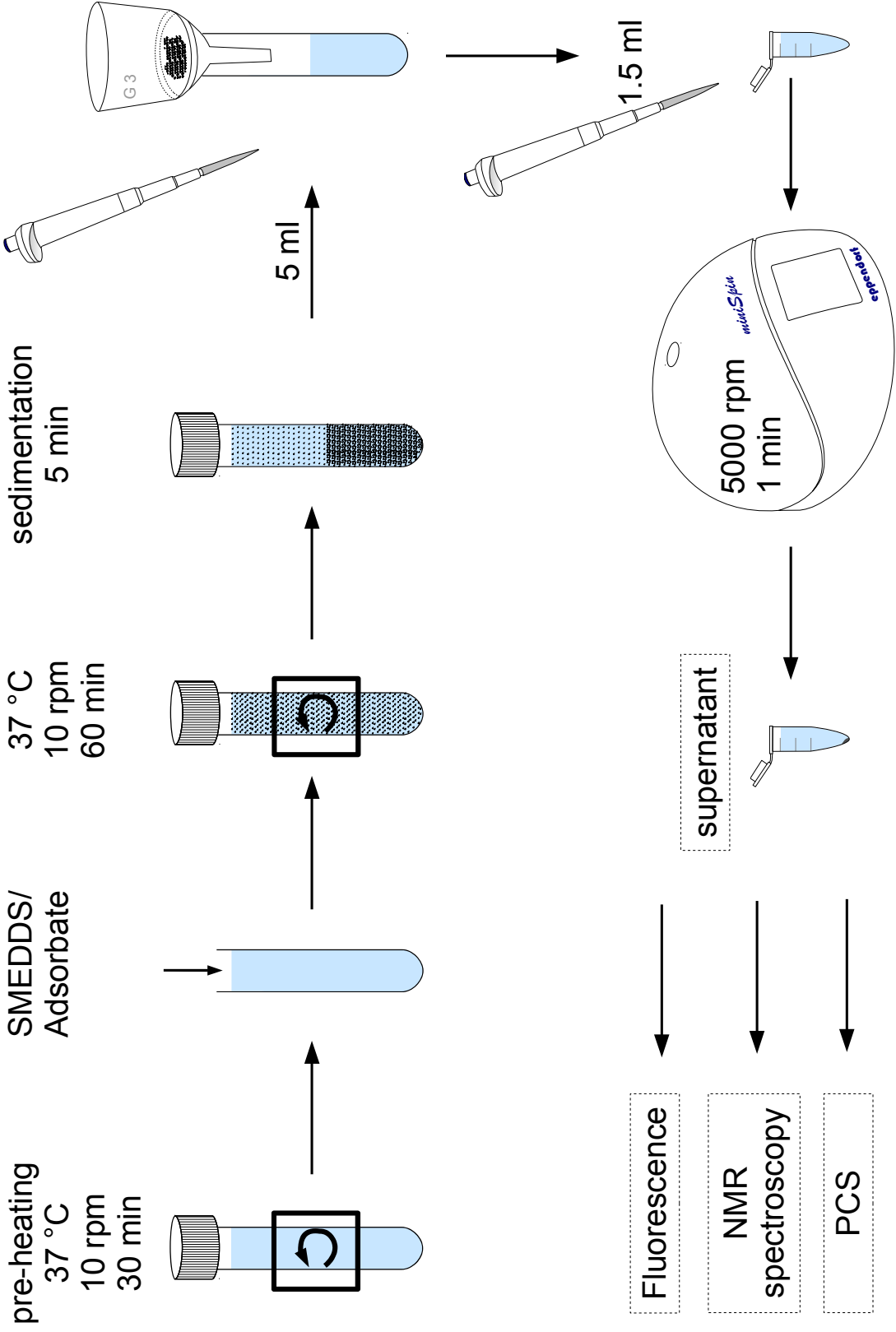
Figure 2: *Sample preparation for the adsorbate release study*

diately blended by use of the SpeedMixer™ programme (see chapter 2.2.1). The mixture was dried under reduced pressure in a rotary evaporator at 40 °C for 30 min. The obtained impregnated raw material was blended with a $0.2 \frac{\text{µg}}{\text{ml}}$ solution of the lipophilic dye DiI in MCT [138]. Rhodamine 110 was excited by a 488 nm laser. DiI was excited by a 543 nm laser. Images were recorded in a sequential scanning mode with the ZEN 2009 software. For adsorbates shown in close-up view a z-stack mode was additionally applied. These pictures are composed of several slices.

2.2.5.3. Reflected-light microscopy

Reflected-light microscopy with a DigiMicro 2.0 was applied for overview pictures of extrudates and pellets. The pictures were taken with the software MicroCapture 2.0.

2.2.6. Absolute density by helium pycnometry

The absolute density was measured with the fully automatic gas displacement helium pycnometer AccuPyc 1330 (Micromeritics, Germany) at room temperature. The sample container was filled with excipient or adsorbat with approximately 50–80 % of the container volume. The number of repeating measurements was fixed automatically during the measuring cycle and ranged between 5 and 10. All in all, two sample series of pure excipient, 10 %, 30 % and 50 % adsorbates were prepared by mortar/pestle and DAC respectively.

2.2.7. Thermogravimetric analysis

The thermogravimetric analysis of the adsorbents was performed with a Netzsch TG 209 (Netzsch-Gerätebau GmbH, Germany). The analyses were conducted in duplicate for each sample with a heating rate of $10 \frac{\text{K}}{\text{min}}$ from 20 °C to 150 °C and a following isothermal period of 10 min at 150 °C.

2.2.8. Nuclear magnetic resonance

Three analytical methods based on nuclear magnetic resonance were applied. Benchtop NMR and MRI were used for investigation of MCT adsorbates (chapter 3.1) and extrusion/spheronization products (chapter 3.2). NMR spectroscopy was used for the investigation of the release media of adsorbed pre-concentrates handled in chapter 3.3.

The benchtop NMR and MRI (BT-NMR/ BT-MRI) measurements were carried out with a low-field (20 MHz) benchtop ^{1}H NMR-MRI spectrometer (MARAN DRX2, Oxford Instruments Molecular Biotools, Oxford, UK) with an included air flow temperature regulation. Samples were prepared according to the procedure in Figure 3. The adsorbate
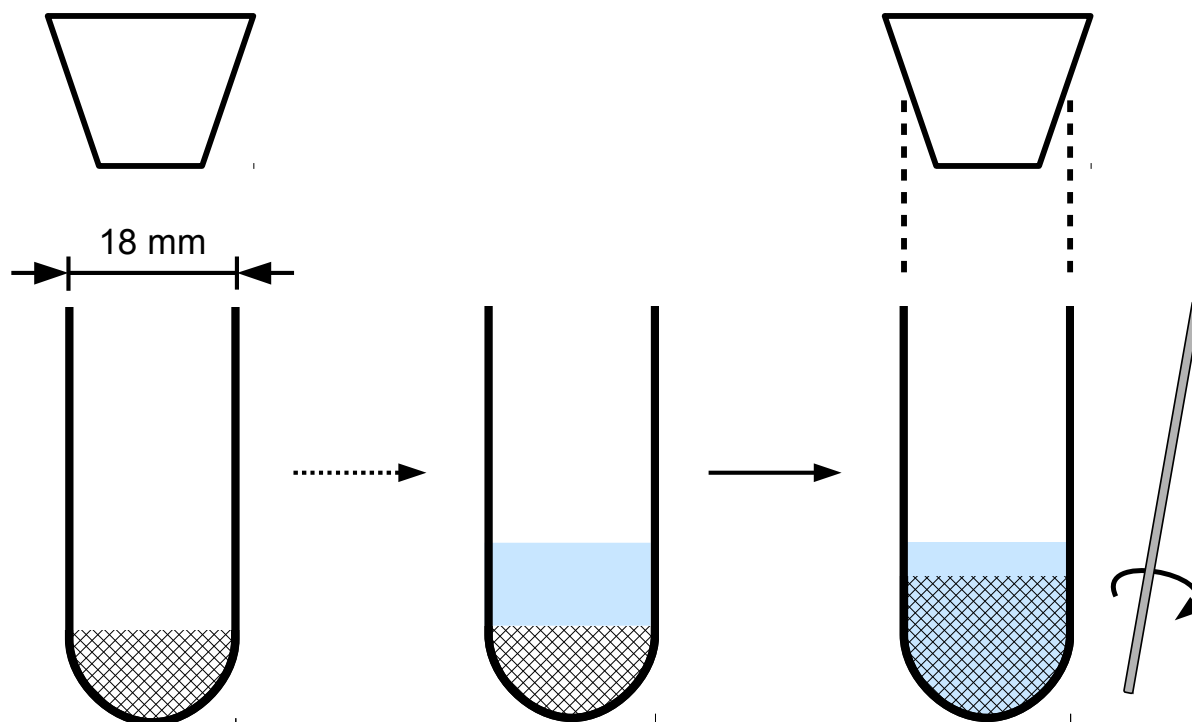
Figure 3: *General sample preparation for Benchtop-NMR relaxometry and -MRI.*

was first filled into a test tube of 18 mm diameter. For the desorption studies of MCT adsorbates, the corresponding medium was then added with a pipette on top of the adsorbate. In case of floating occurrences the sample was shortly and very gently agitated by a stirring rod before starting the measurement. The temperature was generally set to 25 °C. Specifics on sample preparation and parameter settings will be described within the individual method.

2.2.8.1. Benchtop nuclear magnetic resonance relaxometry

For relaxometry measurements, the transverse magnetization decay (T_2 relaxation) was used by applying the Carr-Purcell-Meiboom-Gill (CPMG) pulse sequence [126]. The data were fitted using the WinDXP analysis software (Oxford Instruments Molecular Biotools, Oxford, UK) to obtain the resulting T_2 distribution. A corresponding amount of adsorbate containing 300 mg MCT was filled in a test tube. The relaxation delay time was set to 5 s and the number of echoes between two radio frequency pulses was adjusted for each sample in the range of 512 to 4096. All measurements were performed with 64 scans. Samples were prepared with different MCT loadings in triplicate. The MCT desorption study was done with Fujicalin® adsorbates of 30 and 50 % (w/w) MCT content and with Neusilin® adsorbates of 50 % (w/w) MCT content. Therefore, 2 ml deuterium oxide (D_2O) was added to every test tube containing the adsorbate and the T_2 distribution was measured every 15 minutes over a period of 8 hours. Values of 1 hour are presented.

Table 7: Parameter set of BT-MRI

MRI parameter	Dry adsorbate	Adsorbate with water/ phosphate buffer/ 0.1 M HCl	Adsorbate with D₂O
Repetition time (t_R) [ms]	150	300	600
Gradient echo time (t_E) [ms]	6.7	8	8
Number of measurements (averages)	16	16	16
Gain	100	20	20
Time per image [min]	2.5	5	10

Table 8: Adsorbate quantities used for the BT-MRI study

	Fujicalin®	Neusilin® US2	Neusilin® UFL2
Adsorbate mass [mg]	1000	600	500
Thereof MCT [mg]	300	300	250

Products of extrusion/spheronization process steps and the free liquid concentrate were measured with the same parameters given for the MCT adsorbates. 0.2 g of liquid concentrate and 2 g of every process sample were weighed in a test tube, respectively.

2.2.8.2. Benchtop magnetic resonance imaging

The parameters in table 7 were used for the pilot and the subsequent comparative study. The number of averages is the number of repeating measurements. One measurement (average) comprised 64 scans. "t_R" is the repetition time and defined as the period of time after which a new excitation takes place. "t_E" is defined as the gradient echo time. For reference samples with raw material only, the same parameter settings were used as for the adsorbates. Images were always initiated after the following time points: prior to the addition of the medium, directly after the addition of the medium (start point), after 15 min, after 30 min (not performed in the pilot study) and after 60 min. The adsorbate quantities presented in table 8 were weighed in a test tube to achieve a filling height of approximately 1 cm. First, the image of the dry adsorbate was recorded. Finally, 4 ml aqueous medium were added to the test tube. In case of the Neusilin® adsorbates, a gentle agitation with a stirring rod was applied during the comparative study. The measurement was started immediately.

2.2.8.3. Nuclear magnetic resonance spectroscopy

NMR spectra of the release medium of the adsorbates were recorded with a Gemini 2000 400 MHz NMR spectrometer. The samples were prepared according to the description given in chapter 2.2.4.2 on page 20. Phosphate buffer pH 6.8 (Sørensen) prepared with deuterated water containing 0.75 %(w/w) 3-(trimethylsilyl) propionic-2,2,3,3-d4 acid, sodium salt (TMSP), was used as release medium. 800 µl of the release samples were pipetted in a NMR tube and a spectrum was recorded at 25 °C. Calibration samples with increasing amounts of the lipid component were prepared following the same release procedure. For pre-concentrate A, calibration samples with constant concentration of Solutol® HS 15 ($0.02\,\frac{g}{ml}$) and lipid concentrations of 0; 0.01; 0.02 and $0.03\,\frac{g}{ml}$ were measured. The lipid component is composed of one part Capmul® MCM C10 and two parts Captex 355® EP/NF. Additionally, a pre-concentrate reference ($0.05\,\frac{g}{ml}$ pre-concentrate A) and a Solutol® HS 15 reference ($0.02\,\frac{g}{ml}$) was included. For pre-concentrate B, calibration samples with a constant concentration of the surfactant Cremophor® ELP ($0.025\,\frac{g}{ml}$) and increasing Capmul® PG8 concentrations (0; 0.01; 0.015; 0.02 and $0.025\,\frac{g}{ml}$) were measured. Additionally, a pre-concentrate reference ($0.05\,\frac{g}{ml}$ pre-concentrate B) and a Cremophor® ELP reference ($0.025\,\frac{g}{ml}$) was included. The adsorbate quantity used corresponded to 0.5 g of adsorbed pre-concentrate. The spectra were processed in MestReNova LITE with automatic baseline correction and TMSP as 0 ppm standard. Peak intensities were determined manually.

2.2.9. Electron spin resonance spectroscopy

Electron spin resonance (ESR) spectroscopy was performed with a MiniScope MS 200 X-Band spectrometer (Magnettech, Berlin) at room temperature. Adsorbates with a MCT load of 30 % (w/w) were prepared with both mixing methods in duplicate. Prior to preparation of the adsorbates, MCT and reference solvents (water, methanol, ethanol) were loaded with the spin probe Tempol ($0.5\,\frac{mmol}{l}$). The reference solvents and adsorbates were filled in capillary tubes. The solid Tempol spectrum was generated by molecular distribution of Tempol on pea starch. For this purpose, 2 g pea starch were suspended in 10 ml of a Tempol-water solution ($17.22\,\frac{µg}{ml}$) to achieve a concentration of $0.5\,\frac{mmol}{kg}$ pea starch. The suspension was freeze-dried. The spectra were recorded with the parameters given in table 9 on page 26. The original spectra were simulated with the EPRSIM software (Nitroxide Spectra Simulation - Freeware Version 4.99 - 2005, "Jozef Stefan" Institute, Department of solid state physics, Ljubljana, Slovenia, http://lbf.ijs.si/index.html). Reference spectra were simulated as one isotropic form, the data of the adsorbates as two isotropic domains. The proportion of the species as well as their corresponding rotational correlation time (τ_c) and hyperfine splitting constant (a_N) were calculated directly from the shape of the spectrum by the simulation software.

Table 9: *Summary of ESR parameters*

ESR parameter	Reference solvents	MCT adsorbates	Solid spectrum
B_0-field [mT]	333.9	333.9	333.9
Field sweep [mT]	7.7	7.7	20
Sweep time [min]	10	30	10
Modulation amplitude [mT]	0.02	0.05	0.1
Microwave power [mW]	5	5	20
Number of passes	3	3–5	3

2.2.10. Fluorescence analytic

2.2.10.1. Multispectral optical imaging

Fluorescence imaging was carried out with the Maestro™ fluorescence in vivo imaging system (Cambridge Research & Instrumentation, Inc.). The method is described in detail by Kutza [139], Kutza et al. [140] and Schädlich et al. [141–143]. Nile red (NR) was selected as fluorescence dye because the wavelength of its emission maximum increases with polarity of the environment [132–135]. The adsorbates were prepared with a NR solution in MCT ($0.5\,\frac{\mu g}{ml}$) with both mixing methods. The pure excipient (an amount corresponding to the proportion in the adsorbate) was impregnated with 380 µl of a NR solution in acetone ($0.5\,\frac{\mu g}{ml}$) by the SpeedMixer™ method as comparison specimen. The solvent was removed afterwards in a rotary evaporator for 15 min at room temperature. These samples referred to as "impregnated samples". An appropriate amount of adsorbate containing 300 mg MCT, the equal amount of impregnated excipients and 4 ml of NR containing reference solvents ($0.5\,\frac{\mu g}{ml}$ in methanol, MCT, n-hexane) were transferred in a 12 well microtiter plate. To achieve a similar filling level of the wells Fujicalin® as 30 % (w/w) MCT adsorbate and Neusilin® samples as 50 % MCT adsorbate were compared in the study. Fluorescence images were recorded by use of the green filter set in 2 nm steps. Exposure time was set to automatic mode and the platform height to level 1a. First, the dry adsorbates were measured. Afterwards, 4 ml water were added to the adsorbates and impregnated excipients (desorption study) and the samples were measured again after one hour. All samples were prepared in triplicate.

2.2.10.2. Fluorescence analytic with the NOVOstar micro plate reader

Fluorescence analytic of the release medium of asorbed pre-concentrates was performed by means of the NOVOstar micro plate reader (BMG LABTECH GmbH, Germany). The pre-concentrates A and B were loaded with the fluorescence dye DiI ($1\,\frac{\mu g}{g}$). Sub-

sequently, adsorbates were prepared by the SpeedMixer™ method. The samples of the release medium were obtained following the method described in chapter 2.2.4.2 and figure 2. 200 μl of every supernatant were transferred to a 96 well microtiter plate. The plate was placed in the Novostar microplate reader and the fluorescence of individual wells was measured in plate mode using a 544/10 excitation filter and a 590/20 filter for emission. Every plate was measured with 3 cycles with 100 flashes per well and cycle. The release experiment was carried out in triplicate for both pre-concentrates. All obtained samples from one pre-concentrate series were included in the same microtiter plate. Additionally, 0.5 g of DiI loaded pre-concentrate were suspended in 10 ml phosphate buffer pH 6.8 and served as 100 % release reference. These reference samples were prepared in triplicate and followed the same procedure as done for the adsorbate samples. Furthermore, 7 calibration samples with concentrations of 0.01, 0.02, 0.03, 0.04, 0.05, 0.06 and 0.07 $\frac{g}{ml}$ of DiI loaded pre-concentrates were prepared (equates DiI concentrations in the medium of 0.01, 0.02, 0.03, 0.04, 0.05, 0.06 and 0.07 $\frac{\mu g}{ml}$). 200 μl of every calibration sample as well as a blank were transferred to the same microtiter plate of the corresponding adsorbate release samples.

The mean of 3 measurement cycles of one preparation (one well) was calculated for each sample and the blank value was subtracted. The median was calculated from the three preparations (adsorbate samples and pre-concentrate reference) as well as the positive and negative range. A calibration curve was calculated to prove the linearity for the chosen DiI concentrations.

2.2.11. Particle size characterisation by dynamic light scattering

Particle size characterisation was performed by dynamic light scattering also known as photon correlation spectroscopy (PCS) with the Zetasizer Nano ZS (Malvern Instruments, He-Ne-laser of 633 nm). Samples of pre-concentrate A were diluted 1:10 (v/v), samples of pre-concentrate B were diluted 1:20 (v/v) and samples of pre-concentrate C were diluted 1:40 (v/v) with phosphate buffer pH 6.8 to obtain an optimal sample concentration for the measurement (attenuation values between 6 and 9). The samples were filtrated by a 0.02 μm cellulose acetate filter. The measurement duration was set to automatic mode. Every sample passes 5 measurement cycles at 25 °C and 37 °C at an angle of 173° using non-invasive backscatter optics. A delay of 20 s was inserted between each cycle. The 5 consecutive cycles were performed as a control of the short term stability. Water was set as dispersant in the standard operating procedure with an refractive index of 1.330. One sample was prepared for the selection of pre-concentrates. The experiment was performed in duplicate at 25 °C for the characterisation of the release medium of pre-concentrate A and B. The mean and range of z-average diameter and polydispersity indices were calculated from 5 measurement cycles of every sample.

3. Results and Discussion

3.1. Characterisation of MCT adsorbates

3.1.1. Morphology of the adsorbates

Environmental scanning electron microscopy (ESEM) and confocal laser scanning microscopy (CLSM) were performed to characterise the morphology of the adsorbates. The influence of oil adsorption and production method on the particle surface was investigated.

3.1.1.1. Environmental scanning electron microscopy

Scanning electron micrographs (Fig. 4 on page 29) suggest mostly spherical particles of the pure and the MCT-loaded material of Fujicalin® and Neusilin® US2. The oil adsorption process modified the particle surface. Differences between both mixing methods are visible. The SpeedMixer™ method leads to a smoothing of the particle surface. In contrast, the electron micrographs of the mortar samples show a coarse and uneven particle surface. Partly destroyed powder particles are visible for the Neusilin® US2 sample. Neusilin® UFL2 tends to agglomerate because of its fine powder form (G1 and G2). These agglomerates seem to be more easily destructible by the mortar/pestle method (H1 vs. I1). However, the single particles are too small to get a sufficient resolution to see surface modifications.

Gumaste et al. compared different silicates concerning tableting properties with and without adsorbed liquids [144]. For instance, the surfactant Cremophor® EL was adsorbed at Neusilin® US2 and Neusilin® UFL2. The SEM images of the 1:1 US2-surfactant adsorbate showed a similar rough particle surface as found for the mortar/pestle adsorbate in the present work. Gumaste et al. suggested that Neusilin® US2 adsorbs liquids deeper into its pores because of its porous structure and the presence of relatively large pores of $1\,\mu m$ versus UFL2 with smaller particles. This explanation could be plausible as lipids were adsorbed in form of an organic solution [144]. One the other hand, the treatment of the slurry (intermittent stirring with a spatula) during removal of the organic solvent and the subsequent sieving step could also modify the surface. Hence, the rough and porous appearance of the adsorbate does not necessarily prove the adsorption into the inner pores particularly with regard to the non-visible contrast between adsorbent and liquid. Kang et al. applied scanning electron microscopy to adsorbates with Fujicalin® and Neusilin® US2 and suggested that the liquid SEDDS were retained in micropores and at the particle surface [118].

All in all, ESEM allowed detecting differences in the surface texture of the adsorbate particles. Due to the poor contrast between excipient and oil, it was neither possible to
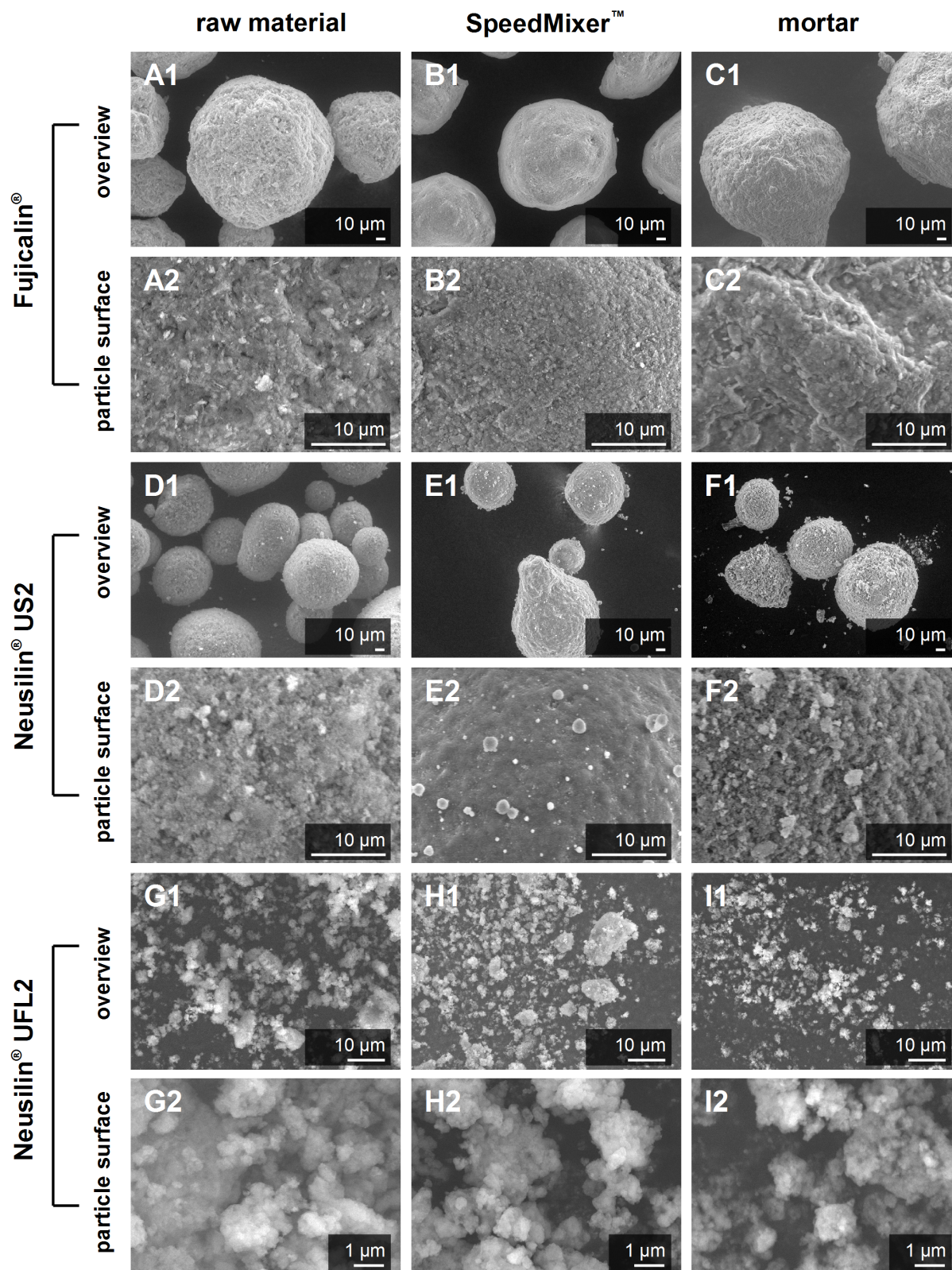
Figure 4: *Scanning electron micrographs of "A1+A2" Fujicalin® raw material; "B1+B2" Fujicalin® loaded with 30 % MCT by speed mixing; "C1+C2" Fujicalin® loaded with 30 % MCT by mortar/pestle; "D1+D2" Neusilin® US2 raw material; "E1+E2" Neusilin® US2 loaded with 50 % MCT by speed mixing; "F1+F2" Neusilin® US2 loaded with 50 % MCT by mortar/pestle; "G1+G2" Neusilin® UFL2 raw material; "H1+H2" Neusilin® UFL2 loaded with 50 % MCT by speed mixing; "I1+I2" Neusilin® UFL2 loaded with 50 % MCT by mortar/pestle.*

obtain information concerning the homogeneity of the oil distribution nor to get a hint if MCT is adsorbed into inner pores. Therefore, a second microscopic method was applied.

3.1.1.2. Confocal laser scanning microscopy

Confocal laser scanning microscopy (CLSM) was able to differentiate visually between particle surface and adsorbed oil by use of two fluorescent dyes. The CLSM images of Fujicalin® and Neusilin® US2 adsorbates are shown in Figure 5 on page 31. The particles of the pure material were covered with Rh 110 (green) prior to the adsorption of a DiI-MCT solution (blue). The pictures indicate a heterogeneous oil adsorption on the excipient particles for the SpeedMixer™ (A,B,D,E) and the mortar/pestle (C,F) blending procedure. Not all of the particles are covered with MCT. Regarding the DiI fluorescence of a single particle in more detail the mortar/pestle method shows a less homogeneous oil distribution on the surface compared to the SpeedMixer™(B versus C, E versus F). Furthermore, the particle surface becomes coarser and particle destruction is visible. Figure 6 on page 32 presents an overview of the mortar samples of all adsorbents. For Neusilin® UFL2, small dots of adsorbed MCT are visible for both methods (C1/C2 and C3/C4). The appearance is comparable. The mortar/pestle sample exhibits a slightly more homogeneous MCT distribution compared to the SpeedMixer™ sample. The poorer agglomerate disintegration of the SpeedMixer™ method leads to bigger MCT accumulations.

The images with close-up view were recorded in a z-stack mode. They are composed of several slices. This mode was selected in order to obtain a better focused surface of the round particle. Furthermore, it was intended to enable a deeper look into the particle and to visualise the inner pores possibly loaded with MCT. Figure 7 and Figure 8 on pages 33 and 34 represent the same image sections used for the detail images of Fujicalin® and Neusilin® US2 (SpeedMixer™) in figure 5 (B1 and E1). The recorded slices from top to bottom are sorted in ascending order by number. The first slice for the Fujicalin® adsorbate (Figure 7) started deeper compared to Figure 5 to focus more on the MCT loaded particle. Both figures demonstrate that the oil is definitely located on the surface or adsorbed in pores close to the outer surface. Additionally, it is visible that the particles disappear more and more on the last slices of the series. The series of the Neusilin® US2 adsorbate in particular goes very deep to a z-position of 81.45 µm from the top of the particle. Slice 7 (61.09 µm) should be the middle of the Neusilin® US2 particle. The last slice of the Fujicalin® series is located in the middle of the non-loaded particle at a z-position of 45.91 µm. For both samples no further slices were recorded because there was almost no fluorescence in deeper layers. The surface of the lower side of the particle is not visible in both cases. Actually, by moving through the particle a circle of Rh 110 fluorescence signal should remain. The outer surface was completely impregnated with
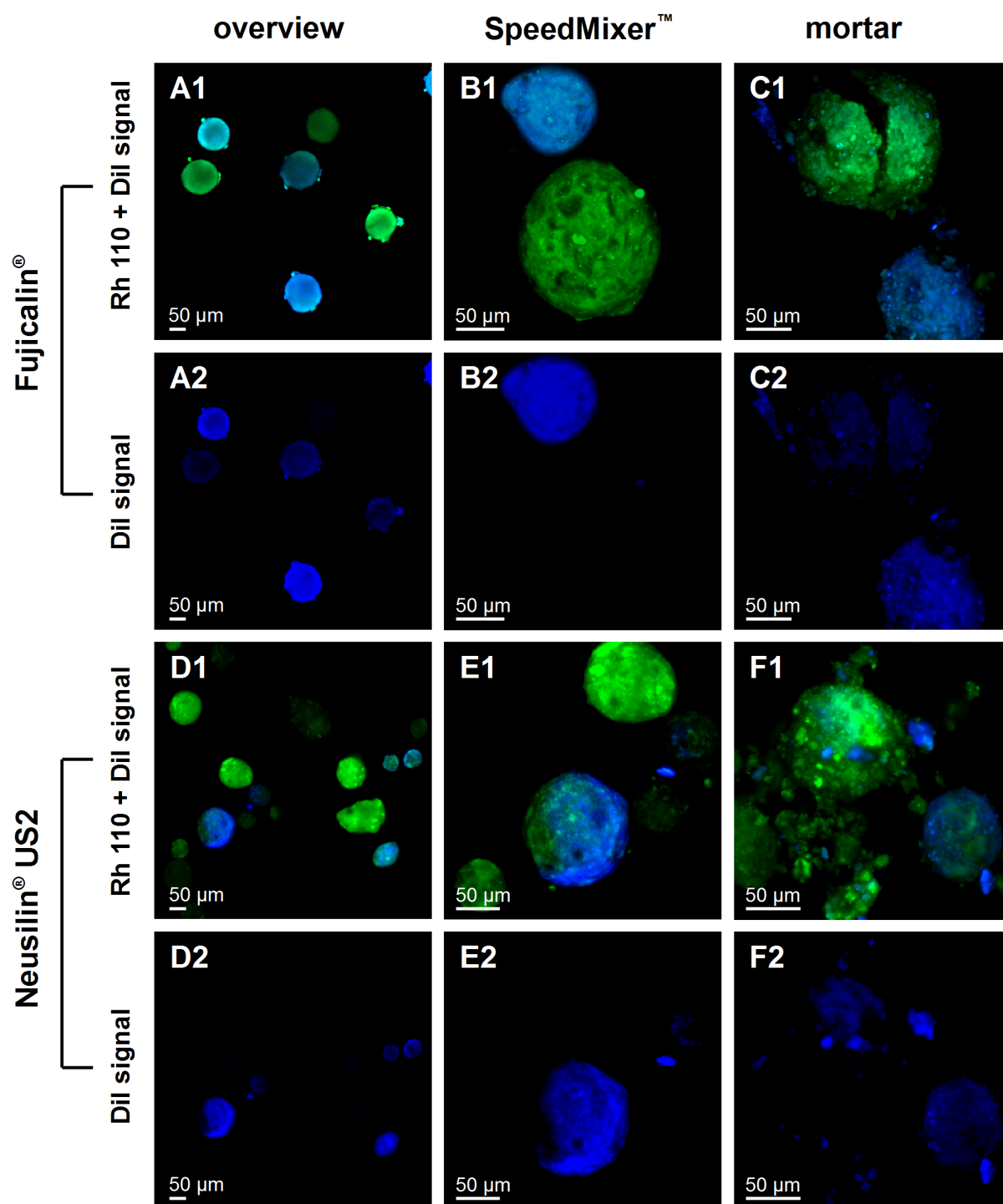
Figure 5: *Confocal laser scanning microscopy images of excipient-MCT adsorbates. Excipient particles are covered with Rh 110 in green, MCT-DiI distribution is shown in blue. Images with number "1" are overlaid images of both dyes. Images with number "2" show the DiI fluorescence only: "A" Fujicalin® with 30 % MCT by SpeedMixer™ - overview; "B" Fujicalin® with 30 % MCT by SpeedMixer™ - close-up view; "C" Fujicalin® with 30 % MCT by mortar/pestle - close-up view; "D" Neusilin® US2 with 50 % MCT by SpeedMixer™ - overview; "E" Neusilin® US2 with 50 % MCT by SpeedMixer™- close-up view; "F" Neusilin® US2 with 50 % MCT by mortar/pestle - close-up view.*
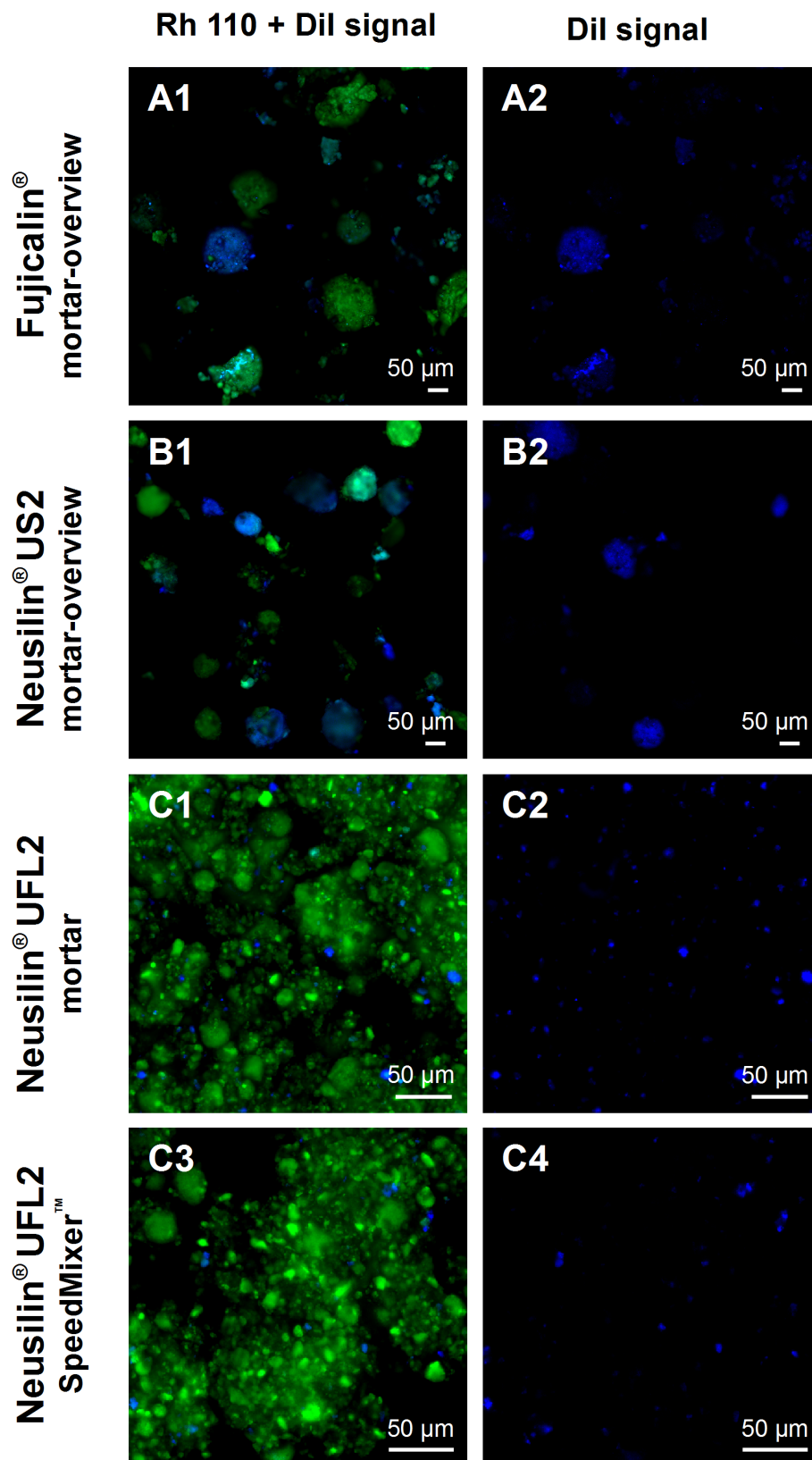
Figure 6: *Confocal laser scanning microscopy images of MCT-excipient adsorbates. Excipient particles are covered with Rh 110 in green, MCT-DiI distribution is shown in blue. Images on the left side are overlaid images of both dyes, images on the right side show the corresponding DiI fluorescence only: "A1+A2" Fujicalin® with 30 % MCT by mortar/pestle - overview; "B1+B2" Neusilin® US2 with 50 % MCT by mortar/pestle - overview; "C1-C4" Neusilin® UFL2 with 50 % MCT by mortar/pestle "C1+C2" and SpeedMixer™ "C3+C4".*
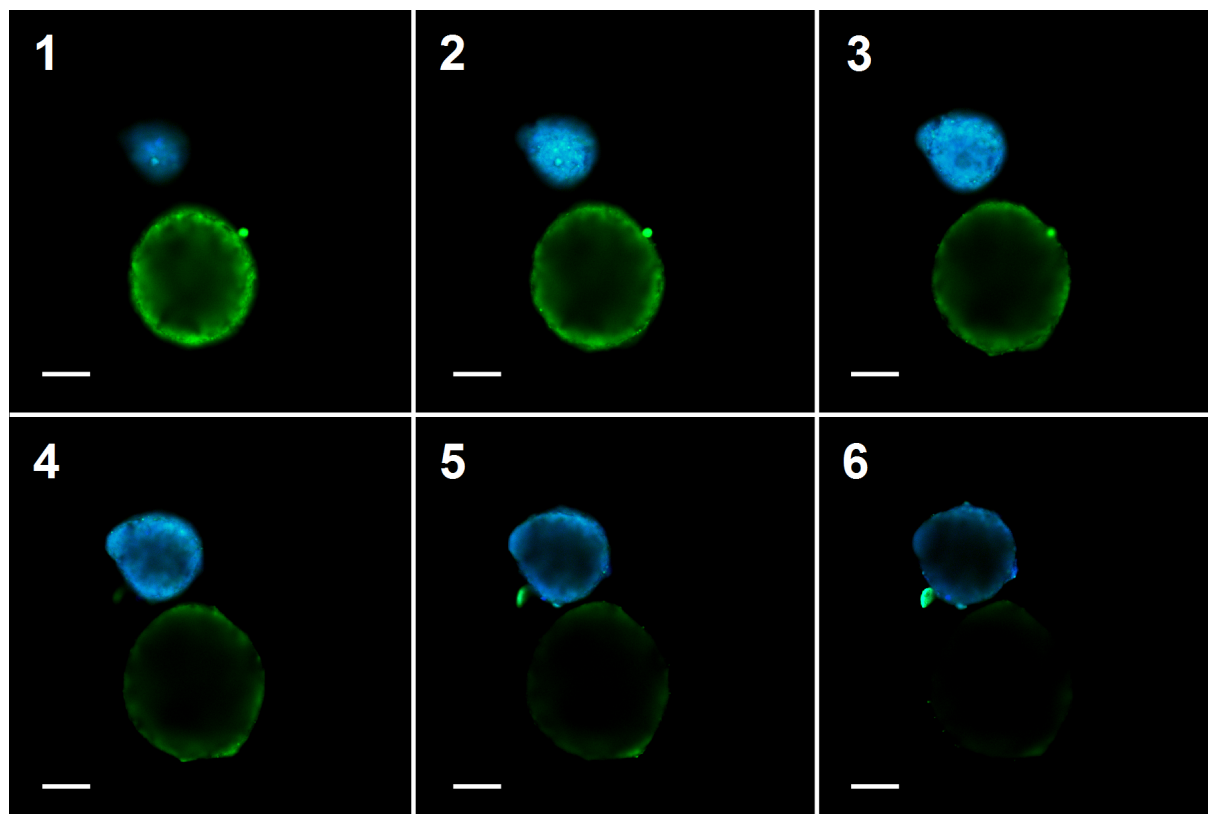
Figure 7: *CLSM image slices of "B1" from Figure 5 - Fujicalin$^®$ with* 30 % *MCT by SpeedMixer^{TM} from top to bottom starting with number 1. The scale bar indicates* 50 µm. *Distance between sequent slices:* 9.18 µm.

this dye. Even if MCT was only located on the surface a blue circle should at least be consistent. Because this cannot be observed, it can be concluded that the particles are too compact and not transparent enough. The light adsorbing barrier is too thick to detect fluorescence signals from the inner pores of the particles and from the opposite particle site. Hence, it cannot be clarified by CLSM whether MCT is adsorbed to the inner pores or not.

3.1.2. Impact of the oil adsorption on the absolute density of the powder

MCT exhibits a density of $0.95 \frac{g}{cm^3}$. The used adsorbents exhibit densities above this value. Consequently, MCT reduces the density of the adsorbate with increasing amounts. Figure 9 on page 36 summarises the data obtained by the helium pycnometry method. All mean data with the corresponding standard deviation are summarised in table 19 on page i (appendix). The graphic shows the much higher starting density for Fujicalin$^®$ ($2.845 \frac{g}{cm^3}$) as pure excipient compared to the Neusilin$^®$ excipients (2.168–$2.235 \frac{g}{cm^3}$). The decrease of density by addition of MCT is therefore more pronounced for Fujicalin$^®$. Apparently,
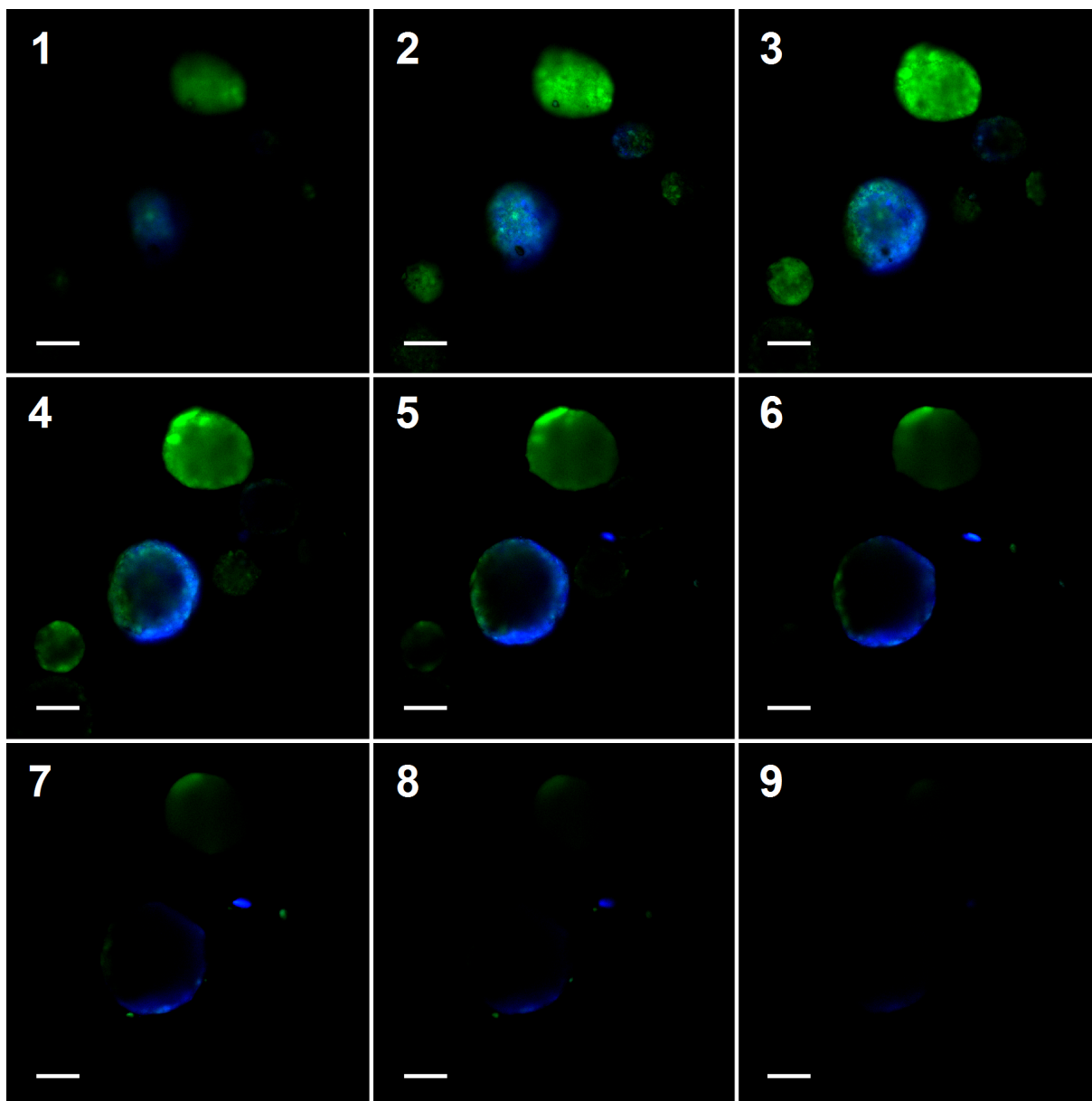
Figure 8: *CLSM image slices of "E1" from Figure 5 - Neusilin® US2 with 50 % MCT by SpeedMixer™ from top to bottom starting with number 1. The scale bar indicates 50 μm. Distance between sequent slices: 10.18 μm.*

the blending method does not influence the absolute density of the adsorbates. But a discrepancy between measured data and theoretically calculated values was identified. The calculated value is composed of the percentages by mass of the density of the pure adsorbent and the density of MCT. For all MCT adsorbates the calculated values are higher compared to the measured data. This suggests that MCT does not reach the inner pores of the particles but is rather located on the surface and outer pores. This hypothesis can be justified as follows. The principle of the used helium pycnometer is based on a gas displacement. The purging process with helium at the beginning of the measurement should displace the air in the sample cell inclusively the air in the pores. If

inner pores are partly closed by a MCT barrier the air in the pores cannot be displaced by helium. The measured sample volume will be false high because the included air contributes to the measured volume and therefore results in a false low absolute density value. Besides, a second impact is imaginable. Helium could dissolve in MCT. A certain solubility in oils was found by different scientists [145–147]. If a certain quantity of helium dissolved in MCT this part would not contribute to the pressure in the sample cell. Consequently, more helium would fill the sample cell than it would be the case without any solubility in MCT. A part of the dissolved helium would return to the gas state after opening of the valve between the sample and the expansion cell. The obtained sample volume will be falsely low and will lead to a false high density. Thus, this impact would not explain a discrepancy between low measured density values and higher theoretically calculated density values. Consequently, the obtained results support the assumption that the adsorption takes place mainly at the surface of the particle and that MCT hardly reach the inner pores. The highest difference between measured and calculated values was found for Fujicalin®(between 0.22 and 0.47 $\frac{g}{cm^3}$). This indicates that the adsorbed oil is mainly located on the outer surface for this adsorbate.

Milović et al. suggests that silicates with the higher surface area and/or bigger pores have a decreasing effect on the release rate of the adsorbate due to partial entrapment of the drug solution into the inner pores [110]. Gumaste et al. also explained the better tableting properties of a Neusilin® US2 adsorbate by the presence of bigger pores or channels and the adsorption of lipids on such structures [144]. Although Fujicalin® exhibits the biggest pores (cp. table 3) it adsorbs most of MCT at the surface according to the present data. Similarly, it can be assumed that Neusilin® US2 do not adsorb MCT to its deeper located pores but rather adsorbs MCT at the surface and partly to inner pores or channels which are located close to the particle surface. The similar data of Neusilin® UFL2 suggest the same for this adsorbent. The single particles are very small. Consequently, an entrapment of MCT inside of inner pores or channels has to be doubted. Probably, the small adsorbate particles form agglomerates with enclosed air and enclosed MCT. All in all, the assumption of an adsorption of an oily solution to the inner pores of the particles has to be questioned.

3.1.3. Microviscosity of the adsorbed oil component

The microviscosity of the oil component serves as measure for the adsorption strength. This parameter was investigated by benchtop nuclear magnetic resonance relaxometry/ imaging and electron spin resonance spectroscopy.
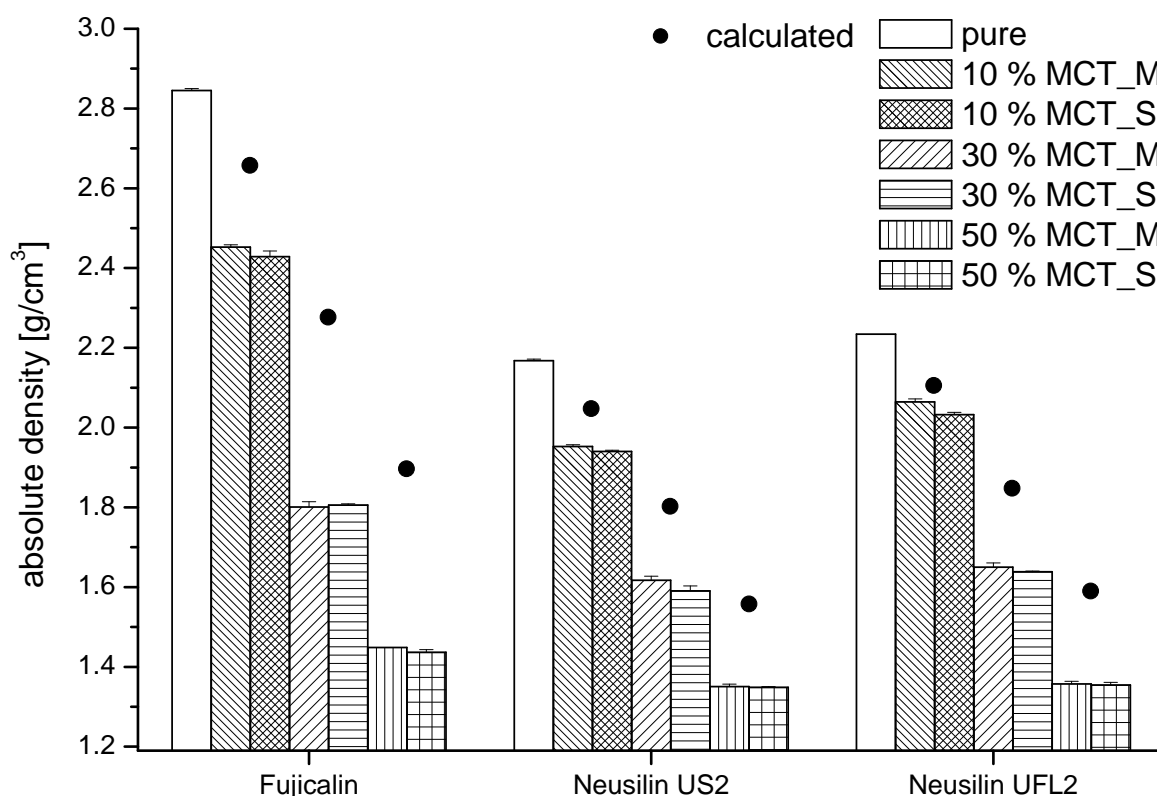
Figure 9: *Absolute density by helium pycnometry of pure excipients and their MCT adsorbates in different percentages produced by mortar/pestle (abbreviation "M") and SpeedMixer™(abbreviation "S"). Two measuring series are presented: The lower value as column, the second value as positive range. Theoretically calculated values are assigned to the* 10 percent, 30 percent *and* 50 percent *adsorbates as circles.*

3.1.3.1. Benchtop nuclear magnetic resonance relaxometry and imaging

The microviscosity can be indirectly estimated by the mobility of the protons of the adsorbed proton bearing liquid. Hence, the MCT mobility in different adsorbates was used as indicator for the excipient's adsorption strength. A weak oil adsorption manifests itself in a high proton mobility, a strong adsorption in a low proton mobility. The proton mobility is detected by the T_2 relaxation time. More precisely, a short relaxation time indicates a lower mobility and therefore a stronger adsorption on the solid excipient. Vice versa, a longer relaxation time indicates a weaker adsorption [127]. The T_2 values of the different excipients were recorded as a function of the oil load and of the relative air humidity which is presented in the following chapters. Besides, the T_2 values of both production methods were compared. An important issue in this work is the release of the MCT component from an adsorbate. This point was investigated by T_2 relaxometry and by MRI. Sample preparation and set up of the experiment is explained in chapter 2.2.8 on page 22.

Table 10: *T_2 relaxation time maxima of adsorbates with different MCT content produced by mortar/pestle method.*

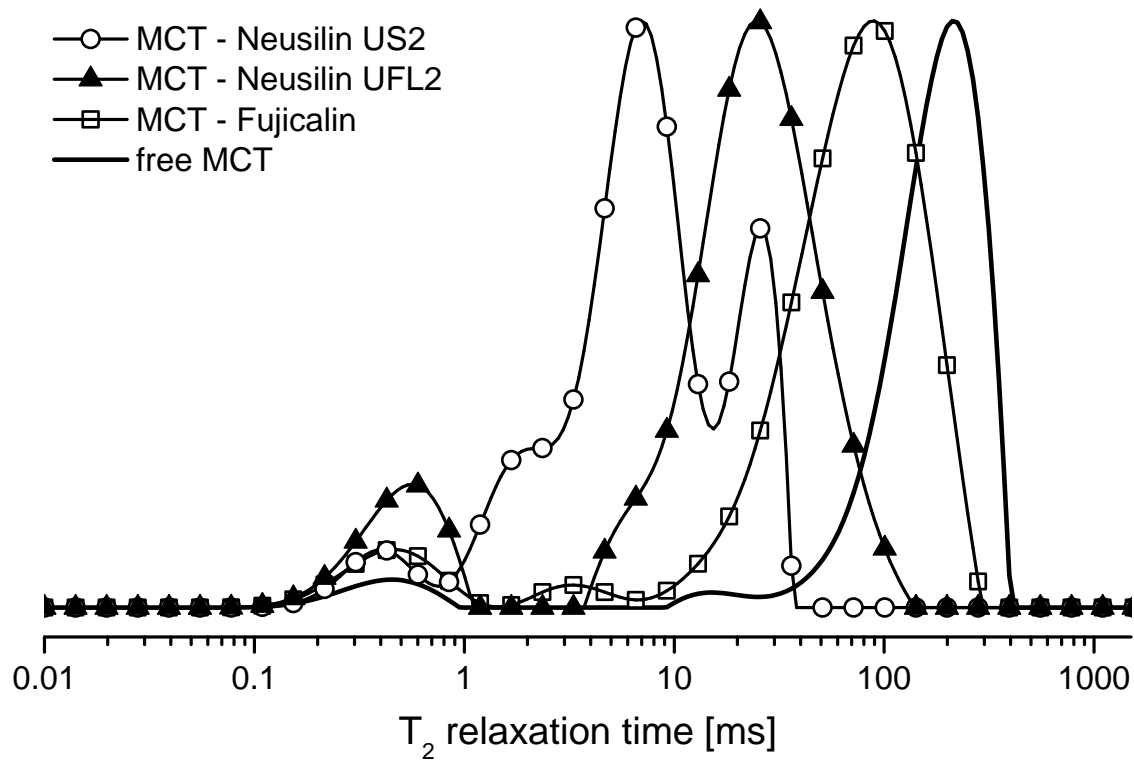| MCT content [% (w/w)]	Fujicalin® [ms]	Neusilin® US2 [ms]	Neusilin® UFL2 [ms]
30	41	2/7/27*	3/9/38*
50	90	7/26*	26
70	-	10/32*	51
100		199–223	

    * Several maxima detected

Figure 10: *T_2 relaxation time distributions of MCT loaded on Fujicalin® and Neusilin® with a content of 50 %. The maximum intensity of each distribution was normalized to 1.*

Influence of the excipient on the T_2 relaxation of adsorbed MCT

For bulk MCT in a non-adsorbed (free) state at 25 °C, a relaxation maximum of 210 ms was observed (table 10 on page 37), which is a typical value for oils [127]. The relaxation values in table 10 and the corresponding distribution curves in figure 10 show the strongest adsorption of MCT for the Neusilin® US2 adsorbent. The T_2 distribution curve is shifted to the lowest relaxation time. Two maxima are visible at 7 and 26 ms. Neusilin® UFL2 follows with a weaker adsorption with a T_2 maximum at 26 ms. The weaker adsorption

can be explained by a tendency for agglomeration. This makes a homogeneous oil incorporation more difficult and is the reason for the presence of more mobile MCT fractions. Fujicalin® with the highest relaxation maximum at 85 ms shows the weakest binding of MCT among these excipients. There are two effects which contribute to the different adsorption properties of the Neusilin® and Fujicalin® products. One point is the surface area. Fujicalin® has a much lower specific surface area compared to both Neusilin® products (see table 3). Hence, the place for adsorption on this excipient is faster saturated. An adsorption of MCT in a second (more mobile) layer is here more probable than for Neusilin® and contributes to the total T_2 relaxation distribution curve. Figure 4 (ESEM) on page 29 showed a more porous structure for Neusilin® US2 than for Fujicalin®. This could be one explanation for the strong reduction of the MCT relaxation time. The porous structure enlarges the surface area. Recent findings of Rao et al. demonstrated that the specific surface area of silica adsorbents had an important impact on the extent of the adsorption of a self-emulsifying system. They suggested an important role of the geometry of the silica network [91]. But the surface area has a stronger influence on the total amount which can be adsorbed than on the adsorption strength. The stronger adsorption at Neusilin® might be caused rather by a more powerful (physico)chemical interaction with MCT. Silicates such as Neusilin® are known to interact via hydrogen bonding [18, 148, 149]. The silanol groups on the surface can serve as proton donor and acceptor. Adhikari et al. [150] and Proctor et al. [151] demonstrated by use of Fourier transform infrared spectroscopy that triglycerides were able to interact via hydrogen bonding with the silanol groups of silicic acid. The spectra provide evidence that mainly the oxygen atom of the ester carbonyl group acts as proton acceptor. Investigations of Larsen et al. [152] and Williams et al. [153] also support the theory of MCT interacting via hydrogen bonding with the surface of Neusilin®. Certainly, the co-existence of other interactions like the weaker van der Waals forces (e.g. London forces) is probable as well. The calcium phosphate Fujicalin® does not present groups able or accessible for hydrogen bonding on the surface. Only the weaker van der Waals forces are possible which results overall in a weaker adsorption of MCT.

Influence of the MCT content

Different amounts of MCT were mixed with the excipients to investigate the influence on the T_2 relaxation of the adsorbed oil. Figure 11 on page 39 shows the macroscopic change of the resulting adsorbates. For a better visualisation MCT was coloured with Sudan red. Row "2" shows adsorbates with 50 % adsorbed MCT. The excipients difference in their oil adsorbing capacity becomes especially apparent comparing these pictures. The Fujicalin® adsorbate (A2) appears much oilier than the Neusilin® examples (B2 and C2). Even a 70 % oil load still has the appearance of a dry powder (B3 and C3). For Fujicalin®, oil loads higher than 50 % were not investigated.
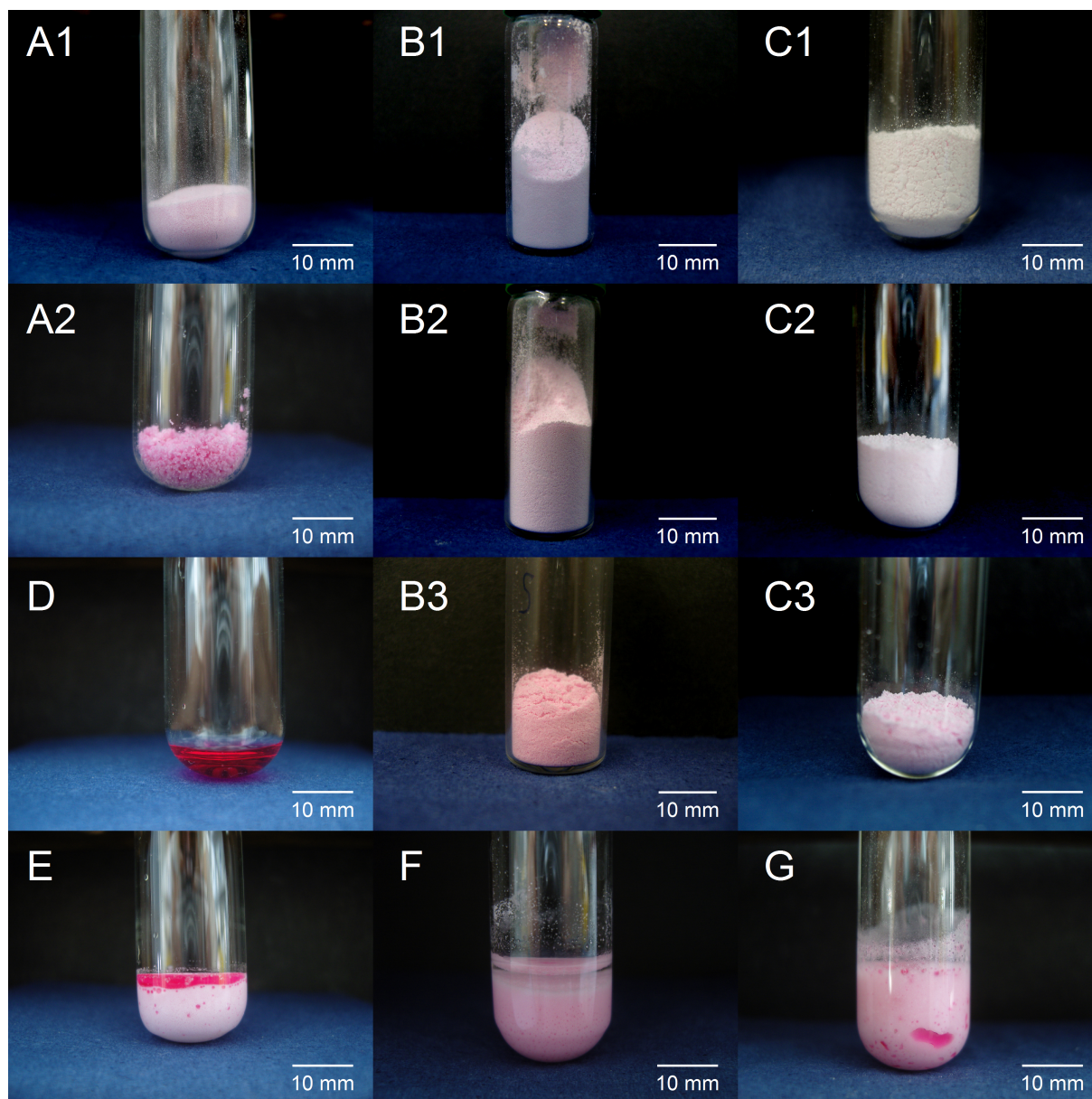
Figure 11: *Pictures of the resulting adsorbates with different MCT contents prepared by mortar/pestle method. MCT was coloured with Sudan Red: "A" Fujicalin®, "B" Neusilin® US2, "C" Neusilin® UFL2 with "1" 30 %, "2" 50 %, "3" 70 % MCT. "D" MCT with Sudan Red. "E-G" Samples of 50 % adsorbates after addition of D_2O as prepared for NMR relaxometry measurements, from left to right: Fujicalin®, Neusilin® US2, Neusilin® UFL2*

Table 11: *T_2 values of MCT adsorbates stored at different relative humidites. Top (adsorption): prior to addition of D_2O. Bottom (desorption):* 60 min *after addition of D_2O.*

	Relative air humidity [%RH]	Fujicalin® with 30 % MCT [ms]	Neusilin® US2 with 50 % MCT [ms]	Neusilin® UFL2 with 50 % MCT [ms]
adsorption	32	23	6/23[*]	6/20[*]
	40	41	7/26[*]	26
	75	54	54	48
desorption	32	223	211	211
	40	211	(51)[**]/199	(60)[**]/211
	75	223	199	211

[*] Several maxima detected
[**] Maximum of a peak shoulder

It is expected that a higher MCT loading leads to more mobile fractions on the excipient and will shift the T_2 distribution curve to higher values. Indeed, increasing amounts of adsorbed MCT lead to a shift of the T_2 distribution curve to higher T_2 values (table 10 on page 37 and figure 12 with the example Fujicalin® and Neusilin® US2 on page 41). This shift indicates various adsorption states which partly converge to a broad distribution curve. An increasing saturation of the particle surface with MCT results in increasing parts of MCT components possessing a higher mobility. Consequently, the T_2 relaxation maximum of the main adsorption state will shift to higher values.

Influence of the relative air humidity

Storage stability and impact of storage conditions play an important role in pharmaceutical production processes. Therefore, the T_2 distribution of the MCT adsorbates under the usual storage condition of 40 %RH was compared to 32 %RH and 75 %RH. Adsorbates with similar powder appearance were exposed to different humidity conditions. Therefore, Fujicalin® as adsorbate with a MCT content of 30 % and Neusilin® US2 and UFL2 as adsorbate with a MCT content of 50 % were chosen for this study.

The excipients reacted differently (adsorption part, table 11 on page 40 and figure 13 on page 42). For Fujicalin®, the storage at lower humidity leads to a visible shift to a lower T_2 relaxation maximum. The storage at 75 %RH caused a slight increase in T_2. Both Neusilin® types are more influenced by humid storage conditions. The T_2 relaxation time of the adsorbed MCT on the Neusilin® US2 material increased from two separate peaks of 7 and 26 ms to one broad peak of 54 ms. The type UFL2 exhibits a similar behaviour.

The stronger dependency on humid conditions can be explained by a higher water
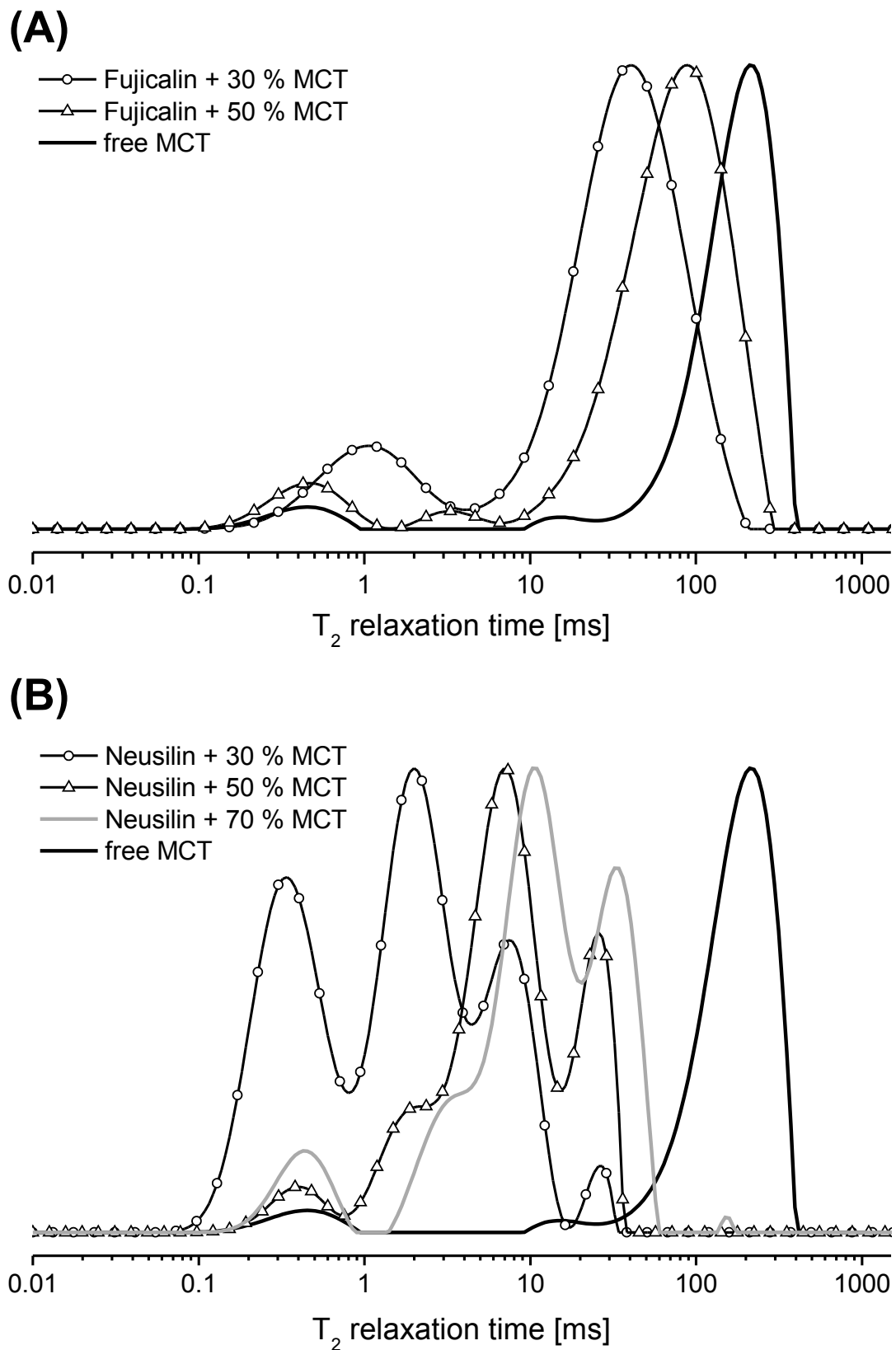
(A)

(B)

Figure 12: T_2 *relaxation time distributions of different MCT quantities adsorbed at (A) Fujicalin® and (B) Neusilin® US2. Due to the higher oil adsorbing capacity, Neusilin® US2 is additionally shown with a MCT content of 70%. The maximum intensity of each distribution was normalized to 1.*
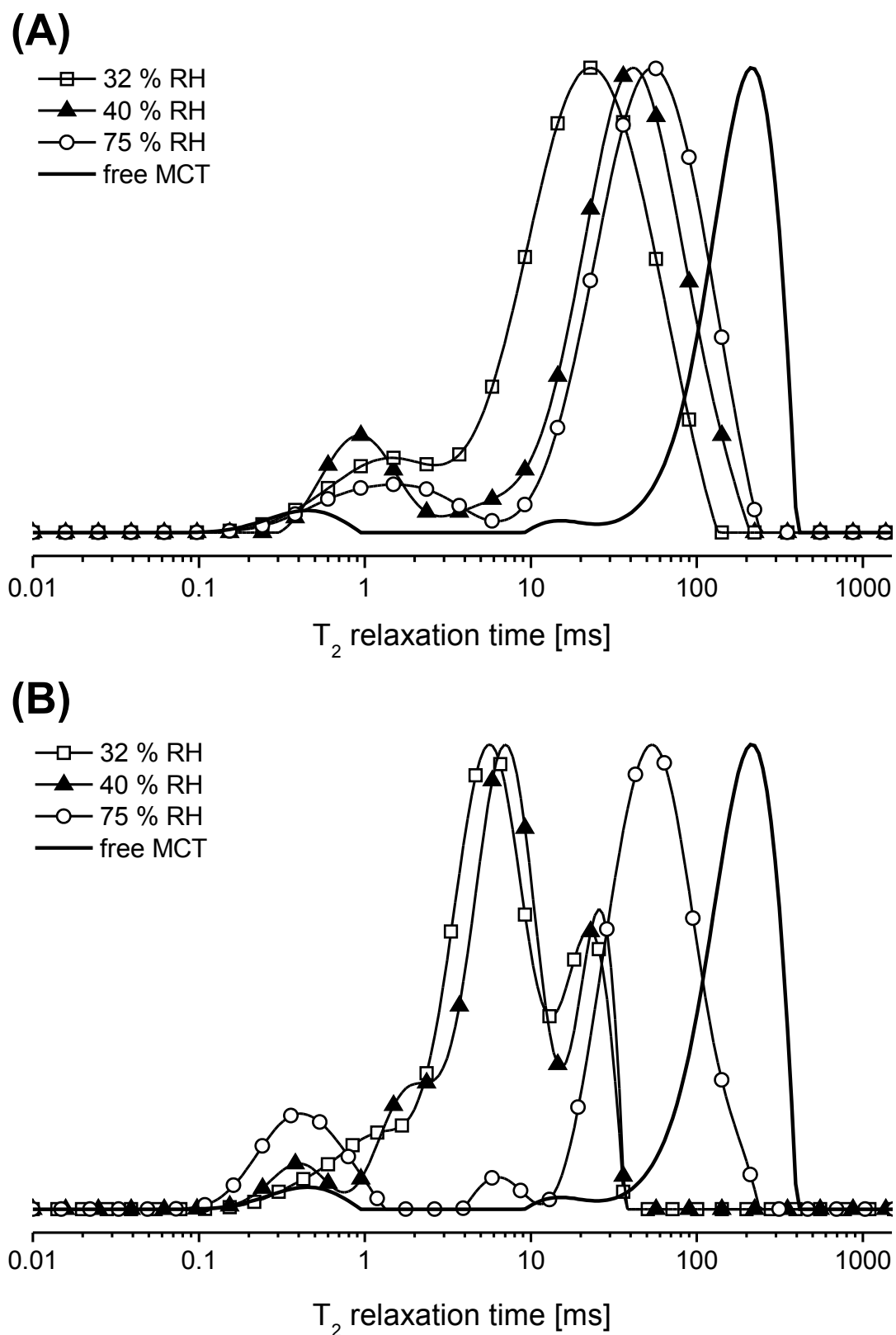
(A)

(B)

Figure 13: *Influence of storage conditions on the T_2 relaxation times of MCT adsorbates of (A) Fujicalin® and (B) Neusilin® US2. The maximum intensity of each distribution was normalized to 1.*

Table 12: *Loss of water of the pure excipients according to thermogravimetric analysis after storage at different relative air humidities.*

Relative air humidity [%RH]	Fujicalin® [%]	Neusilin® US2 [%]	Neusilin® UFL2 [%]
32	1.0	12.3	12.2
40	1.1	12.4	12.4
75	1.5	20.5	20.0

uptake of the Neusilin® excipients and thus a partial saturation of the surface (see thermogravimetric analysis, table 12 on page 43). The graphical presentation of the thermogravimetric analyses can be found in figure 45 on page ii (appendix). The strong water adsorption is caused by the property of Neusilin® to interact via hydrogen bonding. Water molecules are the perfect and stronger partner for this kind of intermolecular interaction. Thus, MCT does not displace the water molecules on the surface or the water molecules displace the triglyceride molecules from the adsorption places. Both possibilities lead to a weakening of the oil adsorption. Similar observations were done by Proctor et al [151]. Different silica materials were investigated for formation of hydrogen bonds. Silica materials with higher water content showed weaker effects of hydrogen bonding. It was assumed that water molecules hinder the triglyceride to bring the ester group in the position for a hydrogen bonding. The same will happen to Neusilin® as long as stored under high relative humidity. Fujicalin® which does not interact via hydrogen bonding is less impacted at high humidity conditions but shows different T_2 relaxation maxima between 32 %RH and 40 %RH.

Influence of the blending method

The impact of blending procedure (mortar/pestle and SpeedMixer™) on the T_2 distribution was investigated. Fujiaclin® adsorbates were compared with a MCT content of 30 % and 50 %, Neusilin® UFL2 and US2 as adsorbates with a MCT content of 50 %. Regarding the T_2-values of table 13 (column adsorption), the SpeedMixer™ had the greatest impact on the Fujicalin® adsorbate. The 30 % adsorbate shows a T_2 shift from 41 ms (mortar/pestle) to 13 ms (SpeedMixer™). For the 50 % adsorbate a shift from 90 to 34 ms is demonstrated. This means that MCT is considerably less mobile and gets stronger adsorbed on Fujicalin® by the SpeedMixer™ method for both MCT contents. A slight decay is also visible for the Neusilin® UFL2. In contrast, for Neusilin® US2, no alteration can be observed (figure 14 on page 44).

The SpeedMixer™ applies more power and thus provides a generally more homogeneous oil distribution on the particle surface compared to the mortar/pestle method. Because of the much smaller surface area of Fujicalin® (see table 3 on page 10), the mortar method
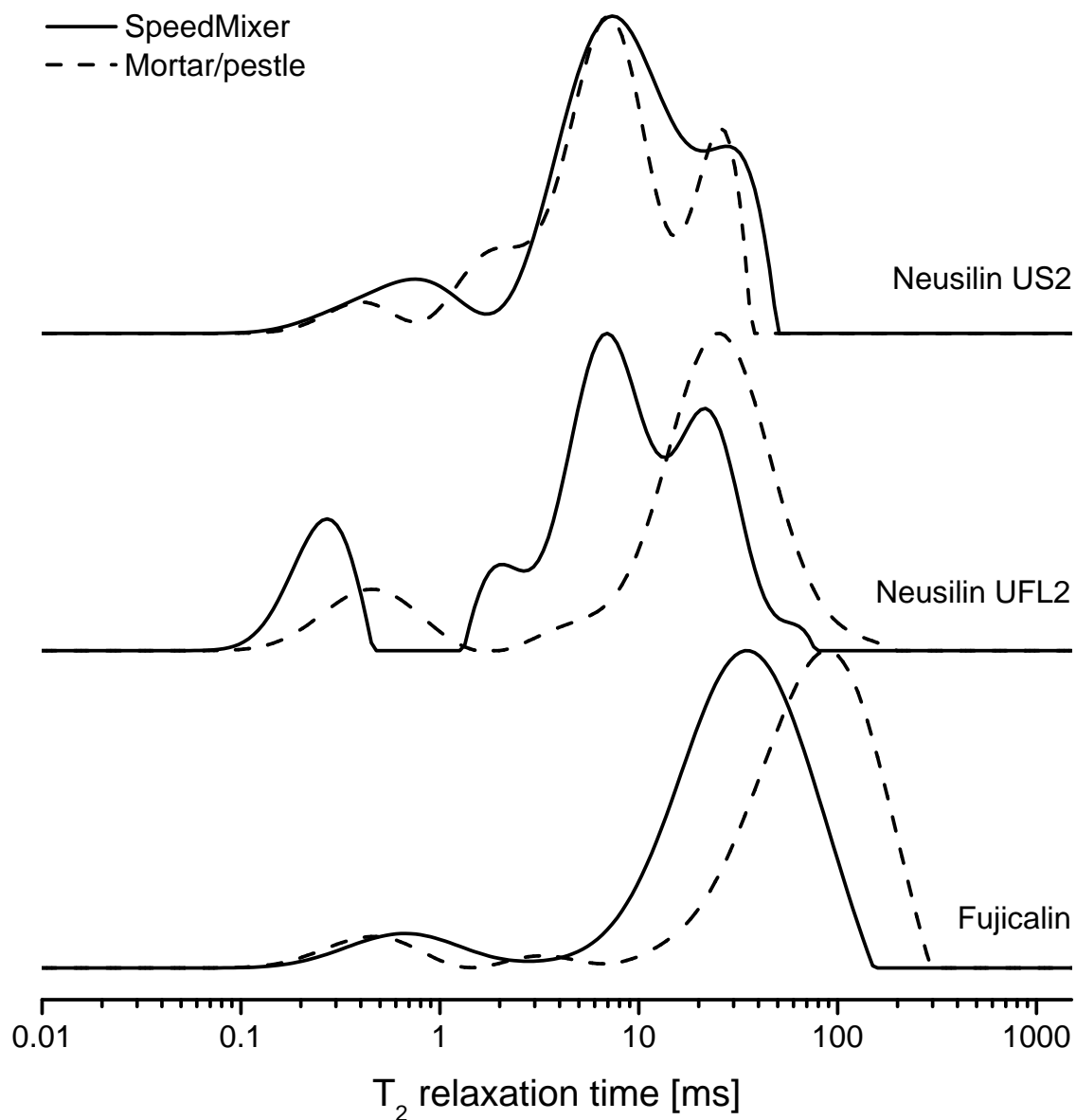
Figure 14: *Influence of the blending method on the T_2 distribution of MCT adsorbates with a MCT content of 50 %. The maximum intensity of each distribution was normalized to 1.*

Table 13: *Influence of the blending method on the T_2 relaxation of MCT after adsorption and desorption (addition of D_2O).*

Adsorbate	SpeedMixer™		Mortar/pestle	
	adsorption	desorption	adsorption	desorption
Fujicalin® with 30 % MCT	13	211	41	211
Fujicalin® with 50 % MCT	34	223	90	211
Neusilin® US2 with 50 % MCT	7/27	199	7/26	199
Neusilin® UFL2 with 50 % MCT	7/22	199	26	211

leads more often to bulk MCT domains with higher T_2 values contributing to the right shift of the distribution curve. The specific surface area of Neusilin® is 7.5 times larger and the chemical bonding of MCT is stronger. Consequently, the distribution homogeneity does not have such a big influence of the T_2 values for the Neusilin® types. Only for Neusilin® UFL2 two separated states were detected by use of the SpeedMixer™. A possible explanation is that adsorbed MCT is distributed in smaller droplets but that already developed agglomerates are less destroyed compared to the treatment with mortar/pestle. Consequently, two states could appear, one for the fine and homogeneously distributed part and one for MCT accumulations in agglomerates.

Behaviour in aqueous media measured by relaxometry

In order to release a dissolved lipophilic drug, the adsorbed oil should separate from the solid excipient when coming into contact with aqueous media. A strong and permanent binding of the oil to the surface of the adsorbent could be disadvantageous for the bioavailability of the dissolved drug. The released MCT component will be detectable as "free MCT" with the already discussed T_2 distribution values. Therefore, the T_2 distributions of the MCT adsorbates were recorded after addition of an aqueous medium. In general, water will also adsorb to the excipient's surface with a probably similar T_2 and would disturb the outcome of the experiment. To avoid water signals in the distribution diagram, deuterium oxide (D_2O) which does not contribute to the NMR signal was chosen as aqueous medium. Only the evaluation after 1 h is shown because most of the alteration in the T_2 distribution occurred within the first 5–15 min (duration of one measurement: approximately 5 min) and there was no further alteration observed within the measurement period of 8 hours. Figure 15 (A) on page 46 visualises the resulting T_2 values. For Fujicalin®, the distribution curve corresponds to the curve of free MCT.
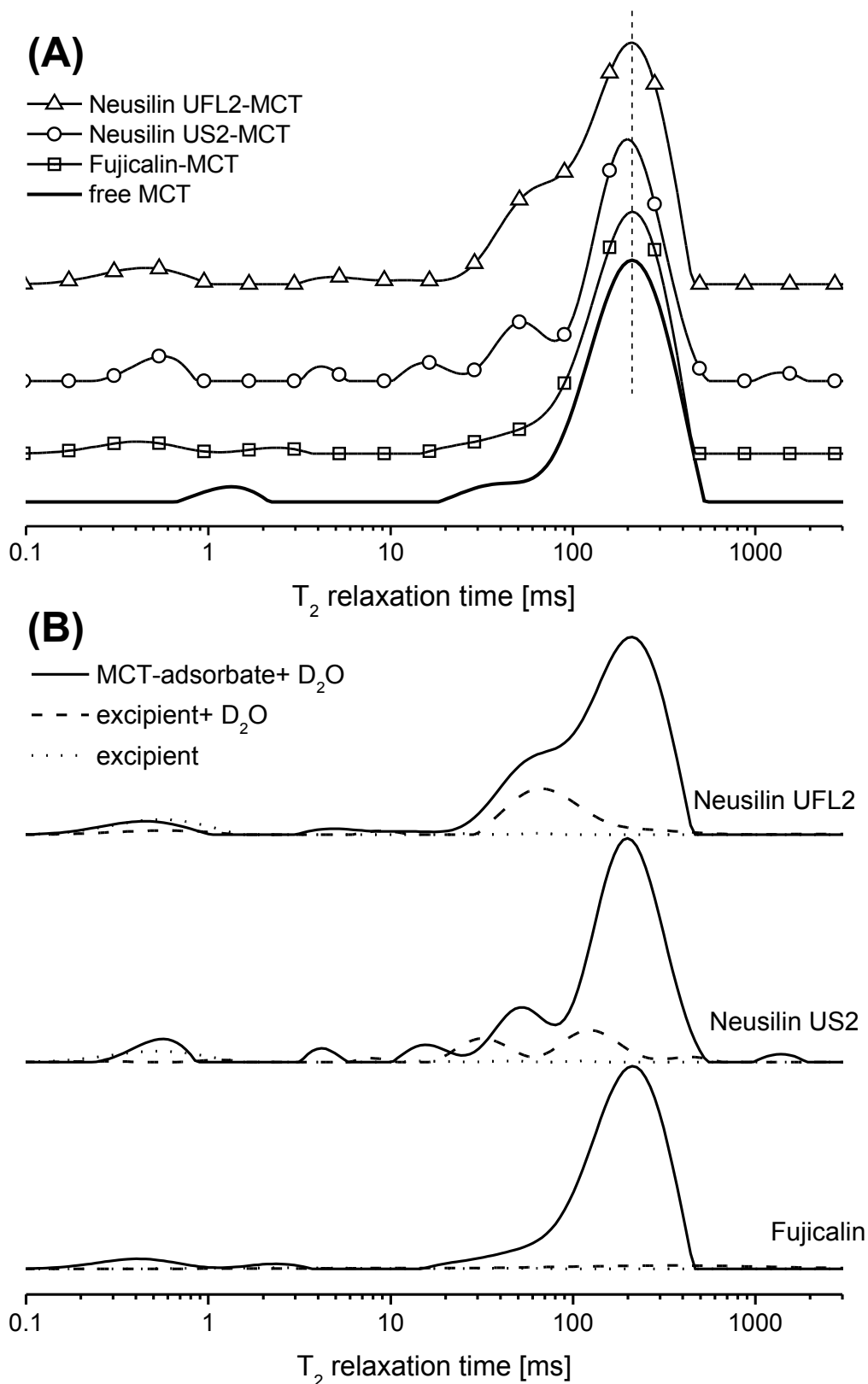
Figure 15: *T_2 distributions of adsorbates 60 min after addition of D_2O: (A) MCT adsorbates in comparison to a MCT-D_2O mixture labelled as free MCT. The maximum intensity was normalized to 1.(B) MCT adsorbates with D_2O (solid line) in comparison to the excipient data with D_2O (dashed line) and the data of the pure excipient (dotted line).*

But for both Neusilin® types an additional broad peak at 50–60 ms appeared which was stronger adsorbed compared to the main peak at circa 210 ms. To verify whether this signal belongs to MCT, the adequate amount of the excipient raw material was measured over time with the same volume of D_2O and under the same conditions (figure 15 (B)). After 60 min, a relevant signal was not detectable for the excipient Fujicalin®. Whereas for the Neusilin® excipients signals were detected approximately at this place where the additional adsorption state was discovered for the MCT adsorbates. Hence, these additional states should belong to adsorbed water. It has already been discussed that water molecules tend to bind to the Neusilin® surface by hydrogen bonding. Thus, exchanges between excipient protons and water protons are possible. The thereby formed HDO, caused by a proton-deuterium exchange, contributes to the NMR signal.

Finally, the results show that in aqueous media the MCT component mostly desorbed from the excipient's surface. But it cannot be excluded that the signal dedicated to adsorbed water does not cover signals of still adsorbed MCT (T_2 at about 30 ms). Furthermore, the investigated storage conditions and blending methods does not influence the MCT desorption. After addition of D_2O the main T_2 relaxation maximum ranges between 199 and 223 ms (table 11 and 13).

To get a visual impression of the MCT release process from the adsorbates, photographs were taken after conducting the measurement. Figure 11 on page 39 shows NMR relaxometry samples after addition of D_2O (E-G). The oil component was coloured with Sudan Red. The photograph "E" reveals a clear red-coloured oil phase on the top of Fujicalin® which seems itself mostly discoloured again. This suggests a good desorption from this excipient. Neusilin® UFL2 (G) exhibits smaller visible oil accumulations and the excipient still shows a slight rose colour. Neusilin® US2 (F) remains clearly coloured. Predominantly, only small droplets of oil seem to be desorbed from the excipient. The sample photographs confirm the good desorption from Fujicalin® and possibly indicate that at least a small part of the oil component or Sudan Red remains adsorbed to the Neusilin® surface. Another explanation can be that the MCT droplets are "free" with respect to their T_2 value but are still stuck between the Neusilin® particles, especially at the type US2. A deeper insight into the wet adsorbate compound and potentially at enclosed oil separations should be possible by MRI which is an imaging method also based on relaxation time distributions and which is not hindered by opaque systems.

Behaviour in aqueous media measured by benchtop MRI

Adsorbate samples were prepared as described in chapter 2.2.8 and imaged prior and after addition of the aqueous medium. The contrast in the MRI images was obtained by the used experimental conditions (parameter set up: see table 7 on page 24). T_1 relaxation time weighted images were generated by the choice of the parameters repetition time

(t_R) and gradient echo time ($_E$). Thereby, free water with long relaxation times could be visually separated from oil with short relaxation times. The change from adsorbed MCT to free MCT could be followed by a visual difference between a homogeneously distributed adsorbed status to locally separated phases of free MCT. Water molecules in an adsorbed state could disturb the visualisation of MCT because they could exhibit similar relaxation times as adsorbed MCT. Hence, image series with D_2O were taken as well. The intensity between the single MRI images cannot be compared but the local distribution of different intensity levels can be followed which was the motivation of the study.

Figure 16 on page 50 shows image series of the pilot study with all MCT adsorbates and distilled water as medium. The highest intensity is painted in white and the colour shifts over grey scales to black for lower intensity values. The column on the left shows the pure excipient where no signal was apparent. The next column shows the reference images from the dry MCT adsorbates and the following columns show the adsorbates after addition of water. Regarding the Fujicalin® series a fast coalescence and separation of MCT on the top of the water surface is visible after 15 min. Some small white spots of free MCT are located within the wet adsorbate sample appearing in a light grey colour. Free water is located at the top in dark grey colour referring to a lower intensity caused by less available protons for an excitation. The oil separation from this adsorbate started immediately after contact with water shown in the starting point image. A coalescence of oil droplets developed on the bottom part of the test tube (white). The corresponding photograph of the wet sample labeled with "F" confirms the oil separation. Before addition of the medium (dry adsorbate), MCT was well distributed on the powder particles and therefore not locally accumulated. Consequently, the colour of the dry adsorbate is less bright and the image signal in general more noisy. MCT on Neusilin® US2 (row 2) appears as homogeneously distributed in the dry adsorbate image as well. But after addition of water, no separation or coalescence of oil droplets took place. According to the T_2 relaxometry measurements in the chapter before most of MCT was found in an desorbed state after 60 min in water. Possibly, small oil droplets remain between the excipient particles visible as a homogeneous white to light grey colour. Only a very thin brighter layer can be identified on top of the water phase. This layer probably contains very small oil droplets still in contact with excipient material which is confirmed by the photograph of the sample. The photograph shows for the US2 type a layer of excipient particles on top in the side view and the existence of very small oil droplets in the top view. But no clear coalescence and local accumulation of MCT droplets occurred. For the Neusilin® UFL2 adsorbate, two brighter spots were noticed within the image of the dry adsorbate. This signal can be explained by the existence of agglomerates and a less homogeneous oil distribution. The tendency for agglomeration was already noticed in the corresponding T_2 distributions in Figure 14. The starting point image of the UFL2 series presents an immediate oil separation and

an accumulation on the bottom of the test tube. The desorption seems to be finished after 15 minutes with a white area located in the inner compound and some droplets on top of the water surface. The oil droplets on top are also present at the top view of the corresponding photograph.

These image series were reproduced and compared with D_2O as medium for a possible improvement of the contrast and phosphate buffer pH 6.8 and 0.1 M HCl respectively. The following observation was found: Most of the Neusilin® samples tended to float on all used media, especially on D_2O. It can be explained by an already lower density of the Neusilin® materials compared to Fujicalin® and a further reduction of the density by blending with MCT (cp. Figure 9 on page 36). Additionally, adsorbed MCT made a complete wetting of the material more difficult leading to entrapped air and floating. Figure 17 on page 51 presents one example of a Neusilin® US2 adsorbate with flotation of the whole material. The MRI images show the still dry interior of the whole compound. The white area indicates adsorbed MCT or adsorbed water due to partial wetting of the excipient. The dark grey to black inner area can be assigned to a cavity filled with air. This upper barrier of the cavity is visibly located above the water surface. To avoid incomplete wetting or floating, further prepared Neusilin® samples were treated with a short and careful agitation using a spatula in the test tube directly after addition of the medium.

The first MRI series with different media in comparison were generated with Fujicalin® adsorbates and are shown in Figure 18 on page 52. As seen in the pilot study, the adsorbate started releasing the adsorbed MCT immediately after addition of water. The light grey to white coloured compound in the starting point image comprises still adsorbed MCT, already desorbed free MCT and adsorbed water. The bottom of the sample in dark grey seems still not to be wetted. From the 15 min image on, a clear coalescence and separation of MCT is visible as white spots. Only a very small part of MCT seems to be located on top of the water surface. This appearance remains unchanged until the image after 60 min. But a very gentle shaking of the test tube was already sufficient to bring the major part of the MCT to the surface (figure 18, right MRI column). The rest of desorbed MCT is still located right in the middle and at the bottom of the test tube. The series with D_2O (row 2) exhibits an improved contrast. The MCT release turned out to be similar to the example with distilled water. A similar behaviour can be noticed for the series with phosphate buffer pH 6.8 and 0.1 M HCl. The acid medium showed a fast floating-up of MCT in this series.

Referring to the Neusilin® samples of figure 19 on page 53, the images of the pilot study were not reproducible as from now on all samples were gently agitated before starting the measurement. The dry adsorbate images confirm a roughly homogeneous MCT distribution for both excipients. Unfortunately, no oil separation can be followed
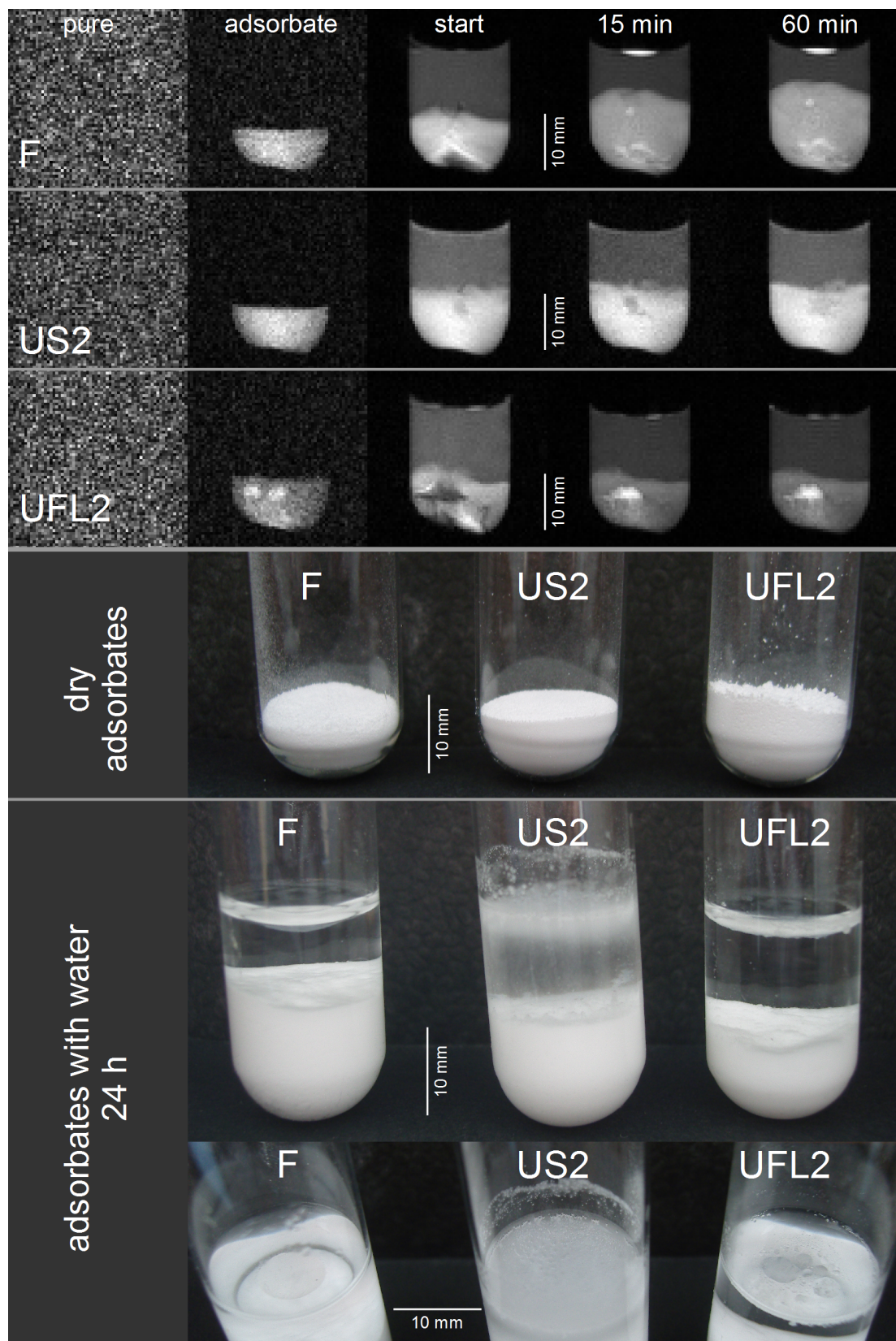
Figure 16: *BT-MRI pilot series (top) and sample photographs (bottom) of adsorbates before and after addition of distilled water. F - Fujicalin®, US2 - Neusilin® US2, UFL2 - Neusilin® UFL2. MRI part: Images were recorded directly after addition of water (start) and after 15 and 60 minutes. White is related to the highest intensity. From left to right: Pure excipient, dry MCT adsorbate, start, 15 min, 60 min. Photographs: (from top to bottom) dry samples, samples with water after 24 h side view and top view.*
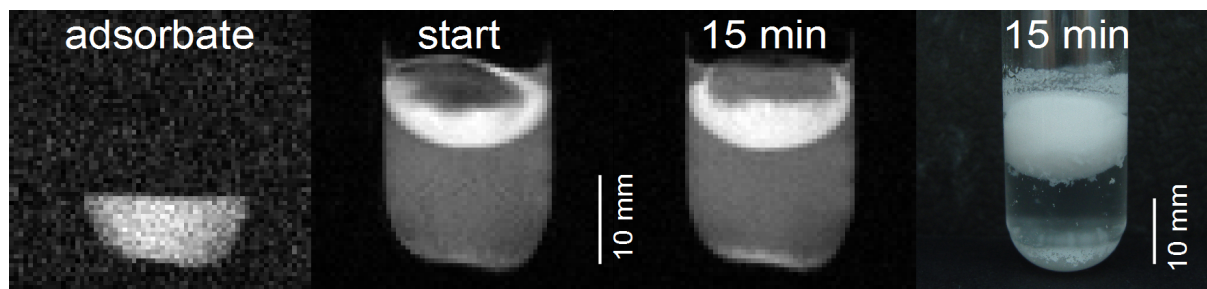
Figure 17: *BT-MRI images of a floating Neusilin® US2 adsorbate with distilled water. Images are shown directly after addition (start) and after* 15 min*. White is related to the highest intensity. From left to right: Dry MCT adsorbate, start,* 15 min*, photograph of the sample.*

for images after addition of aqueous media. Even for the series with D_2O, the exchange of protons as discussed for the relaxometry study (figure 15) leads to a visible signal of adsorbed water (grey coloured). At least, a partly MCT release for the Neusilin® UFL2 adsorbate can be supposed and is visible as small white spot at the bottom for the D_2O row and in poorer contrast for water and 0.1 M HCl, too. The investigation with phosphate buffer has been omitted since a similar behaviour to water was expected and due to the generally low informative value. The same was found for the Neusilin® US2 image series which are not informative enough to exclude or support a MCT desorption. The whole compound is presented in a light grey to white colour. In D_2O, the floating tendency is still apparent (row US2/D_2O). In order to see the influence of MCT on the density of the adsorbate, the pure material without MCT was imaged with D_2O. The corresponding pictures (MR image and photograph) are presented right of the D_2O adsorbate series. A floating was not detectable.

Linking the findings of the MRI study together with the outcome of the T_2 relaxometry desorption study, it is apparent that Fujicalin® releases the adsorbed MCT immediately when getting into contact with aqueous media. A final evaluation for the Neusilin® excipients is not possible due to floating problems. For Neusilin® UFL2, at least a partial desorption and separation of MCT can be assumed based on the MRI and the T_2 relaxometry study. The results of T_2 relaxation definitely support a partial MCT release for Neusilin® US2. The sample photographs of figures 11 (F) and 19 (US2) show small oil droplets on the surface of the test tube. But, the MRI images do not show a clear desorption of MCT. Furthermore, the adsorbate of figure 11 (F) is still coloured. One interpretation could be that most of the initially adsorbed MCT is probably desorbed based on its T_2 value but it remains fixed between excipient particles in form of small droplets. The small droplets which were visible in the sample photographs cannot be resolved in the MRI images. The issue of MCT desorption should be further investigated and is handled again in chapter 3.1.4.2.
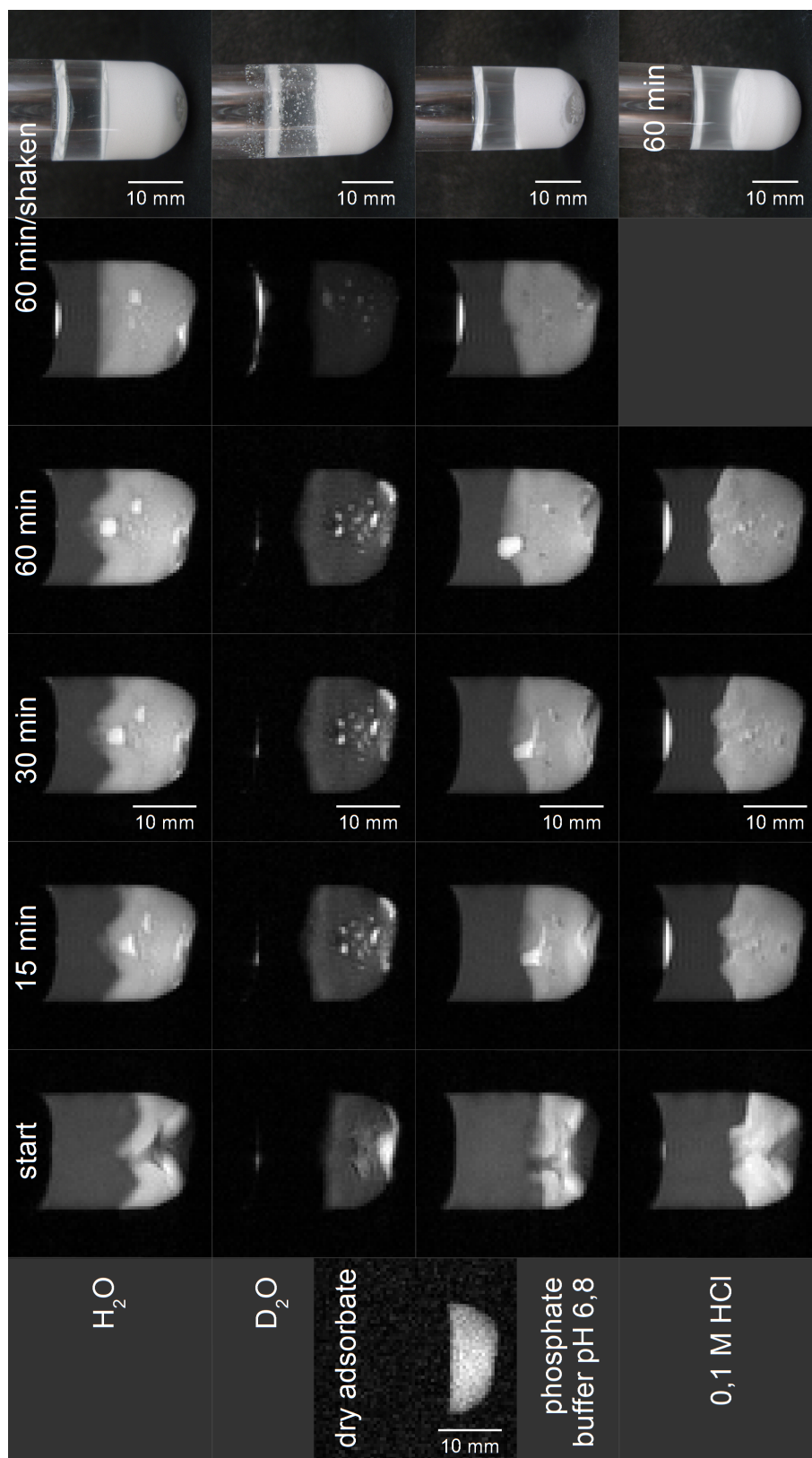
Figure 18: *BT-MRI images of Fujicalin® adsorbates before and after addition of different aqueous media. Images were recorded directly after addition of the medium (start) and after 15, 30 and 60 minutes. White is related to the highest intensity. From left to right: Dry MCT adsorbate, start, 15 min, 30 min, 60 min, 60 min - gently shaken, photograph of the sample. Sample was not shaken when MCT was visibly located on top of the medium. From top to bottom: distilled water, D₂O, phosphate buffer pH 6.8, 0.1 м HCl.*
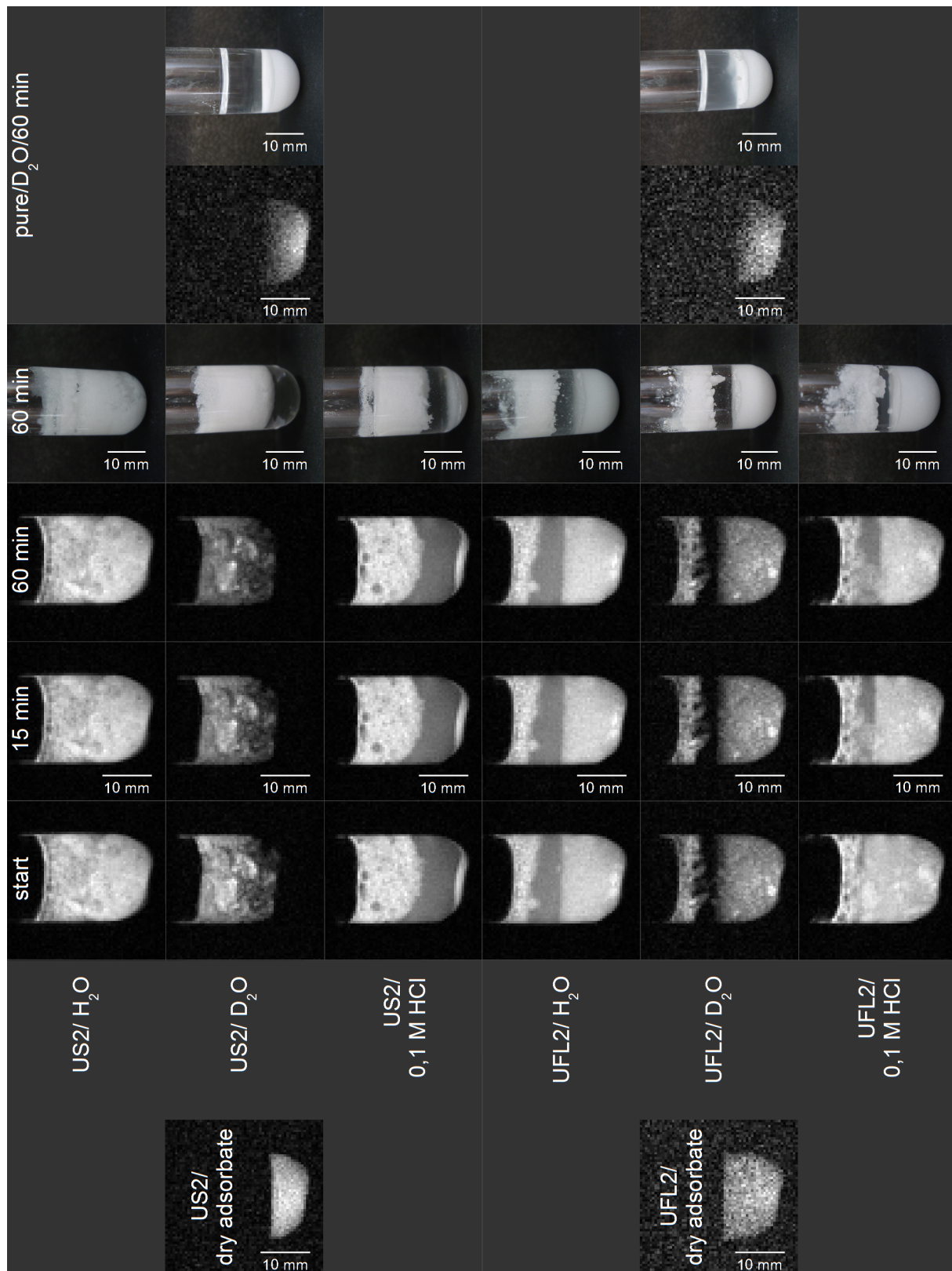
Figure 19: *BT-MRI images of Neusilin® adsorbates before and after addition of different aqueous media. Images are shown for the starting point directly after addition of the medium and for 15 and 60 minutes. White is related to the highest intensity. From left to right: Dry MCT adsorbate, start, 15 min, 60 min, photograph of the sample, MRI of the excipient with D_2O - 60 min, photograph of the excipient sample with D_2O - 60 min. From top to bottom: Type US2 and type UFL2 with the media distilled water, D_2O, 0.1 M HCl.*

3.1.3.2. Electron spin resonance spectroscopy

ESR spectroscopy was chosen as second method to characterise the microviscosity. This technique needs paramagnetic unpaired electrons which have to be included into the sample in form of a spin probe. Spin probes are stable free radicals. The spin probe Tempol was used in this study. Tempol is a stable nitroxide radical which yields an ESR spectrum of three lines (hyperfine splitting - HFS) in its mobile state [129]. Figure 20 on page 55 shows the chemical structure and typical spectra of Tempol in different media as well as adsorbed at solid excipients. Tempol reacts sensitively to its environment. Changes in microviscosity and micropolarity cause alterations in the three-line spectrum. A higher microviscosity results in a line broadening (ΔB_{pp}) and a decreasing signal amplitude (I) predominantly of the third line [128, 130, 131] (e.g. Tempol dissolved in MCT and adsorbed on Neusilin® US2). Tempol in free MCT shows a mobile spectrum characterised by the narrow peak-to-peak line width. A broader line width is visible at the spectrum of the Neusilin® US2 adsorbate. This indicates a lower tumbling rate of the Tempol molecule and therefore a higher microviscosity of the adsorbed oil component. The lower signal amplitude of this spectrum is another indicator for the reduced mobility. But this spectrum still differs from a real solid spectrum where Tempol is molecularly distributed at a solid carrier, here shown for pea starch. The hyperfine splitting constant (a_N) indicates changes of the micropolarity. This evaluation will be handled in detail in chapter 3.1.4.1.

The rotational correlation time (τ_c) is related to the rotation frequency of the spin probe and is used as measure for the microviscosity. It is calculated directly from the shape of the spectrum (ΔB_{pp} and I) by the simulation software. The higher τ_c is, the higher is the microviscosity of the spin probe's environment [154]. It was intended to confirm the differences in the adsorption strength of the excipients. Furthermore, the focus was on the investigation of the impact of the blending method.

MCT adsorbates of the three excipients were prepared using both blending methods (see chapter 2.2.9 on page 25). The spectra simulation by EPRSIM software was based on one species for Tempol in the reference solvents water and MCT. The adsorbate spectra were calculated with two species, one more mobile and one less mobile (accepting that the results are based on this model assumption and do not represent the real adsorption situation). Figure 21 on page 56 presents the rotational correlation time (τ_c) in graph (A) and the hyperfine splitting constant (abbreviated as HFS) in graph (B) for each species. This chapter concentrates on the τ_c results (shown in graph A) as a measure of the MCT mobility. The proportions of the single species which are shown in graph A only are applicable for A and B. The discussion of the results of graph B will be handled in chapter 3.1.4.1 on page 58. All original and simulated spectra which were used for the evaluation of microviscosity and micropolarity parameters are compiled in figure 46 (appendix, page iii).
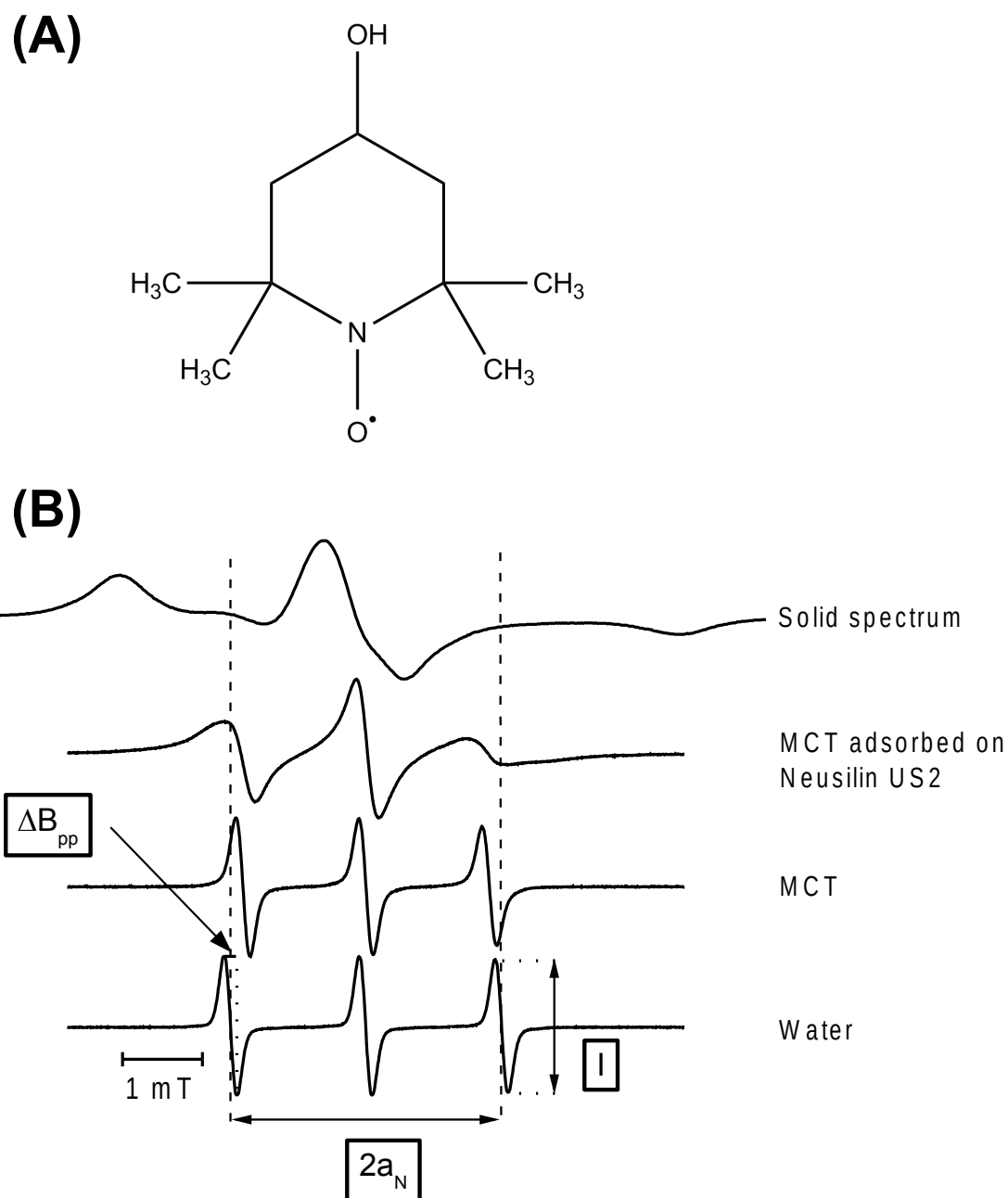
(A)

(B)

Figure 20: *Chemical structure of Tempol (A) and ESR spectra of Tempol in different media and adsorbed at solid excipients (B). Typical ESR parameters are marked for Tempol in water: ΔB_{pp} - line width; a_N - hyperfine splitting constant; I - signal amplitude.*
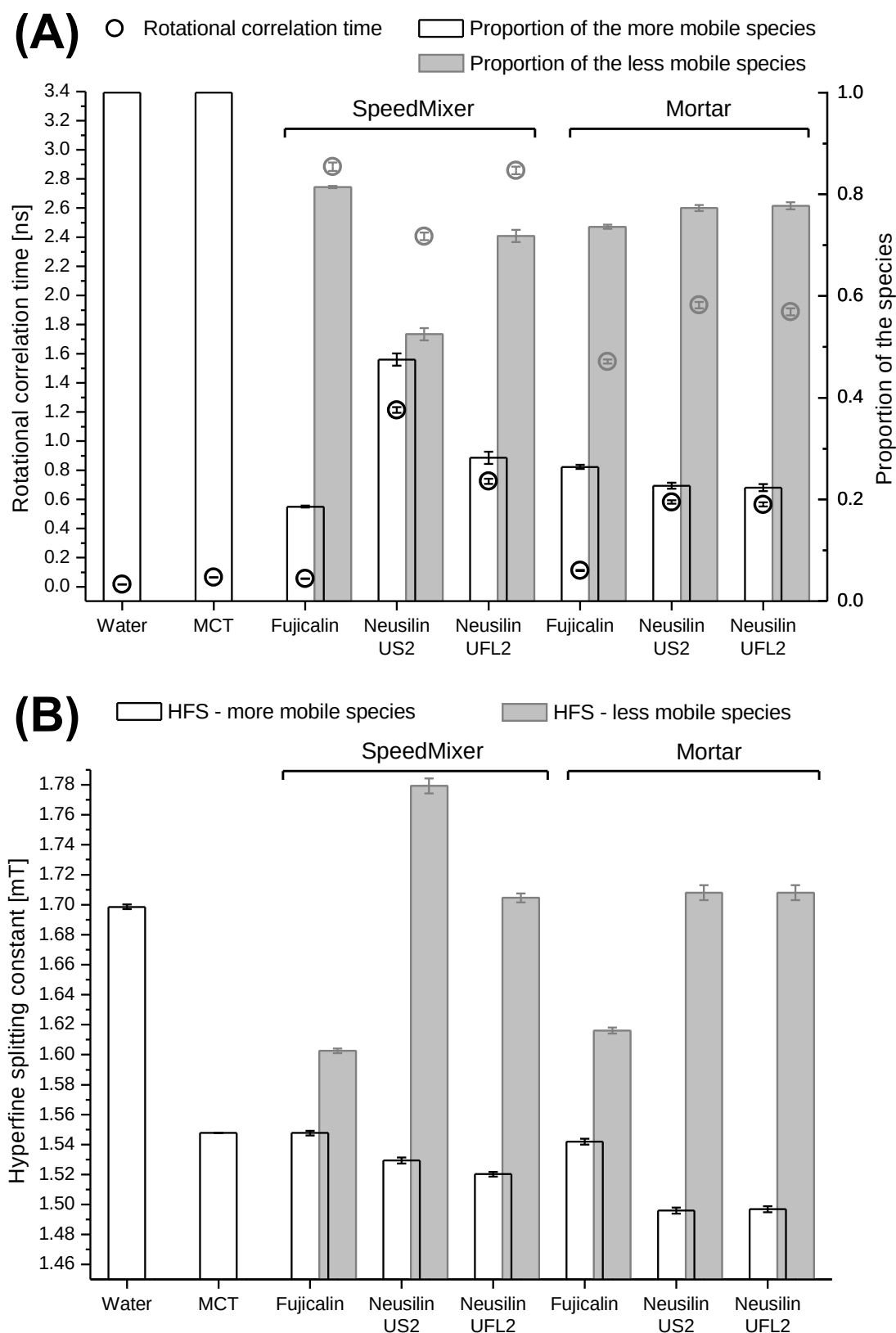
Figure 21: *ESR Simulation data of the spin probe Tempol in reference solvents and MCT-adsorbates: (A) Rotational correlation time (τ_c) shown as circles dedicated to the corresponding simulated species. Species are presented as bars proportionately. (B) Hyperfine splitting constant (a_N) shown as bars. The corresponding proportions of the species are the same as of graph A. For (A) and (B): Error bars derive from the simulation process and denote the accordance of the simulated species to the original data.*

Due to the chosen simulation conditions the adsorbates consist of two species. The more mobile species could be located to the outer part of the MCT layer and the less mobile species closer to the particle surface. Data for τ_c are presented in graph (A). Free MCT exhibits with 0.07 ns a higher τ_c value than water (0.02 ns) because the microviscosity of the oily environment is higher. But both rotational correlation times indicate a relative high tumbling rate and therefore a low microviscosity compared to the τ_c values of the adsorbates. A good distinction between the adsorbates is visible for the mortar samples on the righten site of graph (A) in figure 21. Among the more mobile species (lower τ_c as black circles), Fujicalin® shows a similar τ_c (0.11 ns) as free MCT. The microviscosity is almost unchanged for this part. Both Neusilin® excipients exhibit with about 0.6 ns a much higher τ_c which is related to a slower motion of Tempol and consequently a higher microviscosity. The second species (τ_c as grey circles) which represents the less mobile parts have considerably higher τ_c values. As described before, both Neusilin® excipients have a stronger impact on the MCT environment (about 1.9 ns) than Fujicalin®(about 1.5 ns). The percentages of both species are similar for all three excipients for the mortar samples. Approximately 20 % contributes for the more mobile species, and 80 % for the less mobile species. Basically, it can be concluded that the Neusilin® excipients have a greater influence on the adsorbed MCT than Fujicalin®. This can be explained by a stronger adsorption of MCT. These findings confirm the outcome of the NMR relaxometry experiments (chapter 3.1.3.1. The three data pairs in the middle of graph (A) represent the adsorbates produced by the SpeedMixer™ process. It is noticeable that the proportion of the species as well as the rotational correlation times are altered compared to those from the mortar process. The highest difference between both methods can be found for Fujicalin®. The τ_c of the more mobile species are nearly comparable (0.06 ns and 0.19 ns). But the second species which contribute with 80 % indicate a much lower tumbling rate of Tempol for the SpeedMixer™ method (about 2.9 ns) compared to the mortar/pestle method (about 1.5 ns). The microviscosity of the environment of Tempol is more increased for an adsorbate production by the SpeedMixer™. Regarding Neusilin® US2, the SpeedMixer™ contributes with a higher percentage of around 50 % of the more mobile species compared to mortar/pestle (around 20 %). The corresponding τ_c (1.2 ns) is twice that of the mortar value (0.6 ns). τ_c of the less mobile species counts 2.4 ns and is slightly increased compared to the mortar value (1.9 ns). Neusilin® UFL2 exhibits a higher τ_c value for the less mobile species (2.9 ns), but the proportions remain almost the same between both methods. When τ_c and the proportion value show alterations in parallel, a clear comparison based on the graphical data is not possible. To see the impact of the blending method more clearly, both rotational correlation times of one adsorbate were averaged based on their proportions (table 14). The calculated ratio served as a measure for the sensitivity of the microviscosity of adsorbed MCT to the blending process. The most

Table 14: Proportionately averaged rotational correlation time of MCT adsorbates.

Excipient	SpeedMixer™ [ns]	Mortar/pestle [ns]	Ratio
Fujicalin®	2.36	1.17	2.02
Neusilin® UFL2	2.26	1.59	1.42
Neusilin® US2	1.84	1.63	1.13

explicit difference of the averaged τ_c values between mortar and SpeedMixer™ is shown for the Fujicalin® adsorbate (highest ratio value). The SpeedMixer™ method causes a stronger adsorption of MCT at this excipient, whereas Neusilin® US2 shows the lowest deviation between both methods (lowest ratio value). This confirms the outcome of the T_2 distribution measurements (chapter 3.1.3.1). But it is visible that there are two more balanced states of Tempol for the Neusilin® US2 adsorbate both indicating a higher microviscosity for the SpeedMixer™ method compared to the mortar/pestle method (graph (A) of figure 21). This result is also supported by the CLSM images of the SpeedMixer™ samples which clearly showed a more even oil shell compared to the mortar samples. The more homogeneous MCT distribution is the reason for the two more balanced states of Tempol with a higher environmental microviscosity. The NMR relaxometry probably did not show smaller alterations caused by a more homogeneous oil distribution because the T_2 distribution curves of the Neusilin® US2 adsorbate were relatively broad.

The error bars of the values presented in Figure 21 were derived from the simulation process. Errors were larger for the adsorbates than for the reference spectra. The simulation with two domains is rather an approximation. It is most likely that multiple adsorption states exist as suggested as explanation for the broad distribution curves of the T_2 measurements [155].

3.1.4. Micropolarity of the adsorbed oil component

The micropolarity of the oil component was investigated by electron spin resonance spectroscopy (ESR) and multispectral fluorescence imaging.

3.1.4.1. Electron spin resonance spectroscopy

The hyperfine splitting constant (a_N) from the ESR spectrum can be used as a measure for the surrounding micropolarity of the spin probe [129, 131, 156]. A non-polar environment results in a smaller hyperfine splitting constant compared to a polar environment. Figure 20 (B) shows the spectra of Tempol in water and in MCT. The polar water environment causes the higher a_N value. The data of the simulated species are shown in

Figure 21 (B) on page 56. The a_N value of Tempol in water was 1.70 mT. For comparison, the solvent methanol reached 1.61 mT and ethanol 1.58 mT (data not shown). The data prove the sensitivity of Tempol for polarity changes in its environment. The hyperfine splitting constant for the solvent MCT (1.55 mT) is lower than that of ethanol. In the following, the graphic presents the values for the adsorbates subdivided into both preparation methods. All adsorbates were simulated as two Tempol species. The values of the more mobile MCT component (1.50–1.55 mT) are located close to the value of MCT. All less mobile MCT components are above the value of MCT. Concentrating only on these stronger adsorbed species, the Neusilin® excipients reveal a much higher a_N (1.7–1.8 mT) than the Fujicalin® adsorbate (1.6 mT). This emphasizes the stronger interaction between the Neusilin® excipients and MCT. Tempol indicates an increased environmental micropolarity. The interaction of Tempol in MCT with the Fujicalin® particle surface is less pronounced. A possible explanation could be that the adsorption water of Neusilin® (approximately 12 %, see thermogravimetry data) influences the Tempol molecule and result in hyperfine splitting values similar to that of water. Fujicalin® as anhydrous calcium phosphate does not contain adsorption water. In the literature log P values (octanol/water) of Tempol of 0.5–0.7 are mentioned [157, 158]. Hence, the affinity to MCT should be slightly higher than to water or is at least equal to water. It is theoretically possible that a partial accumulation of Tempol in adsorption water occurs. Furthermore, a_N values below the MCT value and above the water value were found. These values could possibly be caused by errors of the simulation process based on the two species. But the high value for Neusilin® US2 (SpeedMixer™) is far away from the next lower a_N values. In general, such an effect indicates a strong interaction of the spin probe with the particle surface. In the literature, studies of zeolites and aluminium oxides explain such effects on the hyperfine splitting with the existence of Lewis sites in these materials and a wall effect of zeolithes [159–163]. The cations interact as electron acceptor with the oxygen atom of the nitroxide of the spin probe molecule. This leads to a shift of the non-bonding electron pair towards the oxygen atom. As a consequence the spin density at the nitrogen atom and the charge at the oxygen atom is increased [159, 160]. Gutjahr and Pöppl found hyperfine coupling constants for di-tert-butyl nitroxide with up to 4 mT after adsorption at zeolithes. Furthermore, this interaction increases with higher electronegativity potential of the cation [160]. It is remarkable that only the Neusilin® US2 adsorbate prepared by SpeedMixer™ shows this strong interaction and not the Neusilin® US2 adsorbate produced with the mortar method. Moreover, the Neusilin® UFL2 adsorbate does not show such an interaction even though the Neusilin® US2 material is only the spray dried form of the Neusilin® UFL2 material and both are quite similar in their composition of Al_2O_3, MgO and SiO_2. Therefore, the difference can only be explained by a more homogeneous MCT-Tempol distribution on the Neusilin® US2 particles produced by the SpeedMixer™

method. The ESR microviscosity data in figure 21(A) show two more balanced states with a higher microviscosity which supports the assumption of a more homogeneous MCT distribution. Possibly, the strong interaction potential of the silicate surface has more impact on the adsorbed MCT in this case.

Fujicalin® possesses less interaction potential than the Neusilin® excipients. It cannot interact via strong hydrogen bondings as the Neusilin® excipients. Additionally, it has to be discussed whether the overall higher hyperfine splitting constants of the Neusilin® adsorbates are caused by an interaction between centres with high electronegativity and the oxygen atom of the nitroxide group belonging to the spin probe Tempol. Calcium ions possess a lower electronegativity than magnesium, aluminium and silicon ions [164–167]. This is probably the reason why Neusilin® leads to a higher environmental micropolarity of the adsorbed MCT. Apart from the single high value for Neusilin® US2 the hyperfine splitting is hardly influenced by the production method (e.g. 1.55 and 1.60 mT for Fujicalin®-MCT by SpeedMixer™/ 1.54 and 1.62 mT by mortar). This leads to the following assumption: The blending method influences the distribution and homogeneity of MCT in adsorbates and therefore to some degree their τ_c values and also T_2 distributions. But the actual adsorption strength through chemical interaction is not influenced by the production method. However, it is an interesting fact that Neusilin® influences the polarity of MCT. This had to be confirmed by a second analytical method to be sure not to draw conclusions which are eventually based on an individual interaction between the nitroxide group and the silicate surface.

3.1.4.2. Multispectral fluorescence imaging

Multispectral fluorescence imaging was chosen as a second method to study the environmental micropolarity. Nile red (NR) was selected as fluorescent dye because the wavelength of its maximal emission (WME) increases with the surrounding polarity [132–135, 168]. NR is a lipophilic fluorescence dye. A log P of 2.2–2.3 is reported in the literature [169, 170]. Its fluorescence is completely quenched in aqueous media [133, 134, 168, 169]. Hence, impacts from absorption water of the Neusilin® excipients were not expected. The dye was dissolved in MCT prior to preparation of the adsorbates. The change in the emission spectra is apparent on the images of the sample well plates (Figure 22 on page 61). Row A shows the prepared adsorbates. Both Neusilin® types appear in red which refers to a more polar environment. Fujicalin® shows an orange colour. Row B shows the same samples after addition of water. All plate holes appear in yellow, the colour of free MCT (row D, left). References were prepared with MCT (yellow), the more polar methanol (red) and the less polar n-hexane (green). The excipients impregnated with Nile Red show a clear polar character (red). Row E presents photographs of MCT adsorbates coloured with Sudan Red in a well plate. Fujicalin® (left photograph) releases
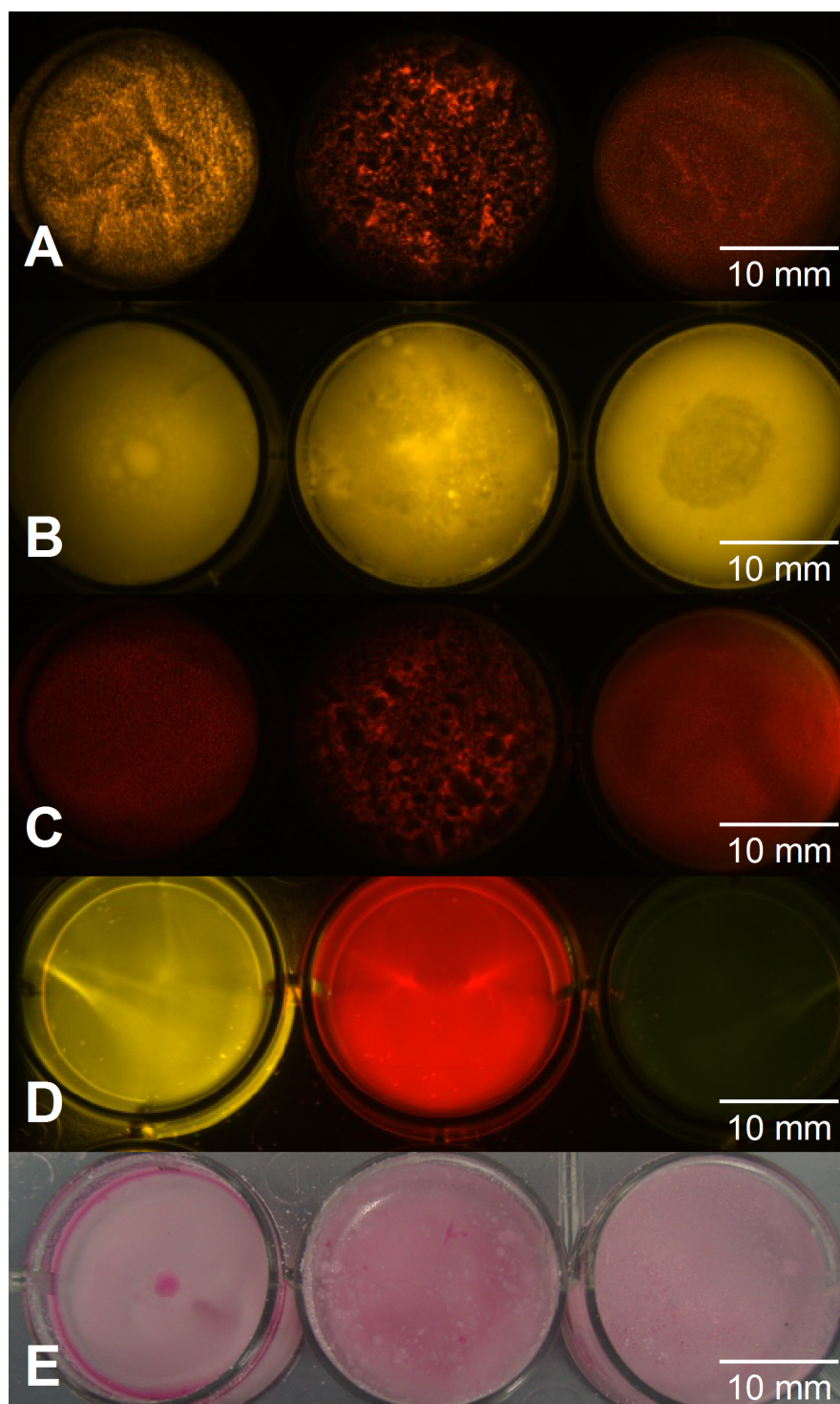
Figure 22: *Fluorescence images – adsorbate rows from left to right: Fujicalin®, Neusilin® UFL2, Neusilin® US2. (A) MCT adsorbates; (B) the same samples from A with water (image after 1 h); (C) impregnated samples; (D) Nile red in reference solvents from left to right: MCT, methanol, n-hexane. (E) Photograph of MCT adsorbates coloured with Sudan Red (taken after 1 h of water addition). The here shown adsorbates were prepared by SpeedMixer™ technique.*
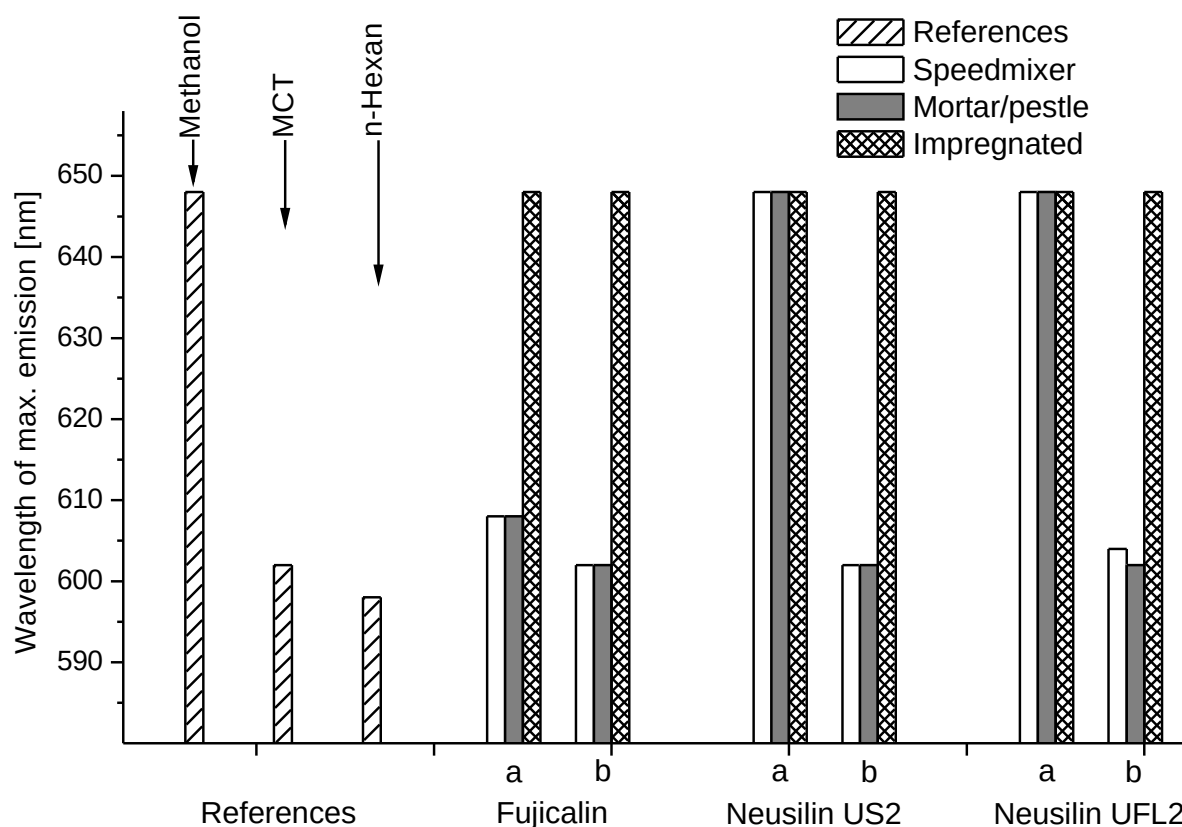
Figure 23: *Wavelength of maximal emission of Nile red in reference solvents (bars with sparse pattern), in MCT adsorbed on excipients and adsorbed on excipients from an acetonic solution (impregnated samples). The MCT adsorbates were produced by SpeedMixer™ technique (white bars) and by mortar/pestle method (grey bars). Impregnated samples (bars with dense pattern) are excipients moistened with an acetonic solution of Nile and dried afterwards. Each excipient group is subdivided in (a) adsorbate samples and (b) the same samples after addition of water.*

the oil which is visible as red accumulation, Neusilin® UFL2 (middle) shows isolated red droplets and for Neusilin® US2, no oil release is apparent. The data behind these images are shown in Figure 23 on page 62 comparing the WME shifts. The group of bars on the left belongs to NR in different reference solvents. The WME value decreases considerably from methanol (648 nm) to hexane (598 nm). The other groups of bars present the data of the adsorbates. Additionally, excipient samples were impregnated with an acetonic solution of NR and dried afterwards to obtain shifts for adsorbed solid NR at the excipient's surface. Comparing all white bars (SpeedMixer™) labelled with "a", the Fujicalin® adsorbate exhibits a slightly higher WME value (608 nm) than free MCT (602 nm). In contrast, the Neusilin® excipients lead to WME values for the adsorbed MCT which are close to the methanol level (648 nm) indicating a more polar environment. The same can be observed for the mortar/pestle method (grey bars). In conclusion, the adsorption of MCT at the Neusilin® products results in a higher micropolarity of the oily component, whereas

Fujicalin® hardly influences the MCT environment for Nile red. The results confirm the outcome of the ESR study. Both NR and Tempol indicate a more polar environment for adsorbed MCT at Neusilin®. The values of the Tempol species which were found to be similar to water in the previous chapter were confirmed. The blending method did not show an impact on the micropolarity which was also estimated from ESR spectroscopy. The impregnated probes of all excipients demonstrate WME values (648 nm) referring to a polarity comparable to the polar methanol solvent. Because of the low solubility of NR in water and the quenching effect, a WME value for water is not available.

Additionally, the multispectral optical imaging method was used for a study of the desorption of MCT. For this purpose, all adsorbate samples were covered with water and a fluorescence image was taken after one hour of incubation. The bars labelled with "b" show a recurrence to WME levels of free MCT (602–604 nm) for the MCT adsorbates. This confirms the data of the NMR relaxometry indicating that the MCT component seems to desorb from the excipient's surface. The extent of desorption or whether droplets stick between excipient particles could not be identified by this method. At least the micropolarity returned to the basic value of free MCT. Regarding the bars representing the impregnated samples, the addition of water has no impact on the high WME value of 648 nm. Due to the poor water solubility [134], NR stayed adsorbed on the solid excipient. Unfortunately, the release of the oil component was not satisfactorily answered. Especially for Neusilin® US2, it was not clear whether the data suggesting a release of MCT are valid. According to NMR imaging and simple photographs no oil separation could be found. This important issue will be handled separately in chapter 3.3.

3.2. Influence of the extrusion/spheronization process on a Fujicalin® adsorbate

The processability of an adsorbate and the influence of the extrusion/spheronization process on the adsorption state of a self-emulsifying concentrate was investigated for the excipient Fujicalin®. Two types of Fujicalin® pellets were produced, one with the extrusion/spheronization aid microcrystalline cellulose (MCC) and a second with pea starch. The process and both formulations are described in chapter 2.2.3 on page 17. The appearance of the products of the sequent process steps (adsorbate blend, extrudate and spheronizate) were observed by means of reflected-light microscopy and ESEM. The influence on the adsorption state was investigated by NMR relaxometry.

3.2.1. Appearance of the products

Photos of adsorbates, extrudates and pellets were taken with a reflected light microscope (figure 47 on page iv, appendix). The adsorbate blends show the different appearance of the solid excipients, the bigger and spherical Fujicalin® granules, the MCC fibres on the left side and the smaller starch granules on the right side. The extrudates with MCC are segmented and appear more stable than those with pea starch. The extrudates with pea starch are hardly segmented, shorter in size and tended to break. This tendency for breakage is visible for the spheronized product as well. Optically, the Fujicalin®-starch-pellets are more inhomogeneous in diameter but appear more spherical than the Fujicalin®-MCC-pellets. More information concerning the distribution of the solid excipients and the surface structure were obtained by ESEM. Figure 24 on page 65 shows all products of the process steps of the MCC pellets. Pictures were taken in GSE and BSE mode and are presented in parallel with the same image section. The GSE mode provides the better resolution but cannot distinguish between both solid materials. In contrast, the BSE mode allows a differentiation between organic and inorganic materials. Thus, Fujicalin® as calcium phosphate appears brighter than MCC as cellulose product. This effect is clearly visible at the pictures A1 and A2. The picture A2 on the right shows the spherical Fujicalin® particles in off-white and the more filamentary MCC in dark grey. Examples of Fujicalin® particles after extrusion and spheronization are marked with an arrow. During extrusion, segmented extrudates were formed (E1). The picture E2 demonstrates that the Fujicalin® particles were destroyed during the extrusion process and that the fragments are homogeneously distributed. The visible off-white particles are much smaller than the original adsorbate particles in picture A2. Furthermore, the grey areas are less dark than the MCC material in picture A2. Obviously, MCC filaments are covered with fine Fujicalin® powder. A close-up image of the extrudate is shown in figure 25 on page 66. The spheronization of the extrudates did not change the appearance of the Fujicalin® particles now incorporated in a more or less spherical pellet (figure 24: P1 and P2). The pellet surface is smooth and does not show any fissures (P1 and the close-up view P3). The adsorbed self-emulsifying concentrate was not distinguishable by ESEM. The same investigation was performed with the process steps of the Fujicalin®-starch-pellets in figure 26 on page 67. The extrudates of the starch blend look less compact than those made of MCC (picture E1). Indeed, these extrudates were more susceptible to degradation than those made of MCC as already shown in the reflected light microscopy images. Besides, no explicit Fujicalin® particles can be found. The starch granules are covered with a fine off-white powder belonging to the destroyed Fujicalin® adsorbate particles. The Fujicalin® powder is also located between the starch granules and possibly stabilize the extruded strand. Obviously, MCC partly protects the adsorbate particles during the extrusion
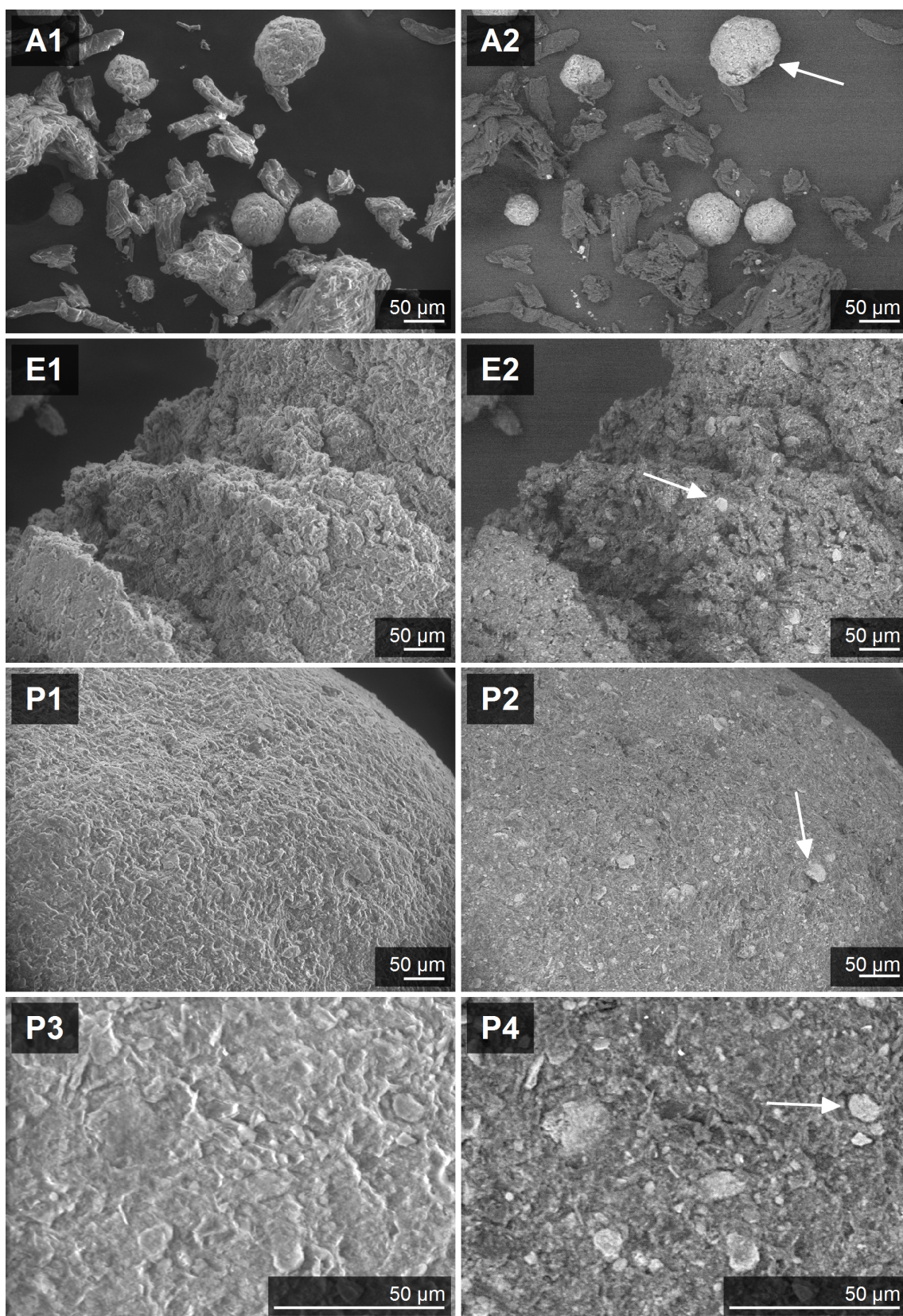
Figure 24: *Scanning electron micrographs of a Fujicalin® adsorbate as blend with MCC (A) as extrudate (E) and pellet (P). Left: GSE mode. Right: BSE mode. The arrow marks the brighter Fujicalin® particles distinguishable by the BSE mode.*
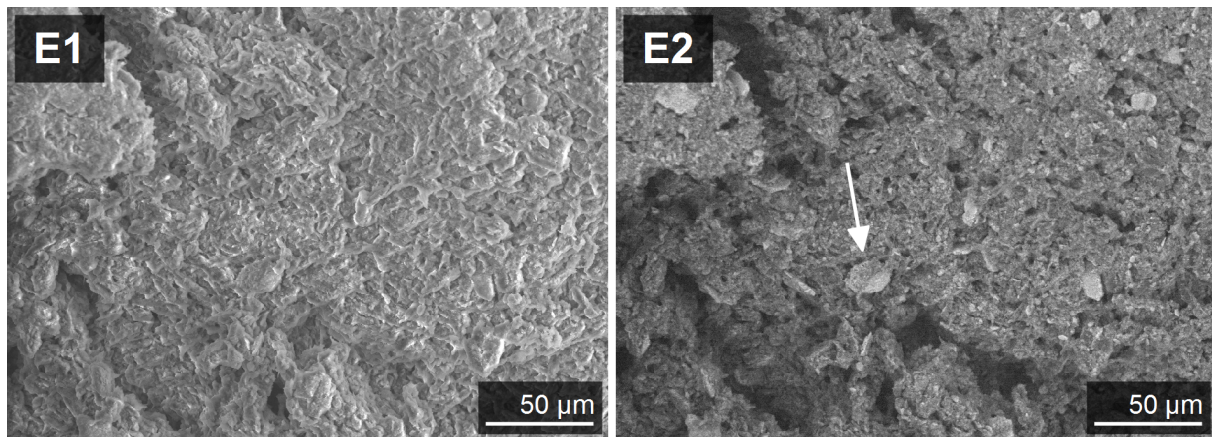
Figure 25: *Scanning electron micrographs of a Fujicalin®-MCC extrudate as close-up view. Left: GSE mode. Right: BSE mode. The arrow marks the brighter Fujicalin® particle.*

process (accompanied by pressure and shear stress) whereas the combination with starch led to more pulverised adsorbate particles (E2 and close-up view E4). After spheronization spherical pellets were obtained (P1 and P2). The surface shows some starch granules which are less covered with Fujicalin® than others, mostly those which slightly protrude from the pellet surface (P2). Possibly, the Fujicalin® cover was abraded during the spheronization process. Furthermore, the surface does not appear as smooth as the MCC example and has clear fissures. A close-up view of the surface can be found in figure 27 on page 68 (P1 and P2). In the close-up view some bigger Fujicalin® particles are visible but clearly smaller in size than those found for the Fujicalin®-MCC-pellets. The fissures in the surface also resulted in broken pellets. An example of a pellet with a fracture site is presented in P3-P6. The white enclosed area marks agglomerated starch granules inside the pellet which are not covered with Fujicalin®. Possibly, fractures mostly occur in such Fujicalin®-poor zones. The accumulation of Fujicalin® to the surface of starch granules could stabilise the extrudate. Consequently, investigations with increasing percentages of Fujicalin® would be interesting but the formulation improvement would go beyond the scope of this thesis. However, pellets containing 70 % of pea starch were produced. As reported by Dukić-Ott et al., starch has poor wetting and plasticity properties [136]. The low water binding capacity makes it difficult to obtain a suitable consistency for extrusion because the range of the water admixture which can be handled in the extruder is narrow. Probably, this could be an advantage of the combination with Fujicalin®. Native starch, like pea starch, naturally contains much more water than Fujicalin®. Loss on drying of pea starch according to the certificate of analysis was 13.5 %. Fujicalin® particles enlarge the range of water admixture to get a suitable mass for extrusion due to its higher water binding capacity. This could be a further benefit of Fujicalin® in addition to the assumed binder-like function between the starch granules.
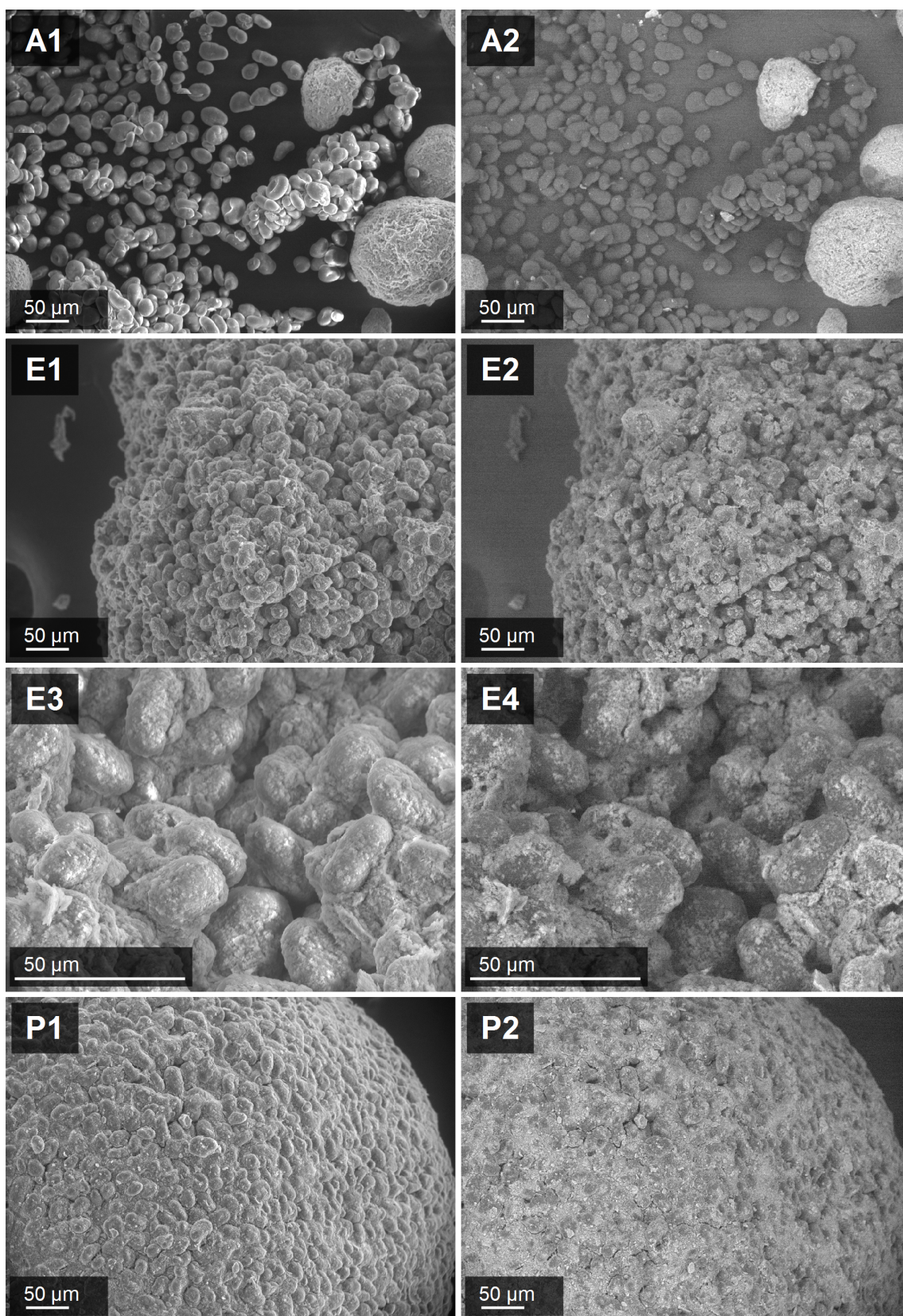
Figure 26: *Scanning electron micrographs of a Fujicalin® adsorbate as blend with pea starch (A) as extrudate (E) and pellet (P). Left: GSE mode. Right: BSE mode. The arrow marks the brighter Fujicalin® particles distinguishable by the BSE mode.*
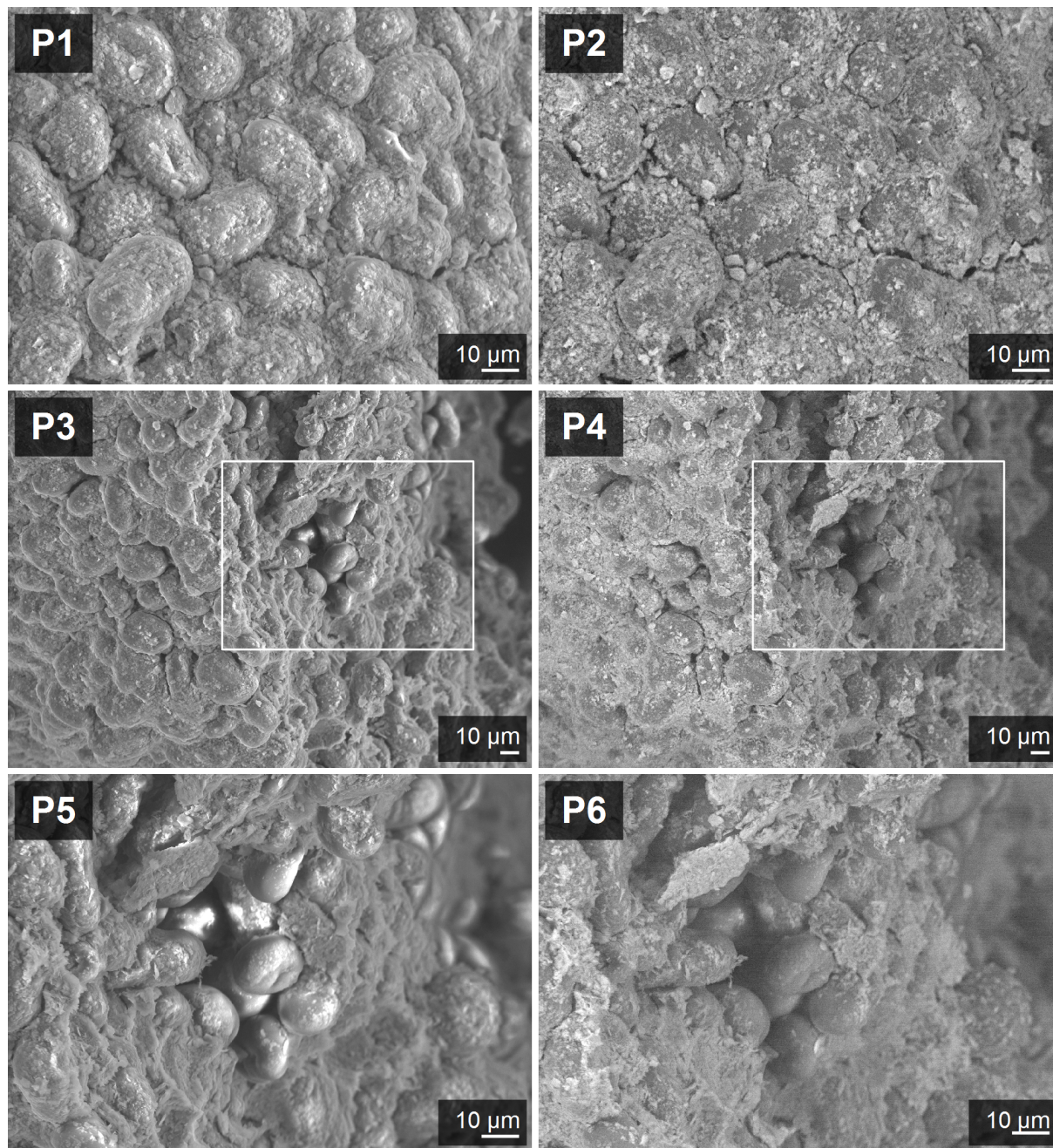
Figure 27: *Scanning electron micrographs of a Fujicalin®starch-pellets. Left: GSE mode. Right: BSE mode. P1 and P2: Close-up view of a intact pellet. P3-P6: Pictures of a fractured pellet. The white marked area is explicit shown in the row below (P5 and P6).*

3.2.2. Benchtop nuclear magnetic resonance relaxometry

NMR relaxometry measurements of the process steps provide more information on the adsorption state of the adsorbed liquid concentrate. The resulting T_2 distributions are compiled in figure 28 on page 70. The T_2 shifts between both pellet types show considerable differences. The adsorption at Fujicalin® and blending with MCC shifted the maximum from $100\,ms$ to $60\,ms$ (A). Hence, the liquid concentrate physically mixed with the solid excipients is less mobile than the free non-adsorbed liquid. After extrusion, the maximum T_2 was further decreased to $20\,ms$ indicating a stronger immobilisation and adsorption. The compressive and shear stress applied during the extrusion process seems to alter the adsorption state of the adsorbed liquid. The spheronization process did not influence the liquid any more as no difference was found between T_2 maximum of the pellet curve and the extrudate curve. This could be expected because extrudates are only rounded out to pellets without the application of pressure during spheronization. Ahmed Abdalla already performed similar investigations with pure MCC pellets and the same liquid concentrate. He found a shift to 30–$40\,ms$ for pellets containing $20\,\%$ of the concentrate [171]. His investigations showed that the physical mixture of the self-emulsifying concentrate with MCC did not differ much from the T_2 maximum of the free concentrate. Therefore, it can be assumed that the extrusion process in particular led to a stronger adsorption at MCC. In graph (A), the physical mixture (adsorbate blend) already decreased the T_2 value compared to the free level. In contrast to the process of Ahmed Abdalla, the liquid concentrate was first mixed and adsorbed at Fujicalin® prior to blending with MCC. Consequently, the visible decay is principally due to the adsorption at Fujicalin®. The extrusion of the wet blend results in a stronger binding of the liquid concentrate compared to the adsorbate blend which could be caused by the presence of Fujicalin® and/or MCC.

The second formulation with $70\,\%$ pea starch appeared differently. Pea starch does not have a good adsorbing capacity. But with a prior adsorption at Fujicalin®, $10\,\%$ of liquid could be easily incorporated. The T_2 distribution of the adsorbate blend shows a split into two physical states, one with a lower T_2 maximum at $50\,ms$ and a second with a higher value of $170\,ms$ (B). The stronger immobilized state is comparable to the state of the Fujicalin®-MCC blend and can be dedicated to the adsorption at Fujicalin®. Interestingly, a part of the liquid is more mobile. Probably, this part can be dedicated to an adsorption at pea starch. The slight right shift compared to the free concentrate could also indicate a fractionation of the liquid mixture. Possibly, the component of mono-, di- and triglycerides separates from the surfactant component Solutol® HS 15 and led to a similar T_2 shift as free MCT (approximately $200\,ms$). However, all distribution curves are very broad and include different adsorption states. Consequently, a separation of
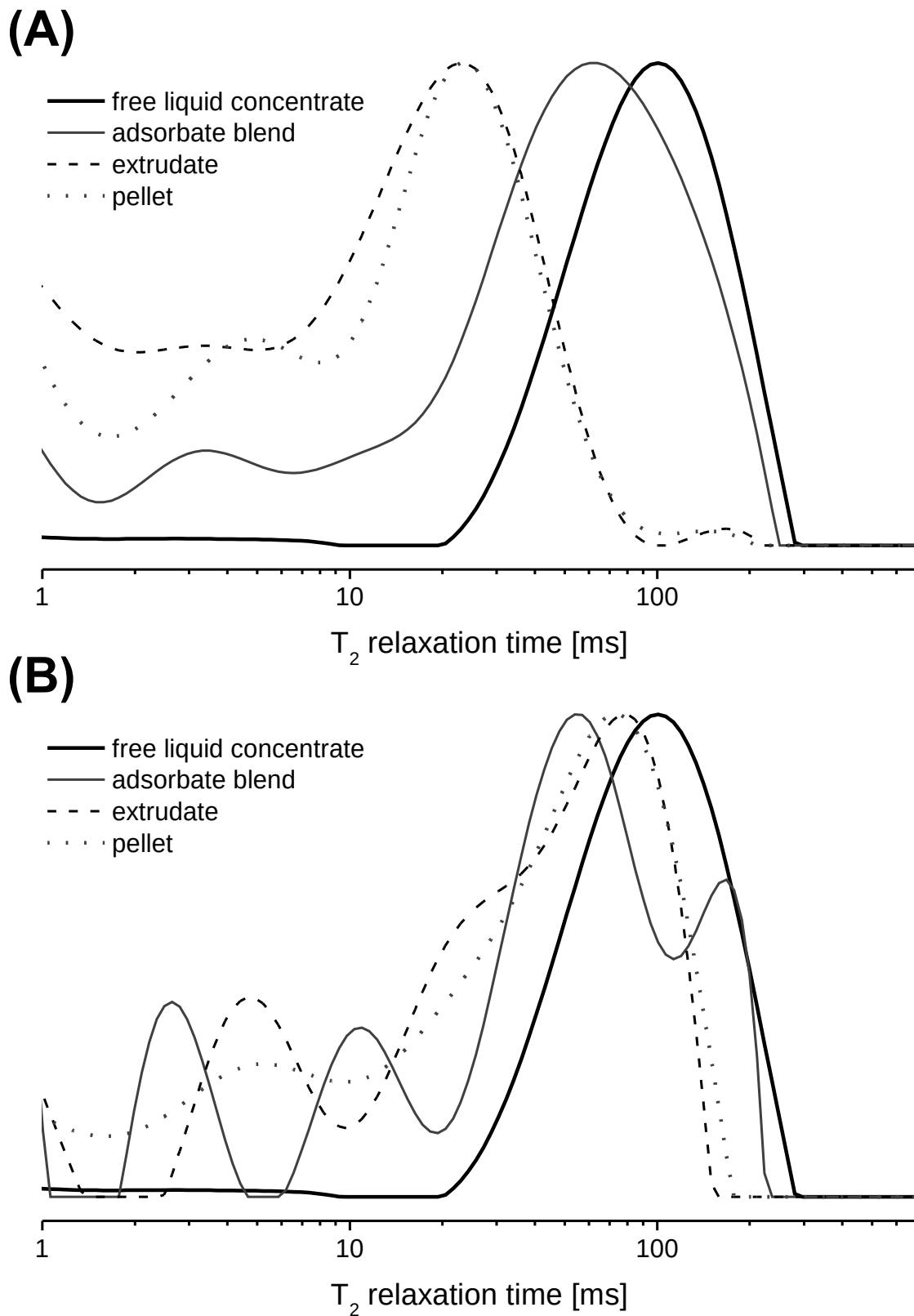
(A)

(B)

Figure 28: *T_2 relaxation time distributions dried products of the different process steps of Fujicalin®-MCC-pellets (A) and Fujicalin®-starch-pellets (B). The maximum intensity of each distribution was normalized to 1.*
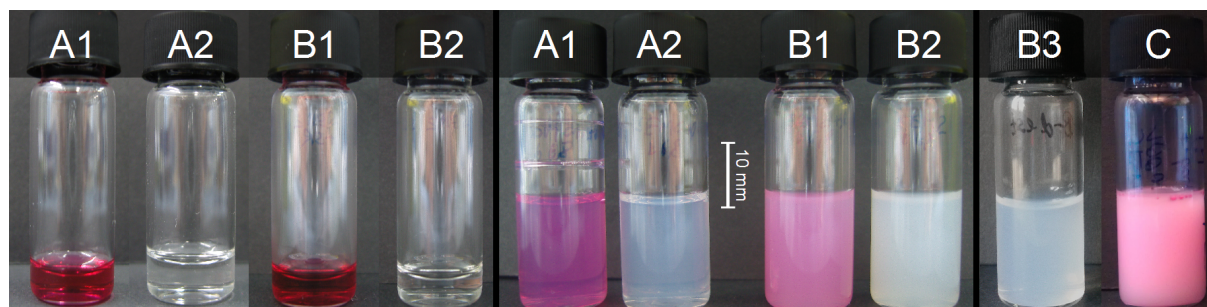
Figure 29: *Pictures of pre-concentrates with self-microemulsifying and self-emulsifying properties. (A) Pre-concentrate A, (B) pre-concentrate B, (C) pre-concentrate C. (1) Pre-concentrates coloured with Sudan red, (2) Pre-concentrates without Sudan red. Left: pre-concentrates, middle: pre-concentrates in phosphate buffer pH 6.8 shaken at 37 °C for 1 h, right: (B3) pre-concentrate B without Sudan red in distilled water and (C) pre-concentrate C in phosphate buffer pH 6.8 shaken at 37 °C for 1 h.*

the pe-concentrate should only be seen as a possible explanation. The extrudate and the pellet products show a T_2 shift to 80 ms based on the adsorbate blend. The slight shoulder on the left indicates a further adsorption state but not as clear as it was for the adsorbate blend. The maximum T_2 value of the extrudate is similar to the adsorbate blend indicating that the extrusion process only slightly impacts the physical state of the liquid. It can be assumed that MCC is the main factor for a compact binding between the excipients during the extrusion process which strengthens the adsorption of the liquid concentrate additionally.

3.3. *In vitro* release of adsorbed self-(micro)emulsifying systems

Three pre-concentrates with self-(micro)emulsifying properties were considered for the investigation of the release properties of the adsorbing excipients. Pre-concentrate A and B tend to form microemulsions upon distribution in an aqueous system. In contrast, pre-concentrate C forms an emulsion and is equivalent to the liquid mixture used for the extrusion/spheronization study. The composition of all three pre-concentrates is described in chapter 2.2.4.1 on page 19.

3.3.1. Selection of self-(micro)emulsifying systems

Figure 29 on page 71 shows pictures of all three pre-concentrates distributed mainly in phosphate buffer pH 6.8 (for experimental explanation see chapter 2.2.4.1). After 1 h at 37 °C pre-concentrate C exhibits a clear coalescence of oil droplets (picture "C"). In pre-concentrate A, one excipient of "C" was exchanged: C8-C10 mono-,di- and triglycerides

by C10 mono-, di- and triglycerides. The mixture forms an almost clear one-phase system in buffer with a characteristic opalescence (pictures A1/A2-middle). The appearance of this aqueous system did not change over the period of one hour at 37 °C. Pre-concentrate B was taken from Li et al. [30] as a microemulsion pre-concentrate for comparison. Instead of Cremophor® EL, Cremophor® ELP was used which is the more purified type of this surfactant. It turned out that the distribution in phosphate buffer pH 6.8 led to a more turbid appearance which generally indicates higher particle sizes and/or the presence of a two-phase system. Pre-concentrate B in distilled water (picture B3 - right) shows a clearer opalescent appearance which is more typical of a microemulsion system. Li et al. investigated the dilution in water only, and found particle sizes around 50 nm by dynamic light scattering. Possibly the "B"-concentrate is more sensitive to the presence of ions. But a phase separation as observed for "C" was not visible. The samples in buffer which were exposed to 37 °C were additionally investigated per light microscopy at ambient temperature. Whereas "A" and "B" did not show the presence of droplets in the micrometer range, "C" clearly exhibits droplet sizes of 5–10 μm (compare figure 49 on page vi, appendix). To get a deeper insight concerning the effect of buffer and temperature, particle size measurements of fresh prepared samples were conducted using dynamic light scattering. Figure 30 on page 73 shows mean particle sizes (intensity weighted) as z-average with the associated polydispersity index (PDI) as a measure of the width of the size distribution. "A" exhibits particle diameters of around 40 nm in phosphate buffer and distilled water at 25 °C and 37 °C as typical for microemulsions. In the literature, Solutol® HS 15 micelles are known with average diameters of 12 nm [172–174]. Diameters of about 40 nm indicate bigger surfactant colloids or microstructures wherein an oil domain can be incorporated as it is reported for microemulsions [175, 176].

Pre-concentrate "B" shows higher particle sizes in buffer (around 80 nm) and at 37 °C the particle size further increased (to more than 100 nm) which is more typical for nano-emulsion droplets. It could indicate a possible aggregation of colloids or the presence of a two-phase system. This would explains the turbid appearance of the sample. The high PDI of the particle size distribution between 0.2 and 0.45 shows a very broad size distribution. The dedicated volume distributions of buffer samples can be viewed in figure 31 on page 74 for 25 °C (black curves) and 37 °C (red curves). For "B" cycle 1 and the last measurement cycle 5 is presented. An increase of particle sizes at 37 °C over the 5 measurement cycles is visible. Obviously, aggregation of colloids takes place which is reversible as the microscopical picture does not show droplets/aggregates in the micrometer range. Distributed in distilled water, pre-concentrate "B" forms more likely a microemulsion with particle sizes around 60 nm, but with a broad size distribution (PDI between 0.2 and 0.3). These diameter results are congruent with the particle sizes found by Li et al [30] and support the existence of microemulsion structures. Cremophor EL
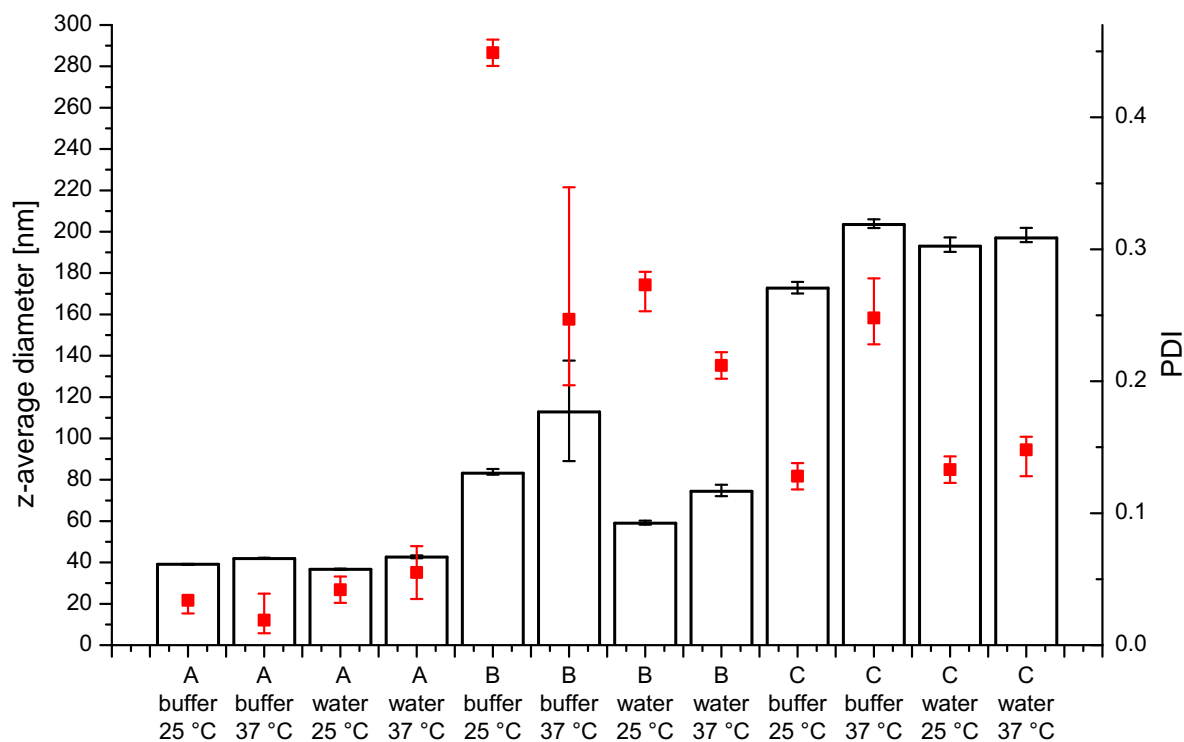
Figure 30: *Z-averages and the corresponding PDI of pre-concentrates A-C in different media and at 25 °C and 37 °C respectively. Mean and range calculated from 5 measurement cycles are presented. Error bars indicate the minimum and maximum of the 5 measurement cycles. Z-average is shown as columns linked to the left ordinate, PDI is shown as red squares linked to the right ordinate.*

micellar systems have smaller particle sizes of 11 nm [177]. Nevertheless, the presence of inorganic electrolytes seems to have a great impact on the properties of the emerging aqueous system. Guering et al. studied the change of the microemulsion structure caused by different salinity levels in 1985 [178]. Iwanaga et al. did similar investigations on liquid crystalline structures of polyoxyethylene-type non-ionic surfactants. The addition of salts lowered the cloud point of the diluted aqueous surfactant solution due to a dehydration effect of the ethylene oxide chains. This effect increases the hydrophobic character of the surfactant [179]. Similar impacts of electrolytes on micellar solutions of non-ionic surfactants were found by Batıgöç and Santos-Ebinuma. The presence of electrolytes reduces the hydrogen bond interactions between the surfactant head groups and the water molecules. This lowers the cloud point of the micellar solution [180, 181]. Obviously, the same influence is shown by dilution of pre-concentrate B in buffer instead of water. The change in its microstructure by altered surfactant-water-interactions (stronger hydrophobic interactions) results in larger aggregates, which was apparent in higher particle sizes during PCS measurements and visually by a stronger turbidity. Rising temperatures have
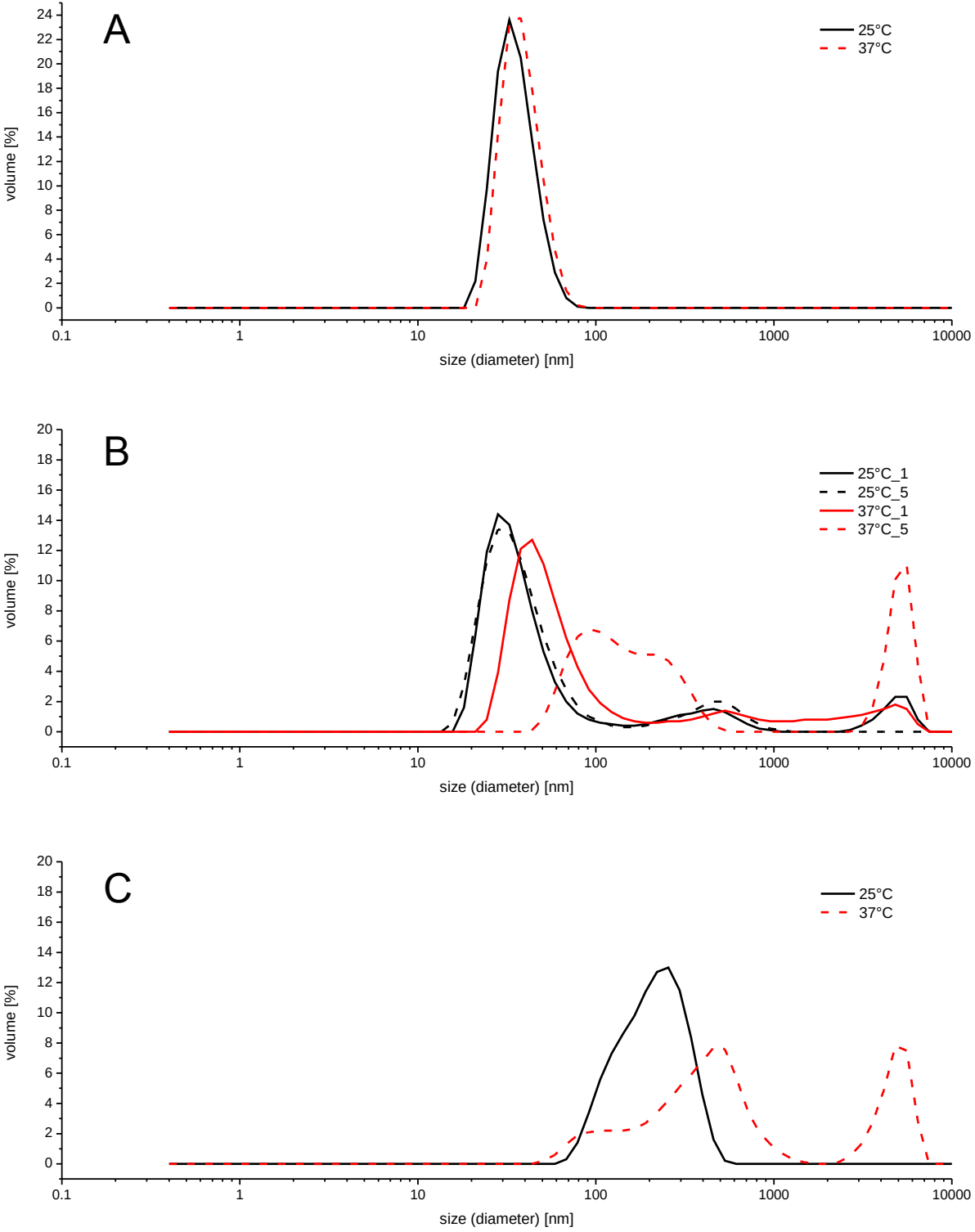
Figure 31: *Volume distribution of pre-concentrates A-C in phosphate buffer pH 6.8 at 25 °C (black line) and 37 °C (red line). (A) Pre-concentrate A, (B) pre-concentrate B with measurement cycle 1 and 5 and (C) pre-concentrate C.*

the same effect. This increases the hydrophobic character of the surfactant and, thereby, alter the microemulsion structure [182]. The higher particle sizes found by PCS confirm that larger aggregates are induced for a diluted pre-concentrate B by an increase of the temperature.

In contrast, pre-concentrate A is not sensitive to the presence of electrolytes or a temperature increased to 37 °C. An explanation is provided by studies of Warisnoicharoen et al [182]. They found that non-ionic microemulsions react differently to buffer used as continuous component in comparison to water. This was dependent on the surfactant and the oil component used. Accordingly, oils with a longer alkyl chain, e.g. soy bean oil, are mostly incorporated as a core, whereas more hydrophilic components as ethyl caprylate with a shorter alkyl chain act more as co-surfactant and are incorporated between the surfactant molecules. Microemulsions made of more hydrophilic lipid components generally reacted with a decrease of its cloud point by dilution with buffer. In the present study, pre-concentrate A contains the more lipophilic lipid component in comparison to pre-concentrate B with propylene glycol caprylate. Probably, the combination of Cremophor® ELP and Capmul® PG8 in pre-concentrate B (bigger surfactant head group with smaller lipid alkyl chain) is more sensitive to altered hydrophilic interactions by electrolytes and temperature and consequently, the amount of incorporated Capmul® PG8 is reduced. This could explain the turbidity seen for "B" caused by formation of aggregates or exclusion of Capmul® PG8 domains and it explains the lower sensitivity of "A" to these factors.

Pre-concentrate "C" forms a nano-emulsion upon distribution in phosphate buffer and distilled water (droplet sizes of about 170–200 nm) at 25 °C. But the PDI for the buffer sample at 37 °C is obviously higher than for the other samples of "C". This indicates a more inhomogeneous system and instability at higher temperatures. Figure 31 shows the detailed volume distribution of both samples in phosphate buffer (C). The emulsion becomes coarse and is shifted to higher particle sizes in the micrometer range at 37 °C. The main peak on the right of the distribution shows a coalescence of oil droplets which is clearly located in a visible particle size range. The size distribution confirms the instability of the emulsion of pre-concentrate C in phosphate buffer of 37 °C. Therefore, pre-concentrate C was excluded from the following release study. Because samples of pre-concentrate B did not change optically during the prevailing temperature of 37 °C (compare B1/B2 of figure 29), it was chosen together with system "A" for the investigation of the release properties of the adsorbents. The corresponding volume distributions of all pre-concentrates A, B and C in distilled water are illustrated for comparison in figure 48 (appendix, page v).

Figure 32 and 33 on page 76 show the selected pre-concentrates freshly diluted in water and buffer. In figure 32 the samples are permeated by a laser beam. System A shows the
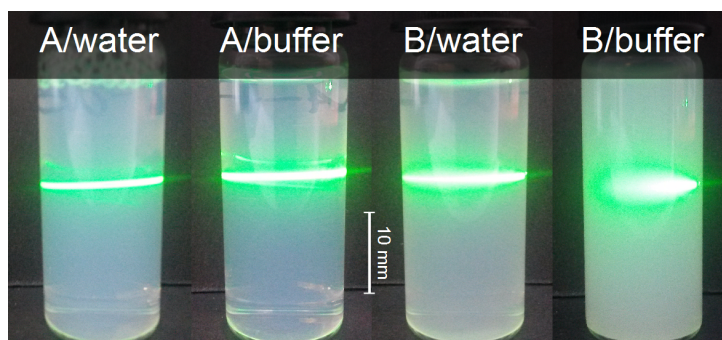
Figure 32: Photographs of freshly prepared samples of 5 % A and B in distilled water and phosphate buffer permeated by a green laser beam.
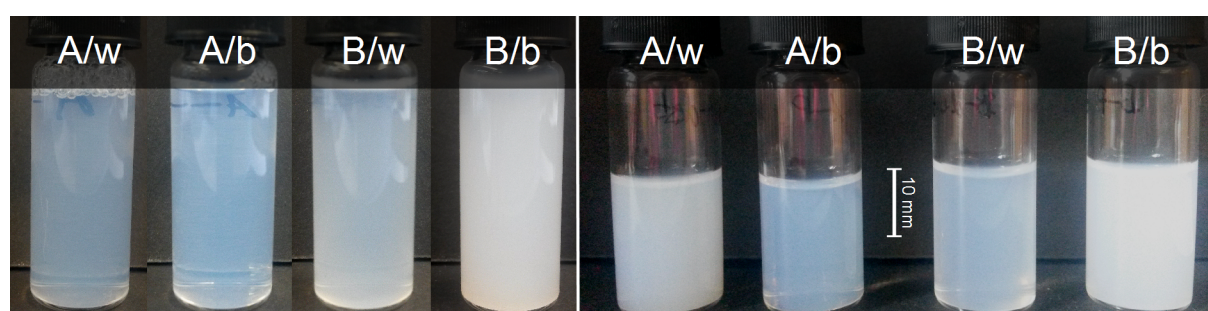

Figure 33: Photographs of 5 % A and B in distilled water and phosphate buffer. Left: Freshly prepared samples. Right: The same samples after 24 h. The scale bar is applicable for left and right.

Tyndall effect which is characteristic for colloidal systems in this particle size range [183]. The laser beam is visible throughout the sample. For samples of "B" the laser beam is visible but shows a more diffuse scattering due to the higher particle sizes, especially for "B" in phosphate buffer. Figure 33 presents the sample alteration occurring during 24 h storage at room temperature. The stored samples on the righten side show a changed appearance for "A" in water. The sample is more turbid indicating a probable aggregation of colloids. In contrast, "A" in buffer and both "B" samples does not show alterations after 24 h. However, all further experiments were conducted in buffer and the analysis was performed within 24 h after dilution of the adsorbate with buffer medium.

3.3.2. Release study of the adsorbed pre-concentrates

The release properties of the adsorbates were characterised by a preliminary visual study using the example of the Sudan Red loaded pre-concentrate A. The subsequent release study with both selected pre-concentrates were performed by means of fluorescence analytics.
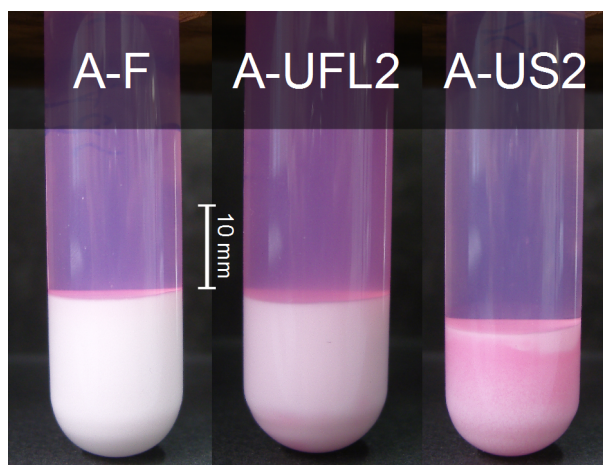
Figure 34: *Release of adsorbed pre-concentrate A (colouration with Sudan red) after centrifugation. (A-F) - Fujicalin® adsorbate, (A-UFL2) - Neusilin® UFL2 adsorbate, (A-US2) - Neusilin® US2 adsorbate.*

3.3.2.1. Visual release study

A preparatory release study was performed with the pre-concentrate A according to the description in chapter 2.2.4.1 on page 19. Figure 34 on page 77 shows photographs of the samples after the centrifugation step. The photographs give a first impression concerning the release properties of the solid excipients. The remaining solid at the bottom of the test tube is for Fujicalin® almost discoloured, followed by the Neusilin® UFL2 sample. Neusilin® US2 exhibits the most residual colour. Consequently, the visual investigation leads to the assumption that Fujicalin® releases more easily the adsorbed pre-concentrate than the Neusilin® excipients. During the centrifugation the whole sample is exposed to mechanical stress. This could influence the released amount of the pre-concentrate. For example, the Fujicalin® sample was centrifuged with 2000 rpm for 1 min to achieve a separation of the solid material. For both Neusilin® samples, 3000 rpm were necessary to separate the solid material from the medium to the bottom of the test tube. Even the higher rotation speed did not discolour the solid material as it is apparent for the Fujicalin® adsorbate. But, the Neusilin® US2 solid is not any more homogeneously coloured (figure 34, right). As expected, an impact of the centrifugation conditions is existent. Therefore, all following release studies were performed according to figure 2 on page 21 where the supernatant is separated without mechanical stress from the majority of solid material.

3.3.2.2. Fluorescence release study

Pre-concentrates A and B were loaded with the lipophilic fluorescence dye DiI to study the release properties of the adsorbents in more detail. The adsorbates were prepared
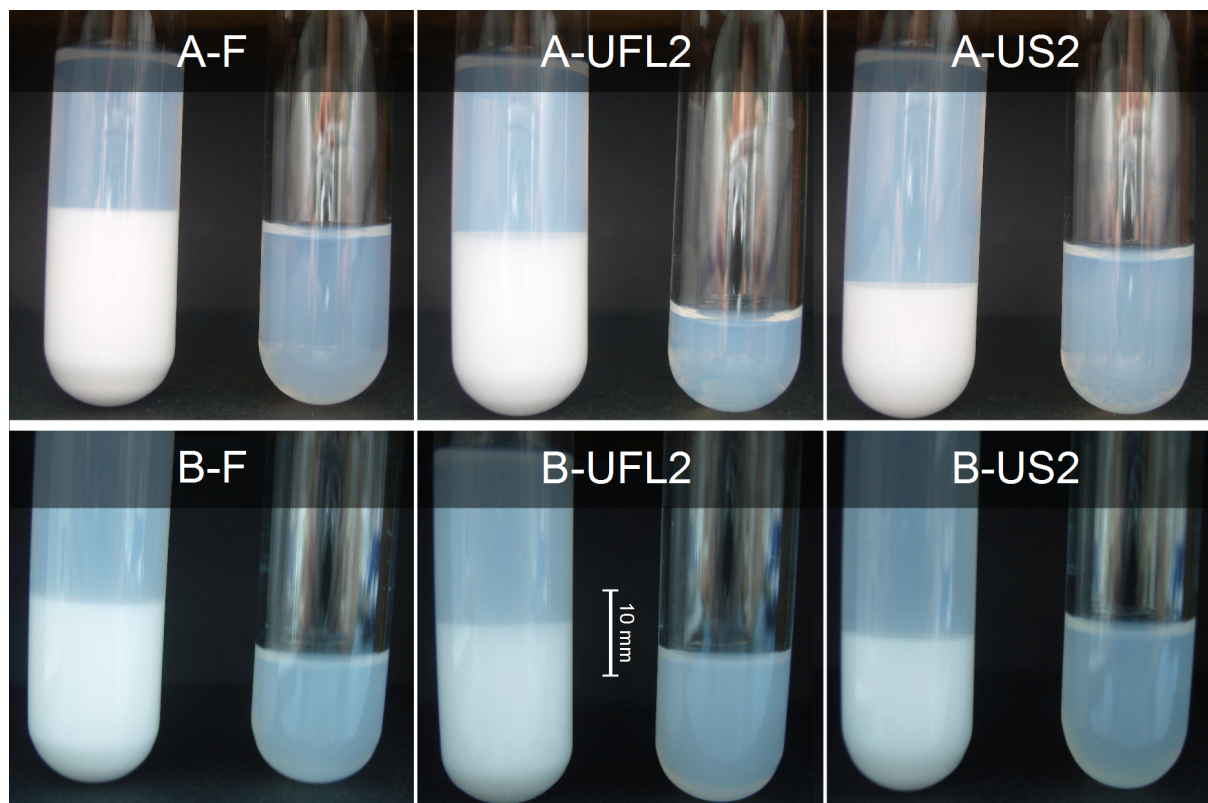
Figure 35: *Release of adsorbed pre-concentrates A and B during the DiI fluorescence study. Top: Series with pre-concentrate A, bottom: Series with pre-concentrate B. (F) - Fujicalin® adsorbate, (UFL2) - Neusilin® UFL2 adsorbate, (US2) - Neusilin® US2 adsorbate. For every picture: Test tube on the left: Release sample after a rest period, test tube on the right: filtrated release medium (see Figure 2).*

by SpeedMixer™ as described in chapter 2.2.1 and with pre-concentrate concentrations presented in table 4. The release procedure is specified in chapter 2.2.4.2 and figure 2.

Figure 35 shows photographs of the release samples after 1 h at 37 °C in an end over end apparatus. As Neusilin® UFL2 exhibits very fine particles the supernatant of this adsorbate looks more turbid than for the other ones. Overall, the supernatant and filtrate of the pre-concentrate A series show the characteristic opalescence indicating that the adsorbed pre-concentrate was at least partly released. The supernatants and filtrates of the pre-concentrate B series appear more turbid than those of the pre-concentrate A series. This was already recognized during the pretest and is caused by electrolytes which have more impact on the pre-concentrate B system (see chapter 3.3.1). It is apparent that the adsorbed pre-concentrate B was at least partly released, too. The supernatant of the Neusilin® US2-B adsorbate is slightly clearer than that of the corresponding Fujicalin® adsorbate. This indicates an incomplete release of the lipid mixture to the buffer medium and/or that the composition of the desorbed liquid mixture is altered.

The results of the fluorescence release experiment of adsorbed pre-concentrate A and B are presented in figure 36 and 37 on page 79 and 80. The reference intensity of the
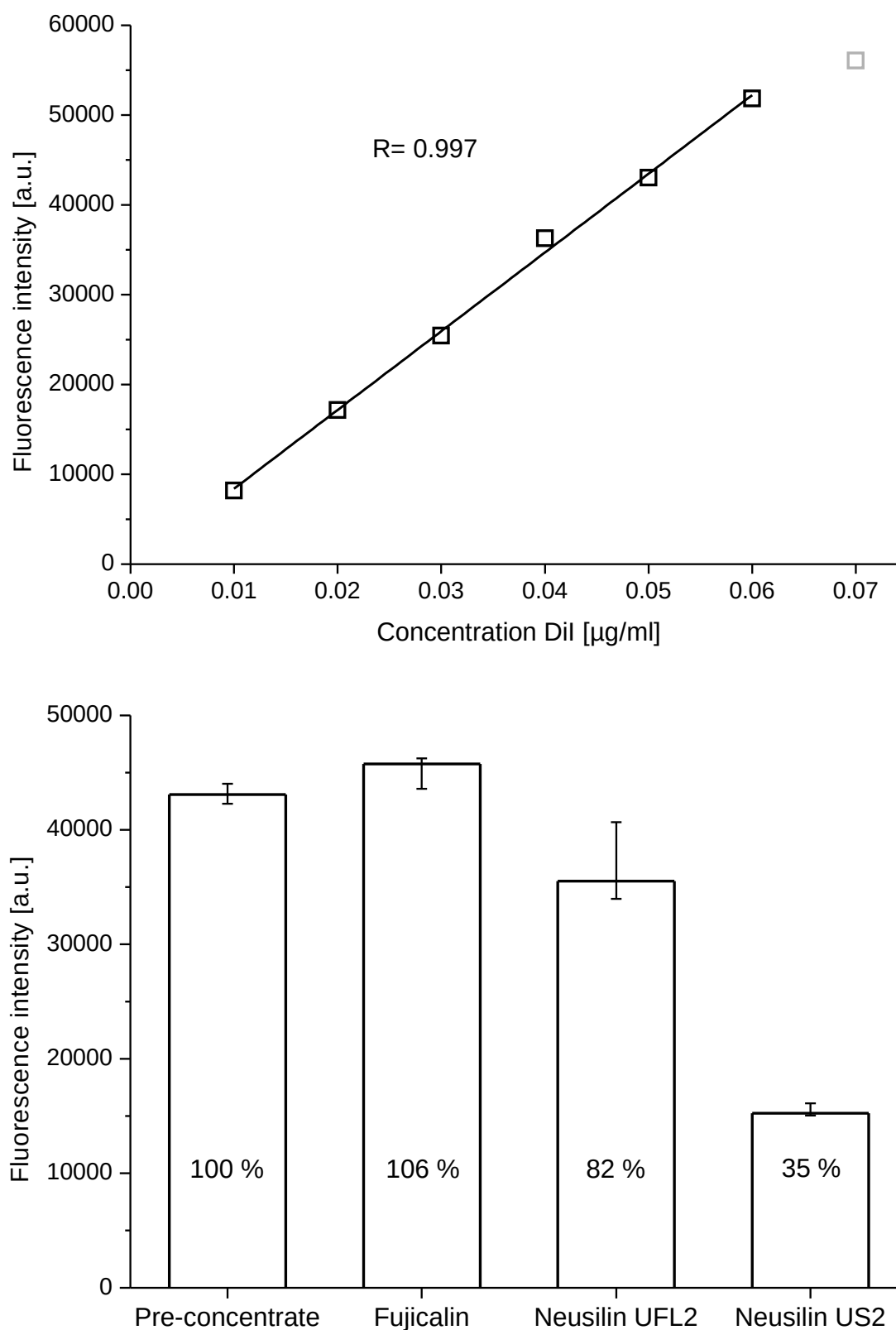
Figure 36: *Release of DiI loaded pre-concentrate A from adsorbates of Fujicalin®, Neusilin® UFL2 and Neusilin® US2 by Novostar micro plate reader. Top: Calibration with increasing concentration of DiI in the release medium. Last data point is excluded. Bottom: Release of adsorbed pre-concentrate A at Fujicalin®, Neusilin® UFL2 and Neusilin® US2 in comparison to the non adsorbed pre-concentrate reference. Data are presented with the median of 3 experiments (columns) and the positive and negative range (error bars).*

Figure 37: *Release of DiI loaded pre-concentrate B from adsorbates of Fujicalin®, Neu-silin® UFL2 and Neusilin® US2 by Novostar micro plate reader. Top: Calibration with in-creasing concentration of DiI in the release medium. Last data point is excluded. Bottom: Release of adsorbed pre-concentrate B at Fujicalin®, Neusilin® UFL2 and Neusilin® US2 in comparison to the non adsorbed pre-concentrate reference. Data are presented with the median of 3 experiments (columns) and the positive and negative range (error bars).*
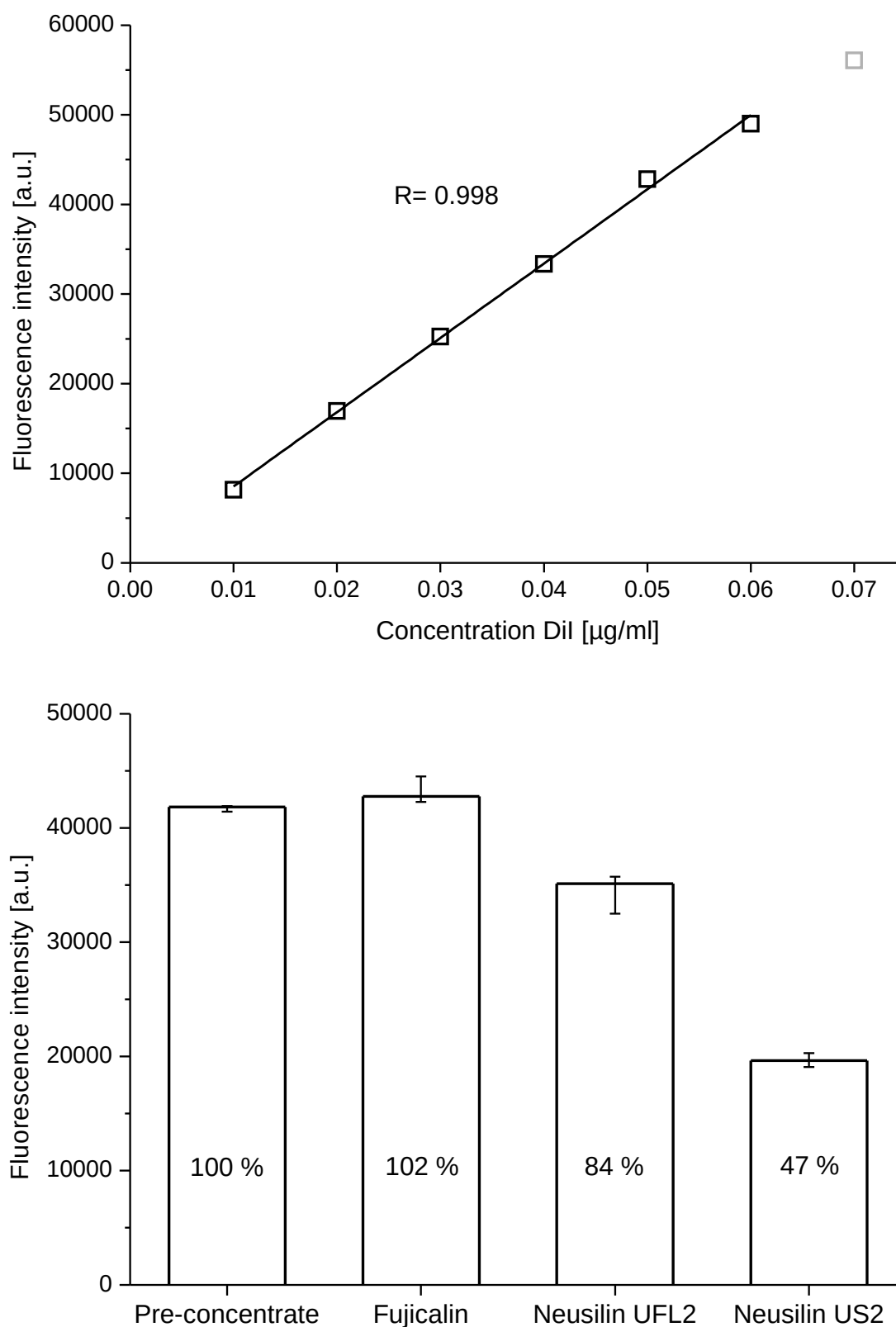
same amount of non-adsorbed pre-concentrate in phosphate buffer pH 6.8 is labelled with "100 %" (left column). It represents the fluorescence intensity value for a pre-concentrate release of 100 %. All other percentage labels are calculated in reference to this intensity value. The graph on the top shows the calibration with increasing amounts of DiI in the release medium. For calibration of pre-concentrate A the 7th sample with a DiI concentration of $0.07\,\frac{\mu g}{ml}$ indicates the beginning of non-linearity by quenching. This value was excluded from calibration of A and B. Both results of linear fit (coefficient of correlation: 0.997 and 0.998) prove the linearity in a DiI concentration range of 0.01–$0.06\,\frac{\mu g}{ml}$. A 100 % release would yield a DiI concentration of $0.05\,\frac{\mu g}{ml}$ and is located within the calibration range.

Figures 36 and 37 demonstrate the varying release properties of Fujicalin®, Neusilin® UFL2 and Neusilin® US2. In both cases, the release medium of the Fujicalin® adsorbate exhibits approximately the same fluorescence intensity like the non adsorbed pre-concentrate which refers to a complete release of the adsorbed liquid. In contrast, the release medium of Neusilin® excipients show lower fluorescence intensities of their release media. Neusilin® UFL2 reaches a release rate of around 80 %. The range of the intensities is considerably higher compared to the other adsorbates. This might be explained by its tendency for agglomerate formation during adsorbate production which causes inhomogeneities in the liquid distribution of the resulting adsorbate. This tendency was already observed during the experiments of NMR imaging and NMR relaxometry for the MCT adsorbates (compare chapter 3.1.3.1). Samples with and without bigger agglomerates result in varying amounts of pre-concentrate of the individual sample. Different released amounts would be the consequence and would result in a broader range of the intensity values. Nevertheless, the median of three values was used which is less impacted by such effects. It can be concluded that Neusilin® UFL2 releases most of the adsorbed pre-concentrate A and B but certainly less than 100 %. According to the intensity values of the release medium of the Neusilin® US2 adsorbate, this excipient retains the highest amount of pre-concentrate at the particle surface. For pre-concentrate A only 35 % and for pre-concentrate B only 47 % of the total quantity were released. More precisely, it can be stated that the release rate probably does not exceed half of the adsorbed quantity of pre-concentrate A and B. In conclusion, the Neusilin® excipients adsorb liquid lipids stronger than Fujicalin® leading to an incomplete desorption. The strongest effect was found for Neusilin® US2. This outcome confirms the assumptions from NMR relaxometry/MRI, ESR spectroscopy and multispectral fluorescence imaging of MCT adsorbates. As root cause a stronger intermolecular binding based on hydrogen bonding was discussed. The investigations with Sudan Red coloured adsorbates already indicated a possible impact on the release quantity. But even though hydrogen bonding should affect the release properties of both Neusilin® excipients there is an obvious difference between both exci-

pients. It can be supposed that again the Neusilin® UFL2 tendency to form solid-liquid agglomerates causes the higher release rate. The liquid adsorption and distribution at the Neusilin® US2 particle surface occurs more homogeneously compared to Neusilin® UFL2. Accordingly, more molecules of the pre-concentrate have direct contact to the particle surface and stay fixed on it or between different Neusilin® US2 particles as concluded from the NMR imaging results.

Kang et al. investigated the release of ibuprofen from self-emulsifying tablets in simulated gastric fluid [118]. They used a liquid SEDDS for dissolving ibuprofen and solidified the liquid by adsorption at Fujicalin® (36 % adsorbate) and Neusilin® UFL2 (52 % adsorbate). The solidified SEDDS was then compressed directly to a tablet upon blending with other excipients. The release rate of the Fujicalin® tablet was similar to the non-adsorbed SEDDS. But for the Neusilin® tablet, the ibuprofen release was retarded and reached only 40 % of the used amount of ibuprofen. Neusilin® UFL2 reached approximately 80 % of release of DiI which can be attributed to several reasons. One probable reason is the further processing of the adsorbate by compression which may enforce the adsorption strength similar to extrusion/spheronization. This was shown for a MCC/Fujicalin®blend processed by extrusion/spheronization presented in chapter 3.2. Another example can be found by Ahmed Abdalla who discovered a stronger adsorption of a self-emulsifying mixture in MCC pellets compared to the physical mixture of the excipients [171]. Secondly, the liquid mixture used by Kang et al. for adsorption differed in the used lipids. This also has an impact on the release rate. For the Neusilin® US2 adsorbate pre-concentrate B was released to a slightly higher extent than pre-concentrate A. A fact which has an impact on the released amount, is the set up of the release experiment and especially in this case the chosen release medium. Kang et al. used simulated gastric fluid, whereas the DiI study was performed in phosphate buffer pH 6.8. Finally, the process of the adsorbate production was different. Kang et al. prepared the adsorbates by the mortar/pestle method. The adsorbates investigated in the present DiI study were prepared by the SpeedMixer™ method. Meanwhile, other interesting release studies on Neusilin® US2 adsorbates were performed by Van Speybroeck et al. and Williams et al [153, 184]. Different lipid based formulations and several drugs were investigated. For all adsorbates, an incomplete drug release was discovered confirming the results presented in this thesis. Furthermore, the desorption was more impacted by the composition of lipid based formulation than by the drug type dissolved. The more lipophilic IIIA formulation adsorbate retained of about 50 % of the drug danazol whereas the less lipophilic IIIB adsorbate released circa 75 % [153]. A comparable difference was also found for the more lipophilic pre-concentrate A and the less lipophilic pre-concentrate B within the present study.

3.3.3. Characterisation of the desorbed pre-concentrates

The release media of all adsorbate types were investigated in detail to find reasons for the different release rates of the adsorbed liquid pre-concentrates. Maybe, one component of the pre-concentrate stays to a higher extent adsorbed at the solid material than the other ones. This could manifest itself for example in altered particle sizes for which reason PCS was applied. NMR spectroscopy was used to get a hint for changed percentages in the pre-concentrate composition.

3.3.3.1. Photon correlation spectroscopy

The particle size analysis of the release medium is shown in figure 38 on page 84. The release procedure was conducted twice per adsorbate. The results are presented in parallel. Thus, one column represent the mean z-average of 5 measurent cycles of the release medium of one sample and error bars indicate the corresponding positive and negative range. The related mean PDI (squares) with positive and negative ranges (error bars) are readable at the right ordinate. The graph at the top shows samples of pre-concentrate A and the graph below samples of pre-concentrate B.

All samples of "A" exhibits narrow size distributions apparent with PDIs mostly lower than 0.1. The release medium of the Fujicalin® adsorbate shows very similar diameters to the non-adsorbed pre-concentrate reference (38–39 nm). The samples of the Neusilin® adsorbates have slightly higher particle diameter (44–45 nm). But the difference is too small to suggest a change in the pre-concentrate composition. However, these diameter sizes support the assumption that microemulsion systems are formed after desorption.

All "B" samples exhibit broad size distributions noticeable with PDIs till 0.7. The particle diameters deviate strongly, also between the parallel measurements. These results do not enable the conclusion concerning a change in the pre-concentrate composition. The mean particle sizes found here (around 50 nm) differs from the first PCS measurement (80 nm, compare figure 30). But the PDI of all measurements for "B" in buffer are high. Consequently, evaluations or a comparison based on these particle size values are not reasonable.

3.3.3.2. Nuclear magnetic resonance spectroscopy

The release medium contains the partly or completely desorbed pre-concentrate. With help of NMR spectroscopy the pre-concentrate composition in the release medium was investigated. Pre-concentrate A is composed of three excipients: a mixture of mono-/di-glycerides, triglycerides and a non-ionic surfactant. Pre-concentrate B is composed of two excipients: the mono fatty acid ester of propylene glycol and a non-ionic surfactant. The spectra evaluation was focused on a two component system: Component 1 - the surfactant
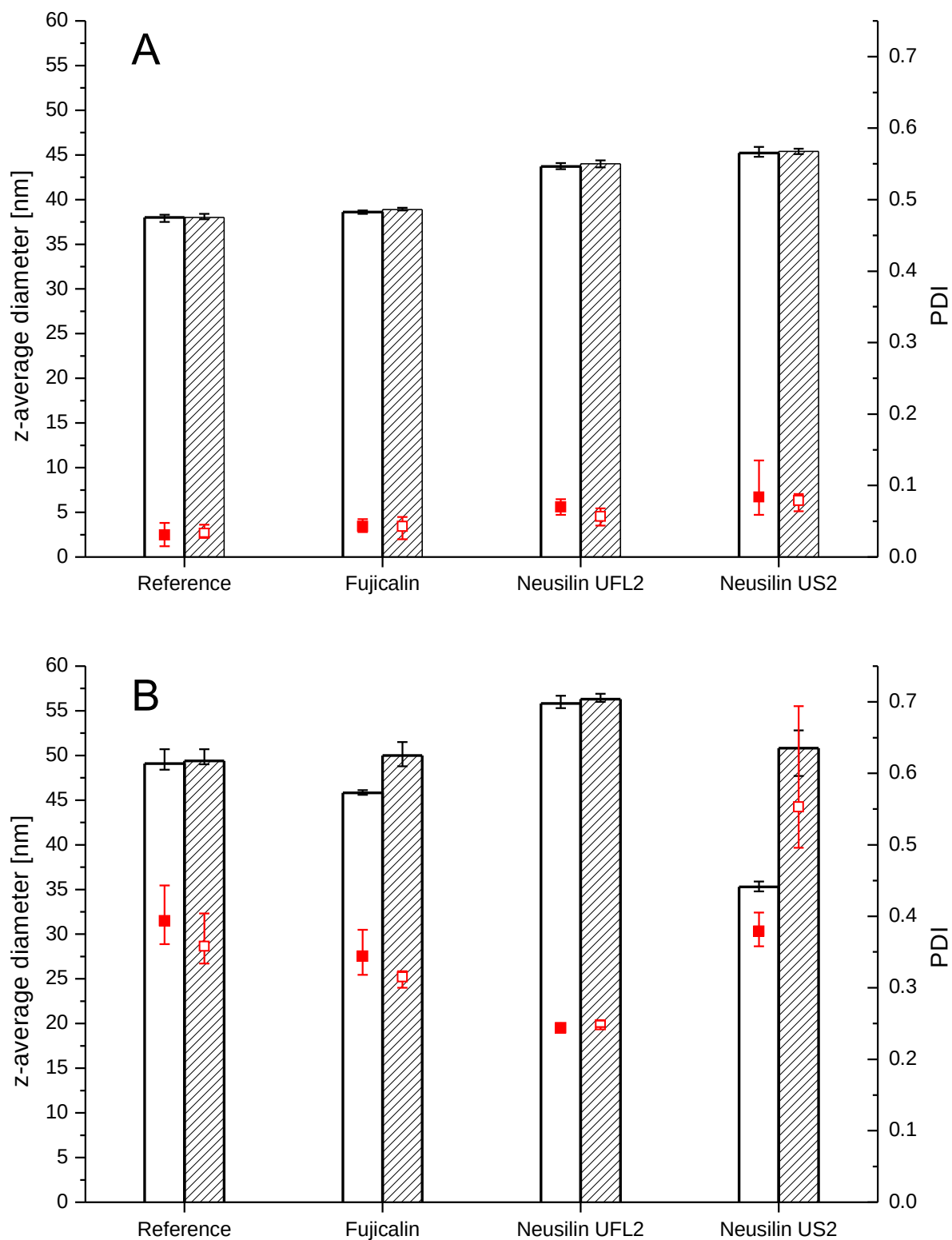
Figure 38: *Z-averages and the corresponding PDI of the release medium from adsorbed pre-concentrates A (top) and B (bottom) in duplicate. Mean and range calculated from 5 measurement cycles at 25 °C are presented. Error bars indicate the minimum and maximum of the 5 measurement cycles. Z-average is shown as columns linked to the left ordinate, PDI is shown as red squares linked to the right ordinate.*

and component 2 - the lipid. For "A", component 1 was the surfactant Solutol® HS 15 and component 2 was mixture of mono-/di-/tri-glycerides Capmul® MCM C10 and Captex® 355 EP/NF. For "B" component 1 was the surfactant Cremophor® ELP and component 2 was the mono fatty acid ester of propylene glycol Capmul® PG8.

It can be assumed that the surfactant (component 1) will desorb more easily from the excipient into the aqueous medium due to its amphiphilic structure. The lipid (component 2) would have a higher tendency to remain adsorbed at the surface. Therefore, the experiment was designed in this direction (see chapter 2.2.8.3 on page 25).

Analysis of the released pre-concentrate A

Calibration samples in deuterated phosphate buffer pH 6.8 were prepared with a constant concentration of Solutol® HS 15 ($0.02 \frac{g}{ml}$) and increasing lipid concentrations (0; 0.01; 0.02 and $0.03 \frac{g}{ml}$). The ratio of the two lipid excipients in the lipid component was the same as used for the original pre-concentrate A. The first calibration sample represents the Solutol® HS 15 reference without the lipid component. The last calibration sample represents the reference for a completely released pre-concentrate in composition and concentration. Figure 39 on page 86 shows NMR spectra of the first sample of the calibration series, Solutol® HS 15 in phosphate buffer (top), and the last sample, containing the amount of a completely released pre-concentrate A in phosphate buffer (bottom). The peak at a chemical shift of 0 ppm represents the standard TMSP. To the left the peak of the aliphatic –CH_3 end group can be found with a chemical shift of 0.9 ppm [185–188]. The aliphatic –CH_2– group appears at a chemical shift of 1.3 ppm [185–188]. The characteristic peak at 3.7 ppm can be assigned to protons of the ethylene oxide group [185–187, 189]. The peak at 4.8 ppm shows the "HDO" which appears due to proton exchange [190, 191].

The graph below shows the spectrum of pre-concentrate A in phosphate buffer. Compared to the spectrum of Solutol® HS 15 some peaks are increased e.g. 0.9; 1.3; 1.6 and 2.3 ppm due to the presence of the lipids Capmul® MCM C10 and Captex® 355. These peaks are increased because of the higher amount of the aliphatic –CH_2– and –CH_3 groups. The peaks at 1.6 ppm and 2.3 ppm can be assigned to –CH_2 groups close to and directly at the acyl group [192–194]. New signals appeared at around 4.1 ppm, 4.3 ppm and 5.2–5.3 ppm which are characteristic of protons of the glyceryl group [194]. A summary of all NMR spectra can be found in figures 50, 51, 52, 53, 54 and 55 on pages vii, viii, ix, x, xi and xii (appendix).

Two peaks were selected, one for the lipid component and one for Solutol® HS 15. For Solutol® HS 15 the characteristic signal at 3.7 ppm was chosen. For the lipids, the calculations were done with the peak at 0.9 ppm. This one was only of low intensity for the Solutol® HS 15 calibration sample (0.0532 relative to the intensity of the peak at 3.7 ppm). The intensity increased (0.4265 relative to the intensity of the peak at
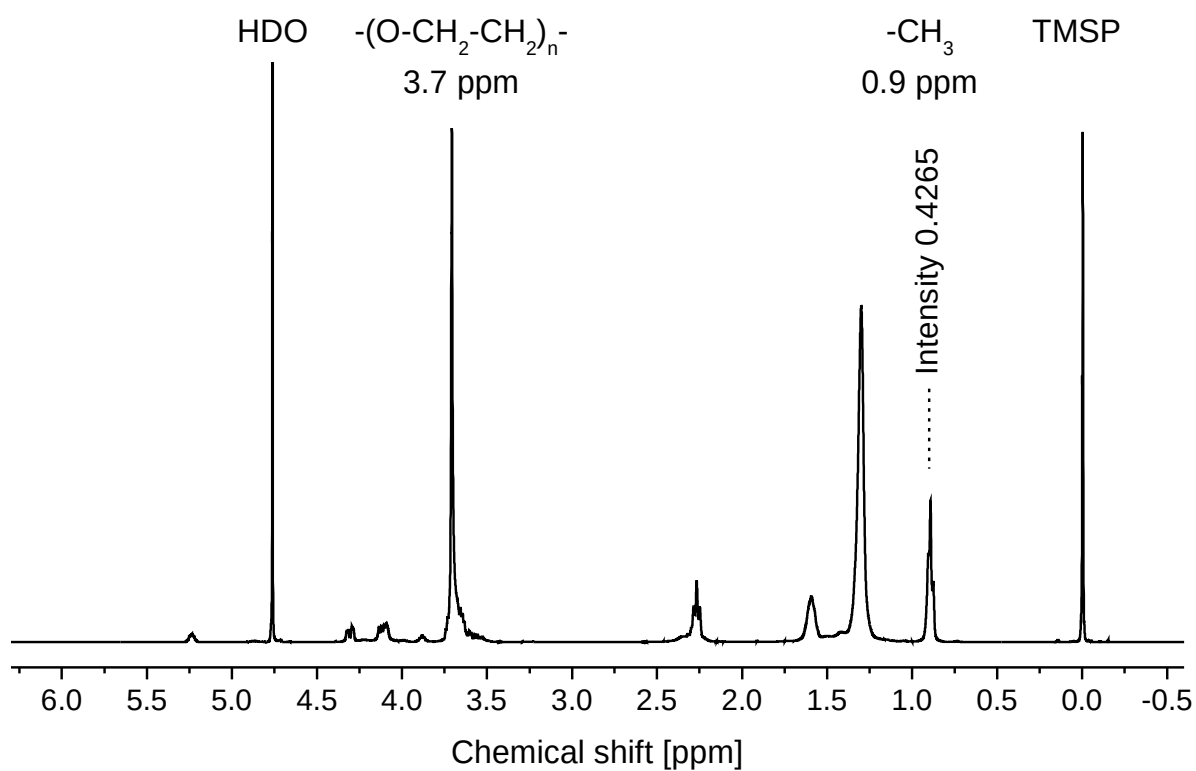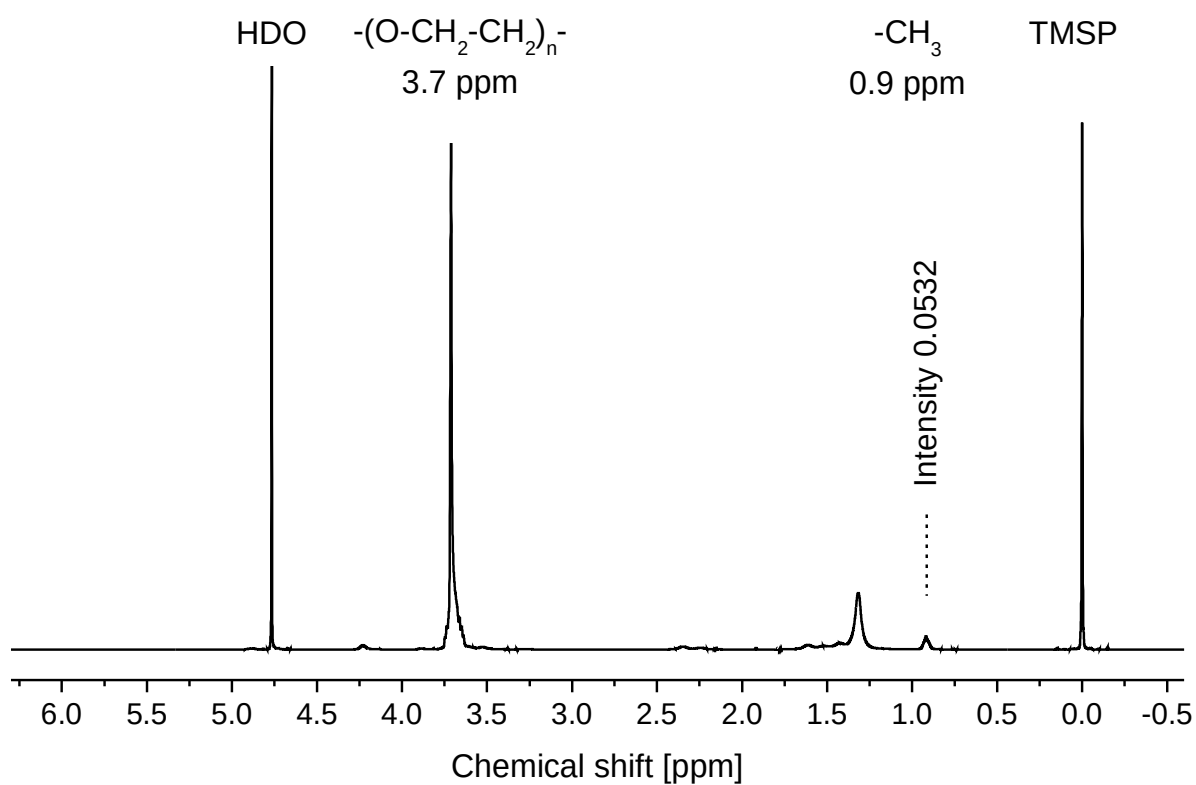
Figure 39: *NMR spectra of Solutol® HS 15 (top) and pre-concentrate A (bottom) in buffer. Chemical shifts are assigned relative to the standard TMSP. The –CH₃ peak intensity is indicated relative to the ethylene oxide peak intensity. The HDO peak is capped in height.*

3.7 ppm) by addition of the lipid component. The peak at 2.3 ppm was not considered because of the lower peak intensity difference between both spectra. The intensities of the peaks 0.9 ppm and 3.7 ppm were set in ratio ($A_{\text{Methyl}}/A_{\text{EO}}$) and were plotted against the known lipid-surfactant weight ratios in figure 40 (top) on page 88. A linear fit of the four calibration points was applied and yielded an coefficient of correlation of 0.9996. The resulting equation 1 was used to calculate the lipid to Solutol® HS 15 ratios (x).

$$y = 0.0554 + 0.2488 \times x \qquad\qquad x = \frac{\frac{A_{\text{Methyl}}}{A_{\text{EO}}} - 0.0554}{0.2488} \qquad (1)$$

"y" is substituted by the intensity ratios obtained from the NMR spectra. Figure 40 (bottom) shows the resulting lipid to Solutol® HS 15 ratios of the adsorbate release samples in comparison to the calibration samples. Table 15 on page 89 gives an overview of the calculated ratios as well as lipid and surfactant percentages.

Two reference samples (marked with ×) were measured additionally. Their composition corresponded to the first and last calibration sample. The first was the surfactant component in buffer and last was the complete amount of non-adsorbed pre-concentrate A in buffer. Both samples led to comparable intensity ratios. Consequently, similar percentages for the lipid and surfactant components were obtained compared to the calibration samples.

The results show that the released pre-concentrate which was adsorbed at Fujicalin® and Neusilin® UFL2 has approximately the same composition as the non-adsorbed pre-concentrate in buffer. That means that the measured incomplete release by fluorescence in chapter 3.3.2.2 concerns both components similarly. A change of the initial composition cannot be identified. By contrast, Neusilin® US2 acted differently. The released pre-concentrate showed an altered composition. The lipid component was reduced from originally 60 % to approximately 44 % and the percentage of the surfactant component Solutol® HS 15 was increased respectively. This means that Neusilin® US2 retains more of the mono-/di-/triglycerides at its surface than of the surfactant. It can be assumed that a selective retention of the pre-concentrate components will change the polarity of the emerging system and may have an influence on a dissolved drug. Consequences could be a direct retention of the drug in the acyl glyceride environment at the excipient surface or a subsequent precipitation of the drug.

Supplementary, the percentage release of Solutol® HS 15 and lipids can be calculated from the NMR data. Normally, the release of the lipid component could be calculated directly by use of the peak intenstity ratio of the methyl and the TMSP peak ($A_{\text{Methyl}}/A_{\text{TMSP}}$). In figure 41 on page 90 the ratios of the calibration samples are plotted against the corresponding release of lipids in percent. The high coefficient of correlation of the applied linear fit close to 1 proves the high accuracy for the quantitative calculation.
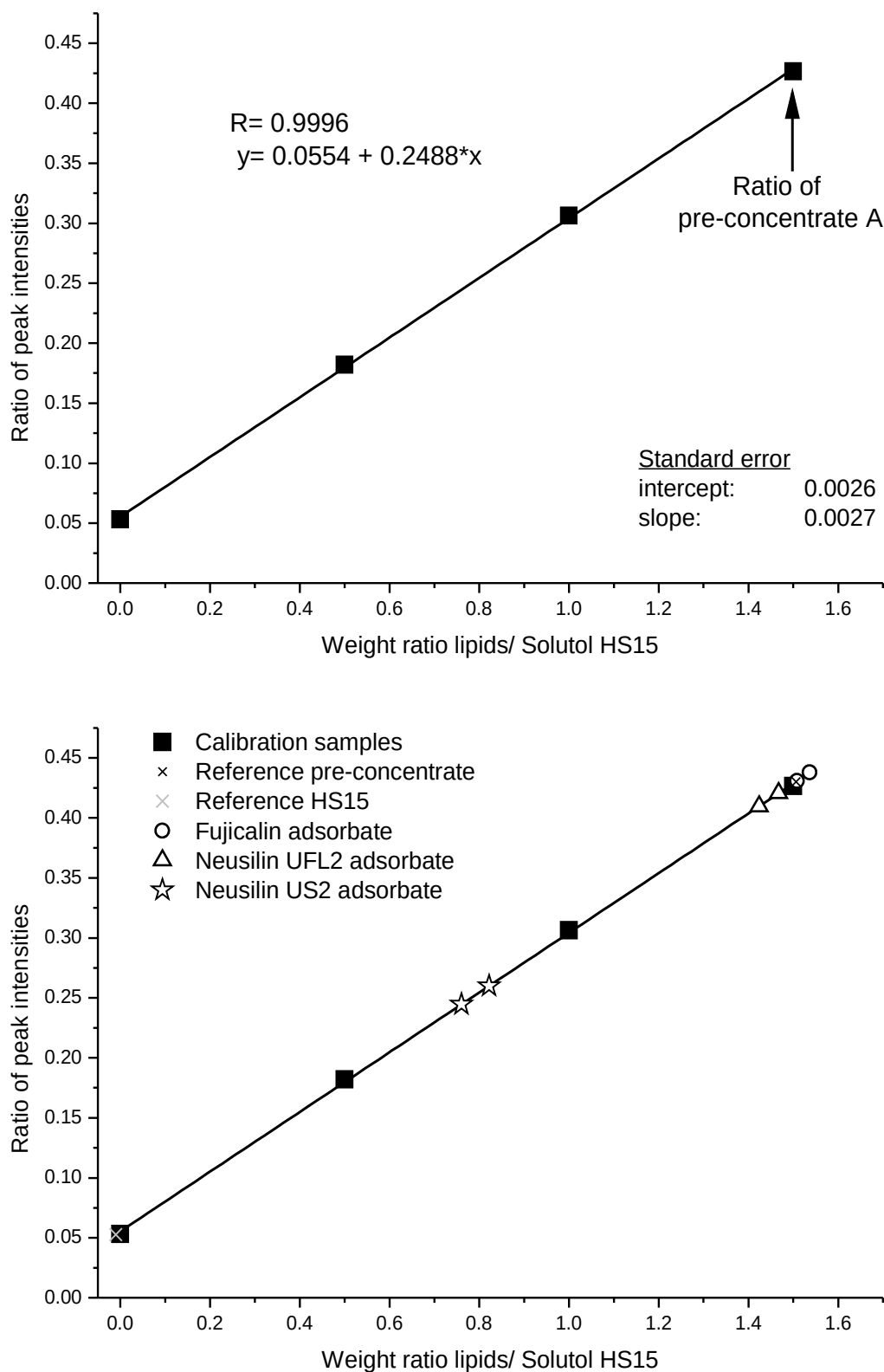
Figure 40: *Intensity ratios (A_{Methyl}/A_{EO}) of the calibration samples (top) and addition-ally with the ratios of the adsorbate samples and two reference samples (bottom) plotted against the lipid to Solutol® HS 15 weight ratio.*

Table 15: *Summary of data from calibration, reference (HS 15 - top, pre-concentrate - bottom) and adsorbate samples of pre-concentrate A. The peak intensity ratio A_{Methyl}/A_{EO} and corresponding/calculated lipid to Solutol® HS 15 weight ratios are presented as well as the calculated percentages of the lipid and surfactant component of the investigated release media. Calculated values are rounded to four decimal places for ratios and are shown as integer for percentages.*

	Intensity ratio $A_{\mathrm{Methyl}}/A_{\mathrm{EO}}$	Ratio lipids to Solutol® HS 15	Lipids [%]	Solutol® HS 15 [%]
Calibration	0.0532	0	0	100
	0.1820	0.5	33	67
	0.3063	1	50	50
	0.4265	1.5	60	40
References	0.0528	-0.0104*	-1*	101
	0.4301	1.5059	60	40
Fujicalin®	0.4378	1.5368	61	39
	0.4307	1.5083	60	40
Neusilin® UFL2	0.4097	1.4240	59	41
	0.4205	1.4675	59	41
Neusilin® US2	0.2600	0.8222	45	55
	0.2446	0.7606	43	57

* Negative values derive from the standard error of the calibration calculation. The standard error is ±4 % based on the residuals from the calibration curve.
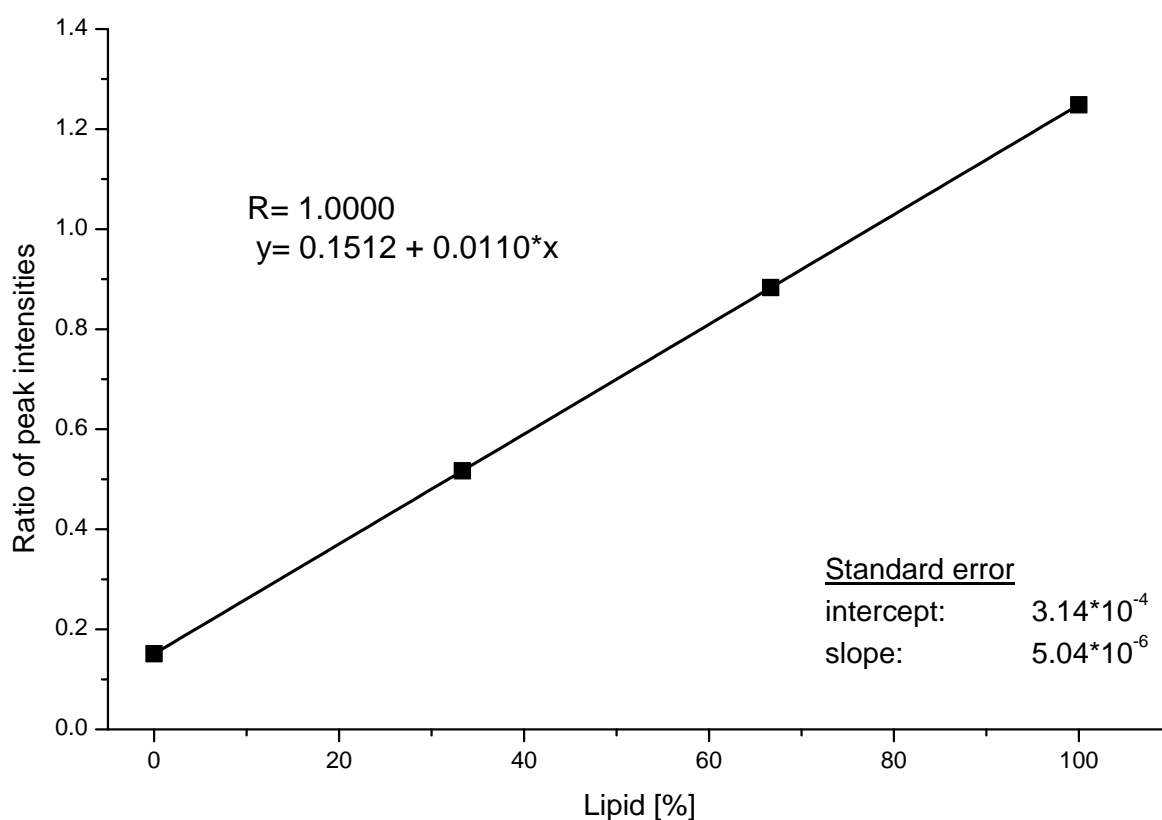
Figure 41: Intensity ratios A_{Methyl}/A_{TMSP} of the calibration samples plotted against the corresponding lipid release in percent.

But this model has one disadvantage. It presumes a 100 % release of Solutol® HS 15 due to the fact that the surfactant also contributes with a small part to the 0.9 ppm peak of the –CH$_3$ group. A 100 % release of Solutol® HS 15 would result in similar ratios of the areas of the ethylene oxide (A_{EO}) and the standard TMSP for reference and adsorbate samples (compare relative peak intensities in table 16 on page 91). By comparing the intensity of ethylene oxide relative to the standard TMSP it is obvious that the reference samples have an intensity around 3 and e.g. for the Neusilin® US2 adsorbate this ratio is decreased to approximately 2. Hence, a calculation based on the equation from figure 41 includes the error of an incomplete release of Solutol® HS 15. Assuming a 0 % release of Solutol® HS 15, a maximum percentage error of 13 % can be expected if the whole amount of lipid would be released. In this case, the integral ratio of 0.05 of the 0.9 ppm peak would count for the lipid part but not be calculated as lipid which causes falsely low lipid percentages. If also the lipid release rate was reduced accompanied with a 0 % release of Solutol® HS 15 the error would even increase.

Even though a 0 % release of Solutol® HS 15 was not observed and thus lower errors can be expected, another approach was chosen. The lipid values were first corrected by subtracting the proportion dedicated to Solutol® HS 15. Therefore, the peak of the NMR

Table 16: *Summary of the peak intensities from NMR spectra relative to the intensity of the standard TMSP and the calculated released percentages of lipids and Solutol®️ HS 15 from reference and adsorbate samples of pre-concentrate A. Relative intensities are rounded to four decimal places and percentages are shown as integer.*

	A_{EO} (3.7 ppm)	A_{Methyl} (0.9 ppm)	Lipids ($w_{\text{Lip}_{\text{rel}}}$) [%]	Solutol®️ HS 15 ($w_{\text{HS15}_{\text{rel}}}$) [%]
HS 15	2.8442	0.1512	-	-
	2.8883	0.1524	-	-
Concentrate	3.0176	1.2979	102	102
	2.9271	1.2483	98	98
Fujicalin®️	3.1885	1.3958	110	107
	3.0269	1.3037	102	102
Neusilin®️ UFL2	2.9178	1.1954	93	98
	2.7799	1.1691	92	94
Neusilin®️ US2	2.2263	0.5787	41	75
	2.1560	0.5274	37	73

standard TMSP was used in relation to the ethylene oxide peak (abbreviated as "EO") in order to calculate the release of Solutol®️ HS 15. The percentage release of Solutol®️ HS 15 (w_{HS15}) is consequently defined by equation (2).

$$w_{\text{HS15}} = \frac{\frac{A_{\text{EO}}}{A_{\text{TMSP}}}}{\frac{A_{\text{EO}_{100\,\%}}}{A_{\text{TMSP}_{100\,\%}}}} = \frac{\frac{A_{\text{EO}}}{A_{\text{TMSP}}}}{2.9723} \tag{2}$$

The peak intensity ratio EO (A_{EO}) to TMSP (A_{TMSP}) of the unknown sample is divided by the equivalent ratio of the pre-concentrate reference sample ($A_{\text{EO}_{100\,\%}}$ to $A_{\text{TMSP}_{100\,\%}}$). These reference values stand for a $100\,\%$ release and the parameters are labelled with "$100\,\%$". The $100\,\%$ release experiment was conducted twice, once as reference sample to the adsorbate experiments and the second was part of the calibration series. Thus, the mean of these calculated $100\,\%$ values was substituted in the equation. In equation (3) on page 92 the relation between the surfactant intensity fraction of the methyl peak ($A_{\text{Methyl}_{\text{HS15}}}$) and the intensity of the EO peak is presented. Both parameters are related to each other with a proportionality factor "k" which was calculated as mean of both Solutol® HS 15 reference samples. The equation was rearranged to "k". Now, this factor could be directly calculated by substituting the values of the HS15 reference samples containing only the amount of Solutol® HS 15 and none of the lipid component. A proximate condition is presented by equation (4). The intensity of the methyl peak (A_{Methyl}) is composed of the proportion of Solutol® HS 15 ($A_{\text{Methyl}_{\text{HS15}}}$) and the proportion of the lipids ($A_{\text{Methyl}_{\text{Lip}}}$) at which $A_{\text{Methyl}_{\text{HS15}}}$ can be substituted by equation (3). The equation can be rearranged to the lipid proportion visible in equation (5).

$$A_{\text{Methyl}_{\text{HS15}}} = A_{\text{EO}} \cdot k \qquad\qquad\qquad k = \frac{A_{\text{Methyl}_{\text{HS15}}}}{A_{\text{EO}}} = 0.0530 \qquad (3)$$

$$A_{\text{Methyl}} = A_{\text{Methyl}_{\text{HS15}}} + A_{\text{Methyl}_{\text{Lip}}} \qquad A_{\text{Methyl}} = A_{\text{EO}} \cdot 0.0530 + A_{\text{Methyl}_{\text{Lip}}} \qquad (4)$$

$$A_{\text{Methyl}_{\text{Lip}}} = A_{\text{Methyl}} - A_{\text{EO}} \cdot 0.0530 \qquad\qquad\qquad (5)$$

Similar to equation (2) the percentage release of lipids is defined in equation (6) and was transformed by substituting $A_{\text{Methyl}_{\text{Lip}}}$ by equation (5). Again, the fraction can be reduced by replacing the $100\,\%$ parameters by its values in equation (7). The final value of 1.1157 represents the mean of both $100\,\%$ reference samples.

$$w_{\text{Lip}} = \frac{\frac{A_{\text{Methyl}_{\text{Lip}}}}{A_{\text{TMSP}}}}{\frac{A_{\text{Methyl}_{\text{Lip}_{100\,\%}}}}{A_{\text{TMSP}_{100\,\%}}}} = \frac{\frac{A_{\text{Methyl}} - A_{\text{EO}} \cdot 0.0530}{A_{\text{TMSP}}}}{\frac{A_{\text{Methyl}_{100\,\%}} - A_{\text{EO}_{100\,\%}} \cdot 0.0530}{A_{\text{TMSP}_{100\,\%}}}} \qquad (6)$$

$$w_{\text{Lip}} = \frac{\frac{A_{\text{Methyl}} - A_{\text{EO}} \cdot 0.0530}{A_{\text{TMSP}}}}{1.1157} \qquad (7)$$

The calculated percentages of released Solutol® HS 15 and released lipids are summarised in table 16. The results of both components confirm the tendency seen from the fluorescence release experiment and part one of the NMR spectroscopy evaluation. The mean of both reference samples yielded a release of $100\,\%$. One of the Fujicalin® measurement series is obviously inaccurate with a result of $110\,\%$ lipid release obviously inaccurate and thus indicates a possible error of $\pm 10\,\%$. The result of released Solutol® HS 15 is

similar and proves that the released pre-concentrate has the initial composition. The second Fujicalin® release study yields a release value of 102 % for both components. This is comparable to the values of the reference sample. Nevertheless, it can be assumed that Fujicalin® neither influences the composition of the desorbed pre-concentrate nor lowers the release rate of both components. The results of both Neusilin® UFL2 samples also confirm the expectations from the fluorescence experiment. The first sample reached an almost complete release of the adsorbed pre-concentrate, the second a slight retention of both components but without any clear influence on the initial composition. Finally, the results of Neusilin® US2 show repeatedly that both components have a lower release quantity than for the other adsorbates and the initial composition of the pre-concentrate was changed to higher percentages of the surfactant. About 40 % release was found for the lipid component and about 74 % for Solutol® HS 15. All in all, the outcome of the previously presented fluorescence experiment has been confirmed. No influence was found on the release quantity for Fujicalin® and a minor influence for Neusilin® UFL2. The lowest release was found for Neusilin® US2. Furthermore, the results of Neusilin® US2 indicate that the release of the lipophilic model DiI is more dependent on the release of the lipid component of the pre-concentrate than on the surfactant. DiI was released to 35 %, which corresponds more to the release rate of the lipid component of averaged 39 % found in the NMR analysis. The stronger dependence of the desorption from the more lipophilic component is also corroborated by the findings of Williams et al. who obtained higher desorption rates for increasing surfactant percentages in the liquid lipid formulation [153].

Analysis of the released pre-concentrate B

The same analysis used for pre-concentrate A was now performed with pre-concentrate B. Calibration samples in deuterated phosphate buffer pH 6.8 were prepared with a constant concentration of the surfactant Cremophor® ELP ($0.025 \frac{g}{ml}$) and increasing Capmul® PG8 concentrations (0; 0.01; 0.015; 0.02 and $0.025 \frac{g}{ml}$). The first calibration sample represents the Cremophor® ELP reference. The last calibration sample represents the reference for a completely released pre-concentrate B in composition and concentration. Figure 42 on page 94 shows NMR spectra of the first sample of the calibration series, Cremophor® ELP in phosphate buffer (top), and the last sample, containing the completely released pre-concentrate B in phosphate buffer (bottom). The spectra resemble those of pre-concentrate A. The peak at a chemical shift of 0 ppm represents again the standard TMSP. In the spectrum below an additional peak appeared at 1.2 ppm between the known –CH$_3$ and –CH$_2$– peaks. This peak can be assigned to the –CH$_3$ group of propylene glycol, component of Capmul® PG8 [190, 195, 196]. The baseline around this peak is not clearly differentiated from the –CH$_2$– at 1.3 ppm. This is why the same relevant peaks, the aliphatic –CH$_3$ end group at 0.9 ppm and the ethylene oxide group peak at 3.7 ppm,
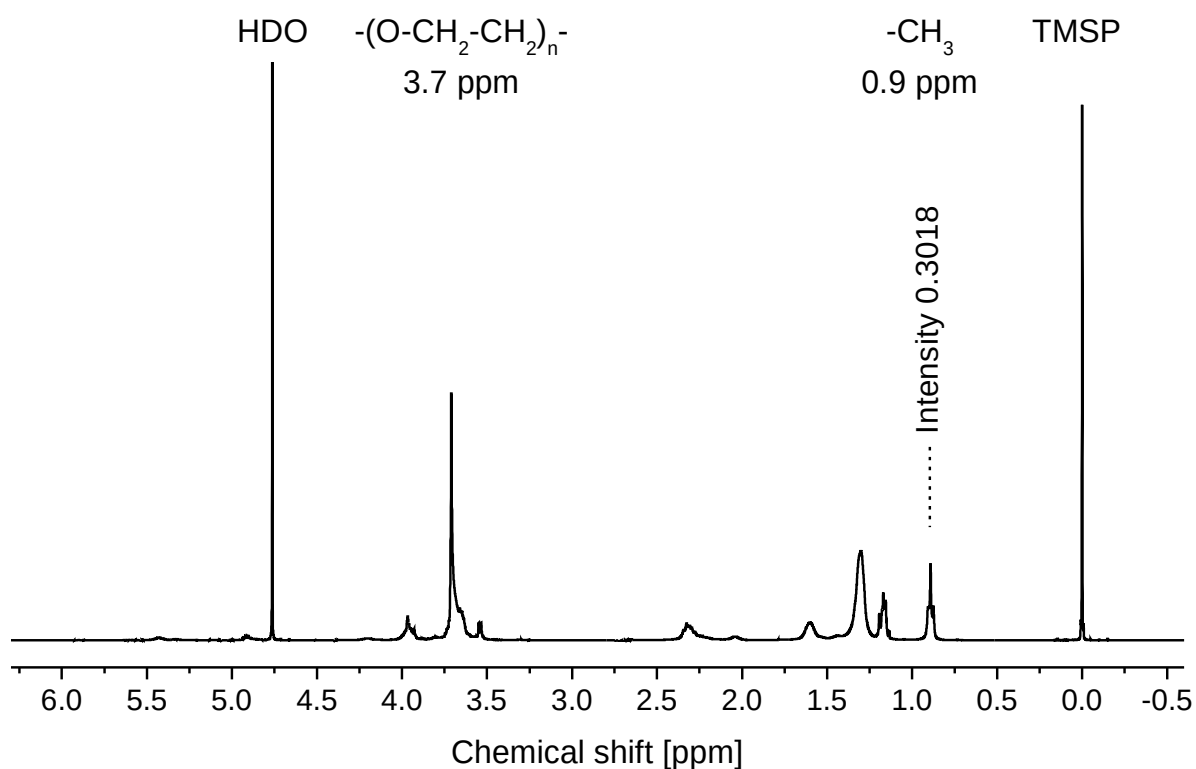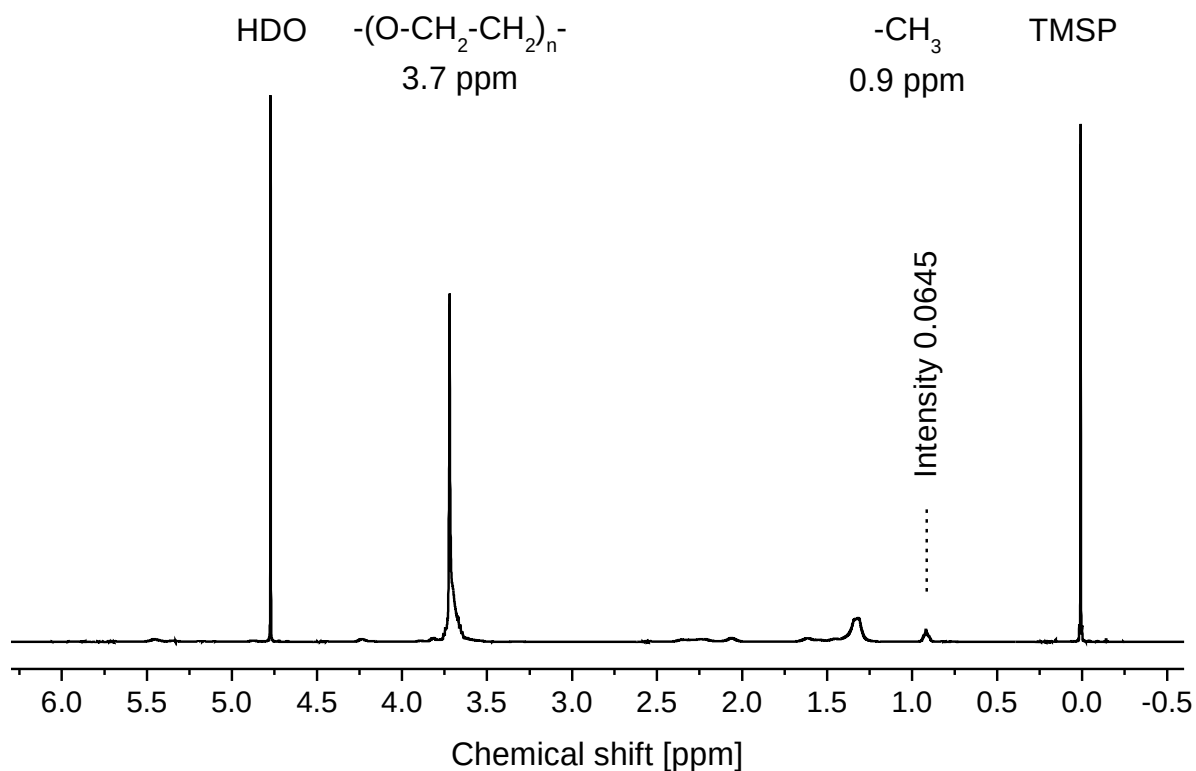
Figure 42: *NMR spectra of Cremophor® ELP (top) and pre-concentrate B (bottom) in buffer. Chemical shifts are assigned relative to the standard TMSP. The –CH₃ peak intensity is indicated relative to the ethylene oxide peak intensity. The HDO peak is capped in height.*

were chosen for evaluation. Compared to the spectrum of Cremophor® ELP the peak at 0.9 ppm in the spectrum below is increased due to the presence of the propylene glycole caprylate (Capmul® PG8). A summary of all NMR spectra can be found in figures 56, 57, 58, 59, 60, 61 and 62 on pages xiii, xiv, xv, xvi, xvii, xviii and xix (appendix).

According to the example pre-concentrate A, the ratios of peak intensities of the methyl and EO peak were calculated ($A_{\text{Methyl}}/A_{\text{EO}}$) and were plotted against the known Capmul® PG8-Cremophor® ELP weight ratios in figure 43 (top) on page 96. A linear fit of the five calibration points was applied and yielded a coefficient of correlation of 0.9930. The resulting equation 8 on page 95 was used to calculate the Capmul® PG8 to Cremophor® ELP ratios (x) of the adsorbate release samples. "y" was substituted by the intensity ratios obtained from the NMR spectra. Figure 43 (bottom) shows the resulting Capmul® PG8 to Cremophor® ELP ratios of the adsorbate release samples in comparison to the calibration samples. Table 17 on page 97 gives an overview of the calculated ratios and the Capmul® PG8 and Cremophor® ELP percentages.

$$y = 0.0700 + 0.2404 \times x \qquad\qquad x = \frac{\frac{A_{\text{Methyl}}}{A_{\text{EO}}} - 0.0700}{0.2404} \tag{8}$$

Two reference samples (marked with ×) were measured additionally as performed for pre-concentrate A. Similar percentages were calculated for the Capmul® PG8 and the Cremophor® ELP component compared to the calibration samples. The higher standard error may be attributed to the slight turbidity found for diluted pre-concentrate B samples.

The samples of pre-concentrate B show similar tendencies as found for pre-concentrate A. The pre-concentrate released from Fujicalin® and Neusilin® UFL2 has approximately the same composition as the non-adsorbed pre-concentrate in buffer. Both excipients do not alter the initial composition. For the Neusilin® US2 excipient a slightly reduced release of Capmul® PG8 is visible (from 50 % to approximately 45 %). But, this effect is considerably less pronounced as for pre-concentrate A. One reason could be the more hydrophilic properties of Capmul® PG8 compared to the lipid mixture of Capmul® MCM C10 and Captex® 355 EP/NF. Lipids with rather hydrophilic properties seem to have a weaker binding to the surface of Neusilin® particles. By contact to a hydrophilic buffer medium this lipid desorbs more easily from the excipient's surface. This explains the different results between the single Neusilin® US2 samples. While having a lower affinity to the Neusilin® US2 excipient mechanical stress during the release procedure will have a greater impact and can lead to the different outcomes for composition and release of the pre-concentrate.

The percentage release of Cremophor® ELP and Capmul® PG8 were calculated from the NMR data according to the method used for pre-concentrate A. The linear correlation of the intensity ratio ($A_{\text{EO}}/A_{\text{TMSP}}$) to the PG8 release in percent is shown in figure 44
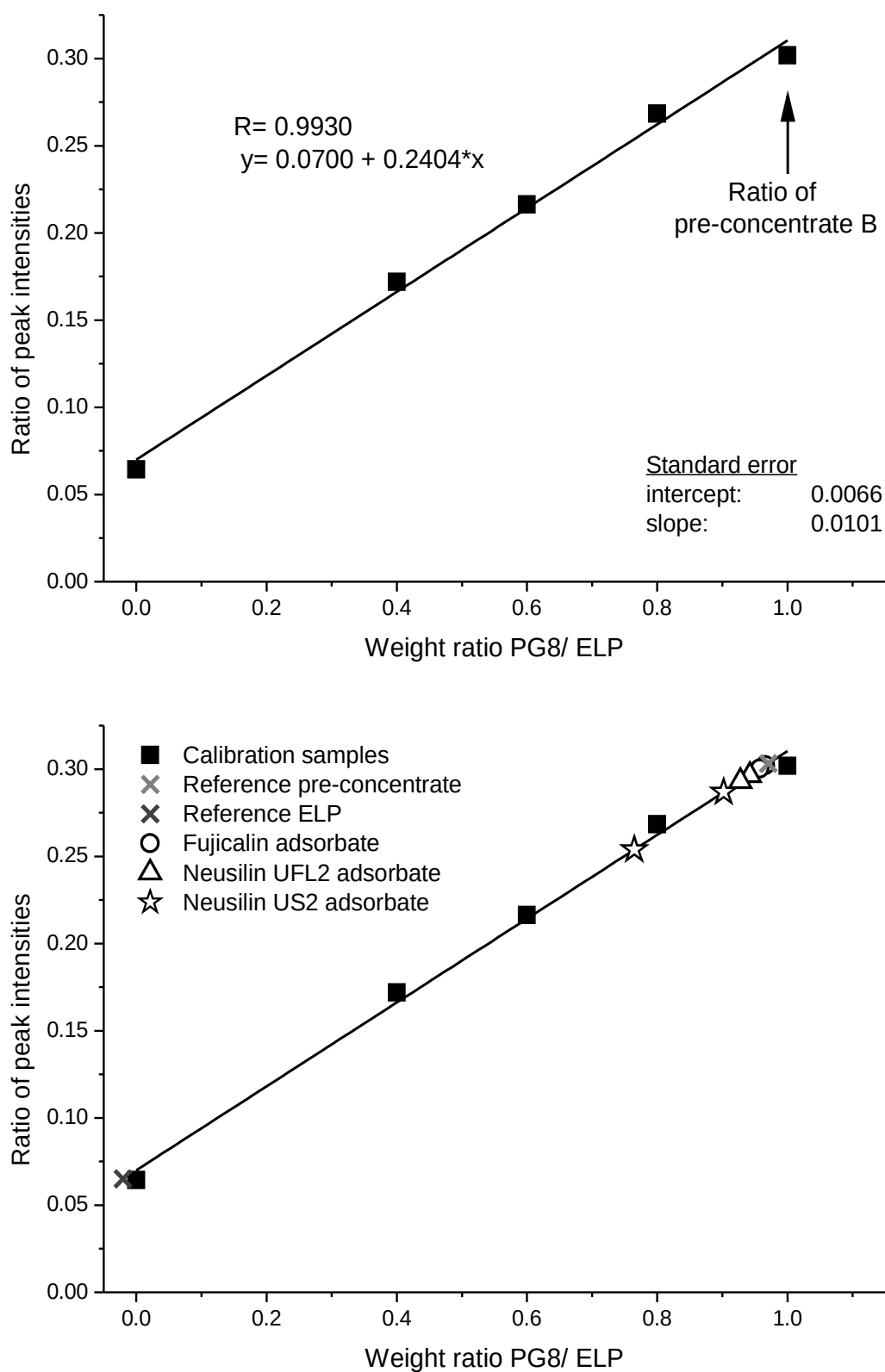
Figure 43: *Intensity ratios (A_{Methyl}/A_{EO}) of the calibration samples (top) and additionally with the ratios of the adsorbate samples and two reference samples (bottom) plotted against the Capmul® PG8 to Cremophor® ELP weight ratio.*

Table 17: *Summary of data from calibration, reference (ELP - top, pre-concentrate - bottom) and adsorbate samples of pre-concentrate B. The peak intensity ratio A_{Methyl}/A_{EO} and corresponding/calculated Capmul® PG8 to Cremophor® ELP weight ratios are presented as well as the calculated percentages of Capmul® PG8 and Cremophor® ELP of the investigated release media. Calculated values are rounded to four decimal places for ratios and are shown as integer for percentages.*

	Intensity ratio $A_{\mathrm{Methyl}}/A_{\mathrm{EO}}$	Ratio Capmul® PG8 to Cremophor® ELP	Capmul® PG8 [%]	Cremophor® ELP [%]
Calibration	0.0645	0	0	100
	0.1719	0.4	29	71
	0.2164	0.6	37.5	62.5
	0.2685	0.8	44	56
	0.3018	1	50	50
References	0.0651	-0.0206*	-2*	102
	0.3032	0.9703	49	51
Fujicalin®	0.3022	0.9661	49	51
	0.3002	0.9577	49	51
Neusilin® UFL2	0.2965	0.9421	49	51
	0.2931	0.9280	48	52
Neusilin® US2	0.2896	0.9021	47	53
	0.2538	0.7647	43	57

* Negative values derive from the standard error of the calibration calculation. The standard error is ±8 % based on the residuals from the calibration curve.
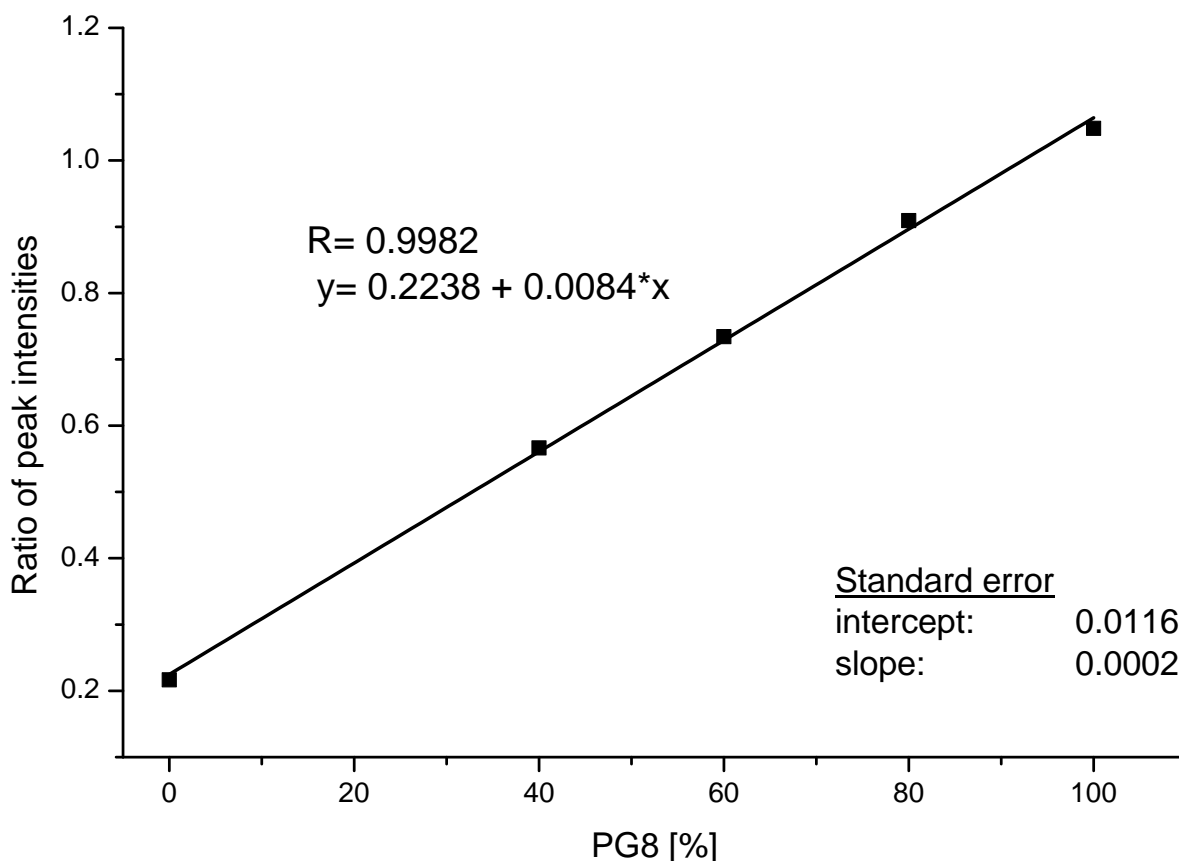
Figure 44: Intensity ratios of the calibration samples plotted against the corresponding lipid release in percent.

on page 98. The coefficient of correlation of the applied linear fit amounts to 0.9982. Again, the use of this correlation presumes a 100 % release of Cremophor® ELP. This is not the case because the peak intensity ratios of the ethylene oxide group (A_{EO}) and the standard TMSP (A_{TMSP}) differ from 3.5 for the pre-concentrate references to ratios below 3 for Neusilin® US2 adsorbate samples (compare table 18 on page 100). Therefore, the peak intensity of the –CH$_3$ group was corrected by subtracting the proportion dedicated to Cremophor® ELP. The percentage release of Cremophor® ELP (w_{ELP}) is defined by equation (9). The peak intensity ratio EO (A_{EO}) to TMSP (A_{TMSP}) of the unknown sample is divided by the same ratio of the pre-concentrate reference sample ($A_{\text{EO}_{100\,\%}}$ to $A_{\text{TMSP}_{100\,\%}}$). The mean of both samples was substituted in the equations.

$$w_{\text{ELP}} = \frac{\frac{A_{\text{EO}}}{A_{\text{TMSP}}}}{\frac{A_{\text{EO}_{100\,\%}}}{A_{\text{TMSP}_{100\,\%}}}} = \frac{\frac{A_{\text{EO}}}{A_{\text{TMSP}}}}{3.4811} \tag{9}$$

Equation (10) shows the relation between the surfactant intensity fraction of the –CH$_3$ peak ($A_{\text{Methyl}_{\text{ELP}}}$) and the intensity of the EO peak. The equation was rearranged to the proportionality factor "k". It was calculated as mean of both Cremophor® ELP reference

samples. In equation (11) the intensity of the $-CH_3$ peak (A_{Methyl}) is composed of the proportion of Cremophor® ELP ($A_{\text{Methyl}_{\text{ELP}}}$) and the proportion of Capmul® PG8 ($A_{\text{Methyl}_{\text{PG8}}}$). $A_{\text{Methyl}_{\text{ELP}}}$ can be substituted by equation (10). The equation can be rearranged to the PG8 proportion shown in equation (12). Similar to equation (9) the percentage release of PG8 is defined in equation (13). $A_{\text{Methyl}_{\text{PG8}}}$ was substituted by equation (12). Again, the fraction can be reduced by replacing the 100 % parameters by its values in equation (14). The final value of 0.8277 represents the mean of both pre-concentrate reference samples.

$$A_{\text{Methyl}_{\text{ELP}}} = A_{\text{EO}} \cdot k \qquad\qquad\qquad k = \frac{A_{\text{Methyl}_{\text{ELP}}}}{A_{\text{EO}}} = 0.0648 \qquad (10)$$

$$A_{\text{Methyl}} = A_{\text{Methyl}_{\text{ELP}}} + A_{\text{Methyl}_{\text{PG8}}} \qquad A_{\text{Methyl}} = A_{\text{EO}} \cdot 0.0648 + A_{\text{Methyl}_{\text{PG8}}} \qquad (11)$$

$$A_{\text{Methyl}_{\text{PG8}}} = A_{\text{Methyl}} - A_{\text{EO}} \cdot 0.0648 \qquad (12)$$

$$w_{\text{PG8}} = \frac{\frac{A_{\text{Methyl}_{\text{PG8}}}}{A_{\text{TMSP}}}}{\frac{A_{\text{Methyl}_{\text{PG8}_{100\,\%}}}}{A_{\text{TMSP}_{100\,\%}}}} = \frac{\frac{A_{\text{Methyl}} - A_{\text{EO}} \cdot 0.0648}{A_{\text{TMSP}}}}{\frac{A_{\text{Methyl}_{100\,\%}} - A_{\text{EO}_{100\,\%}} \cdot 0.0648}{A_{\text{TMSP}_{100\,\%}}}} \qquad (13)$$

$$w_{\text{PG8}} = \frac{\frac{A_{\text{Methyl}} - A_{\text{EO}} \cdot 0.0648}{A_{\text{TMSP}}}}{0.8277} \qquad (14)$$

The calculated percentages of released Cremophor® ELP and released Capmul® PG8 are summarised in table 18. Fujicalin® shows an 100 % release of the adsorbed pre-concentrate B. Approximately 90 % was desorbed from Neusilin® UFL2 without any difference between both components. The PG8 release of Neusilin® UFL2 (86–89 %) is comparable to the result of the DiI release of 84 % in figure 37. The contrast to Neusilin® US2 is less pronounced than it was for pre-concentrate A. Sample 1 showed a surfactant release of approximately 80 %, sample 2 of 65 %. The release of the lipid component PG8 is lower compared to the surfactant component. The reason for generally smaller differences between the excipients could be explained by the lower lipophilic properties of Capmul® PG8 compared to Capmul® MCM C10 and Captex® 355. Consequently, the affinity to desorb into an aqueous system is increased. This also explains the findings by Williams et al. who obtained a higher desorption rate for increasing surfactant percentages in lipid based formulations. Sample 2 of Neusilin® US2 with circa 50 % of released Capmul® PG8 is comparable to the release rate of 47 % DiI. This supports the conclusion that mostly the lipid component is responsible for the release of the dissolved lipophilic compound. The varying results between both Neusilin® US2 samples can be explained by weaker interactions between pre-concentrate B and Neusilin® US2. Hence, mechanical stress caused by the experimental release procedure could more easily influence the amount of desorbed pre-concentrate B.

Table 18: *Summary of the peak intensities from NMR spectra relative to the intensity of the standard TMSP and the calculated released percentages of Capmul® PG8 and Cremophor® ELP from reference and adsorbate samples of pre-concentrate B. Relative intensities are rounded to four decimal places and percentages are shown as integer.*

	A_{EO} (3.7 ppm)	A_{Methyl} (0.9 ppm)	Capmul® PG8 $(w_{\mathrm{PG8_{rel}}})$ [%]	Cremophor® ELP $(w_{\mathrm{ELP_{rel}}})$ [%]
ELP	3.3136	0.2156	-	-
	3.3314	0.2148	-	-
Concentrate	3.4552	1.0429	99	99
	3.5073	1.0636	101	101
Fujicalin®	3.5864	1.0839	103	103
	3.5065	1.0527	100	101
Neusilin® UFL2	3.1963	0.9476	89	92
	3.1259	0.9161	86	90
Neusilin® US2	2.8784	0.8257	77	83
	2.2581	0.5731	52	65

4. Summary and perspectives

During this thesis it was shown that lipid adsorbates of Fujicalin®, Neusilin® US2 and Neusilin® UFL2 with different lipid formulation systems could be obtained by standard mixing technologies. Two simple homogenisation methods, mortar/pestle and dual asymmetric centrifugation (SpeedMixer™), were successfully applied. For Fujicalin® and Neusilin® US2, a more homogeneous MCT distribution and a smoother adsorbate particle surface were found for the production by SpeedMixer™ compared to the mortar/pestle method. An advantage of the SpeedMixer™ method is not apparent for the adsorbent Neusilin® UFL2. On the contrary, there was a tendency for bigger agglomerates with MCT. With help of helium pycnometry it was confirmed that both homogenisation methods mostly lead to an adsorption at the surface of the particles and into pores close to the particle's surface but hardly into the inner pores. These could only be reached due to particle destruction occurring during homogenisation per mortar/pestle. The results of NMR relaxometry and ESR spectroscopy detected an increase in the microviscosity of MCT by application of the SpeedMixer™ method. Consequently, the adsorption of MCT is stronger if homogenisation took place by SpeedMixer™ compared to mortar/pestle. This effect was strongly pronounced for Fujicalin®, less for Neusilin® UFL2 and hardly for Neusilin® US2. But release studies did not show any influence on lipid desorption from Fujicalin®. An impact of the homogenisation method on the micropolarity in the lipid environment was not observed. All in all, the SpeedMixer™ is the more feasible method because of the better reproducibility and applicability from the industrial point of view. Based on the results of this thesis it will be necessary to test other homogenisation technologies often used in industrial solid formulation as rotary-drum mixing (e.g. the double cone mixer). Furthermore, the feasibility of a scale-up should be investigated regarding reproducibility and homogeneity.

NMR relaxometry and ESR spectroscopy were successfully applied to figure out the different adsorption properties of the adsorbents. The microviscosity served as measure for differences in their adsorption strength for MCT. This parameter was most reduced for the Neusilin® US2 adsorbate. Consequently, this excipient exhibits the highest adsorption strength followed by Neusilin® UFL2 and Fujicalin®. All adsorbents were sensitive to the relative humidity concerning their adsorption strength but reacted in different humidity ranges. For Fujicalin®, the shift in the microviscosity of MCT happened at lower relative humidity. Both Neusilin® types showed an decrease of the microviscosity at more humid conditions. All in all, storage conditions turned out to be a crucial factor for lipid adsorbates regarding the adsorbing capacity and adsorption strength of the adsorbents and should therefore be controlled. Interesting results were obtained regarding the micropolarity. ESR and multispectral fluorescence imaging detected an increased polarity

in the adsorbed MCT environment for both Neusilin® adsorbents. No influence on the micropolarity was found for Fujicalin®. The higher micropolarity could possibly impact a poorly water-soluble drug dissolved in the adsorbed oil. Further studies with different oils would be interesting in order to see an impact of the oil composition, e.g. medium versus long-chain or saturated versus non-saturated components.

The impact of a pharmaceutical process on the adsorption state of the liquid is an important issue for future industrial applications. The extrusion/spheronization process was chosen using the example of Fujicalin® and a known self-emulsifying system. It was possible to produce visually spherical pellets. In addition to the conventional extrusion/spheronization aid MCC, pellets could also be obtained by use of pea starch as filling excipient additional to the adsorbate. The extrusion with MCC has an impact on the adsorption state of the liquid mixture resulting in a higher microviscosity and therefore stronger adsorption. This strong alteration was not observed for extrusion with pea starch. Prospectively, more investigations with starches in combination with Fujicalin® should be performed with e.g. starches of different sources and with increasing Fujicalin® contents. Higher Fujicalin® percentages could improve the physical stability of the pellets and would increase the capacity for liquid adsorption. Furthermore, the Neusilin® excipients were not included in the present study and should be investigated as well. Moreover, future studies should also include the direct compression process because direct compression into tablets is a favoured pharmaceutical process. It would be interesting to see the impact of e.g. the compression force on the adsorption state of an adsorbed liquid to get knowledge about the risk of oil leakage.

Finally, release experiments using different analytical methods were performed. According to the results of NMR relaxometry and multispectral fluorescence imaging, a complete desorption appeared to be probable, but the images obtained by MRI suggested a rather different desorption behaviour of MCT between Fujicalin® and Neusilin®. Deeper insights into the release characteristic were obtained by investigation of self-(micro)emulsifying adsorbates. Thereby, an impact of the adsorption strength on the desorption was found as expected. A new self-(micro)emulsifying system modified from the mixture of Ahmed Abdalla was developed and investigated in comparison to a more polar self-(micro)emulsifying system from the literature. The performed visual study with the lipophilic dye Sudan red verified the assumption of a poorer desorption from Neusilin® excipients. This was finally confirmed by a fluorescence study with the lipophilic fluorescence dye DiI. The analysis of the desorbed pre-concentrate indicated a complete release of the dye from the Fujicalin® adsorbate but a release of less than 50 % from the Neusilin® US2 adsorbate. The higher release of approximately 80 % for Neusilin® UFL2 was probably caused by the presence of agglomerates containing an increased proportion of liquid. The results of ^{1}H NMR spectroscopy of the released pre-concentrate

offered significant indications for a selective release of multi-component lipid systems. The applied adsorption at Fujicalin® and Neusilin® UFL2 did not impact the composition of the released self-emulsifying systems, whereas for Neusilin® US2, the more lipophilic self-emulsifying system showed an altered composition after desorption. The surfactant proportions were increased compared to the original mixture (from 40 % 55 % for pre-concentrate A). The more lipophilic mono,-di-and triglycerides of the mixture tend to retain at the surface of the Neusilin® US2 particles because of their poorer affinity to an aqueous buffer medium. The impact on the composition of the pre-concentrate B was lower because the component Capmul® PG8 is more hydrophilic than Capmul® MCM C10 and Captex® 355. It was additionally found that the released proportions of the fluorescence dye DiI correspond approximately to the released proportions resulting from ¹H NMR spectroscopy data of the more lipophilic component of both mixtures. The highly lipophilic dye DiI is predominantly located in the more lipophilic component of the self-emulsifying systems. The release of this dye is controlled by the release of the more lipophilic component. A change in the composition of a lipid system can be crucial for the release profile of a poorly water-soluble drug, not only by the overall desorption quantity of the lipid mixture but also by an increase of the more polar component. Consequently, an impact on the performance of the lipid formulation e.g. drug precipitation cannot be excluded.

In summary, Fujicalin® is the most suitable and promising adsorbent among the studied excipients. Although it exhibits the weakest oil adsorbing capacity and adsorption strength, it ensures a constant micropolarity and release property of the lipid system and moreover a complete desorption. Neusilin® UFL2 shows a high oil adsorption strength with impact on the micropolarity and a slight impact on the desorption. The tendency for agglomeration and inhomogeneous lipid distribution is a disadvantage and probably caused the better release outcome. Neusilin® US2 showed a strong influence on the lipid system, e.g. micropolarity, incomplete and selective desorption. More investigations are necessary to get a thorough understanding of adsorption processes at Neusilin®. Multi-component lipid formulation systems of type II to IV should be studied according to their desorption properties. The impact of APIs of different polarity in effective dosage should be investigated. The analytic procedure presented in this thesis makes it easier to select excipients for use in solid lipid adsorbates. The chemical and mechanical stress for an adsorbate formulation in the gastrointestinal system would not be sufficiently covered by use of a buffer medium in an end-over-end device. Selected formulations should be further investigated in simulated gastric and intestinal fluid and preferably in a simulated gastric and intestinal environment to obtain more knowledge about the performance in the gastrointestinal tract.

A. Supplementary Material

Table 19: *Values of absolute density of pure excipients and their MCT adsorbates: F - Fujicalin®, US - Neusilin® US2, UFL - Neusilin® UFL2; number - percentage of adsorbed MCT; (M) - mortar/pestle, (S) - SpeedMixer™.*

| Sample	Absolute density ρ $[\frac{g}{cm^3}]$				ρ (calc.) $[\frac{g}{cm^3}]$	Difference $[\frac{g}{cm^3}]$	
	$\bar{x}_1$	σ_1	$\bar{x}_2$	σ_2		[1]	[2]
F	2.8450	0.0033	2.8500	0.0031	-	-	
F10(M)	2.4582	0.0036	2.4524	0.0028	2.6573	0.1991	0.2049
F10(S)	2.4428	0.0023	2.4285	0.0022		0.2145	0.2288
F30(M)	1.8009	0.0012	1.8142	0.0012	2.2769	0.4760	0.4627
F30(S)	1.8059	0.0017	1.8088	0.0012		0.4710	0.4681
F50(M)	1.4485	0.0004	1.4487	0.0008	1.8965	0.4480	0.4478
F50(S)	1.4434	0.0004	1.4368	0.0008		0.4531	0.4597
US	2.1718	0.0052	2.1679	0.0038	-	-	
US10(M)	1.9571	0.0036	1.9526	0.0026	2.0475	0.0904	0.0949
US10(S)	1.9401	0.0038	1.9432	0.0034		0.1074	0.1043
US30(M)	1.6272	0.0033	1.6170	0.0017	1.8026	0.1754	0.1856
US30(S)	1.6032	0.0013	1.5908	0.0019		0.1994	0.2118
US50(M)	1.3570	0.0008	1.3506	0.0009	1.5577	0.2007	0.2071
US50(S)	1.3489	0.0009	1.3504	0.0009		0.2088	0.2073
UFL	2.2345	0.0083	2.2345	0.0048	-	-	
UFL10(M)	2.0719	0.0019	2.0646	0.0048	2.1056	0.0337	0.0410
UFL10(S)	2.0326	0.0010	2.0380	0.0046		0.0730	0.0676
UFL30(M)	1.6605	0.0048	1.6500	0.0033	1.8478	0.1873	0.1978
UFL30(S)	1.6383	0.0021	1.6402	0.0007		0.2095	0.2076
UFL50(M)	1.3573	0.0013	1.3640	0.0002	1.5900	0.2327	0.2260
UFL50(S)	1.3546	0.0018	1.3612	0.0012		0.2354	0.2288
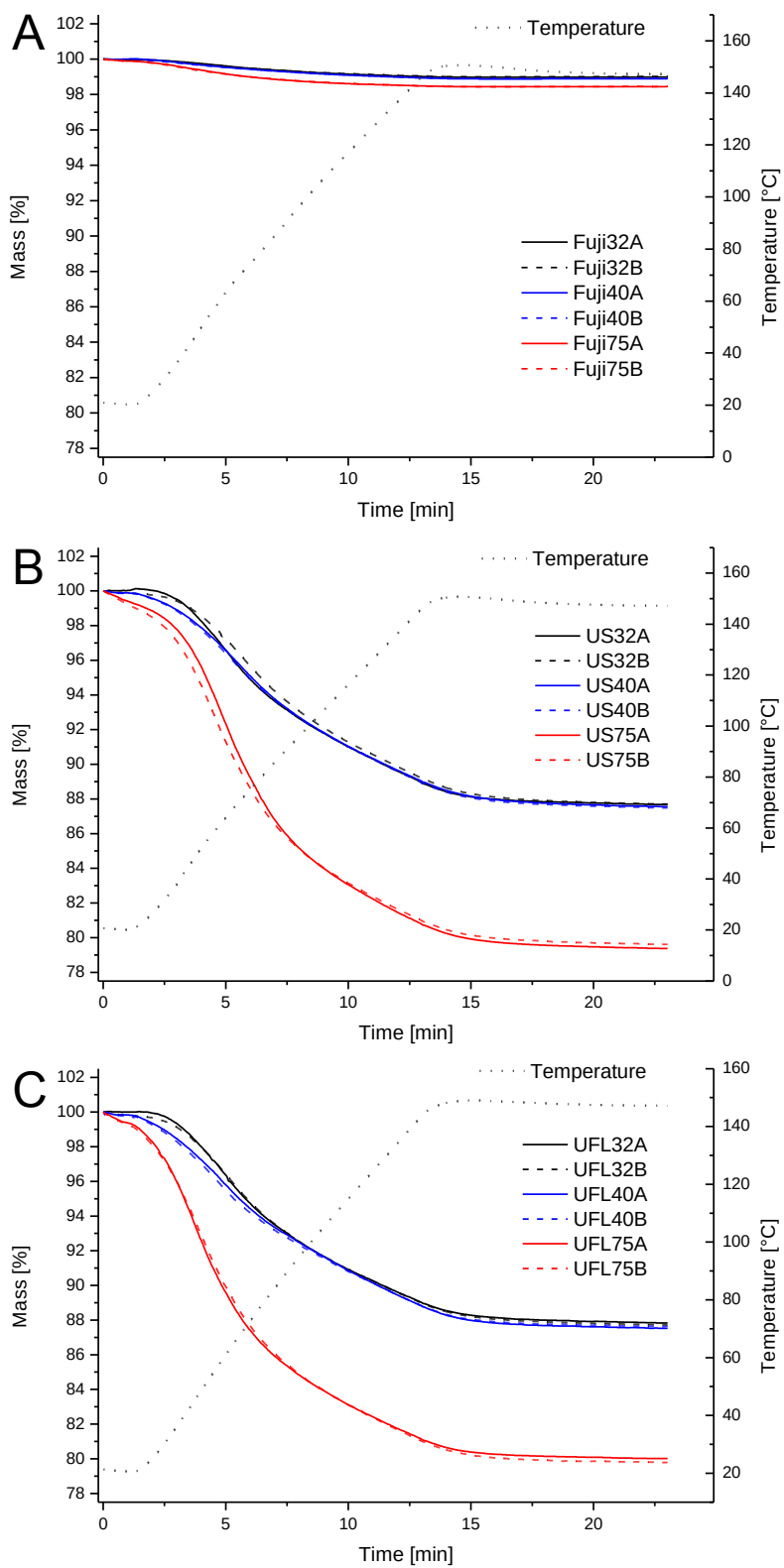
Figure 45: *Thermogravimetry data of : A Fujicalin®, B Neusilin® US2 and C Neusilin® UFL2 stored at 32 %RH, 40 %RH and 75 %RH. Analyses were conducted with n = 2.*
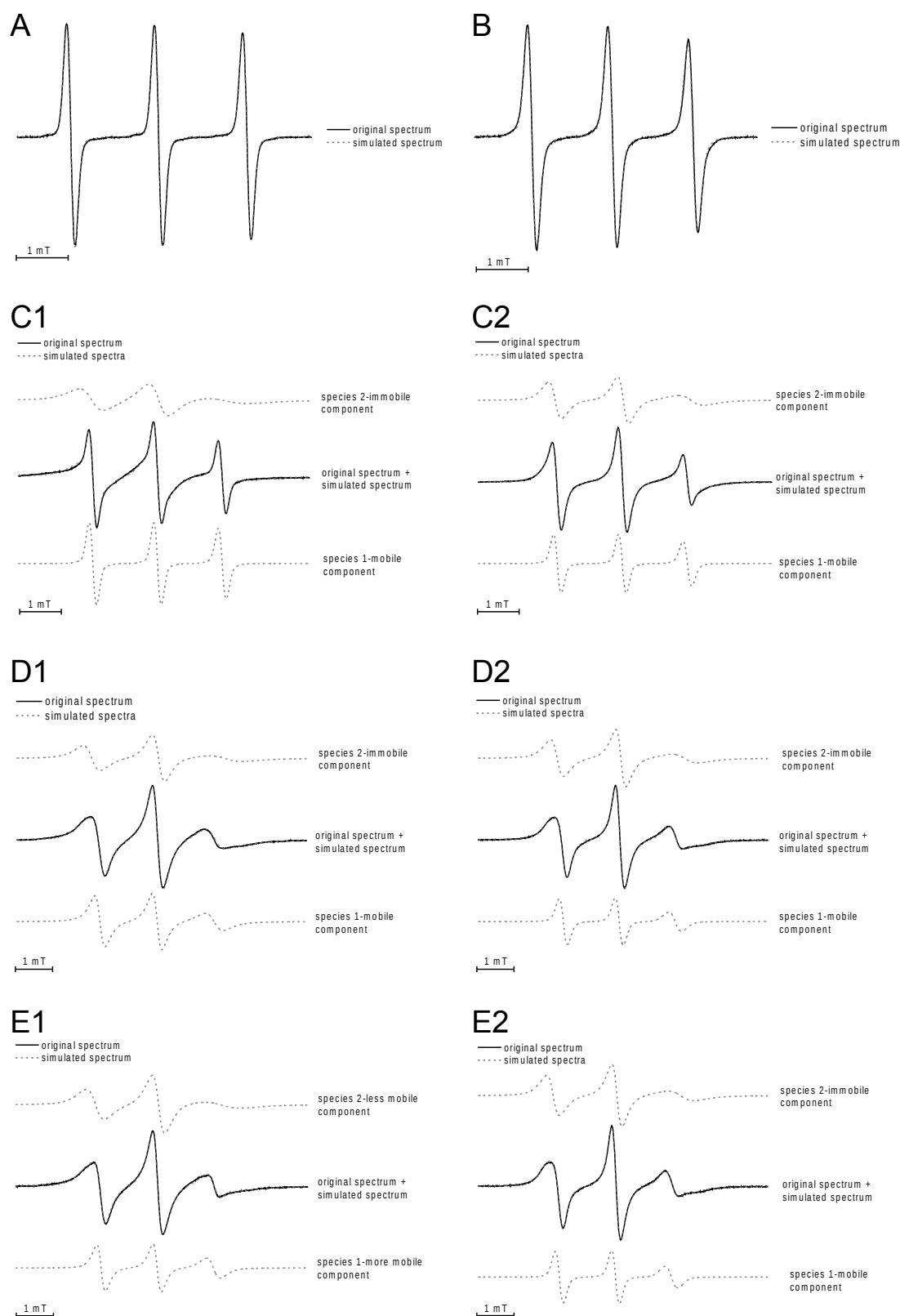
Figure 46: *Compilation of the ESR spectra of TEMPOL in reference solvents and MCT-adsorbates - original spectra and the corresponding simulated species. Graphic illustrations with number (1) are adsorbates produced with the SpeedMixer™ technique and with number (2) by the mortar/pestle method: (A) Water, (B) MCT, (C1+C2) MCT adsorbate at Fujicalin®, (D1+D2) MCT adsorbate at Neusilin® US2, (E1+E2) MCT adsorbate at Neusilin® UFL2.*
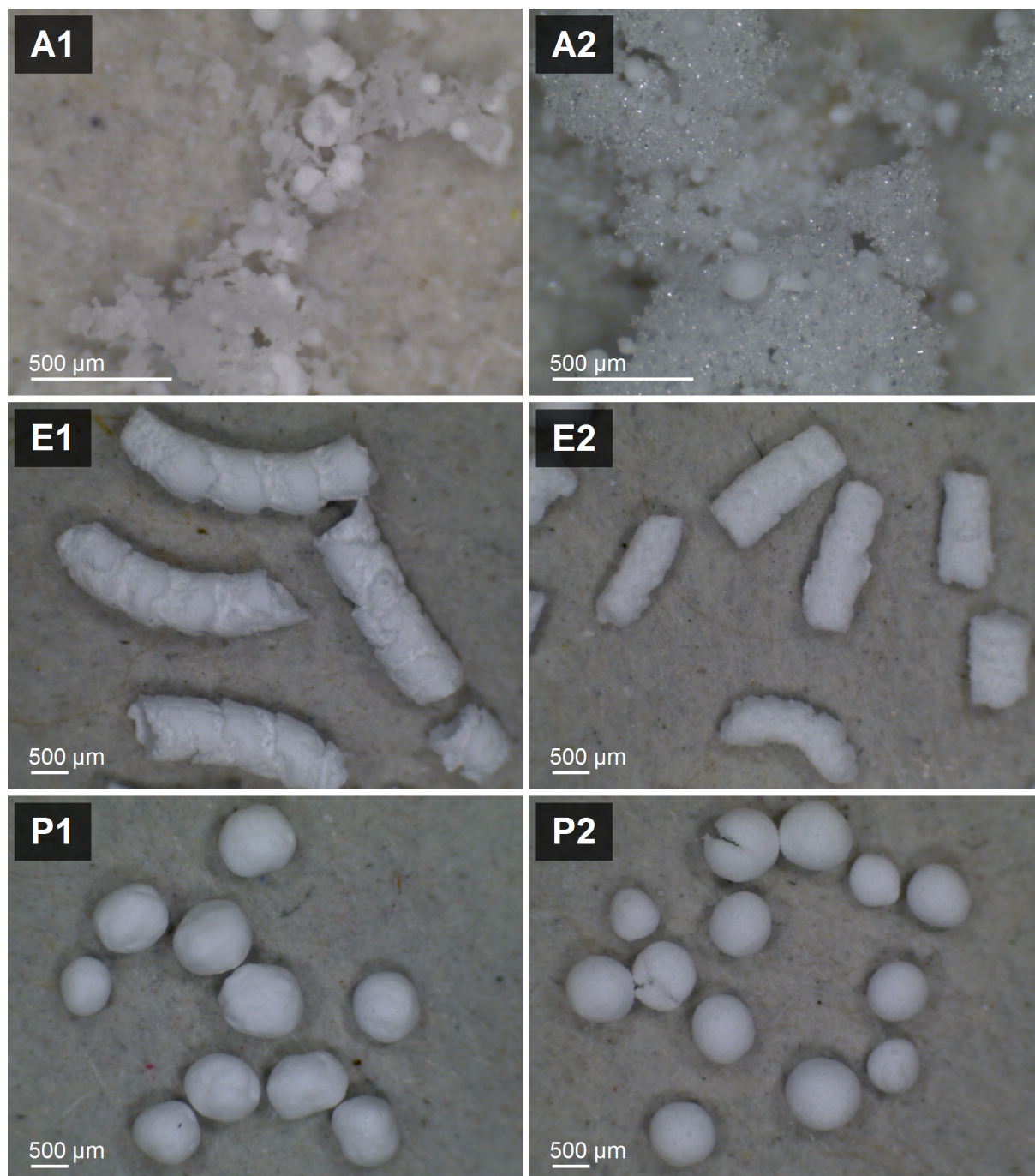
Figure 47: *Micrographs of a Fujicalin® adsorbate as blend (A), as extrudate (E) and pellet (P). Left (1): In combination with MCC. Right (2): In combination with pea starch.*
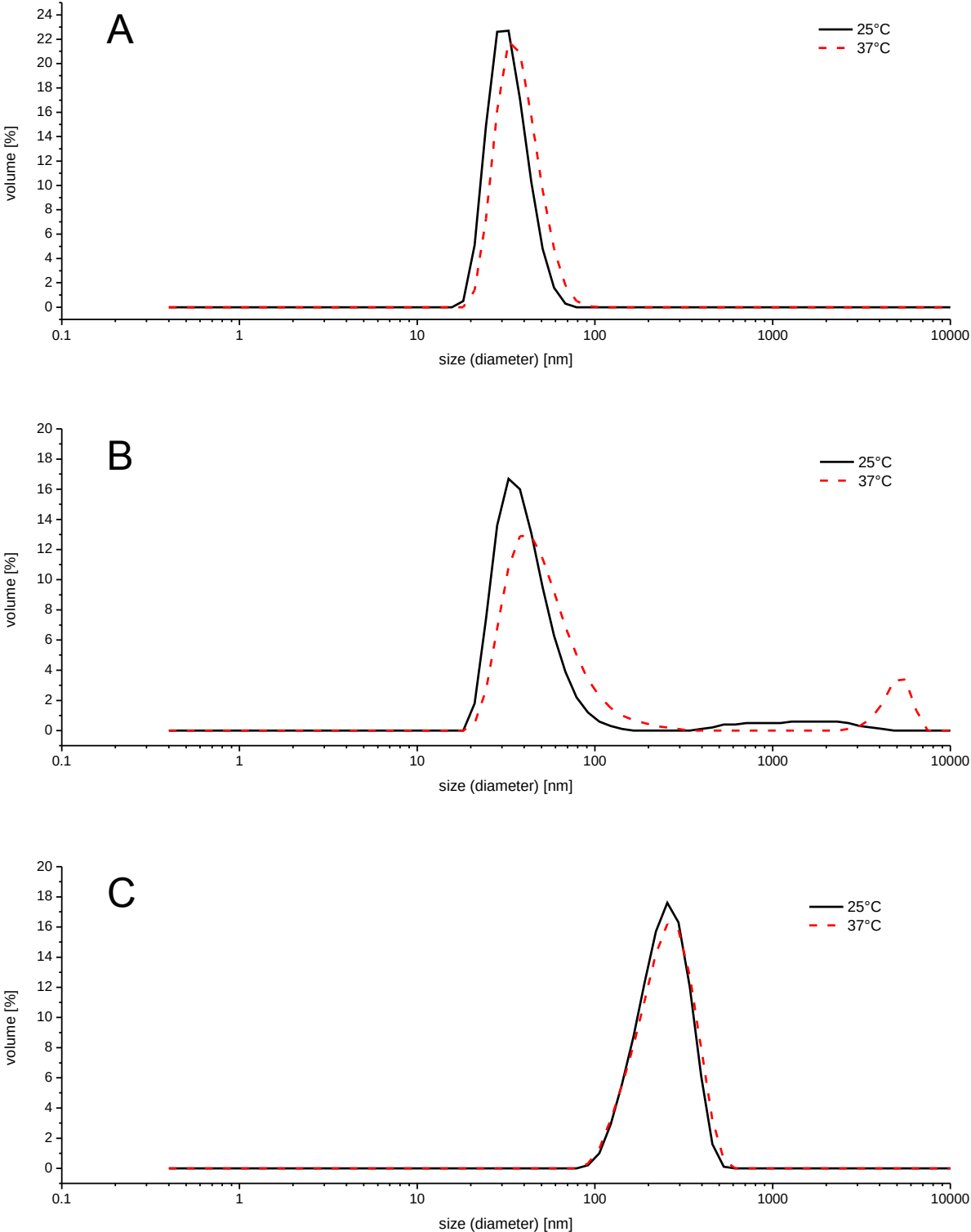
Figure 48: *Volume distribution of pre-concentrates A, B and C in distilled water at* 25 °C *(black line) and* 37 °C *(red line). (A) pre-concentrate A, (B) pre-concentrate B and (C) pre-concentrate C.*
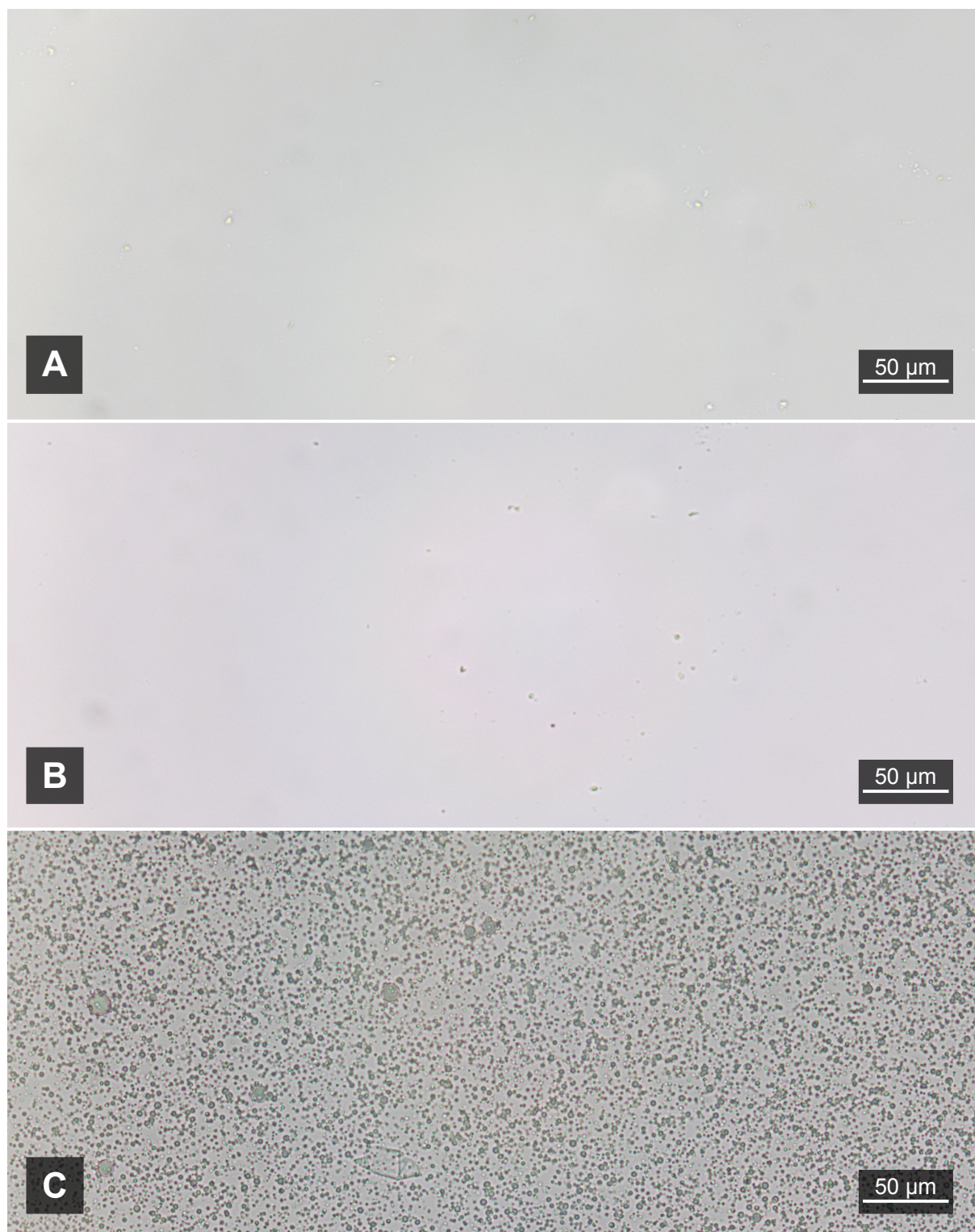
Figure 49: *Micrographs of 5 % microemulsion systems A and B and the emulsion C in phosphate buffer pH 6.8 exposed to 37 °C.*
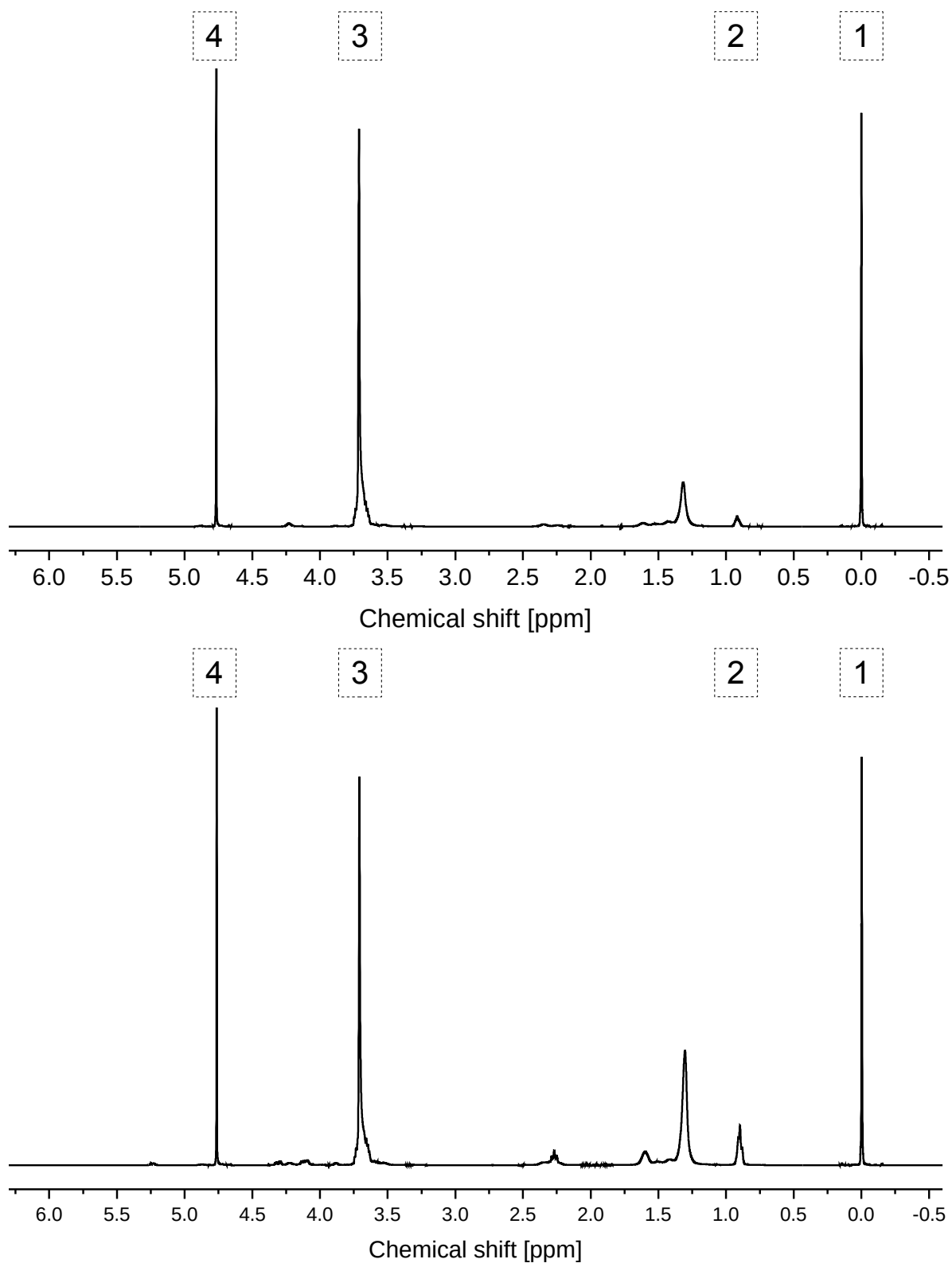
Figure 50: *NMR spectra of calibration sample 1 (top) and 2 (bottom) of pre-concentrate A series. Peak label from right to left: (1) TMSP, (2) aliphatic –CH₃ end group, (3) ethylene oxide group, (4) HDO. Spectra were normalized to the peak area of the ethylene oxide peak. Integral values are specified for peak (2) and (3). Peak (4) is capped in height.*
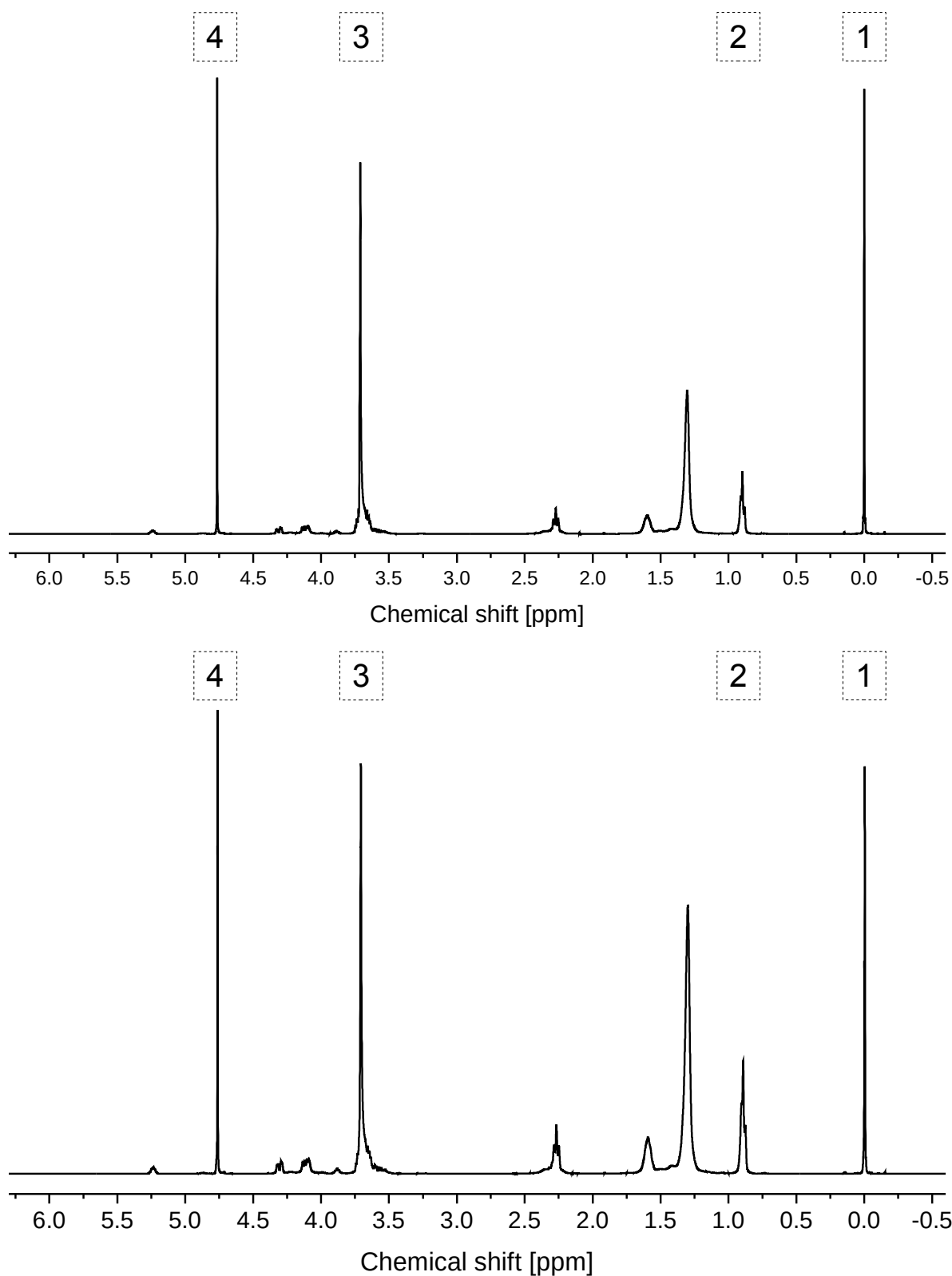
Figure 51: *NMR spectra of calibration sample 3 (top) and 4 (bottom) of pre-concentrate A series. Calibration sample 4 is equivalent to a reference sample with* 100 % *release. Peak label from right to left: (1) TMSP, (2) aliphatic –CH₃ end group, (3) ethylene oxide group, (4) HDO. Spectra were normalized to the peak area of the ethylene oxide peak. Integral values are specified for peak (2) and (3). Peak (4) is capped in height.*
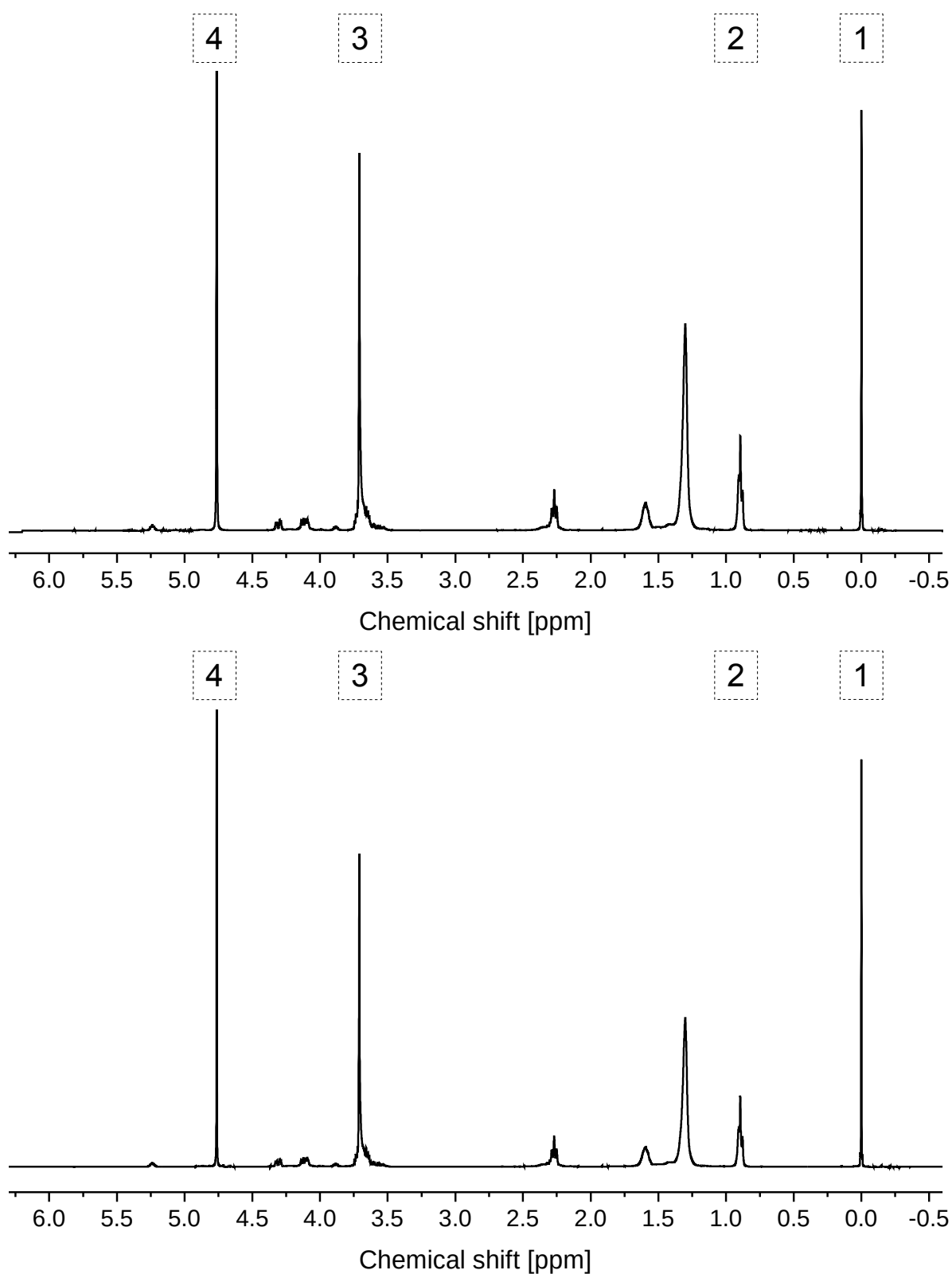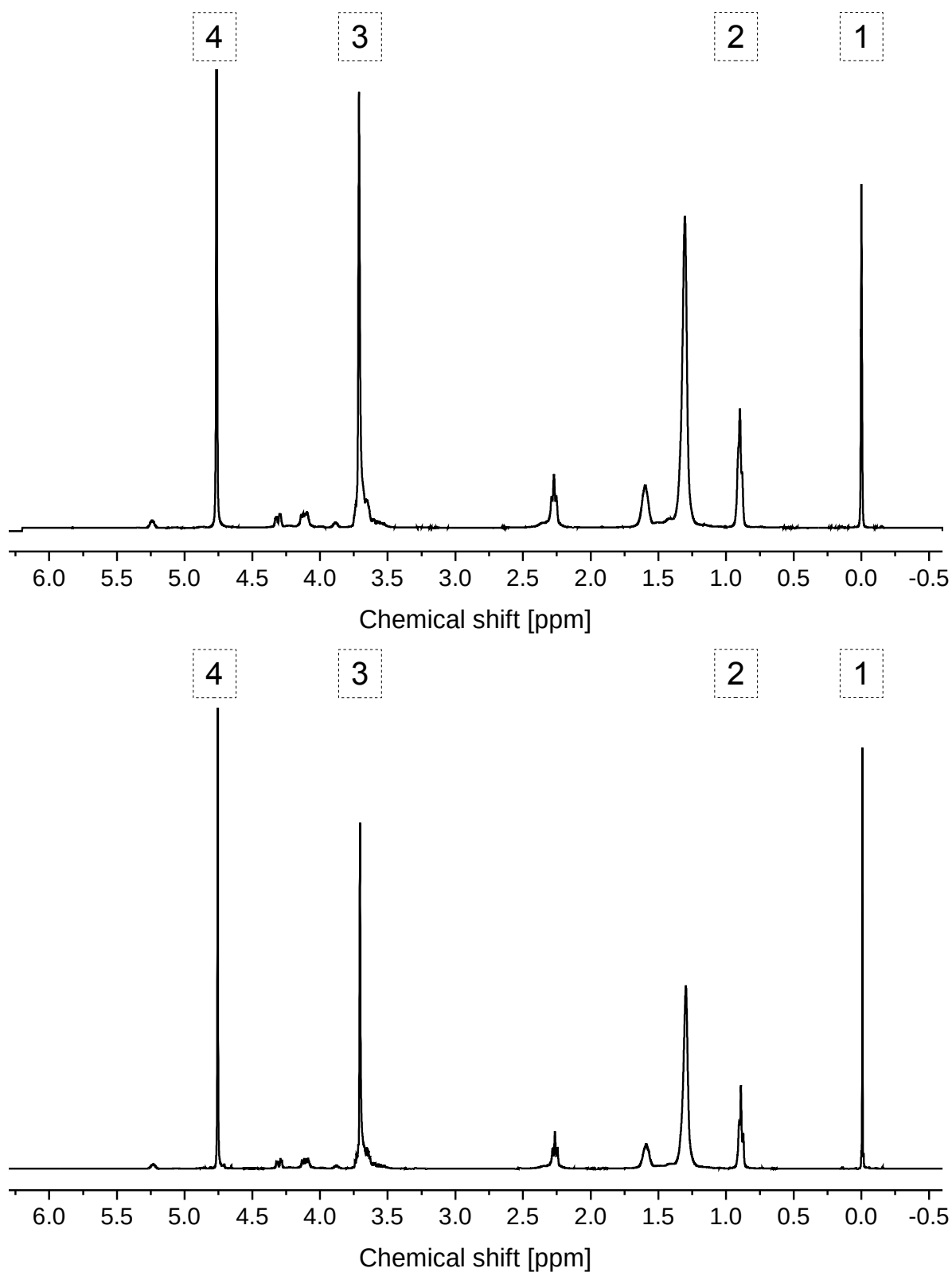
Figure 52: *NMR spectra of Fujicalin$^{\circledR}$ adsorbate sample 1 (top) and 2 (bottom) of pre-concentrate A series. Peak label from right to left: (1) TMSP, (2) aliphatic –CH$_3$ end group, (3) ethylene oxide group, (4) HDO. Spectra were normalized to the peak area of the ethylene oxide peak. Integral values are specified for peak (2) and (3). Peak (4) is capped in height.*

Figure 53: *NMR spectra of Neusilin® UFL2 adsorbate sample 1 (top) and 2 (bottom)of pre-concentrate A series. Peak label from right to left: (1) TMSP, (2) aliphatic –CH₃ end group, (3) ethylene oxide group, (4) HDO. Spectra were normalized to the peak area of the ethylene oxide peak. Integral values are specified for peak (2) and (3). Peak (4) is capped in height.*
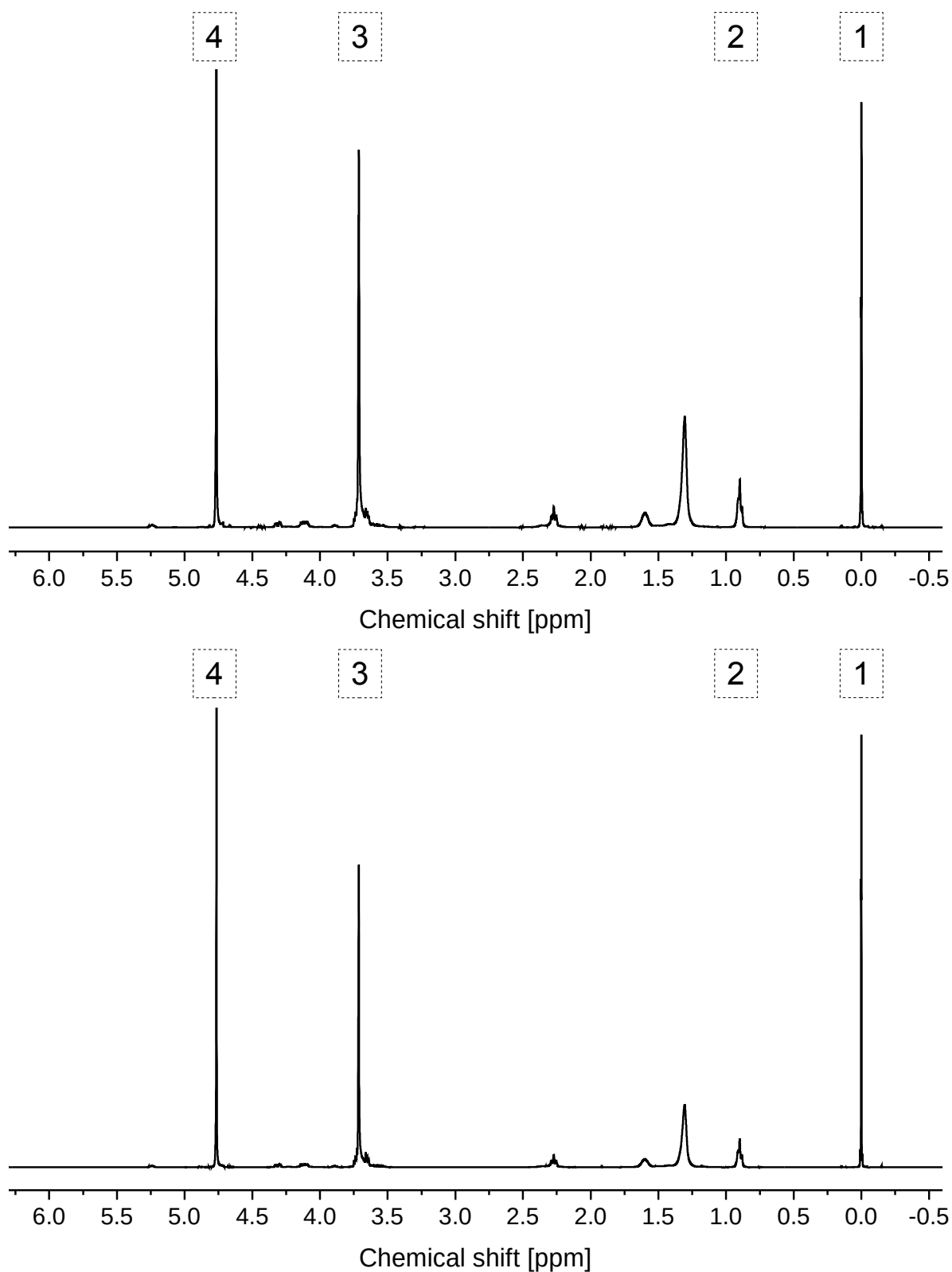
Figure 54: *NMR spectra of Neusilin® US2 adsorbate sample 1 (top) and 2 (bottom) of pre-concentrate A series. Peak label from right to left: (1) TMSP, (2) aliphatic –CH₃ end group, (3) ethylene oxide group, (4) HDO. Spectra were normalized to the peak area of the ethylene oxide peak. Integral values are specified for peak (2) and (3). Peak (4) is capped in height.*
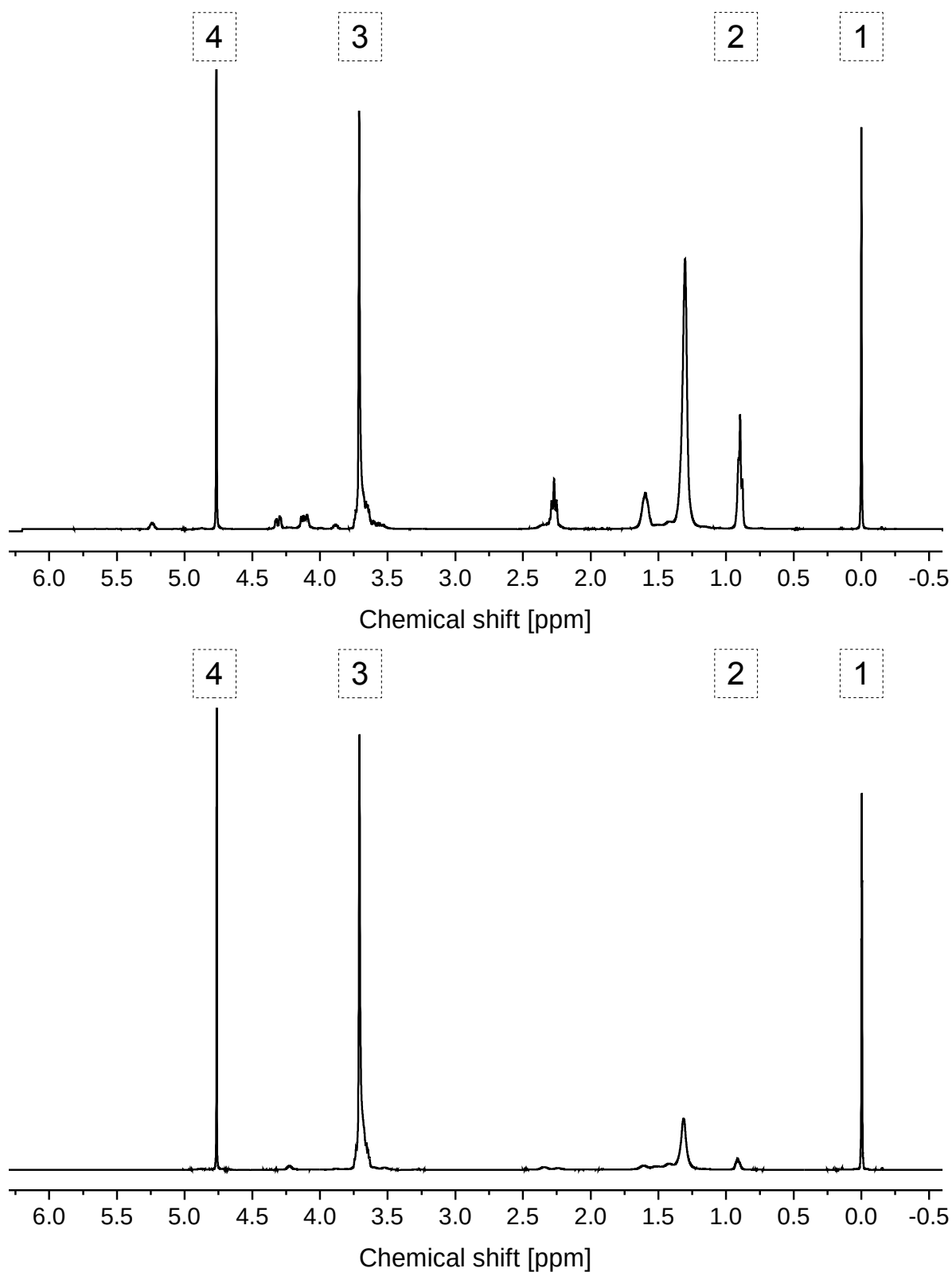
Figure 55: *NMR spectrum of the pre-concentrate A reference sample (top) and the Solutol® HS 15 reference sample (bottom). Peak label from right to left: (1) TMSP, (2) aliphatic –CH₃ end group, (3) ethylene oxide group, (4) HDO. Spectra were normalized to the peak area of the ethylene oxide peak. Integral values are specified for peak (2) and (3). Peak (4) is capped in height.*

Figure 56: *NMR spectra of calibration sample 1 (top) and 2 (bottom) of pre-concentrate B series. Peak label from right to left: (1) TMSP, (2) aliphatic –CH₃ end group, (3) ethylene oxide group, (4) HDO. Spectra were normalized to the peak area of the ethylene oxide peak. Integral values are specified for peak (2) and (3). Peak (4) is capped in height.*
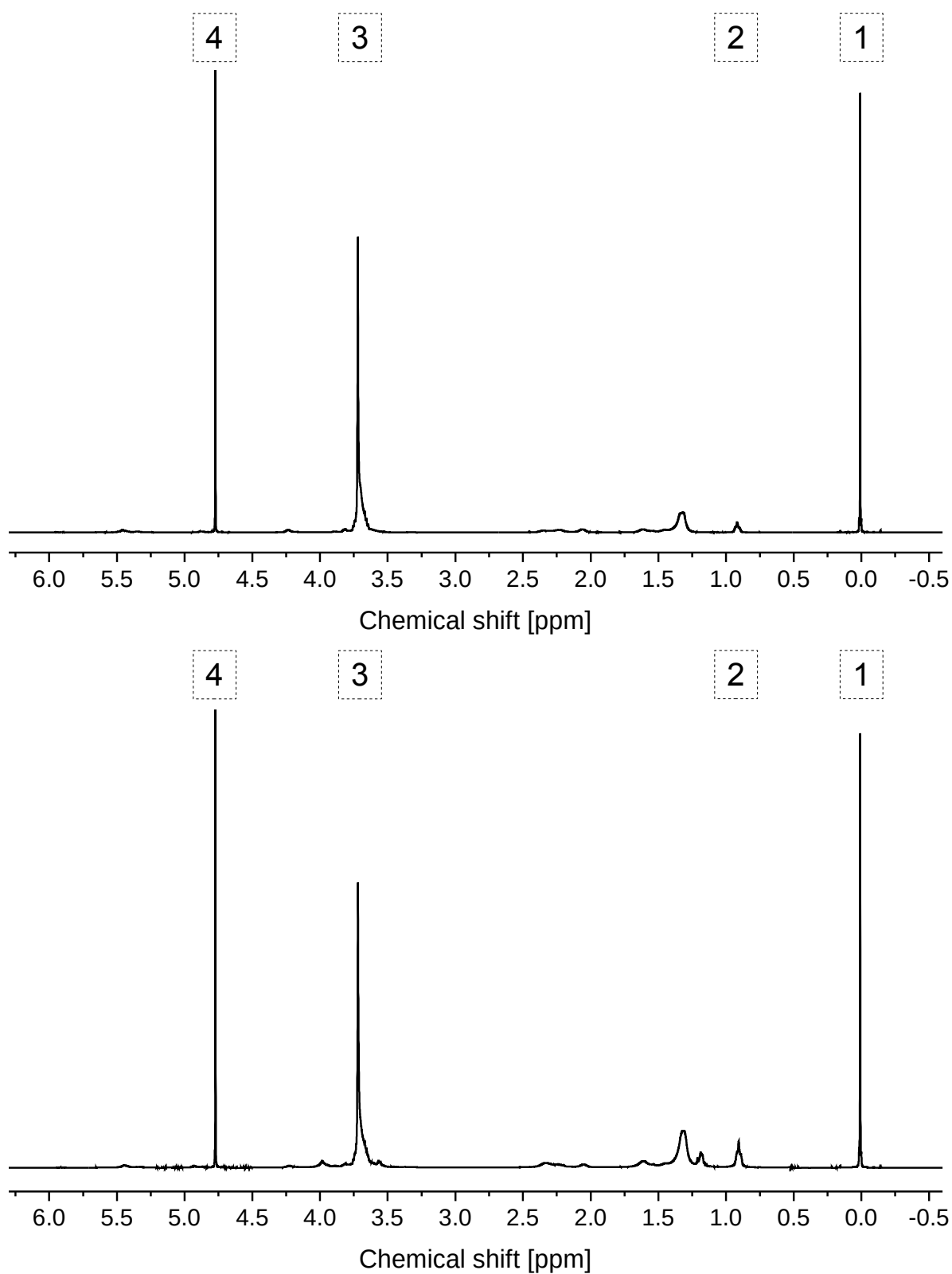
Figure 57: *NMR spectra of calibration sample 3 (top) and 4 (bottom) of pre-concentrate B series. Peak label from right to left: (1) TMSP, (2) aliphatic –CH₃ end group, (3) ethylene oxide group, (4) HDO. Spectra were normalized to the peak area of the ethylene oxide peak. Integral values are specified for peak (2) and (3). Peak (4) is capped in height.*
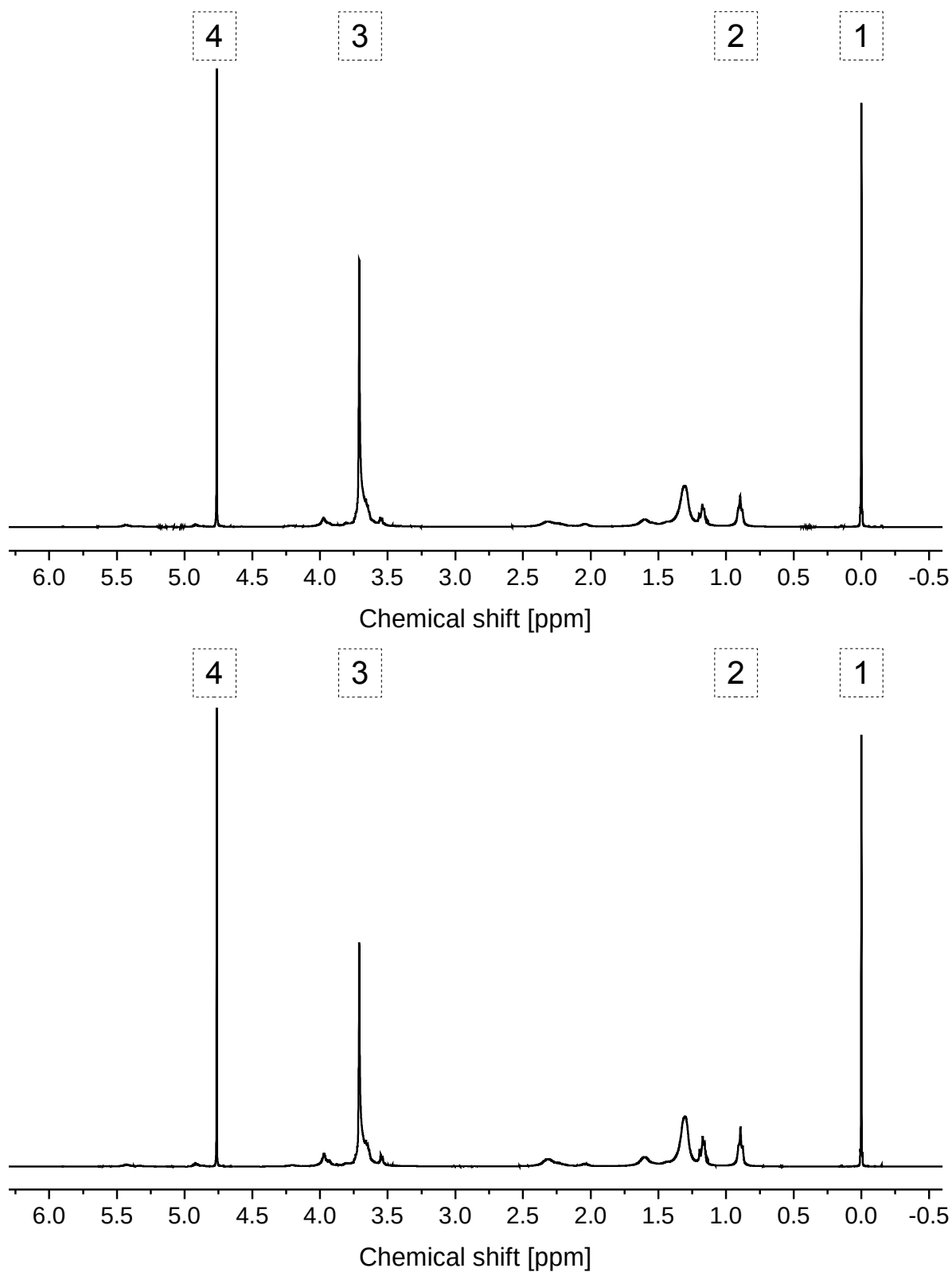
Figure 58: _NMR spectra of calibration sample 5 (top) and the pre-concentrate B reference sample (bottom) of pre-concentrate B series. Peak label from right to left: (1) TMSP, (2) aliphatic –CH₃ end group, (3) ethylene oxide group, (4) HDO. Spectra were normalized to the peak area of the ethylene oxide peak. Integral values are specified for peak (2) and (3). Peak (4) is capped in height._
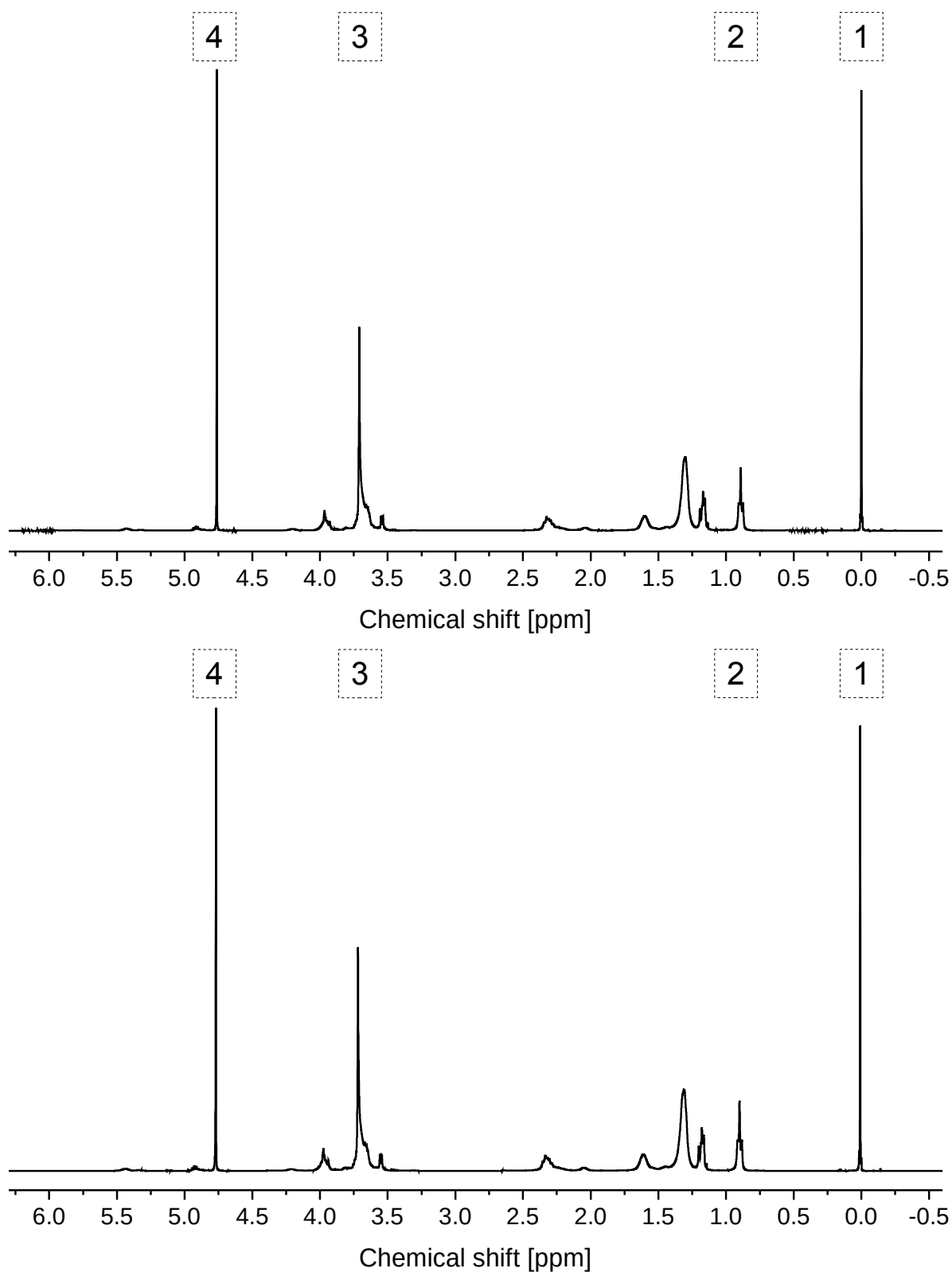
Figure 59: *NMR spectra of Fujicalin® adsorbate sample 1 (top) and 2 (bottom) of pre-concentrate B series. Peak label from right to left: (1) TMSP, (2) aliphatic –CH$_3$ end group, (3) ethylene oxide group, (4) HDO. Spectra were normalized to the peak area of the ethylene oxide peak. Integral values are specified for peak (2) and (3). Peak (4) is capped in height.*

Figure 60: *NMR spectra of Neusilin® UFL2 adsorbate sample 1 (top) and 2 (bottom) of pre-concentrate B series. Peak label from right to left: (1) TMSP, (2) aliphatic –CH₃ end group, (3) ethylene oxide group, (4) HDO. Spectra were normalized to the peak area of the ethylene oxide peak. Integral values are specified for peak (2) and (3). Peak (4) is capped in height.*
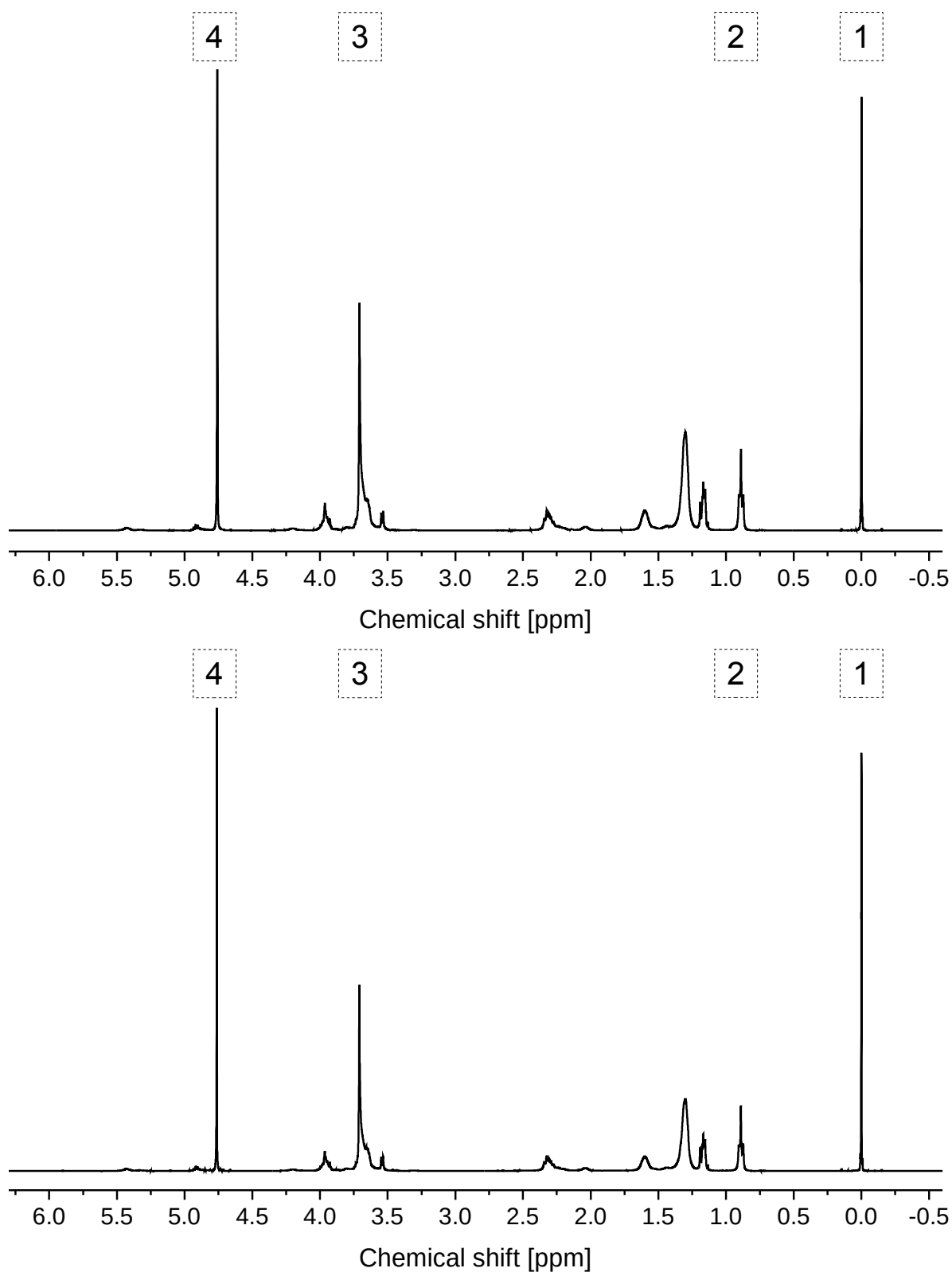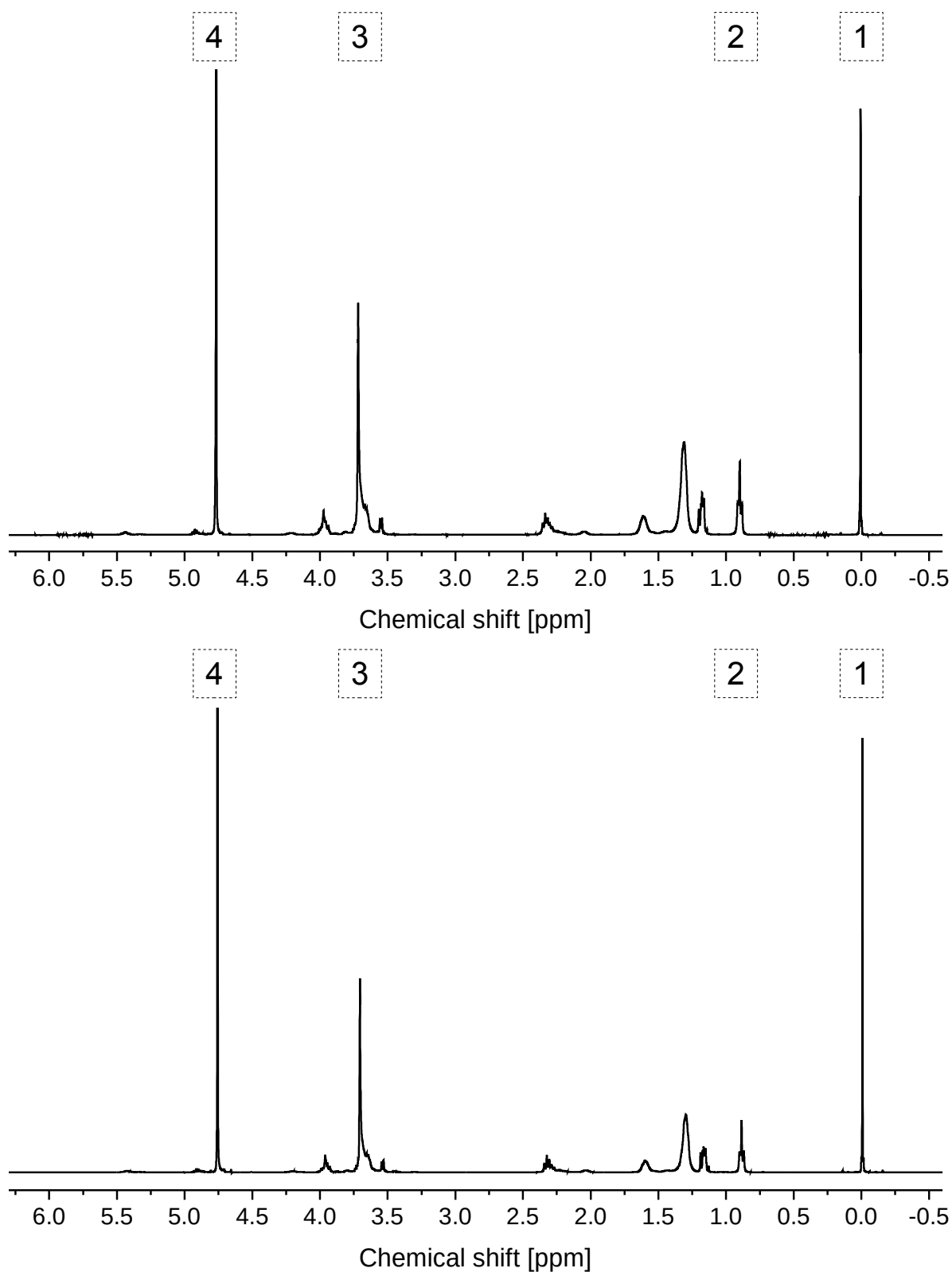
Figure 61: *NMR spectra of Neusilin® US2 adsorbate sample 1 (top) and 2 (bottom) of pre-concentrate B series. Peak label from right to left: (1) TMSP, (2) aliphatic –CH₃ end group, (3) ethylene oxide group, (4) HDO. Spectra were normalized to the peak area of the ethylene oxide peak. Integral values are specified for peak (2) and (3). Peak (4) is capped in height.*
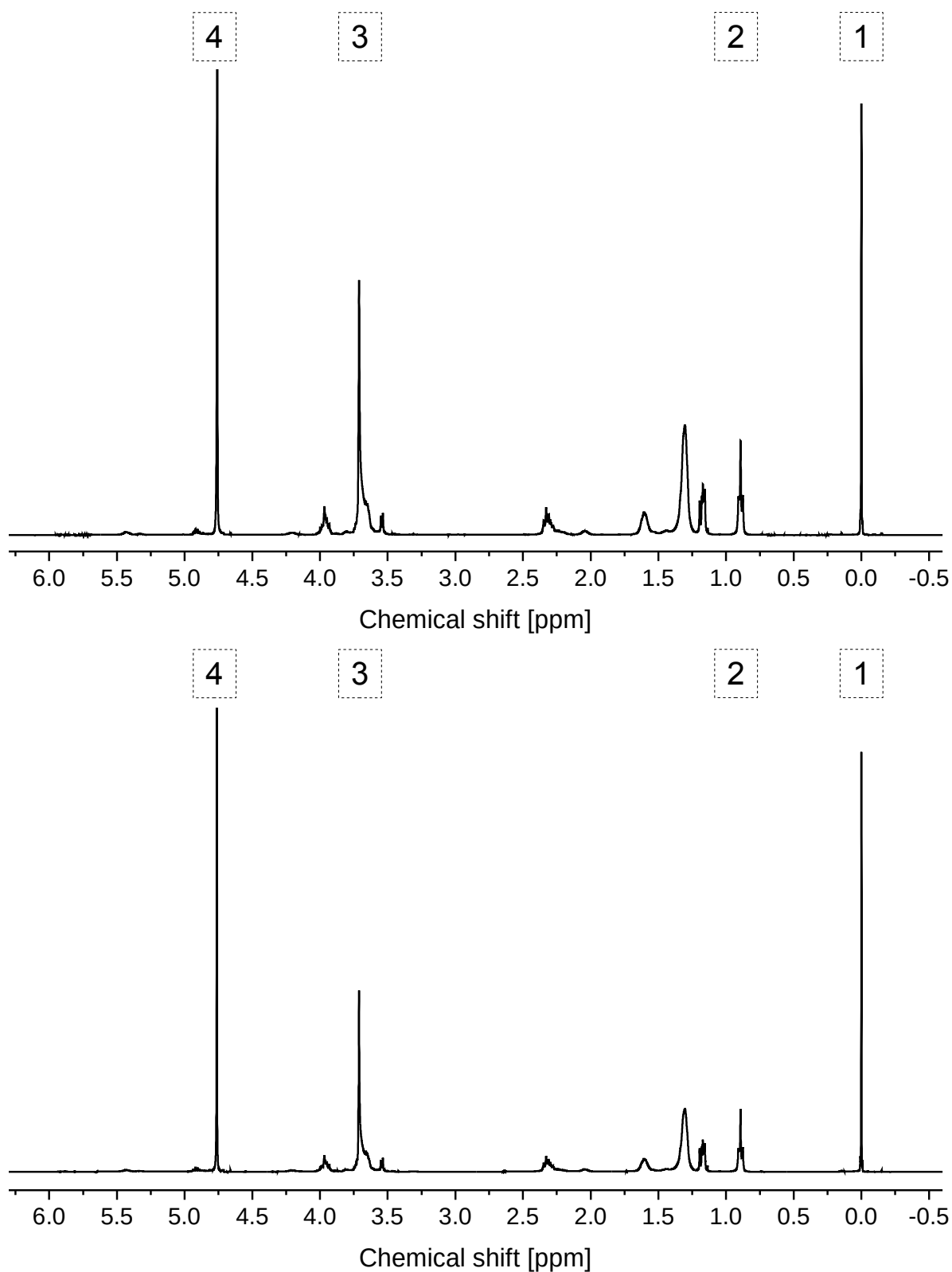
Figure 62: *NMR spectrum of the Cremophor® ELP reference sample. Peak label from right to left: (1) TMSP, (2) aliphatic –CH₃ end group, (3) ethylene oxide group, (4) HDO. Spectra were normalized to the peak area of the ethylene oxide peak. Integral values are specified for peak (2) and (3). Peak (4) is capped in height.*
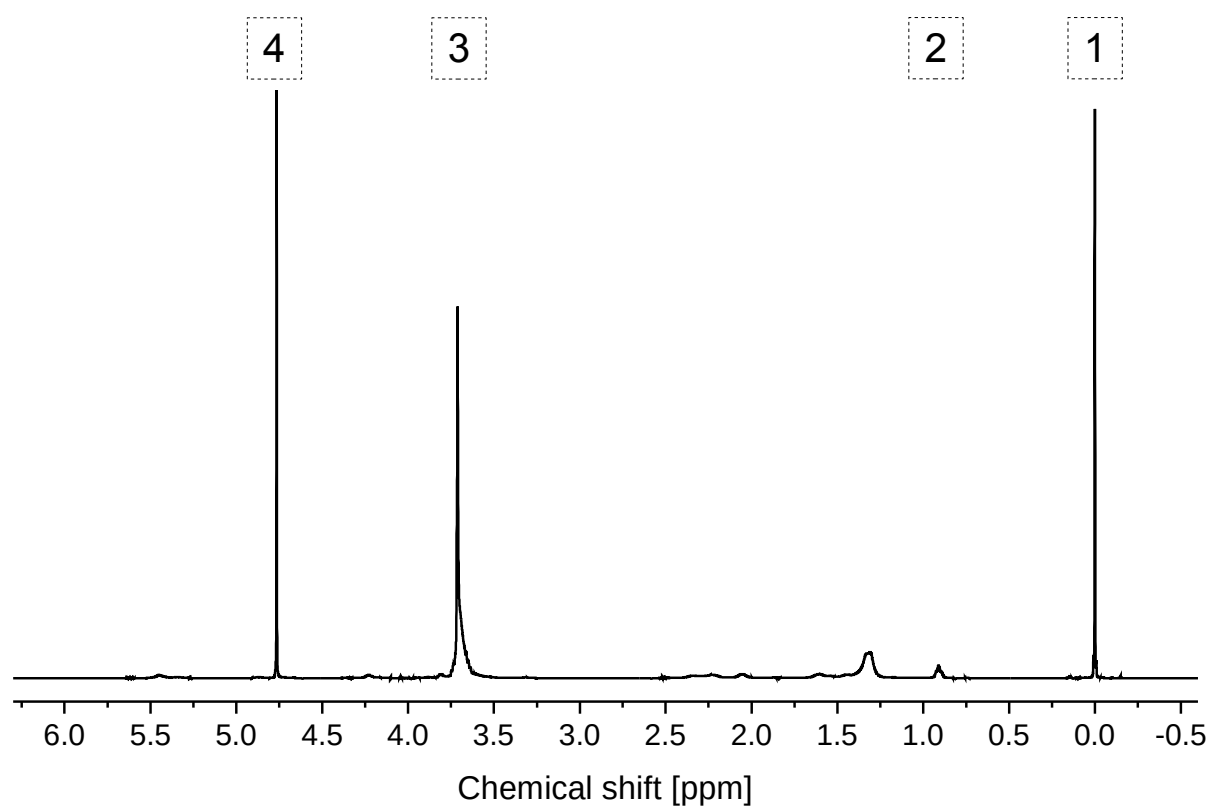
B. List of abbreviations

2a$_n$ Distance between the two outer ESR signals of a nitroxide radical

a$_n$ Hyperfine splitting constant

API Active pharmaceutical ingredient

BSE Backscatter electron

BT Benchtop

CLSM Confocal laser scanning microscopy

D$_2$O Deuterium oxide

DAC Dual asymmetric centrifugation

DiI 1,1-Dioctadecyl-3,3,3',3'-tetramethyl-indocarbocyanine perchlorate

EO Ethylene oxid

ESEM Environmental scanning electron microscopy

ESR Electron spin resonance

GSE Gaseous secondary electron

HLB Hydrophilic lipophilic balance

HPMC Hydroxypropylmethyl cellulose

HS15 Solutol$^{®}$ HS 15

LCT Long-chain tryglycerides

LEMS Liquid encapsulation by microspray

LFCS Lipid formulation classification system

MCC Microcrystalline cellulose

MCT Medium-chain triglycerides

MRI Magnetic resonance imaging

NMR Nuclear magnetic resonance

NR Nile red

o/w	oil in water
PCS	Photon correlation spectroscopy
PEG	Polyethylene glycol
pH	negative decimal logarithm of the hydrogen ion activity
PVP	Polyvinyl pyrrolidone
RH	relative humidity
Rh 110	Rhodamine 110
rpm	rounds per minute
t_E	Gradient echo time
TMSP	3-(trimethylsilyl) propionic-2,2,3,3-d4 acid, sodium salt
t_R	Repetition time
WME	Wavelenght of maximal emission

C. Bibliography

[1] J. Alsenz, M. Kansy, High throughput solubility measurement in drug discovery and development, Advanced Drug Delivery Reviews 59 (7) (2007) 546–567.

[2] C. A. Lipinski, Drug-like properties and the causes of poor solubility and poor permeability, Journal of Pharmacological and Toxicological Methods 44 (1) (2000) 235–249.

[3] C. A. Lipinski, F. Lombardo, B. W. Dominy, P. J. Feeney, Experimental and computational approaches to estimate solubility and permeability in drug discovery and development settings, Advanced Drug Delivery Reviews 64 (2012) 4–17.

[4] W. G. Dai, C. Pollock-Dove, L. C. Dong, S. Li, Advanced screening assays to rapidly identify solubility-enhancing formulations: High-throughput, miniaturization and automation, Advanced Drug Delivery Reviews 60 (6) (2008) 657–672.

[5] R. Takano, K. Sugano, A. Higashida, Y. Hayashi, M. Machida, Y. Aso, S. Yamashita, Oral absorption of poorly water-soluble drugs: Computer simulation of fraction absorbed in humans from a miniscale dissolution test, Pharmaceutical Research 23 (6) (2006) 1144–1156.

[6] S. L. Morissette, r. Almarsson, M. L. Peterson, J. F. Remenar, M. J. Read, A. V. Lemmo, S. Ellis, M. J. Cima, C. R. Gardner, High-throughput crystallization: Polymorphs, salts, co-crystals and solvates of pharmaceutical solids, Advanced Drug Delivery Reviews 56 (3) (2004) 275–300.

[7] Y. Kawabata, K. Wada, M. Nakatani, S. Yamada, S. Onoue, Formulation design for poorly water-soluble drugs based on biopharmaceutics classification system: Basic approaches and practical applications, International Journal of Pharmaceutics 420 (1) (2011) 1–10.

[8] D. Hauss, Oral lipid-based formulations, Advanced Drug Delivery Reviews 59 (7) (2007) 667–676.

[9] B. Tang, G. Cheng, J. C. Gu, C. H. Xu, Development of solid self-emulsifying drug delivery systems: Preparation techniques and dosage forms, Drug Discovery Today 13 (13/14) (2008) 606–612.

[10] G. L. Amidon, H. Lennernäs, V. P. Shah, J. R. Crison, A theoretical basis for a biopharmaceutic drug classification: The correlation of in vitro drug product dissolution and in vivo bioavailability, Pharmaceutical Research 12 (3) (1995) 413–420.

[11] R. Löbenberg, G. L. Amidon, Modern bioavailability, bioequivalence and biopharmaceutics classification system. New scientific approaches to international regulatory standards, European Journal of Pharmaceutics and Biopharmaceutics 50 (1) (2000) 3–12.

[12] M. Lindenberg, S. Kopp, J. B. Dressman, Classification of orally administered drugs on the world health organization model list of essential medicines according to the biopharmaceutics classification system, European Journal of Pharmaceutics and Biopharmaceutics 58 (2) (2004) 265–278.

[13] A. Dahan, J. M. Miller, G. L. Amidon, Prediction of solubility and permeability class membership: Provisional BCS classification of the world's top oral drugs, The AAPS journal 11 (4) (2009) 740–746.

[14] K. Mäder, U. Weidenauer (Eds.), Innovative Arzneiformen, Wissenschaftliche Verlagsgesellschaft Stuttgart, 2010.

[15] A. K. Shah, S. A. Agnihotri, Recent advances and novel strategies in pre-clinical formulation development: An overview, Journal of Controlled Release 156 (3) (2011) 281–296.

[16] C. Porter, N. Trevaskis, W. Charman, Lipids and lipid-based formulations: Optimizing the oral delivery of lipophilic drugs, Nature Reviews Drug Discovery 6 (3) (2007) 231–248.

[17] H. Chen, C. Khemtong, X. Yang, X. Chang, J. Gao, Nanonization strategies for poorly water-soluble drugs, Drug Discovery Today 16 (7) (2011) 354–360.

[18] R. Laitinen, K. Löbmann, C. J. Strachan, H. Grohganz, T. Rades, Emerging trends in the stabilization of amorphous drugs, International Journal of Pharmaceutics 453 (1) (2013) 65–79.

[19] C. L.-N. Vo, C. Park, B. J. Lee, Current trends and future perspectives of solid dispersions containing poorly water-soluble drugs, Eur.J.Pharm.Biopharm 85 (3, Part B) (2013) 799–813.

[20] S. Shah, S. Maddineni, J. Lu, M. A. Repka, Melt extrusion with poorly soluble drugs, International Journal of Pharmaceutics 453 (1) (2013) 233–252.

[21] C. W. Pouton, Formulation of self-emulsifying drug delivery systems, Advanced Drug Delivery Reviews 25 (1) (1997) 47–58.

[22] A. Humberstone, W. Charman, Lipid-based vehicles for the oral delivery of poorly water soluble drugs, Advanced Drug Delivery Reviews 25 (1) (1997) 103–128.

[23] K. Mohsin, M. Long, C. Pouton, Design of lipid-based formulations for oral administration of poorly water-soluble drugs: Precipitation of drug after dispersion of formulations in aqueous solution, Journal of Pharmaceutical Sciences 98 (10) (2009) 3582–3595.

[24] C. Pouton, Lipid formulations for oral administration of drugs: Non-emulsifying, self-emulsifying and 'self-microemulsifying' drug delivery systems, European Journal of Pharmaceutical Sciences 11 (2000) S93–S98.

[25] C. Pouton, Formulation of poorly water-soluble drugs for oral administration: Physicochemical and physiological issues and the lipid formulation classification system, European Journal of Pharmaceutical Sciences 29 (3-4) (2006) 278–287.

[26] C. Pouton, C. Porter, Formulation of lipid-based delivery systems for oral administration: Materials, methods and strategies, Advanced Drug Delivery Reviews 60 (6) (2008) 625–637.

[27] S. M. Caliph, W. N. Charman, C. J. Porter, Effect of short-, medium-, and long-chain fatty acid-based vehicles on the absolute oral bioavailability and intestinal lymphatic transport of halofantrine and assessment of mass balance in lymph-cannulated and non-cannulated rats, Journal of Pharmaceutical Sciences 89 (8) (2000) 1073–1084.

[28] S. A. Charman, W. N. Charman, M. C. Rogge, T. D. Wilson, F. J. Dutko, C. W. Pouton, Self-emulsifying drug delivery systems: formulation and biopharmaceutic evaluation of an investigational lipophilic compound, Pharmaceutical Research 9 (1) (1992) 87–93.

[29] K. B. Seljak, K. Berginc, J. Trontelj, A. Zvonar, A. Kristl, M. Gasperlin, A self-microemulsifying drug delivery system to overcome intestinal resveratrol toxicity and presystemic metabolism, Journal of Pharmaceutical Sciences (2014) –.

[30] P. Li, S. Hynes, T. Haefele, M. Pudipeddi, A. Royce, A. Serajuddin, Development of clinical dosage forms for a poorly water-soluble drug ii: Formulation and characterization of a novel solid microemulsion preconcentrate system for oral delivery of a poorly water-soluble drug, Journal of Pharmaceutical Sciences 98 (5) (2009) 1750–1764.

[31] R. Strickley, Solubilizing excipients in oral and injectable formulations, Pharmaceutical Research 21 (2) (2004) 201–230.

[32] T. Gershanik, S. Benita, Self-dispersing lipid formulations for improving oral absorption of lipophilic drugs, European Journal of Pharmaceutics and Biopharmaceutics 50 (1) (2000) 179–188.

[33] J. F. Cuiné, W. N. Charman, C. W. Pouton, G. A. Edwards, C. J. Porter, Increasing the proportional content of surfactant (cremophor el) relative to lipid in self-emulsifying lipid-based formulations of danazol reduces oral bioavailability in beagle dogs, Pharmaceutical Research 24 (4) (2007) 748–757.

[34] K. Kawakami, K. Miyoshi, Y. Ida, Solubilization behavior of poorly soluble drugs with combined use of gelucire 44/14 and cosolvent, Journal of Pharmaceutical Sciences 93 (6) (2004) 1471–1479.

[35] K. Kawakami, N. Oda, K. Miyoshi, T. Funaki, Y. Ida, Solubilization behavior of a poorly soluble drug under combined use of surfactants and cosolvents, European Journal of Pharmaceutics and Biopharmaceutics 28 (1–2) (2006) 7–14.

[36] A. Müllertz, A. Ogbonna, S. Ren, T. Rades, New perspectives on lipid and surfactant based drug delivery systems for oral delivery of poorly soluble drugs, Journal of Pharmacy and Pharmacology 62 (11) (2010) 1622–1636.

[37] A. M. S. Villar, B. C. Naveros, A. C. C. Campmany, M. A. Trenchs, C. B. Rocabert, L. H. Bellowa, Design and optimization of self-nanoemulsifying drug delivery systems (SNEDDS) for enhanced dissolution of gemfibrozil, International Journal of Pharmaceutics 431 (1–2) (2012) 161–175.

[38] J. Cuiné, C. Mcevoy, W. Charman, C. Pouton, G. Edwards, H. Benameur, C. Porter, Evaluation of the impact of surfactant digestion on the bioavailability of danazol after oral administration of lipidic self-emulsifying formulations to dogs, Journal of Pharmaceutical Sciences 97 (2) (2008) 995–1012.

[39] H. Mu, R. Holm, A. Müllertz, Lipid-based formulations for oral administration of poorly water-soluble drugs, International Journal of Pharmaceutics 453 (1) (2013) 215–224.

[40] A. Dahan, A. Hoffman, The effect of different lipid based formulations on the oral absorption of lipophilic drugs: The ability of in vitro lipolysis and consecutive ex vivo intestinal permeability data to predict in vivo bioavailability in rats, European Journal of Pharmaceutics and Biopharmaceutics 67 (1) (2007) 96–105.

[41] K. Mohsin, Design of lipid-based formulations for oral administration of poorly water-soluble drug fenofibrate: Effects of digestion, AAPS PharmSciTech 13 (2) (2012) 637–646.

[42] J. Christensen, K. Schultz, B. Mollgaard, H. Kristensen, A. Müllertz, Solubilisation of poorly water-soluble drugs during in vitro lipolysis of medium- and long-chain triacylglycerols, European Journal of Pharmaceutical Sciences 23 (3) (2004) 287–296.

[43] S. f. Han, T. t. Yao, X. x. Zhang, L. Gan, C. Zhu, H. z. Yu, Y. Gan, Lipid-based formulations to enhance oral bioavailability of the poorly water-soluble drug anethol trithione: Effects of lipid composition and formulation, International Journal of Pharmaceutics 379 (1) (2009) 18–24.

[44] M. Grove, G. P. Pedersen, J. L. Nielsen, A. Müllertz, Bioavailability of seocalcitol i: Relating solubility in biorelevant media with oral bioavailability in rats–effect of medium and long chain triglycerides, Journal of Pharmaceutical Science 94 (8) (2005) 1830–1838.

[45] M. Grove, A. Müllertz, J. L. g. Nielsen, G. P. Pedersen, Bioavailability of seocalcitol ii: Development and characterisation of self-microemulsifying drug delivery systems (smedds) for oral administration containing medium and long chain triglycerides, European Journal of Pharmaceutical Sciences 28 (3) (2006) 233–242.

[46] C. J. Porter, A. M. Kaukonen, A. Taillardat-Bertschinger, B. J. Boyd, J. M. O'Connor, G. A. Edwards, W. N. Charman, Use of in vitro lipid digestion data to explain the in vivo performance of triglyceride-based oral lipid formulations of poorly water-soluble drugs: Studies with halofantrine, Journal of Pharmaceutical Science 93 (5) (2004) 1110–1121.

[47] D. G. Fatouros, B. Bergenstahl, A. Müllertz, Morphological observations on a lipid-based drug delivery system during *in vitro* digestion, European Journal of Pharmaceutical Sciences 31 (2) (2007) 85–94.

[48] D. G. Fatouros, G. Deen, L. Arleth, B. Bergenstahl, F. S. Nielsen, J. S. Pedersen, A. Müllertz, Structural development of self nano emulsifying drug delivery systems (snedds) during *in vitro* lipid digestion monitored by small-angle x-ray scattering, Pharmaceutical Research 24 (10) (2007) 1844–1853.

[49] D. Fatouros, F. Nielsen, D. Douroumis, L. Hadjileontiadis, A. Müllertz, *In vitro-in vivo* correlations of self-emulsifying drug delivery systems combining the dynamic lipolysis model and neuro-fuzzy networks, European Journal of Pharmaceutics and Biopharmaceutics 69 (3) (2008) 887–898.

[50] C. Porter, C. Pouton, J. Cuine, W. Charman, Enhancing intestinal drug solubilisation using lipid-based delivery systems, Advanced Drug Delivery Reviews 60 (6) (2008) 673–691.

[51] A. Müllertz, D. G. Fatouros, J. R. Smith, M. Vertzoni, C. Reppas, Insights into intermediate phases of human intestinal fluids visualized by atomic force microscopy and cryo-transmission electron microscopy ex vivo, Molecular Pharmaceutics 9 (2) (2011) 237–247.

[52] W.-G. Dai, L. C. Dong, X. Shi, J. Nguyen, J. Evans, Y. Xu, A. A. Creasey, Evaluation of drug precipitation of solubility-enhancing liquid formulations using milligram quantities of a new molecular entity (NME), Journal of Pharmaceutical Sciences 96 (11) (2007) 2957–2969.

[53] N. Thomas, R. Holm, A. Müllertz, T. Rades, *In vitro* and *in vivo* performance of novel supersaturated self-nanoemulsifying drug delivery systems (super-SNEDDS), Journal of Controlled Release 160 (1) (2012) 25–32.

[54] A. T. Larsen, A. G. Ohlsson, B. Polentarutti, R. A. Barker, A. R. Phillips, R. Abu-Rmaileh, P. A. Dickinson, B. Abrahamsson, J. Østergaard, A. Müllertz, Oral bioavailability of cinnarizine in dogs: Relation to SNEDDS droplet size, drug solubility and in vitro precipitation, European Journal of Pharmaceutical Sciences 48 (1–2) (2013) 339–350.

[55] J. Dressman, J. Butler, J. Hempenstall, C. Reppas, The BCS: Where do we go from here?, Pharmaceutical Technology 25 (7) (2001) 68–77.

[56] J. M. Kovarik, E. A. Mueller, B. van, W. Tetzloff, K. Kutz, Reduced inter- and intraindividual variability in cyclosporine pharmacokinetics from a microemulsion formulation, Journal of Pharmaceutical Sciences 83 (3) (1994) 444–446.

[57] E. A. Mueller, J. M. Kovarik, B. van, W. Tetzloff, J. Grevel, K. Kutz, Improved dose linearity of cyclosporine pharmacokinetics from a microemulsion formulation, Pharmaceutical Research 11 (2) (1994) 301–304.

[58] E. A. Mueller, J. M. Kovarik, J. B. van Bree, J. Grevel, P. W. Lücker, K. Kutz, Influence of a fat-rich meal on the pharmacokinetics of a new oral formulation of

cyclosporine in a crossover comparison with the market formulation, Pharmaceutical Research 11 (1) (1994) 151–155.

[59] R. G. Strickley, Currently marketed oral lipid-based dosage forms: Drug products and excipients in: Oral lipid-based formulations: Enhancing the bioavailability of poorly water soluble drugs, Informa Healthcare, Inc., New York, 2007.

[60] K. Kohli, S. Chopra, D. Dhar, S. Arora, R. K. Khar, Self-emulsifying drug delivery systems: An approach to enhance oral bioavailability, Drug Discovery Today 15 (21) (2010) 958–965.

[61] V. Jannin, J. Musakhanian, D. Marchaud, Approaches for the development of solid and semi-solid lipid-based formulations, Advanced Drug Delivery Reviews 60 (6) (2008) 734–746.

[62] M. Kuentz, Lipid-based formulations for oral delivery of lipophilic drugs, Drug Discovery Today: Technologies 9 (2) (2012) e97–e104.

[63] E. T. Cole, D. Cadé, H. Benameur, Challenges and opportunities in the encapsulation of liquid and semi-solid formulations into capsules for oral administration, Advanced Drug Delivery Reviews 60 (6) (2008) 747–756.

[64] S. Chakraborty, D. Shukla, B. Mishra, S. Singh, Lipid - an emerging platform for oral delivery of drugs with poor bioavailability, European Journal of Pharmaceutics and Biopharmaceutics 73 (1) (2009) 1–15.

[65] J. Breitenbach, Melt extrusion: From process to drug delivery technology, Eur.J.Pharm.Biopharm 54 (2) (2002) 107–117.

[66] M. M. Crowley, F. Zhang, M. A. Repka, S. Thumma, S. B. Upadhye, S. Kumar Battu, J. W. McGinity, C. Martin, Pharmaceutical applications of hot-melt extrusion: Part I, Drug Development and Industrial Pharmacy 33 (9) (2007) 909–926.

[67] M. A. Repka, S. K. Battu, S. B. Upadhye, S. Thumma, M. M. Crowley, F. Zhang, C. Martin, J. W. McGinity, Pharmaceutical applications of hot-melt extrusion: Part II, Drug Development and Industrial Pharmacy 33 (10) (2007) 1043–1057.

[68] P. Kleinebudde, Solid lipid extrusion, in: Melt Extrusion, Springer, 2013, pp. 299–328.

[69] F. Siepmann, S. Muschert, M. Flament, P. Leterme, A. Gayot, J. Siepmann, Controlled drug release from gelucire-based matrix pellets: Experiment and theory, International Journal of Pharmaceutics 317 (2) (2006) 136–143.

[70] M. Windbergs, C. J. Strachan, P. Kleinebudde, Influence of the composition of glycerides on the solid-state behaviour and the dissolution profiles of solid lipid extrudates, International Journal of Pharmaceutics 381 (2) (2009) 184–191.

[71] M. Windbergs, C. J. Strachan, P. Kleinebudde, Understanding the solid-state behaviour of triglyceride solid lipid extrudates and its influence on dissolution, European Journal of Pharmaceutics and Biopharmaceutics 71 (1) (2009) 80–87.

[72] Y. W. Chen, M. R. Mackley, Flexible chocolate, Soft Matter 2 (4) (2006) 304–309.

[73] J. Engmann, M. Mackley, Semi-solid processing of chocolate and cocoa butter: The experimental correlation of process rheology with microstructure, Food and Bioproducts Processing 84 (2) (2006) 95–101.

[74] C. Reitz, C. Strachan, P. Kleinebudde, Solid lipid extrudates as sustained-release matrices: The effect of surface structure on drug release properties, European Journal of Pharmaceutical Sciences 35 (4) (2008) 335–343.

[75] C. Reitz, P. Kleinebudde, Solid lipid extrusion of sustained release dosage forms, European Journal of Pharmaceutics and Biopharmaceutics 67 (2) (2007) 440–448.

[76] A. Abdalla, K. Mäder, Preparation and characterization of a self-emulsifying pellet formulation, European Journal of Pharmaceutics and Biopharmaceutics 66 (2) (2007) 220–226.

[77] N. Passerini, B. Albertini, B. Perissutti, L. Rodriguez, Evaluation of melt granulation and ultrasonic spray congealing as techniques to enhance the dissolution of praziquantel, International Journal of Pharmaceutics 318 (1–2) (2006) 92–102.

[78] C. Cavallari, L. Rodriguez, B. Albertini, N. Passerini, F. Rosetti, A. Fini, Thermal and fractal analysis of diclofenac/gelucire 50/13 microparticles obtained by ultrasound-assisted atomization, Journal of Pharmaceutical Sciences 94 (5) (2005) 1124–1134.

[79] I. Ilić, R. Dreu, M. Burjak, M. Homar, J. Kerč, S. Srčič, Microparticle size control and glimepiride microencapsulation using spray congealing technology, International Journal of Pharmaceutics 381 (2) (2009) 176–183.

[80] T. Yi, J. Wan, H. Xu, X. Yang, A new solid self-microemulsifying formulation prepared by spray-drying to improve the oral bioavailability of poorly water soluble drugs, European Journal of Pharmaceutics and Biopharmaceutics 70 (2) (2008) 439–444.

[81] K. Christensen, G. Pedersen, H. Kristensen, Preparation of redispersible dry emulsions by spray drying, International Journal of Pharmaceutics 212 (2) (2001) 187–194.

[82] K. Heinzelmann, K. Franke, Using freezing and drying techniques of emulsions for the microencapsulation of fish oil to improve oxidation stability, Colloids and Surfaces B: Biointerfaces 12 (3-6) (1999) 223–229.

[83] H. Adelmann, B. P. Binks, R. Mezzenga, Oil powders and gels from particle-stabilized emulsions, Langmuir 28 (3) (2012) 1694–1697.

[84] K. Christensen, G. Pedersen, H. Kristensen, Physical stability of redispersible dry emulsions containing amorphous sucrose, European Journal of Pharmaceutics and Biopharmaceutics 53 (2) (2002) 147–153.

[85] K. Christensen, G. Pedersen, H. Kristensen, Technical optimisation of redispersible dry emulsions, International Journal of Pharmaceutics 212 (2) (2001) 195–202.

[86] A. Tan, A. K. Davey, C. A. Prestidge, Silica-lipid hybrid (SLH) versus non-lipid formulations for optimising the dose-dependent oral absorption of celecoxib, Pharmaceutical Research 28 (9) (2011) 2273–2287.

[87] T. H. Nguyen, A. Tan, L. Santos, D. Ngo, G. A. Edwards, C. J. Porter, C. A. Prestidge, B. J. Boyd, Silica-lipid hybrid (SLH) formulations enhance the oral bioavailability and efficacy of celecoxib: An in vivo evaluation, Journal of Controlled Release 167 (1) (2013) 85–91.

[88] K. E. Bremmell, A. Tan, A. Martin, C. A. Prestidge, Tableting lipid-based formulations for oral drug delivery: A case study with silica nanoparticle-lipid-mannitol hybrid microparticles, Journal of Pharmaceutical Sciences 102 (2) (2013) 684–693.

[89] A. Tan, S. Simovic, A. K. Davey, T. Rades, B. J. Boyd, C. A. Prestidge, Silica nanoparticles to control the lipase-mediated digestion of lipid-based oral delivery systems, Molecular Pharmaceutics 7 (2) (2010) 522–532.

[90] A. Tan, A. Martin, T. Nguyen, B. Boyd, C. Prestidge, Hybrid nanomaterials that mimic the food effect: Controlling enzymatic digestion for enhanced oral drug absorption, Angewandte Chemie – International Edition 51 (22) (2012) 5475–5479.

[91] S. Rao, A. Tan, B. J. Boyd, C. A. Prestidge, Synergistic role of self-emulsifying lipids and nanostructured porous silica particles in optimizing the oral delivery of lovastatin, Nanomedicine 9 (18) (2014) 2745–2759.

[92] I. S. Ahmed, M. H. Aboul-Einien, In vitro and in vivo evaluation of a fast-disintegrating lyophilized dry emulsion tablet containing griseofulvin, European Journal of Pharmaceutical Sciences 32 (1) (2007) 58–68.

[93] C. Ratti, Hot air and freeze-drying of high-value foods: A review, Journal of Food Engineering 49 (4) (2001) 311–319.

[94] T. Rogers, A. Nelsen, M. Sarkari, T. Young, K. Johnston, R. Williams, Enhanced aqueous dissolution of a poorly water soluble drug by novel particle engineering technology: Spray-freezing into liquid with atmospheric freeze-drying, Pharmaceutical Research 20 (3) (2003) 485–493.

[95] E. A. Boss, R. M. Filho, E. C. V. de Toledo, Freeze drying process: Real time model and optimization, Chemical Engineering and Processing: Process Intensification 43 (12) (2004) 1475–1485.

[96] W. Abdelwahed, G. Degobert, S. Stainmesse, H. Fessi, Freeze-drying of nanoparticles: Formulation, process and storage considerations, Advanced Drug Delivery Reviews 58 (15) (2006) 1688–1713.

[97] S. M. Patel, T. Doen, M. J. Pikal, Determination of end point of primary drying in freeze-drying process control, AAPS PharmSciTech 11 (1) (2010) 73–84.

[98] J. Unga, F. Tajarobi, O. Norder, G. Frenning, A. Larsson, Relating solubility data of parabens in liquid PEG 400 to the behaviour of PEG 4000-parabens solid dispersions, European Journal of Pharmaceutics and Biopharmaceutics 73 (2) (2009) 260–268.

[99] J. Unga, P. Matsson, D. Mahlin, Understanding polymer-lipid solid dispersions - the properties of incorporated lipids govern the crystallisation behaviour of PEG, International Journal of Pharmaceutics 386 (1-2) (2010) 61–70.

[100] D. Mahlin, A. Ridell, G. Frenning, S. Engström, Solid-state characterization of PEG 4000/monoolein mixtures, Macromolecules 37 (7) (2004) 2665–2667.

[101] D. Mahlin, J. Unga, A. Ridell, G. Frenning, S. Engström, Influence of polymer molecular weight on the solid-state structure of PEG/monoolein mixtures, Polymer 46 (26) (2005) 12210–12217.

[102] R. M. Dannenfelser, H. He, Y. Joshi, S. Bateman, A. T. Serajuddin, Development of clinical dosage forms for a poorly water soluble drug I: Application of polyethylene glycol-polysorbate 80 solid dispersion carrier system, Journal of Pharmaceutical Sciences 93 (5) (2004) 1165–1175.

[103] C. Hentzschel, A. Sakmann, C. Leopold, Suitability of various excipients as carrier and coating materials for liquisolid compacts, Drug Development and Industrial Pharmacy 37 (10) (2011) 1200–1207.

[104] A. Abdalla, S. Klein, K. Mäder, A new self-emulsifying drug delivery system (SEDDS) for poorly soluble drugs: Characterization, dissolution, *in vitro* digestion and incorporation into solid pellets, European Journal of Pharmaceutical Sciences 35 (5) (2008) 457–464.

[105] L. Boltri, N. Coceani, D. D. Curto, L. Dobetti, P. Esposito, Enhancement and modification of etoposide release from crospovidone particles loaded with oil-surfactant blends, Pharmaceutical Development and Technology 2 (4) (1997) 373–381.

[106] Fujicalin - technical details (http://www.fujicalin.com/product/general_properties.php) (10 2013).

[107] Neusilin - technical details (http://www.neusilin.com/product/general_properties.php) (10 2013).

[108] Y. Ito, H. Arai, K. Uchino, K. Iwasaki, N. Shibata, K. Takada, Effect of adsorbents on the absorption of lansoprazole with surfactant, International Journal of Pharmaceutics 289 (1) (2005) 69–77.

[109] Y. Ito, T. Kusawake, M. Ishida, R. Tawa, N. Shibata, K. Takada, Oral solid gentamicin preparation using emulsifier and adsorbent, Journal of Controlled Release 105 (1) (2005) 23–31.

[110] M. Milović, J. Djuriš, L. Djekić, D. Vasiljević, S. Ibrić, Characterization and evaluation of solid self-microemulsifying drug delivery systems with porous carriers as systems for improved carbamazepine release, International Journal of Pharmaceutics 436 (1) (2012) 58–65.

[111] S. S. Spireas, C. I. Jarowski, B. D. Rohera, Powdered solution technology: Principles and mechanism, Pharmaceutical Research 9 (10) (1992) 1351–1358.

[112] S. Spireas, S. Sadu, Enhancement of prednisolone dissolution properties using liquisolid compacts, International Journal of Pharmaceutics 166 (2) (1998) 177–188.

[113] S. Spireas, S. Sadu, R. Grover, In vitro release evaluation of hydrocortisone liquisolid tablets, Journal of Pharmaceutical Sciences 87 (7) (1998) 867–872.

[114] S. Spireas, T. Wang, R. Grover, Effect of powder substrate on the dissolution properties of methyclothiazide liquisolid compacts, Drug Development and Industrial Pharmacy 25 (2) (1999) 163–168.

[115] M. Saeedi, J. Akbari, K. Morteza-Semnani, R. Enayati-Fard, S. Sar-Reshteh-dar, A. Soleymani, Enhancement of dissolution rate of indomethacin using liquisolid compacts, Iranian Journal of Pharmaceutical Research 10 (1) (2011) 25–33.

[116] C. Hentzschel, M. Alnaief, I. Smirnova, A. Sakmann, C. Leopold, Enhancement of griseofulvin release from liquisolid compacts, European Journal of Pharmaceutics and Biopharmaceutics 80 (1) (2012) 130–135.

[117] C. Sander, P. Holm, Porous magnesium aluminometasilicate tablets as carrier of a cyclosporine self-emulsifying formulation, AAPS PharmSciTech 10 (4) (2009) 1388–1395.

[118] M. Kang, S. Jung, W. Song, J. Park, S. Choi, K. Oh, H. Choi, Y. Choi, J. Lee, B. Lee, S. Chi, Immediate release of ibuprofen from Fujicalin®-based fast-dissolving self-emulsifying tablets, Drug Development and Industrial Pharmacy 37 (11) (2011) 1298–1305.

[119] V. R. Kallakunta, S. Bandari, R. Jukanti, P. R. Veerareddy, Oral self emulsifying powder of lercanidipine hydrochloride: Formulation and evaluation, Powder Technology 221 (2012) 375–382.

[120] J. Adrian, A. Wolf, A. Steinbach, J. Rössler, R. Süss, Targeted delivery to neuroblastoma of novel siRNA-anti-GD2-liposomes prepared by dual asymmetric centrifugation and sterol-based post-insertion method, Pharmaceutical Research 28 (9) (2011) 2261–2272.

[121] M. Hirsch, V. Ziroli, M. Helm, U. Massing, Preparation of small amounts of sterile sirna-liposomes with high entrapping efficiency by dual asymmetric centrifugation (DAC), Journal of Controlled Release 135 (1) (2009) 80–88.

[122] U. Massing, S. Cicko, V. Ziroli, Dual asymmetric centrifugation (DAC)–a new technique for liposome preparation, Journal of Controlled Release 125 (1) (2008) 16–24.

[123] W. Tian, S. Schulze, M. Brandl, G. Winter, Vesicular phospholipid gel-based depot formulations for pharmaceutical proteins: Development and in vitro evaluation, Journal of Controlled Release 142 (3) (2010) 319–325.

[124] I. Aursand, L. Gallart-Jornet, U. Erikson, D. Axelson, T. Rustad, Water distribution in brine salted cod (gadus morhua) and salmon (salmo salar): A low-field ^{1}H NMR study, Journal of Agricultural and Food Chemistry 56 (15) (2008) 6252–6260.

[125] S. Lu, J. Chen, Y. Chen, C. Lii, P. Lai, H. Chen, Water mobility, rheological and textural properties of rice starch gel, Journal of Cereal Science 53 (1) (2011) 31–36.

[126] M. Bastrop, A. Meister, H. Metz, S. Drescher, B. Dobner, K. Mäder, A. Blume, Water dynamics in bolaamphiphile hydrogels investigated by ^{1}H NMR relaxometry and diffusometry, Journal of Physical Chemistry B 115 (1) (2011) 14–22.

[127] H. Metz, K. Mäder, Benchtop- NMR and MRI–a new analytical tool in drug delivery research, International Journal of Pharmaceutics 364 (2) (2008) 170–175.

[128] K. Mäder, B. Bittner, Y. Li, W. Wohlauf, T. Kissel, Monitoring microviscosity and microacidity of the albumin microenvironment inside degrading microparticles from poly(lactide-co-glycolide) (PLG) or ABA-triblock polymers containing hydrophobic poly(lactide-co-glycolide) A blocks and hydrophilic poly(ethylene oxide) B blocks, Pharmaceutical Research 15 (5) (1998) 787–793.

[129] D. J. Lurie, K. Mäder, Monitoring drug delivery processes by EPR and related techniques - principles and applications, Advanced Drug Delivery Reviews 57 (8) (2005) 1171–1190.

[130] A. Besheer, K. M. Wood, N. A. Peppas, K. Mäder, Loading and mobility of spin-labeled insulin in physiologically responsive complexation hydrogels intended for oral administration, Journal of Controlled Release 111 (1-2) (2006) 73–80.

[131] S. Kempe, H. Metz, K. Mäder, Application of electron paramagnetic resonance (EPR) spectroscopy and imaging in drug delivery research - chances and challenges, European Journal of Pharmaceutics and Biopharmaceutics 74 (1) (2010) 55–66.

[132] A. K. Dutta, K. Kamada, K. Ohta, Spectroscopic studies of nile red in organic solvents and polymers, Journal of Photochemistry and Photobiology A: Chemistry 93 (1) (1996) 57–64.

[133] S. D. Fowler, P. Greenspan, Application of nile red, a fluorescent hydrophobic probe, for the detection of neutral lipid deposits in tissue sections: comparison with oil red o., Journal of Histochemistry and Cytochemistry 33 (8) (1985) 833–836.

[134] P. Greenspan, S. D. Fowler, Spectrofluorometric studies of the lipid probe, nile red, Journal of Lipid Research 26 (7) (1985) 781–789.

[135] D. L. Sackett, J. Wolff, Nile red as a polarity-sensitive fluorescent probe of hydrophobic protein surfaces, Analytical Biochemistry 167 (2) (1987) 228–234.

[136] A. Dukić-Ott, M. Thommes, J. Remon, P. Kleinebudde, C. Vervaet, Production of pellets via extrusion-spheronisation without the incorporation of microcrystalline cellulose: A critical review, European Journal of Pharmaceutics and Biopharmaceutics 71 (1) (2009) 38–46.

[137] L. Greenspan, Humidity fixed points of binary saturated aqueous solutions, Journal of Research of the National Bureau of Standards. Section A: Physics and Chemistry 81 (1) (1977) 89–96.

[138] F. Rashid, R. Horobin, Interaction of molecular probes with living cells and tissues. part 2. A structure-activity analysis of mitochondrial staining by cationic probes, and a discussion of the synergistic nature of image-based and biochemical approaches, Histochemistry 94 (3) (1990) 303–308.

[139] J. Kutza, Oleogele auf 12-Hydroxystearinsäurebasis als injizierbare Implantate zur kontrollierten Proteinfreisetzung, Ph.D. thesis, Martin-Luther-Universität (2014).

[140] C. Kutza, H. Metz, J. Kutza, F. Syrowatka, K. Mäder, Toward a detailed characterization of oil adsorbates as "solid liquids", European Journal of Pharmaceutics and Biopharmaceutics 84 (1) (2013) 172–182.

[141] A. Schädlich, T. Naolou, E. Amado, R. Schops, J. Kressler, K. Mäder, Noninvasive in vivo monitoring of the biofate of 195 k Da poly(vinyl alcohol) by multispectral fluorescence imaging, Biomacromolecules 12 (10) (2011) 3674–3683.

[142] A. Schädlich, H. Caysa, T. Mueller, F. Tenambergen, C. Rose, A. Göpferich, J. Kuntsche, K. Mäder, Tumor accumulation of NIR fluorescent PEG-PLA nanoparticles: Impact of particle size and human xenograft tumor model, ACS Nano 5 (11) (2011) 8710–8720.

[143] A. Schädlich, C. Rose, J. Kuntsche, H. Caysa, T. Mueller, A. Göpferich, K. Mäder, How stealthy are PEG-PLA nanoparticles? an NIR *in vivo* study combined with detailed size measurements, Pharmaceutical Research 28 (8) (2011) 1995–2007.

[144] S. G. Gumaste, S. A. Pawlak, D. M. Dalrymple, C. J. Nider, L. D. Trombetta, A. T. Serajuddin, Development of solid SEDDS, IV: Effect of adsorbed lipid and surfactant on tableting properties and surface structures of different silicates, Pharmaceutical Research 30 (12) (2013) 3170–3185.

[145] A. R. Behnke, O. Yarbrough, Respiratory resistance, oil-water solubility, and mental effects of argon, compared with helium and nitrogen, American Journal of Physiology–Legacy Content 126 (2) (1939) 409–415.

[146] J. Lawrence, W. Loomis, C. Tobias, F. Turpin, Preliminary observations on the narcotic effect of xenon with a review of values for solubilities of gases in water and oils, The Journal of physiology 105 (3) (1946) 197–204.

[147] W. A. Gerth, Applicability of Henry's law to hydrogen, helium, and nitrogen solubilities in water and olive oil at 37 °C and pressures up to 300 atmospheres, Archives of Biochemistry and Biophysics 241 (1) (1985) 187–199.

[148] M. K. Gupta, Y. C. Tseng, D. Goldman, R. H. Bogner, Hydrogen bonding with adsorbent during storage governs drug dissolution from solid-dispersion granules, Pharmaceutical Research 19 (11) (2002) 1663–1672.

[149] D. Bahl, R. H. Bogner, Amorphization of indomethacin by co-grinding with Neusilin US2: Amorphization kinetics, physical stability and mechanism, Pharmaceutical Research 23 (10) (2006) 2317–2325.

[150] C. Adhikari, A. Proctor, G. Blyholder, Diffuse-reflectance fourier-transform infrared spectroscopy of vegetable oil triglyceride adsorption on silicic acid, Journal of the American Oil Chemists' Society 71 (6) (1994) 589–594.

[151] A. Proctor, C. Adhikari, G. Blyholder, Lipid adsorption on commercial silica hydrogels from hexane and changes in triglyceride complexes with time, Journal of the American Oil Chemists' Society 73 (6) (1996) 693–698.

[152] D. B. Larsen, K. Fredholt, C. Larsen, Addition of hydrogen bond donating excipients to oil solution: Effect on *in vitro* drug release rate and viscosity, European Journal of Pharmaceutical Sciences 13 (4) (2001) 403–410.

[153] H. D. Williams, M. Van Speybroeck, P. Augustijns, C. J. Porter, Lipid-based formulations solidified via adsorption onto the mesoporous carrier Neusilin® US2: Effect of drug type and formulation composition on *in vitro* pharmaceutical performance, Journal of Pharmaceutical Sciences 103 (6) (2014) 1734–1746.

[154] S. Lüsse, K. Arnold, Water binding of polysaccharides - NMR and ESR studies, Macromolecules 31 (20) (1998) 6891–6897.

[155] M. Romanelli, M. Ottaviani, G. Martini, L. Kevan, Adsorption of nitroxide solutions on X zeolite. 3. Electron spin resonance and electron spin echo modulation study of deuteriated methanol solutions, The Journal of Physical Chemistry 93 (1) (1989) 317–322.

[156] S. Kempe, H. Metz, P. Pereira, K. Mäder, Non-invasive *in vivo* evaluation of in situ forming PLGA implants by benchtop magnetic resonance imaging (BT-MRI) and EPR spectroscopy, European Journal of Pharmaceutics and Biopharmaceutics 74 (1) (2010) 102–108.

[157] U. A. Nilsson, L. I. Olsson, G. Carlin, A. C. Bylund-Fellenius, Inhibition of lipid peroxidation by spin labels. Relationships between structure and function, Journal of Biological Chemistry 264 (19) (1989) 11131–11135.

[158] S. Thaler, M. Fiedorowicz, P. Grieb, Z. Wypych, N. Knap, T. Borowik, K. Zawada, J. Kaminski, M. Wozniak, R. Rejdak, Neuroprotective effects of tempol acyl esters against retinal ganglion cell death in a rat partial optic nerve crush model, Acta ophthalmologica 89 (7) (2011) e555–e560.

[159] M. Gutjahr, A. Pöppl, W. Böhlmann, R. Böttcher, Electron pair acceptor properties of alkali cations in zeolite Y: An electron spin resonance study of adsorbed di-tert-butyl nitroxide, Colloids and Surfaces A: Physicochemical and Engineering Aspects 189 (1) (2001) 93–101.

[160] A. Pöppl, M. Gutjahr, T. Rudolf, Paramagnetic adsorption complexes as studied by advanced electron paramagnetic resonance techniques, in: Molecules in Interaction with Surfaces and Interfaces, Springer, 2004, pp. 185–215.

[161] M. Ottaviani, M. Garcia-Garibay, N. J. Turro, TEMPO radicals as EPR probes to monitor the adsorption of different species into X zeolite, Colloids and Surfaces A: Physicochemical and Engineering Aspects 72 (1993) 321–332.

[162] E. J. Hensen, D. G. Poduval, V. Degirmenci, D. J. Ligthart, W. Chen, M. Françoise, M. S. Rigutto, J. R. v. Veen, Acidity characterization of amorphous silica–alumina, The Journal of Physical Chemistry C 116 (40) (2012) 21416–21429.

[163] T. Konovalova, A. Volodin, V. Chesnokov, E. Paukshtis, G. Echevskii, ESR measurements of concentration for strong surface acceptor centers on zeolites and $Al_2 O_3$ using nitroxide radical TEMPON, Reaction Kinetics and Catalysis Letters 43 (1) (1991) 225–229.

[164] Y. Zhang, Electronegativities of elements in valence states and their applications. 1. Electronegativities of elements in valence states, Inorganic Chemistry 21 (11) (1982) 3886–3889.

[165] R. T. Sanderson, Electronegativity and bond energy, Journal of the American Chemical Society 105 (8) (1983) 2259–2261.

[166] R. G. Parr, R. G. Pearson, Absolute hardness: Companion parameter to absolute electronegativity, Journal of the American Chemical Society 105 (26) (1983) 7512–7516.

[167] R. G. Pearson, Absolute electronegativity and hardness: Application to inorganic chemistry, Inorganic Chemistry 27 (4) (1988) 734–740.

[168] J. Jose, K. Burgess, Syntheses and properties of water-soluble nile red derivatives, The Journal of organic chemistry 71 (20) (2006) 7835–7839.

[169] P. Greenspan, E. P. Mayer, S. D. Fowler, Nile red: A selective fluorescent stain for intracellular lipid droplets, The Journal of cell biology 100 (3) (1985) 965–973.

[170] L. E. Bromberg, D. P. Barr, Aggregation phenomena in aqueous solutions of hydrophobically modified polyelectrolytes. A probe solubilization study, Macromolecules 32 (11) (1999) 3649–3657.

[171] A. Abdalla, Development and characterization of self-emulsifying pellets by extrusion/spheronization, Ph.D. thesis, Martin-Luther-Universität (2008).

[172] A. K. Kirchherr, A. Briel, K. Mäder, Stabilization of indocyanine green by encapsulation within micellar systems, Molecular Pharmaceutics 6 (2) (2009) 480–491.

[173] M. Türk, R. Lietzow, Stabilized nanoparticles of phytosterol by rapid expansion from supercritical solution into aqueous solution, AAPS PharmSciTech 5 (4) (2004) 36–45.

[174] Solutol® HS 15 – technical information (2003).

[175] D. P. Acharya, P. G. Hartley, Progress in microemulsion characterization, Current Opinion in Colloid & Interface Science 17 (5) (2012) 274–280.

[176] A. S. Narang, D. Delmarre, D. Gao, Stable drug encapsulation in micelles and microemulsions, International Journal of Pharmaceutics 345 (1) (2007) 9–25.

[177] H. M. Aliabadi, A. Mahmud, A. D. Sharifabadi, A. Lavasanifar, Micelles of methoxy poly (ethylene oxide)-*b*-poly (ϵ-caprolactone) as vehicles for the solubilization and controlled delivery of cyclosporine a, Journal of Controlled Release 104 (2) (2005) 301–311.

[178] P. Guering, B. Lindman, Droplet and bicontinuous structures in microemulsions from multicomponent self-diffusion measurements, Langmuir 1 (4) (1985) 464–468.

[179] T. Iwanaga, M. Suzuki, H. Kunieda, Effect of added salts or polyols on the liquid crystalline structures of polyoxyethylene-type nonionic surfactants, Langmuir 14 (20) (1998) 5775–5781.

[180] Ç. Batıgöç, H. Akbaş, Spectrophotometric determination of cloud point of Brij 35 nonionic surfactant, Fluid Phase Equilibria 303 (1) (2011) 91–95.

[181] V. C. Santos-Ebinuma, A. M. Lopes, A. Converti, J. Pessoa, Adalberto, C. d. O. Rangel-Yagui, Behavior of Triton X-114 cloud point in the presence of inorganic electrolytes, Fluid Phase Equilibria 360 (2013) 435–438.

[182] W. Warisnoicharoen, A. Lansley, M. Lawrence, Nonionic oil-in-water microemulsions: The effect of oil type on phase behaviour, International Journal of Pharmaceutics 198 (1) (2000) 7–27.

[183] H. Saint Ruth, D. Attwood, G. Ktistis, C. Taylor, Phase studies and particle size analysis of oil-in-water phospholipid microemulsions, International Journal of Pharmaceutics 116 (2) (1995) 253–261.

[184] M. Van Speybroeck, H. D. Williams, T. H. Nguyen, M. U. Anby, C. J. Porter, P. Augustijns, Incomplete desorption of liquid excipients reduces the *in vitro* and *in vivo* performance of self-emulsifying drug delivery systems solidified by adsorption onto an inorganic mesoporous carrier, Molecular Pharmaceutics 9 (9) (2012) 2750–2760.

[185] K. Itoh, S. Matsui, Y. Tozuka, T. Oguchi, K. Yamamoto, Improvement of physicochemical properties of n-4472. part II: Characterization of n-4472 microemulsion and the enhanced oral absorption, International Journal of Pharmaceutics 246 (1-2) (2002) 75–83.

[186] K. I. Momot, P. W. Kuchel, B. E. Chapman, P. Deo, D. Whittaker, NMR study of the association of propofol with nonionic surfactants, Langmuir 19 (6) (2003) 2088–2095.

[187] M. A. Schubert, M. Harms, C. C. Müller-Goymann, Structural investigations on lipid nanoparticles containing high amounts of lecithin, European Journal of Pharmaceutical Sciences 27 (2) (2006) 226–236.

[188] V. Teeranachaideekul, P. Boonme, E. B. Souto, R. H. Müller, V. B. Junyaprasert, Influence of oil content on physicochemical properties and skin distribution of nile red-loaded NLC, Journal of Controlled Release 128 (2) (2008) 134–141.

[189] K. I. Momot, P. W. Kuchel, Pulsed field gradient nuclear magnetic resonance as a tool for studying drug delivery systems, Concepts in Magnetic Resonance Part A 19 (2) (2003) 51–64.

[190] H. E. Gottlieb, V. Kotlyar, A. Nudelman, N MR chemical shifts of common laboratory solvents as trace impurities, The Journal of Organic Chemistry 62 (21) (1997) 7512–7515.

[191] D. S. Wishart, C. G. Bigam, J. Yao, F. Abildgaard, H. Dyson, E. Oldfield, J. L. Markley, B. D. Sykes, ^{1}H, ^{13}C and ^{15}N chemical shift referencing in biomolecular NMR, Journal of Biomolecular NMR 6 (2) (1995) 135–140.

[192] K. Jores, W. Mehnert, K. Mäder, Physicochemical investigations on solid lipid nanoparticles and on oil-loaded solid lipid nanoparticles: A nuclear magnetic resonance and electron spin resonance study, Pharmaceutical Research 20 (8) (2003) 1274–1283.

[193] E. Hatzakis, A. Agiomyrgianaki, S. Kostidis, P. Dais, High-resolution NMR spectroscopy: An alternative fast tool for qualitative and quantitative analysis of diacylglycerol (DAG) oil, Journal of the American Oil Chemists' Society 88 (11) (2011) 1695–1708.

[194] P. Sopelana, I. Arizabaleta, M. L. Ibargoitia, M. D. Guillen, Characterisation of the lipidic components of margarines by 1 H nuclear magnetic resonance, Food Chemistry 141 (4) (2013) 3357–3364.

[195] S. He, M. Timmer, M. Yaszemski, A. Yasko, P. Engel, A. Mikos, Synthesis of biodegradable poly(propylene fumarate) networks with poly(propylene fumarate)-diacrylate macromers as crosslinking agents and characterization of their degradation products, Polymer 42 (3) (2001) 1251–1260.

[196] X. J. Loh, K. B. Colin Sng, J. Li, Synthesis and water-swelling of thermo-responsive poly (ester urethane)s containing poly (ε-caprolactone), poly(ethylene glycol) and poly(propylene glycol), Biomaterials 29 (22) (2008) 3185–3194.

D. List of publications

Articles

- C. Kutza, H. Metz, J. Kutza, F. Syrowatka, K. Mäder, Toward a detailed characterization of oil adsorbates as "'solid liquids"', European Journal of Pharmaceutics and Biopharmaceutics 84 (1) (2013) 172–182.

Oral presentations

- C. Kegel, A. Abdalla, H. Metz, K. Mäder, How liquids and solids interact – a study by Benchtop-NMR, 36th Annual Meeting of the Controlled Release Society, Copenhagen (2009).

Book chapter

- C. Kegel, S. Klein, K. Mäder, Neue Hilfsstoffe - Mehrwert oder nur Mehrkosten?, K. Mäder, U. Weidenauer: Innovative Arzneiformen, WVG Stuttgart, 2010

Poster presentations

- C. Kegel, A. Abdalla, H. Metz, K. Mäder, Benchtop-NMR – a powerful analytical tool to study solid-liquid-interactions, CRS Germany Local Chapter, Halle (2009).

- C. Kegel, H. Metz, K. Mäder, Investigation of the state of solidified lipid formulation systems by Benchtop-NMR, 7th World Meeting on Pharmaceutics, Biopharmaceutics and Pharmaceutical Technology, Valetta (2010).

- C. Kegel, K. Mäder, Monitoring of alterations in solid lipid formulation systems, CRS Germany Local Chapter, Jena (2011).

- C. Kegel, H. Metz, J. Kutza, K. Mäder, Investigation of solid oil adsorbates – Influence of excipient surfaces on polarity and mobility of the oil component under different storage conditions by Benchtop-NMR, 8th World Meeting on Pharmaceutics, Biopharmaceutics and Pharmaceutical Technology, Istanbul (2012).

E. Acknowledgement

This work would not have been possible without the assistance and help of many persons. Therefore, I would like to thank

- Kerstin Schwarz for performing the thermogravimetric analysis

- Ute Menzel for her laboratory assistance and help with the PCS measurements

- Claudia Bertram for all the assistance in organisational issues

- Dr. rer. nat. Martin G. Hahn for the great atmosphere in our office

- All alumnae and current members of the work group "Pharmaceutics" for the great atmosphere in research and beyond the work remembering the joint lunch breaks and trips

- Anke Hinder, Dr. rer. nat. Tanja Engelbrecht, Dr. rer. nat. Sandra Klein, Dr. rer. nat. Stefan Hoffmann and Juliane Frank for a very pleasant time during realisation of the practical student courses

- My family for the encouragement and support during the finalisation of this thesis

F. Curriculum Vitae

Name	Claudia Kutza, geb. Kegel
Adresse	V. Vereinsstr. 13
	06110 Halle/Saale
Geburtsdatum	13. Juli 1983
Geburtsort	Dresden

2002	Abitur, Julius-Ambrosius-Hülße-Gymnasium, Dresden
2002 – 2006	Studium der Pharmazie, Universität Leipzig
11/2006 – 05/2007	Pharmaziepraktikantin, Merck KGaA, Darmstadt
05/2007 – 12/2007	Pharmaziepraktikantin, Apotheke im SEC, Dresden
12/2007	Abschluss der Pharmazeutischen Prüfung
03. Januar 2008	Approbation als Apotheker
01/2008	Angestellte Apothekerin, Apotheke im SEC, Dresden
02/2008 – 09/2012	Wissenschaftliche Mitarbeiterin, AG Prof. Dr. K. Mäder, Pharm. Technologie, Institut für Pharmazie der Martin-Luther-Universität Halle-Wittenberg
04/2008 – 07/2011	Teilzeittätigkeit als angestellte Apothekerin (Chefvertretung) in der Apotheke am Händelhaus in Halle/Saale
Seit 09/2012	Angestellte Apothekerin, Bayer Bitterfeld GmbH, Bitterfeld-Wolfen
	09/2012 – 10/2013 Prozesstechnologie
	Seit 10/2013 Qulaitätssicherung und Qualitätskontrolle

Halle/Saale, den 22. Juli 2015

_____

Claudia Kutza

G. Selbstständigkeitserklärung

Hiermit erkläre ich an Eides statt, dass ich die vorliegende Arbeit selbständig und ohne fremde Hilfe verfasst habe, keine anderen als die von mir angegebenen Quellen und Hilfsmittel benutzt habe und die den benutzten Werken wörtlich oder inhaltlich entnommenen Stellen als solche kenntlich gemacht habe.

Darüber hinaus erkläre ich, dass ich noch keine vergeblichen Promotionsversuche unternommen habe und dass diese Dissertation weder in der gegenwärtigen noch in einer anderen Fassung bereits einer anderen Fakultät vorgelegen hat.

Halle/Saale, den 22. Juli 2015

_____

Claudia Kutza